Evolving *In Vitro* and *In Silico* Methods for Predicting Performance in Respiratory Drug
Delivery Applications

by

Conor Aidan Ruzycki

A thesis submitted in partial fulfillment of the requirements for the degree of

Doctor of Philosophy

Department of Mechanical Engineering
University of Alberta

Abstract

The overarching theme of this work is the investigation and development of *in vitro* and *in silico* methods used to characterize inhaled pharmaceutical aerosols. The ultimate aim is to expand and strengthen the links between applied science and clinical practice for inhaled medications. Chapter 1 introduces the structure of the thesis. Chapter 2 consists of a review of literature. Relevant metrics used in the characterization of inhaled therapies are discussed, together with advanced *in vitro* and *in silico* methods for characterizing respiratory tract deposition and drug disposition.

Chapter 3 describes an *in vitro* study on deposition from commercially available pharmaceutical inhalers in the Alberta Idealized Throat. This mouth-throat geometry has been used to accurately characterize aerosol deposition in terms of extrathoracic and total lung doses, though its ability to replicate *in vivo* deposition from some inhalers requires careful consideration of the underlying aerosol mechanics. We hypothesized that differences between *in vitro* and *in vivo* data may be partly caused by variations in factors not typically considered during *in vitro* testing, primarily the insertion angle of the inhaler into the mouth-throat geometry itself. Three of six examined inhalers showed sensitivity to the angle of insertion. For DPIs, this sensitivity may be reduced using larger diameter mouthpieces and smaller particle sizes in powder formulations. For pMDIs, lower momentum sprays demonstrated more consistent performance. Consideration of these factors in future devices and formulations may improve the consistency of dosing during real-world use.

Chapter 4 describes a combined *in vitro – in silico* methodology to predict systemic exposure of budesonide from dry powder inhalers, incorporating *in vitro* measurements of intrathoracic particle size distributions, regional lung deposition modeling, and pharmacokinetics. Good agreement between predictions and *in vivo* data were obtained without the requirement of extraneous fit factors, suggesting the model is robust for well-characterized therapeutic agents like budesonide.

Comparatively modest deposition in the small conducting airways was predicted to occur with each dry powder inhaler despite large *in vitro* differences in performance. Tracheobronchial deposition was predicted to correlate poorly with systemic drug concentrations, suggesting that overt reliance on systemic exposure data in establishing bioequivalence of locally acting inhaled therapies may not properly elucidate differences between formulations. Rather, a combination of methods like that proposed in the present work may aid in better predicting bioequivalence.

In Chapter 5, a novel *in vitro – in silico* methodology was developed to characterize nebulizer performance in the context of methacholine challenge testing. The incorporation of experimental methods with hygroscopic theory and lung deposition modeling allowed for the quantification of regional deposition of methacholine and better estimation of the provocative dose than is provided by existing methods, which likely overestimate the relevant dose by considerable and device-dependent margins. Measurements of airstream conditions suggested that droplets exiting nebulizer mouthpieces exist in highly concentrated states compared to stock solutions, and upon inhalation these droplets can be expected to undergo significant hygroscopic growth. The procedure outlined in Chapter 5 may serve as step towards standardizing the determination of provocative doses obtained with methacholine challenge testing, which could improve the translatability of results currently obtained with disparate methods and protocols.

Finally, Chapter 6 summarizes major conclusions, identifies contributions to knowledge, and proposes potential avenues for future work. Methods described in this thesis provide a framework for improving upon the standard pharmacopeial methods used to characterize pharmaceutical aerosols. With increased focus on the use of inhaled aerosols as a vehicle for both local and systemic delivery of medication, such methods are of interest in streamlining the drug development process and in optimizing future devices and formulations.

Preface

Chapter 2 has been submitted as a book chapter:

> Ruzycki, Conor A., Warren H Finlay, and Andrew R. Martin. Estimating Clinically Relevant Measures of Inhaled Pharmaceutical Aerosol Performance with Advanced In Vitro and In Silico Methods. In Organ Specific Drug Delivery and Targeting to the Lungs, edited by Ajit S Narang and Ram I. Mahato, CRC Press; Taylor & Francis Group.

Portions have been edited to reduce redundancy with other chapters in this thesis. I performed the literature review and wrote the chapter, with supervisors WHF and ARM providing content feedback. Luba Slabyj provided copy-editing/editorial assistance.

Chapter 3 is published as:

> Ruzycki, Conor A., Andrew R. Martin, and Warren H. Finlay. 2019. "An Exploration of Factors Affecting in Vitro Deposition of Pharmaceutical Aerosols in the Alberta Idealized Throat." Journal of Aerosol Medicine and Pulmonary Drug Delivery 32 (6): 405–17.

Portions therein were presented as a conference abstract:

> Ruzycki, Conor A., Andrew R. Martin, and Warren H. Finlay. Exploring in vitro deposition of pharmaceutical aerosols in the Alberta Idealized Throat. International Society for Aerosols in Medicine (ISAM) 22nd Congress (international), Montreux, Switzerland. May 25-29, 2019 (poster presentation).

I was responsible for the experimental design, operating inhalers, rinsing samples, data analysis and interpretation, and preparing the manuscript as the primary author. ARM and WHF supervised the study. Helena Orszanska performed the chemical assays for quantifying drug mass in rinsate samples via UV spectroscopy.

Chapter 4 is published as:

> Ruzycki Conor A, Brynn Murphy, Hafeez Nathoo, Andrew R. Martin, and Warren H. Finlay. "Combined in Vitro-in Silico Approach to Predict Deposition and Pharmacokinetics of Budesonide Dry Powder Inhalers." Pharmaceutical Research. (2020, 37:10,209).

Portions therein were presented in conference abstracts:

> Ruzycki Conor A, Brynn Murphy, Hafeez Nathoo, Andrew R. Martin, and Warren H. Finlay. Predicting local and systemic distributions of inhaled budesonide powders using in vitro experiments combined with numerical modeling. 10th International Aerosol Conference (international), St. Louis, MO. Sep 2-7, 2018 (poster presentation)

> Ruzycki CA, Finlay WH, Martin AR. Predicting Pharmacokinetics from Three Marketed Dry Powder Inhalers. American Thoracic Society (ATS) 2020, Philadelphia, PA. May 15-20, 2020 (abstract accepted for presentation during thematic poster session, cancelled due to COVID-19 pandemic).

I was responsible for the experimental design, operating inhalers, rinsing samples, data analysis and interpretation, numerical modeling of lung deposition and pharmacokinetics, and preparing the manuscript as the primary author. ARM and WHF supervised the study. ARM provided the original excel code for the PK model that was expanded upon in the present work. BM assisted in early experimental design work and sample collection. NH assisted in the development of the dissolution model. Helena Orszanska performed the chemical assays for quantifying drug mass in rinsate samples via UV spectroscopy.

Chapter 5 will be submitted as a journal article. Portions have been submitted as a conference abstract:

> Ruzycki, Conor A., David Pawluski, Eric Y.L. Wong, Warren H. Finlay, and Andrew R. Martin. In Vitro – In Silico Characterization of Lung Deposition for Nebulizers used in Methacholine Challenge Testing. American Thoracic Society 2022 International Conference.

Preliminary work has been presented in conference abstracts:

> Ruzycki, Conor A., Tully Underhill, David Pawluski, Eric Y.L. Wong, Warren H. Finlay, and Andrew R. Martin. Comparing In Vitro Performance of the RX160 Wright-Type and Misty Max 10 Nebulizers for Methacholine Challenge Testing. American Thoracic Society (ATS) 2020, Philadelphia, PA. May 15-20, 2020 (abstract accepted for presentation during thematic poster session, cancelled due to COVID-19 pandemic).

Ruzycki, Conor A., Tully Underhill, David Pawluski, Eric Y.L. Wong, Warren H. Finlay, and Andrew R. Martin. Establishing In Vitro Equivalence of Legacy and Replacement Wright-Type Nebulizers for Methacholine Challenge Testing. Canadian Respiratory Conference (CRC), Niagara Falls, ON. Apr 16-18, 2020, abstract accepted for presentation; cancelled due to COVID-19 pandemic.

I was responsible for all aspects of the experimental design (including operating nebulizers, chemical assays via UV spectroscopy, measuring airstream conditions, and operating the ELPI+), data analysis and interpretation, numerical modeling of lung deposition and hygroscopic behaviour, primary authorship of conference abstracts and an upcoming journal article, and associated literature review. ARM and WHF supervised the study. WHF performed simulations on an older Fortran version of the lung deposition model to provide validation data. TU assisted in preliminary experimental design work and prototyped adapters for connecting various components. DP and EYLW provided nebulizers for experimental testing and advised on aspects of clinical experience of their use in the University of Alberta Hospital Pulmonary Function Laboratory. Emmadin Javaheri provided an earlier version of the C code for the hygroscopic lung deposition model upon which the current model was structured.

Dedication

"Thou mayest"

John Steinbeck, *East of Eden*

Acknowledgements

I cannot properly express my appreciation for the mentorship, support, and guidance I have received from my supervisors, Prof. Warren H. Finlay and Prof. Andrew R. Martin. Having the opportunity to bounce ideas around with these two has made my PhD experience immensely rewarding. Their support and helpful feedback when things were going well, and their patience and understanding when things were not, have ensured that this thesis is finally complete. Thank you both for providing the perfect environment for academic research and personal development. Their trust in my abilities, even when I lacked it myself, has meant more than either can ever know.

Thanks as well to Prof. Reinhard Vehring for serving on my supervisory committee and for providing invaluable guidance and feedback on numerous projects (his honest opinions were always appreciated). The numerous professors at the department of mechanical engineering that I have had the pleasure of learning under deserve kudos as well. Thank you to the members of the Aerosol Research Laboratory of Alberta that I have had the pleasure of working with (particularly Scott Tavernini, who has become a great friend), both past and present, and to staff throughout the University of Alberta that have aided me throughout. Special thanks to Luba Slabyj as well for her editorial assistance (and wit). Simply put, there are too many people who have played an important role during my PhD to provide all the necessary acknowledgements here.

In the summer of 2020, we learned that our long-time lab technician, Helena Orszanska, was terminally ill. Helena was a unique character who left her mark on everyone in the research lab, and I had the pleasure of working with her for almost a decade. Her love of literature, her disdain for bureaucracy, and her understanding nature ("men plan, god laughs") made her a fixture of my time in the lab, and she was both a good friend and a trusted confidant. Helena passed away in 2020 after a brief illness. She is missed.

Thank you as well to my family for their love and support. Thank you to my parents William and Peggy for instilling in me an appreciation for education and science, and for always believing in me. Thank you to my sister Kayley (and her partner Matt) for always being a voice of reason. And from the bottom of my heart, thank you to my partner Luanne for the love, support, and sarcastic humour that has pulled me through the dark times and made the good times even better.

Table of Contents

List of Tables

List of Figures

1 Introduction

The overarching theme of this work is the investigation of *in vitro* and *in silico* methods used to examine inhaled pharmaceutical aerosols. These aerosols are a mainstay of modern medicine and provide numerous unique advantages over other delivery routes. The ability to deliver medication directly to the site of intended action in lung tissue makes therapeutic aerosols particularly useful for treating lung diseases such as asthma, cystic fibrosis, and chronic obstructive pulmonary disease (Gross and Barnes 2017; Tarrant et al. 2017). The rapid uptake facilitated by fast absorption from the pulmonary region for small molecules, and generally high bioavailability for macromolecules, also hint at the utility of aerosols for systemic drug delivery (Patton and Byron 2007). This is further evidenced by increasing interest in the use of the inhalation route for drug delivery of numerous therapeutics (Newman 2017). Such advantages are balanced somewhat by the complicated physics governing the behaviour of aerosols (from generation in devices through to deposition in the respiratory tract) that often result in large variability in performance. Considering the rich history of inhaled therapies and the accelerating development of new formulations and devices (Stein and Thiel 2016), there is an increasing need for more clinically-relevant measures of performance than are provided by existing pharmacopeial methods. Broadly, the present work describes how such measures can be obtained using experimental and numerical methods and illustrates their use in important real-world problems. This thesis thus aims to strengthen the links between applied science and medicine that aid in the development of inhaled therapies.

Chapter 2 provides a review of the literature. Clinical measures that are commonly used to characterize inhaled therapies are described, along with the limitations of current pharmacopeial methods. Discussions of existing *in vitro* methods used to characterize aerosol performance, deposition models used to predict the mass of drug delivered to the totality (or portions) of the respiratory tract, and pharmacokinetic models used to translate predictions of deposition into measures of systemic exposure are included. Particular attention is given to extrathoracic deposition modeling and characterization via experimental methods, as variability in extrathoracic deposition *in vivo* is considered a primary cause of variability in the dose of inhaled medication reaching the lungs (Borgström, Olsson, and Thorsson 2006). The influence of various factors on

inhaled pharmaceutical performance in real-world use are also discussed to identify important parameters for consideration when developing predictive *in vitro* and *in silico* methods.

Chapter 3 describes an *in vitro* study on deposition from six commercially available pharmaceutical inhalers in the Alberta Idealized Throat. Previous work had demonstrated the ability of the Alberta Idealized Throat to replicate average pharmaceutical aerosol deposition in adults, but that notion was recently challenged in a comparison of deposition among a number of extrathoracic geometries (Wei et al. 2018). We hypothesized that differences in one of two factors, inhaler insertion angle and ambient relative humidity, may have been the cause of the discrepancy. The goal of the study is to therefore investigate the influence of these factors on *in vitro* deposition from marketed inhalers in the Alberta Idealized Throat and identify whether device or formulation characteristics play a role in sensitivity to these factors. By identifying these characteristics, guidance may be provided for future device and formulation design to reduce variability in real-world use.

Chapter 4 describes a combined *in vitro – in silico* study characterizing the performance of three budesonide dry powder inhalers with identical label claims to inform bioequivalence testing. The issue of how best to establish bioequivalence for orally inhaled drug products remains an important one given the recognized importance of inhaled medications in treating disease and the general need for affordable therapies globally (Lee et al. 2015). The specifics involved in establishing bioequivalence vary depending on jurisdiction (Lu et al. 2015), often involving some or all of *in vitro* pharmacopeial measurements, pharmacokinetic studies for systemic exposure, and clinical trials. For medications like inhaled corticosteroids and bronchodilators, where local action in lung tissue is thought to be of more concern than systemic exposure, there are recognized limitations in using pharmacokinetic metrics like peak systemic concentration and area under the curve to characterize bioequivalence. In Chapter 4, advanced *in vitro* methods building upon those developed in Chapter 3 are used to characterize extrathoracic deposition and the intra-thoracic particle size distributions in a manner accounting for differences in device design. This information is used to inform lung deposition modeling and elucidate generational deposition in the thoracic airways. Trends in regional deposition in the large and small conducting airways and the alveolar region are considered owing to hypothesized local action of corticosteroids (Usmani et al. 2016). A pharmacokinetic model incorporating dissolution in the conducting airways is used to predict

the net influence of dissolution, mucociliary clearance, and absorption on systemic exposure as would be measured in traditional clinical studies on bioequivalence. The goals of this study are (a) to examine if a combined *in vitro – in silico* methodology can replicate systemic exposure of budesonide observed *in vivo* for dry powder inhalers and (b) to investigate how predictions in regional deposition correlate with systemic exposure. Successful demonstration of (a) would imply that leveraging the separate strengths of *in vitro* and *in silico* methods is a particularly useful strategy in the early stages of drug development, when iterations on device and formulation design are easier to incorporate, while (b) can inform whether additional information beyond systemic exposure is required in establishing bioequivalence of generics.

Chapter 5 describes an *in vitro – in silico* investigation into methacholine challenge testing to inform determination of the provocative dose obtained with disparate nebulizers and test protocols. The European Respiratory Society (ERS) technical standard on challenge testing (Coates et al. 2017) supports a shift towards reporting results in terms of provocative doses but does not incorporate a means for estimating e.g. exhaled doses or the influence of hygroscopic effects. As such, existing methods for characterizing the provocative dose may be of limited utility in standardizing the reporting of test results across disparate protocols. The goals of this study are (a) to develop an *in vitro* methodology for comparing the performance of nebulizers emitting aerosols with considerable differences in characteristics that complicate the use of traditional measurement techniques, (b) to investigate the behaviour of nebulized droplets via hygroscopic theory, and (c) to numerically model regional deposition of methacholine aerosols to inform determination of the provocative dose. With chapter 4 focusing on regional lung deposition modeling of stable particles, Chapter 5 expands this modeling to consider hygroscopic effects that occur with nebulized aerosols prior to and after inhalation into the respiratory tract. Considering the widespread use of challenge testing in modern pulmonary function laboratories, the improved information provided by (c) in characterizing the provocative dose may be useful in standardizing its determination, in ensuring that results obtained with different protocols are translatable, and in optimizing future protocol designs.

Chapter 6 provides the main conclusions of the thesis, identifies unique contributions to current knowledge, and outlines potential directions for future work. Following the bibliography, additional information supporting Chapters 3, 4, and 5 are included in the appendices.

2 Estimating Clinically Relevant Measures of Inhaled Pharmaceutical Aerosol Performance with Advanced In Vitro and In Silico Methods

This chapter is based on a submitted book chapter; Ruzycki, Conor A., Warren H. Finlay, Andrew R. Martin. Submitted November 12th, 2021. "Estimating Clinically Relevant Measures of Inhaled Pharmaceutical Aerosol Performance with Advanced In Vitro and In Silico Methods." In Organ Specific Drug Delivery and Targeting to the Lungs*, edited by Ajit S Narang and Ram I. Mahato, CRC Press; Taylor & Francis Group. Portions have been edited to reduce redundancy with other chapters in this thesis.*

2.1 Introduction

Inhaled pharmaceutical aerosols, having proved useful in the treatment of disease, are now a mainstay of modern medicine. The direct delivery of medication to the respiratory tract offers a number of advantages as a route of drug administration, including rapid onset of action, reduced systemic dosing for drugs targeting respiratory tract disease, and ease of use for patients. Consequently, therapeutic aerosols are routinely prescribed in the treatment of respiratory tract diseases and disorders, among them asthma, chronic obstructive pulmonary disease (COPD), and cystic fibrosis. Common inhaled therapies include corticosteroids, anticholinergic agents, and beta-agonists in the standard treatment of asthma and COPD (Cazzola et al. 2012; Bateman et al. 2008; Gross and Barnes 2017); antibiotics for managing lung infections that frequently occur in patients who suffer from cystic fibrosis, undergo prolonged mechanical ventilation, or experience lengthy stays in intensive care (Quon, Goss, and Ramsey 2014; Döring et al. 2012); and mucoactive agents such as hypertonic saline to increase mucociliary clearance in patients with chronic lung disease (Tarrant et al. 2017). For these therapies, whose goal is the treatment of disease locally within the lungs, the aerosol route allows for targeted delivery to the site of intended action, achieving local therapeutic doses while bypassing large systemic doses—a major advantage over other routes of administration.

There also exists a largely untapped potential for pharmaceutical aerosols in systemic drug delivery, for example, inhaled insulin for the treatment of diabetes (Santos Cavaiola and Edelman 2014), anti-psychotic (San et al. 2018) and anti-migraine (Tepper 2013; Stapleton 2018) medications, and levodopa for treating Parkinson's disease (Olanow and Stocchi 2018). Systemic delivery of macromolecules via the respiratory tract has been shown to yield higher bioavailability

than other non-invasive delivery routes, which may help reduce the total dose required for efficacious treatment, while the large surface area provided by the alveolar airways allows for the rapid uptake of small molecules (Patton and Byron 2007). Formulations comprising dry powders for inhalation can remain stable for years when stored at room temperatures, making these an ideal vehicle for drug delivery in regions where access to refrigeration is limited (S. H. Wang et al. 2012). Stable dry powder formulations of anti-tubercular therapies may thus prove extremely useful in treating tuberculosis in the developing world (Parumasivam et al. 2016).

Such advantages of inhaled pharmaceutical aerosols are countered somewhat by a number of factors that can reduce treatment success with these medications. For one, the drug must enter the airways to reach the site of intended action. Modern delivery devices typically lose a significant fraction of the nominal drug dose to deposition in the extrathoracic airways before it reaches the lungs, a process that can lead to deleterious side effects and reduced treatment efficacy (Agertoft and Pedersen 1993; Buhl 2006). Extrathoracic deposition, being subject-specific and variable (Martin, Moore, and Finlay 2018; Ruzycki et al. 2017), can also cause a high degree of variability in the total dose delivered to the lungs, and complicates titration to efficacious minimal doses in patients with chronic conditions (Borgström, Olsson, and Thorsson 2006). In addition to inflammation and associated immune responses, chronic lung diseases often cause pathophysiological and histological alterations in the airways that increase in severity with disease progression (Usmani and Barnes 2012). The site of intended action for some inhaled medications may therefore become a moving target as the disease advances.

An additional consideration with inhaled aerosols is the reliance of treatment efficacy on patient adherence to correct administration techniques. A large proportion of patients demonstrate improper technique when self-administering with inhalers, leading to jeopardized device performance and reduced treatment efficacy (Fink and Rubin 2005). Noting the wide range of inhaler designs on the market, Laube et al. (2011) provided a number of specific device recommendations for practitioners working with different patient groups to alleviate issues related to improper technique. And while pharmacist intervention can certainly improve inhalation technique and treatment outcomes (Hämmerlein, Müller, and Schulz 2011; Basheti et al. 2007), the requirement of proper patient technique for treatment efficacy remains a key consideration.

With both local and systemic delivery of inhaled therapeutics, the deposition of aerosol particles in the airways of the respiratory tract is critical in determining the effective dose. The respiratory tract can be broadly classified into three regions: the extrathoracic, which comprises the mouth, nose, and throat airways; the conducting region of the tracheobronchial airways; and the alveolar region, which facilitates gas exchange over the large surface area provided by hundreds of millions of alveoli. For local delivery, certain drugs may provide a more therapeutic effect when delivered to specific portions of the respiratory tract, as in the case of the proximal conducting airways for beta-agonists (Usmani, Biddiscombe, and Barnes 2005) or the more peripheral small airways for anti-inflammatories (Usmani and Barnes 2012; Bjermer 2011). For systemic delivery, general consensus places the ideal location of deposition as the alveolar (gas-exchange) region, where the thin barrier between the alveolar lumen and surrounding capillaries facilitates rapid uptake and increased bioavailability compared to other administration routes (Patton and Byron 2007). With either form of delivery, deposition in the extrathoracic region for many inhaled pharmaceutical aerosols is often considered lost or wasted, as this dose is either swallowed (later undergoing first-pass metabolism) or expectorated.

2.1.1 Clinically Relevant Measures

Measures of inhaled pharmaceutical aerosol performance *in vivo* typically rely on clinical trials with quantifiable endpoints. Along with the classic endpoints of morbidity and mortality from large-scale clinical trials, quantifiable test metrics for use in evaluating inhaled pharmaceutical aerosol performance are invaluable. One of the most commonly used metrics in characterizing lung disease and treatment efficacy is the forced expiratory volume in 1 second (FEV1; Pellegrino et al. 2005). Measured via spirometry, the FEV1 sees widespread use in the characterization and treatment of asthma (Reddel et al. 2009), cystic fibrosis (Szczesniak et al. 2017), and chronic obstructive pulmonary disease (COPD; Kakavas et al. 2021). Correlations between the FEV1 and *in vitro* measures of pharmaceutical aerosol performance would thus be useful in optimizing therapies, and while the exact relation between dose and efficacy is depends on numerous factors (Daley-Yates 2015), some basic inferences can be made for certain drug classes based on the literature.

Numerous dose-ranging studies have demonstrated relationships between the total administered dose and improvements in FEV1, reinforcing the logical notion that the amount of drug delivered

6

to the lungs is related to treatment efficacy. Such relationships have been clinically demonstrated with both corticosteroids (Dahl et al. 1993; G. Shapiro et al. 1998; Montanaro et al. 2021; Daley-Yates et al. 2021) and bronchodilators (Caillaud et al. 2007; Singh et al. 2014; Kerwin et al. 2020), and the opposite effect (i.e., reductions in FEV1) are observed with challenge aerosols like methacholine (Coates et al. 2017).

For some drugs, deposition in specific regions of the lungs may be more determinate of treatment efficacy than the total administered dose. Usmani, Biddiscombe, and Barnes (2005) demonstrated in vivo that regional deposition was a larger determinant of the effect of albuterol on improvements to FEV1 for asthmatic patients than the total lung dose. 30 µg doses of albuterol delivered via large 6 µm mass median aerodynamic diameter particles (posited to deposit predominantly in the proximal airways) achieved greater improvements in FEV1 than 200 µg doses delivered via pressurized metered dose inhaler plus spacer, while equivalent 30 µg doses delivered via smaller 1.5 µm and 3.0 µm aerosols that demonstrated higher total lung doses than the 6.0 µm aerosol and more distal deposition showed reduced treatment efficacy. The authors surmised that since airway smooth muscle is predominately located in the conducting airways, and that the β2-agonist albuterol acts on this tissue to induce bronchodilation, treatment efficacy was increased by preferentially targeting deposition in this region (Usmani, Biddiscombe, and Barnes 2005).

With inhaled corticosteroids, recent focus has shifted towards increasing deposition in the more peripheral regions of the lungs to treat small airway (< 2 mm diameter) inflammation (Scichilone et al. 2013). In a recent study on extra-fine beclomethasone dipropionate delivered via pressurized metered dose inhaler, Montanaro et al. (2021) found the improvement in FEV1 in asthmatics plateaued at 200 µg, with 400 µg showing increased adverse events at no additional clinical benefit. These results support the analysis of Beasley et al. (2019), who note that the traditional definition of a "low" dose of inhaled corticosteroids (100 to 250 µg of fluticasone propionate or equivalent for adults) actually captures 80 to 90% of the maximum achievable clinical effect for moderate to severe asthma. However, because these doses are the nominal doses metered by devices (not the actual doses depositing in the lungs or portions therein), the influence of regional deposition on clinical effect of corticosteroids is not well-established.

Regional targeting may also be of benefit with inhaled antibiotics. Ramsey et al. (1999) demonstrated that inhaled tobramycin improved the FEV1 and decreased the need for

hospitalizations of cystic fibrosis patients with *Pseudomonas aeruginosa* infections. Administration of high (300 mg) doses of tobramycin were performed using a jet nebulizer emitting relatively large droplets (4 μm), with the aim of preferentially targeting infection in the airways while limiting systemic absorption via the alveolar region. A companion study by Geller et al. (2002) evaluated the pharmacokinetics and bioavailability of tobramycin, demonstrating that the majority of patients achieved sufficiently high concentrations of tobramycin in sputum to treat infection, with low systemic availability via the inhalation route (11.7%) helping to limit potential toxic systemic side effects that would otherwise be associated with such high doses. Inhaled antibiotics, in general, aim to provide the highest concentration of active drug at the site of infection while avoiding systemic toxicity (Maselli, Keyt, and Restrepo 2017).

Common among the above examples is the notion that the quantification of the dose of drug delivered to the lungs, and even to specific regions of the lung, can aide in understanding treatment efficacy and the parameters that influence clinical outcomes. Beyond basic measures of total or regional dose, models allowing for the characterization of disposition are also useful in predicting drug concentrations in airway surface liquid, free vs. bound drug in specific tissues, and in characterizing systemic exposure. With novel treatments in development for various classes of therapeutics, having *in vitro* and *in silico* methods that can accurately inform these fundamental characterizations of therapeutic agents are of interest in optimizing the drug development process.

2.1.2 *Pharmacopeial Measures of Inhaler Performance*

Methods for predicting where the aerosol generated by a particular inhaler and/or with a particular formulation will deposit within the respiratory tract are invaluable in characterizing existing treatments and creating new ones. Standard practice for examining and describing device and formulation performance follows the recommendations of compendial organizations such as the United States Pharmacopeia (2019a; 2019b) and the European Pharmacopoeia (2019), or the guidance of regulatory bodies such as the United States Food and Drug Administration (2018) and European Medicines Agency (2006). These recommendations, which can vary depending on whether the device in question is a dry powder inhaler (DPI), pressurized metered dose inhaler (pMDI), soft mist inhaler (SMI), or nebulizer, aim at ensuring that manufactured devices on the market adhere to quality control metrics such as consistency and accuracy in delivered dose (Shur et al. 2019). Less focus is placed on predicting *in vivo* performance. The delivered dose uniformity

test, for example, provides no information concerning how much drug reaches the site of intended action, or the fate of the drug following deposition.

Fundamentally, this scarcity of information may hamper the development of new products, as the goalposts used in the early stages of inhaler and formulation design (delivered dose, basic aerodynamic particle size distribution groupings) are only tangentially related to *in vivo* deposition and disposition. Given such limitations, the development of new test methods that are more predictive of *in vivo* performance is an attractive prospect. Such methods may help streamline the development process for novel treatments by providing additional information on device and formulation performance in preclinical phases of drug development—well in advance of expensive clinical trials and associated ethical issues—while also providing quality control measures more applicable to health outcomes.

2.1.3 Defining Test Systems

Test systems for inhaled pharmaceutical aerosols can be broadly classified into several categories, including *in vitro* methods, *in silico* computational models, *ex vivo* experiments, and animal models. The present chapter focuses on *in vitro* methods for estimating extrathoracic and thoracic deposition together with aspects of *in silico* computational modeling, including algebraic deposition correlations, one-dimensional lung deposition models, and pharmacokinetic models of disposition following deposition (wherein some aspects of dissolution and absorption are discussed). Other categories of test systems, such as *in vitro* and *ex vivo* dissolution and translocation testing (Radivojev et al. 2019; Selo et al. 2021), 3-dimensional lung deposition modeling (Hofmann 2020), and animal models (Phalen, Oldham, and Wolff 2008) lie outside the scope of the present work and are not described in detail.

2.2 *In Vitro* Methods

In vitro methods are experimental methods performed in a laboratory setting under controlled conditions. With inhaled pharmaceutical aerosols, such methods allow for the in-depth examination of a multitude of parameters for device and formulation performance. A basic *in vitro* experiment to examine deposition may consist of an inhaler, extrathoracic geometry, and filter connected in a series to an inhalation source. As aerosol is emitted from the inhaler, some particles or droplets will impact on and deposit along the interior surfaces of the extrathoracic geometry, while others will continue downstream to be captured in the filter. In the absence of a large exhaled

dose, the dose depositing on this filter provides an estimate of the total dose delivered to the lungs, while the dose depositing in the extrathoracic geometry provides an estimate of oropharyngeal deposition (Finlay and Martin 2008; Weers and Clark 2017; Martin, Moore, and Finlay 2018). Additional information can be gained by replacing the filter with a sizing instrument, such as a cascade impactor, from which the initial particle size distribution entering the thoracic airways can be inferred (Wei et al. 2018; Ruzycki et al. 2018).

The development of *in vitro* correlations capable of accurately predicting *in vivo* deposition has long been a topic of particular interest in the pharmaceutical industry (Byron et al. 2010), leading to a number of recent advances that may improve the predictive capabilities of benchtop experiments. There are several factors to consider in the design of predictive *in vitro* methods, broadly summarized into categories of (i) airway geometry, (ii) inhalation maneuver, (iii) hygroscopic behavior, and (iv) real-world use.

2.2.1   Airway Geometry

Given the importance of extrathoracic deposition in determining the total dose delivered to the lungs, the design of *in vitro* geometries capable of replicating extrathoracic deposition is an obvious starting point in improving the clinical relevance of *in vitro* tests. The United States Pharmacopeia – Induction Port (USP-IP; United States Pharmacopeia 2019a) is a commonly used geometry for interfacing with inhalers *in vitro* and consists of a simple design (two constant diameter tubes joined with a 90° elbow) allowing for ease of manufacture. Unfortunately, this simple design fails to replicate the complex fluid-dynamical interactions that occur within the extrathoracic airways and as a result consistently underestimates extrathoracic deposition of pharmaceutical aerosols in adults (Cheng et al. 2001; Zhang, Gilbertson, and Finlay 2007; Zhou, Sun, and Cheng 2011).

A natural progression from the USP-IP is the use of geometries that more accurately replicate the complex nature of the extrathoracic airways. Modern examples of this approach generally fall into one of two camps: the use of realistic (or semi-realistic) geometries that aim to directly replicate anatomical structures, or the use of idealized geometries that mimic important anatomical features to capture the function of the airways. In either case, advances in medical imaging over the past few decades have proven extremely useful in the development of such geometries, which were previously obtainable only through airway casts on human cadavers (Guilmette, Wicks, and Wolff

1989). Several examples of both realistic and idealized extrathoracic airway geometries for *in vitro* tests can be found in the literature. For drug delivery to the lungs, the relevant extrathoracic airway is age-dependent: infants are obligate nose breathers, while older children and adults typically self-administer aerosols via the mouth. Thus, for treatments targeting delivery to the lungs, extrathoracic geometries for infants have focused on the nasal extrathoracic airways, while extrathoracic geometries for children and adults have focused on the oral extrathoracic airways. Table 2-1 and the following sections summarize some of the extrathoracic geometries that have been described in the literature for use *in vitro*.

Table 2-1: Examples of extrathoracic airway geometries for *in vitro* testing.

Geometry	Type	Age Group	Airway
Oropharyngeal Consortium (OPC) Models (Burnell et al. 2007)	Realistic	Adults	Oral
Virginia Commonwealth University (VCU) Models (Delvadia, Longest, and Byron 2012)	Semi-Realistic	Adults	Oral
Sophia Anatomical Infant Nose-Throat (SAINT) Model (Janssens et al. 2002)	Realistic	Infants (~9 months)	Nasal
Premature Infant Nose Throat (PrINT) Model (Minocchieri et al. 2008)	Realistic	Premature Infants (32-week gestation)	Nasal
Alberta Idealized Throat (Stapleton et al. 2000)	Idealized	Adults	Oral
Alberta Idealized Child Throat (Golshahi and Finlay 2012)	Idealized	Children (6 to 14 years)	Oral
Idealized Infant Nasal Model (Javaheri, Golshahi, and Finlay 2013)	Idealized	Infants (3 – 18 months)	Nasal
Idealized Neonatal Nasal Model (Tavernini et al. 2018)	Idealized	Neonatal Infants (0 – 3 months)	Nasal
Alberta Idealized Nasal Inlet (Kiaee et al. 2019)	Idealized	Adults	Nasal

2.2.1.1   Realistic and Semi-Realistic Extrathoracic Geometries

Drawing on a series of studies on human oropharyngeal airspaces using magnetic resonance imaging (McRobbie, Pritchard, and Quest 2003; Pritchard and McRobbie 2004; McRobbie and Pritchard 2005), Burnell et al. (2007) presented a set of three realistic extrathoracic airway models designed to predict low, median, and high oropharyngeal deposition in healthy adults using nebulizers, pMDIs, and DPIs. These three upper airway models were isolated from a large set of

80 MRI scans of 20 adult patients inhaling from four separate mouthpieces and were based on a statistical analysis of 11 dimensional variables and series of *in vitro* measurements using a DPI, pMDI, and nebulizer. Referred to as the Oropharyngeal Consortium (OPC) models, these geometries have been used to confirm the idea that the dose escaping deposition in an extrathoracic airway model is predictive of the total lung dose when the exhaled dose is negligible (Olsson et al. 2013).

Delvadia, Longest, and Byron (2012) described a semi-realistic upper airway model spanning from the mouth and throat into the upper bronchi of the third airway generation. The mouth-throat model was adapted from Xi and Longest (2007)'s reconstruction of a fully realistic geometry using elliptical cross sections of equal hydraulic diameter and flow area, while the upper airways from the trachea to the third generation were based on morphological data from the literature (Yeh and Schum 1980; Tian, Longest, Su, Walenga, et al. 2011). The geometry, with a mouth-throat volume of 61.6 cm^3 and tracheobronchial dimensions corresponding to a lung volume of 3.5 L, was presented as a "medium-sized" geometry for the general adult population. Additional "small" and "large" geometries were created by a scaling procedure aimed at capturing the variations in airway sizes observed in adults. For the mouth-throat, scaling factors were obtained by adding and subtracting a volume of 37.8 cm^3 (corresponding to two times the standard deviation of the average mouth-throat volume reported by Burnell et al. [2007]) to and from the original 65 cm^3 volume Xi and Longest (2007) geometry, and then taking the cube root of the volume ratios. In effect, this approach created an isotropic scaling along each dimension of 1.165 for the large geometry and 0.748 for the small geometry. Here, Delvadia, Longest, and Byron (2012) presumed that the "small" and "large" geometries generated via isometric scaling of the "medium" geometry would capture the 95th percentiles of physical dimensions observed in adult population, and hypothesized that these would translate into estimates of the median and variability of lung deposition when used *in vitro* to examine deposition from pharmaceutical inhalers. This approach does not account for geometric dissimilarity in extrathoracic geometries *in vivo*, however, (see discussion later in this chapter based on Ruzycki et al. [2017]), and it is therefore unclear if these geometries provide rigorous estimates of variability in real populations. The geometries described by Delvadia, Longest, and Byron (2012) are together referred to as the Virginia Commonwealth University (VCU) models, and a number of studies have used the VCU models, or portions thereof, to examine factors such as insertion angle (Delvadia et al. 2013), the effects of realistic inhalation

maneuvers on DPI performance (Delvadia et al. 2012; Wei et al. 2017), and relative performance in comparisons with other throat models (Wei et al. 2018; Kaviratna et al. 2019).

Janssens et al. (2002) presented the Sophia Anatomical Infant Nose-Throat (SAINT) model, a realistic nasopharyngeal geometry created from a computed tomography (CT) scan of a 9-month-old Caucasian female infant. The model, which included portions of the infant's face, provides a realistic interface for aerosol administration via facemasks and spacers. Janssens et al. (2002) used the SAINT model to examine initial thoracic particle sizes and total lung doses of a budesonide pMDI delivered with a spacer and facemask using realistic inhalations. Deposition within the SAINT model itself was not directly measured, as the polymer resin of the model interfered with high performance liquid chromatographs (HPLCs) for the selected solvent, ethanol. The SAINT model has seen use in a number of studies on aerosol administration to infants, including investigations on high flow nebulization (Réminiac et al. 2016), active dry powder inhalers (Laube et al. 2012), and facemask seal leaks (Esposito-Festen et al. 2004).

Minocchieri et al. (2008) developed a realistic nasopharyngeal airway model of a premature newborn from MRI scans of a healthy male with a gestational age of 32 weeks to address the absence of such a model in the literature. The authors noted somewhat limited scan resolution due to long acquisition times and coarse voxel sizes provided by MRI as compared to CT imaging, which was not used because of ethical issues concerning radiation exposure for preterm infants. A physical model including the face was rapid prototyped using a photopolymer, with post-build CT scans of the physical model confirming that the printing process adequately replicated the airways. Minocchieri et al. (2008) then used a facemask to deliver a nebulized budesonide solution through the model at various inspiratory flow rates, measuring the total lung dose and particle sizes escaping deposition with a Next Generation Impactor. As with the study by Janssens et al. (2002), solvent interactions with the plastic extrathoracic airway geometry interfered with HPLC measurements, preventing the direct determination of deposition within the model itself.

2.2.1.2 Idealized Extrathoracic Geometries

The first idealized throat model for aerosol deposition measurements was developed by Stapleton et al. (2000) using data from CT scans, MRI scans, observations of living subjects, and archival literature on extrathoracic airway dimensions in adults. The development of this geometry, called the Alberta Idealized Throat, was motivated in part by the desire to remove the bias of a particular

individual's airway from studies using limited numbers of realistic airway replicas. Comprised of simplified analogues of important anatomical features including the pharynx, epiglottis, and larynx, the Alberta Idealized Throat can be reliably manufactured to tight tolerances with existing technologies while still capturing the function of the extrathoracic airways. Having been shown to predict the average deposition expected for various pharmaceutical aerosols in adult populations (Zhang, Gilbertson, and Finlay 2007; Zhou, Sun, and Cheng 2011; Weers et al. 2015; Wei et al. 2018), the Alberta Idealized Throat has seen extensive use following its commercialization through Copley Scientific. Recent examples include *in vitro* examinations of inhaler performance at altitude (Morin et al. 2014; Ruzycki et al. 2018), evaluation of novel inhaler designs and formulations (Fink et al. 2017; Ung et al. 2016; Weers et al. 2015), and performance comparisons of various devices (Shemirani et al. 2013; Ciciliani, Langguth, and Wachtel 2017; Ruzycki, Martin, and Finlay 2019; Ruzycki et al. 2020). Ruzycki, Martin, and Finlay (2019) recently demonstrated that the insertion angle used with high-momentum pMDIs and certain DPIs with large particle sizes or high mouthpiece exit velocities can significantly influence *in vitro* measurements obtained with the AIT. Their observations suggest that stronger correlations between *in vitro* measurements and *in vivo* scintigraphy data with inhalers demonstrating these characteristics are obtained with the AIT when the inhaler mouthpiece is aligned with the transverse plain, rather than directed towards the back of the oral cavity: such effects may explain disparities in *in vitro – in vivo* correlations reported by different authors (see e.g. Wei et al. [2018]).

Golshahi and Finlay (2012) found that an isometric scaling down of the Alberta Idealized Throat by a factor of 0.62 yielded a throat model that captures average extrathoracic deposition in school-age children. This particular scale factor was selected so that the characteristic diameter (equal to the throat volume divided by surface area) of the scaled model matched the average characteristic diameter measured in nine realistic airway models of children ages 6 to 14 that had been used to examine deposition in an earlier study (Golshahi, Noga, and Finlay 2012). Ruzycki et al. (2014) then showed that this geometry, named the Alberta Idealized Child Throat, successfully replicated *in vivo* deposition of therapeutic aerosols from both pMDIs and DPIs in school-age children.

Javaheri, Golshahi, and Finlay (2013) developed an idealized nasopharyngeal airway using CT scans from ten infants aged 3 to 18 months. Cross sections of airway scans were used to develop idealized cross sections that were then joined using two-dimensional splines to create the general

form of the idealized model, incorporating such important airway features as the meatus, turbinates, nasal valve, and septum. This model was then scaled such that its hydraulic diameter (i.e., four times the volume divided by the airway surface area) matched the average hydraulic diameter measured in the ten infant airways. *In vitro* measurements suggested that deposition in this idealized geometry closely matched the trends in deposition observed in the ten realistic airway models, although Tavernini et al. (2018) demonstrated that an additional isotropic scaling of 0.8 on this geometry yielded a geometry more predictive of the average deposition across the entire 3 to 18 month age range. An additional isotropic scale factor of 0.75 on this version of the geometry (i.e. a total isotropic scaling of 0.6 on the Javaheri, Golshahi and Finlay [2013] geometry) provided an idealized geometry representative of deposition in neonates with an average age of 1 month. At present, a lack of suitable *in vivo* deposition data in infants or neonates has prevented the full validation of either the idealized infant nasal geometry or the idealized neonate nasal geometry. Nevertheless, both may prove useful in guiding studies on aerosol administration to very young patients, a topic for which *in vitro* methods are particularly useful owing to ethical concerns.

Recent interest in intranasal drug delivery (Keller, Merkel, and Popp 2021) has motivated the development of the Alberta Idealized Nasal Inlet (Kiaee et al. 2019; Chen et al. 2020), representative of adult nasal extrathoracic airways. Kiaee et al. (2019) developed the geometry via a sophisticated computational approach wherein airway geometries of 10 subjects (obtained via computed tomography) were decomposed into cross sections that served as a basis for a heuristic and iterative development of an idealized model. Average numerical deposition of spray droplets in regions of interest including the vestibule, valve, anterior and posterior turbinates, olfactory mucosa, and nasopharynx observed in an earlier computational study (Kiaee et al. 2018) was used as a basis for iterating the design of the geometry. Chen et al. (2020) demonstrated good *in vitro* agreement between deposition in this idealized model and the average deposition measured across 5 realistic nasal airway geometries, as well with *in vivo* data from the literature. Together these results suggest that the Alberta Idealized Nasal Inlet may serve as a useful platform for quantifying *in vitro* regional nasal-extrathoracic deposition for nasal sprays.

2.2.1.3   In Vitro Measures of Thoracic Deposition

The basic measurement of *in vitro* thoracic deposition is the total lung dose, typically measured by placing a high efficiency filter downstream of an extrathoracic geometry to capture any dose that would penetrate into the lungs. Such a procedure cannot differentiate between the dose that would deposit in the lungs and the dose that might be exhaled, but for many DPIs and pMDIs for which a long breath hold is advised during administration the exhaled dose is negligible (Clark 2012).

More in-depth characterization of thoracic deposition *in vitro* is complicated by the intricate anatomy of these airways: the fractal bifurcating nature of sequential airway generations with varying and continually decreasing dimensions quickly renders attempts to replicate such a complex geometry with a physical prototype untenable. While a full *in vitro* model of the airways is not possible, partial upper-airway models consisting of the first few conducting airway generations and bifurcations have been described (Cheng, Zhou, and Chen 1999; Borojeni et al. 2015; Huynh et al. 2018). Such models have proven useful in exploratory research and in the development of empirical correlations (Chan and Lippmann 1980) but are not widely used in practice.

An alternative is to combine the practice of particle size characterization via cascade impactors with extrathoracic deposition measurements using realistic or idealized mouth-throat geometries. Rather than simply providing a measure of the total lung dose as provided by a filter, the use of a cascade impactor downstream of a mouth-throat geometry allows for the estimation of the particle size distribution entering the thoracic airways (Wei et al. 2017; Burnell et al. 2007). These data can in turn be used as input in regional deposition models (Bhagwat et al. 2017; Ruzycki et al. 2018; 2020; Tavernini et al. 2021) to gather and elucidate more information on thoracic deposition than is provided by traditional *in vitro* measures such as the mass median aerodynamic diameter or fine particle dose.

The use of filters designed to mimic regional deposition is a promising development that may allow for the more direct estimation of broad trends in regional deposition without requiring numerical modeling and cascade impactor measurements. The physics of deposition in the human airways via impaction, sedimentation, and diffusion is in many ways analogous to that of deposition in filters, and in theory a properly designed filter should be able to replicate *in vivo* deposition of inhaled pharmaceutical aerosols in, for example, the tracheobronchial region.

Tavernini et al. (2019) described the development of such a filter capable of replicating numerical predictions of tracheobronchial deposition for various physiologically relevant inhalation profiles. Recent proof-of-concept tests have demonstrated good agreement between the *in vitro* tracheobronchial filter for four commercially available DPIs and *in vitro* NGI measurements plus *in silico* predictions of regional deposition (Tavernini et al. 2021). A comparison of the *in vitro* aspects of these experiments is shown in Figure 2-1. The simplified nature of the setup using the tracheobronchial filter is attractive from the viewpoint of device development and method standardization, and these successful pilot studies suggest that such an approach may prove useful in expediting the development of innovative and generic inhalation products.
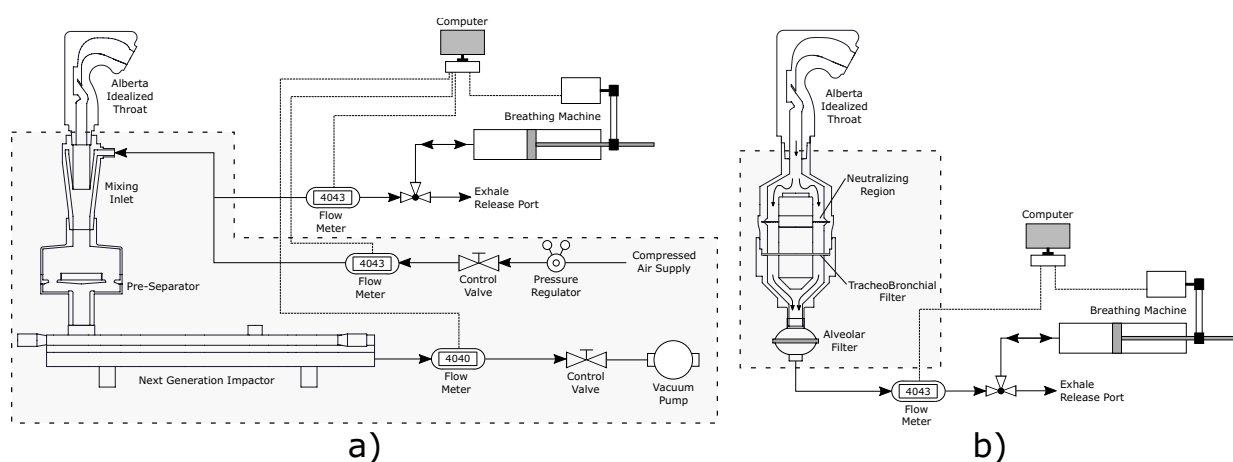
Figure 2-1: Schematic diagrams of the experimental apparatus for a) cascade impactor measurements or b) regional deposition filter measurements for characterizing inhaler performance *in vitro* using realistic inhalation profiles. Grey shaded regions identify different equipment required for each setup. Reproduced from Tavernini et al. (2021) with permission from Springer Nature, *Pharmaceutical Research.*

2.2.2   Inhalation Maneuver

In vivo inhalation maneuvers vary widely among the various types of devices: for some, the appropriate form is a sinusoidal-like tidal breath, for others, a fast and deep inhalation. With the advent of computer-controlled breathing machines (e.g., ASL 5000 Breathing Simulator, IngMar Medical, Pittsburg, PA, USA), it is often a straightforward matter to deliver physiologically realistic inhalation patterns when examining many inhalation devices *in vitro*. The following sections discuss appropriate inhalation profiles to use for the various classes of devices.

2.2.2.1 pMDIs and SMIs

The nominal inhalation maneuver for pMDIs consists of a slow and steady inhalation followed by an extended breath hold (Mitchell, Suggett, and Nagel 2016). Ideally, the flowrate generated by a patient inhaling through a pMDI is as low as reasonably possible (Pauwels, Newman, and Borgström 1997), with a typical target of 30 L/min (Laube et al. 2011; Broeders et al. 2009). PMDIs generally have a very low airflow resistance (Hira et al. 2018), making it quite easy for most patient groups to generate 30 L/min through these devices. SMIs have a similarly low airflow resistance (Hira et al. 2018), making 30 L/min a reasonable target flowrate here as well (Newman et al. 1998). In some circumstances, a slow and deep inhalation (repeated 3 to 5 times) may be recommended when pMDIs and SMIs are used in conjunction with add-on devices such as spacers or valved holding chambers, although tidal inhalations are more common (Broeders et al. 2009; Mitchell, Suggett, and Nagel 2016).

In practice, *in vitro* examinations of pMDI and SMI performance are carried out using a constant inhalation flowrate generated by a vacuum source (i.e., a pump). This method is somewhat analogous to trained pMDI and SMI use, according to which the patient begins inhaling prior to actuating the device. One benefit of this approach is that it avoids issues coordinating the device actuation with a particular moment in the inhalation maneuver, as would otherwise be necessary when using more realistic inhalation profiles. Furthermore, droplet sizes initially generated by such devices are essentially independent of inhalation flowrate (Mitchell, Suggett, and Nagel 2016); flowrate-dependent performance is instead caused by differing rates of impaction, turbulence levels, and hygroscopic effects that occur at different airflow velocities during transit through the airways (Shemirani et al. 2013; Finlay 2019).

The aerosol spray emitted by a pMDI generally has a significant velocity exceeding that of the surrounding ambient air inhaled by the patient (Liu, Doub, and Guo 2012). The development of this spray in a confined space (i.e. the oral cavity) and in the presence of a surrounding sheath of air (i.e. ambient air inhaled by the patient) is an extremely complex process (Finlay 2019) that can be influenced by the inhalation flowrate via shear-induced turbulence along the edges of the spray plume (Shemirani et al. 2013). While the momentum of the spray alone can cause a significant amount of extrathoracic deposition owing to its inertia, these turbulent effects may play an additional role (Shemirani et al. 2013).

The question then arises as to whether a constant inhalation flowrate is sufficient for capturing any of the aforementioned effects on pMDI performance *in vivo*, or if a fully realistic inhalation profile should be used instead. Limited work has explored the use of realistic inhalation profiles with pMDIs and SMIs. Drawing on data collected from several volunteers, Olsson et al. (2013) developed a sophisticated *in vitro* setup incorporating a computer-controlled pneumatic hand to actuate pMDIs at specific moments in the inhalation maneuver. They found that volunteers actuated the pMDI an average of 0.25 seconds after the start of inhalation (noting a high degree of intra-subject variability) and selected three profiles they deemed as representative of the 5th, 50th, and 95th percentiles for (1) the flowrate at device actuation and (2) the average flowrate for a period of 1 second after actuation. Olsson et al. (2013) then compared *in vitro* measurements of the ex-cast dose obtained with these inhalation profiles to *in vivo* lung doses estimated via plasma concentrations, finding a reasonable agreement. Unfortunately, no comparison was made to the use of steady inhalation flowrates, leaving this issue unresolved. There is evidence that extrathoracic deposition of a bolus of stable aerosol is governed more by the flowrate at which particles reach the site of deposition than by the flowrate at which they were inhaled, and that the process of bolus deposition for stable particles in the extrathoracic region can be considered quasi-steady (Grgic, Martin, and Finlay 2006). With pMDIs and SMIs, however, large hygroscopic size changes can certainly occur (Finlay 2019). If the effects of inhalation flowrate on these hygroscopic effects are negligible (i.e., if hygroscopic behavior is more or less the same at, for instance, 30 L/min as at 40 L/min, flowrates representing the average and maximum achieved by properly trained subjects [Olsson et al. 2013]), *in vitro* experiments using appropriately set steady inhalation flowrates with pMDIs and SMIs are likely indicative of deposition obtained with realistic inhalations *in vivo*.

The duration for which air is drawn through the pMDI/SMI *in vitro* is typically set to obtain an inhaled volume of 4.0 L (United States Pharmacopeia 2019a). This setting provides an ample volume of air to ensure that the bolus of aerosol emitted from these devices transits the entire volume of sizing instruments in use today (Mohammed et al. 2012).

2.2.2.2 DPIs

Most DPIs are passive, relying on a patient's inhalation to generate the energy required for powder aerosolization, deagglomeration, and delivery into the respiratory tract. These devices tend to

demonstrate high degrees of flowrate-dependent performance, and as such, are sensitive to the magnitude and shape of the inhalation profile used during their operation (Weers and Clark 2017). With DPIs, patients are typically instructed to inhale deeply, rapidly, and forcefully, and then follow up with a long breath hold (Mitchell, Suggett, and Nagel 2016; Broeders et al. 2009). The non-negligible airflow resistances of these devices necessitates a fair amount of effort on the part of the patient to achieve a strong inhalation, and typical use generates pressure drops of 1 to 6 kPa across the DPI (Weers and Clark 2017). Exactly how this pressure drop translates into an inhalation flowrate depends on the value of the airflow resistance of the specific device in question; a wide range of airflow resistances—anywhere from 0.015 to 0.06 $kPa^{1/2}min/L$ (Frijlink and De Boer 2005)—are encountered with existing DPIs, resulting in a similarly wide range of inhalation flowrates.

Standard *in vitro* DPI tests use a solenoid valve to deliver a step inhalation through the device up to the peak inhalation flowrate (United States Pharmacopeia 2019a). This setup facilitates repeatability but provides no control over the acceleration of flowrate, a factor known to influence the performance of some DPIs (Everard, Devadason, and Le Souëf 1997; Kamin et al. 2002; Dorosz, Penconek, and Moskal 2016). The actual acceleration of flowrate developed across an inhaler using a step inhalation can vary with the magnitude of the peak flowrate and device resistance and is further influenced by the amount of "dead-space," or internal volume, of the sampling apparatus used during testing (Greguletz et al. 2010; 2020; Versteeg et al. 2020). In effect, the acceleration of flowrate is more rapid when an inhaler is actuated with a solenoid valve directly into a filter than when it is actuated with a solenoid valve into an extrathoracic geometry attached to a Next Generation Impactor. In some circumstances, *in vitro* data obtained with these forms of inhalation can provide good predictions of *in vivo* deposition, provided inhalation flowrates are set appropriately (Finlay and Gehmlich 2000). For devices that demonstrate greater sensitivity to the acceleration of flowrate, however, more realistic inhalation patterns may be required to obtain predictive measures of *in vivo* performance (Ung and Chan 2016).

Realistic profiles can be delivered using programmable breathing machines, allowing for the direct replication of inhalation profiles generated by volunteers inhaling from various devices (Finlay and Gehmlich 2000). This method relies on *in vivo* data from subjects inhaling through devices and is somewhat cumbersome from a development perspective. A compromise may take the form

of semi-realistic inhalation patterns that capture the general form of inhalations achieved *in vivo* through DPIs of varying resistance, as advocated by Delvadia et al. (2016). For a device with a specific inhalation resistance R, this method provides tunable semi-realistic inhalation profiles of a sinusoidal form for the 10th, 50th, and 90th percentiles of peak inspiratory flowrate generated by adult volunteers that can be further modified for varying inhaled volume, duration of inhalation, and the time required to reach the peak inspiratory flowrate—relevant equations are presented in Chapter 3; equations (3-1) and (3-2).

A caveat to using time-varying inhalation profiles *in vitro* is that cascade impactors must be operated at a constant flowrate to provide meaningful aerodynamic size classification data. The combination of a time-varying inhalation profile through a DPI and particle size measurements with a cascade impactor thus requires a more complicated *in vitro* setup incorporating a mixing inlet (Wei et al. 2017; Olsson et al. 2013; Tavernini et al. 2021)—see Figure 2-1 above. The mixing inlet allows for a fully constant flowrate to be maintained through the cascade impactor that is balanced by an equal flow of bypass air before an inhalation through the DPI. Operating the breathing machine perturbs the mass balance of airflow across the mixing inlet, which is reestablished by airflow drawn through the DPI. Upon exiting the distal end of the throat, aerosol is diluted with the bypass airstream and enters the cascade impactor at a constant flowrate. Although the setups described in Figure 2-1 are more complicated than the pharmacopeial method for examining DPIs (i.e., using a step inhalation controlled via a solenoid valve), they are more likely to emulate DPI performance *in vivo* for devices that are sensitive to the effects of parameters such as the acceleration of flowrate. One limitation with the NGI is the maximum allowable flowrate of 100 L/min for which the NGI is properly characterized. Extension beyond this range without implementing a full compendial characterization of impactor performance (i.e., evaluating performance with well-characterized monodisperse particles) may result in off-spec impactor performance and mischaracterization of results.

2.2.2.3 Nebulizers, Spacers, Valved Holding Chambers, and Facemasks

The administration of therapeutic aerosols using nebulizers occurs over several breaths and a timespan of minutes, with patients typically being instructed to breathe in a relaxed, normal manner (Laube et al. 2011; Mitchell, Suggett, and Nagel 2016). Many nebulizers operate continuously during administration, with the drug delivered into the respiratory tract during

inhalation and lost to the environment upon exhalation (through, for example, a one-way expiratory valve in the mouthpiece). Various designs are available, including traditional jet nebulizers (both vented and unvented), which are driven by a compressed air source, and vibrating mesh nebulizers, which generate droplets from a liquid solution via the action of a piezoelectric element on a fine mesh of nozzles. For such devices, primary droplet production is likely independent of inhalation flowrate, but the subsequent evolution of these droplets via impaction with interior baffles (when present), aerodynamic loading, and hygroscopic effects may be more sensitive (Finlay 2019).

Spacers and valved holding chambers act to reduce the ballistic nature of the jet emitted from a pMDI upon actuation and provide additional time for the propellant to evaporate prior to inhalation. This delay results in a slower-moving aerosol comprised of smaller particles that are less likely to deposit in the extrathoracic region and more likely to penetrate into deeper airways (Mitchell and Dolovich 2012). Use of such devices also removes the need to coordinate device actuation and inhalation, making them an extremely useful tool for administering pharmaceutical aerosols to uncoordinated or uncooperative patients, and allows patients to inhale relatively normally during administration. Aerosol delivery to uncoordinated or non-compliant patients can be further facilitated using facemasks, as is standard practice with pediatrics (Smaldone, Berg, and Nikander 2005), again allowing the patient to inhale relatively normally during administration.

With respect to normal patient use, predictive *in vitro* tests for many types of nebulizers, spacers, valved holding chambers, and facemasks may best be performed using tidal inhalations over several breaths, including both the inhalation and exhalation portions of the breathing cycle. Depending on the parameter of interest, the full simulation of tidal breathing may be unnecessary; with unvented nebulizers, the inhaled dose can be estimated given knowledge both of the duration of inhalation relative to the full breath and of the total delivered dose measured using conventional methods.

While one can use realistic inhalations measured from patients directly, a more adaptable method involves the use of sinusoidal curves (Mitchell and Dolovich 2012). Roth, Lange, and Finlay (2003) showed that sinusoidal inhalation profiles provide an excellent approximation of realistic inhalation profiles for subjects inhaling through vented nebulizers, as the *in vitro* particle size measurements they obtained with sinusoidal and realistic inhalations and subsequent simulations

of regional lung deposition were essentially identical. Sinusoidal curves carry the added benefit of being easily modified to adjust the breathing pattern for the varying tidal volumes, duty cycles, and durations representative of various patient groups (Dolovich and Mitchell 2004). In practice, a full breath is typically modeled in two portions consisting of separate inhalations and exhalations, with pauses between cycles considered negligible. The mathematical form of the profile for the flowrate at a given time, $Q_{\text{tidal}}(t)$, is shown in equation (2-1), where V_{T} is the tidal volume, f is the breathing frequency (expressed as the number of breathing cycles per minute), and δ_{c} is the duty cycle (the ratio of the durations of inhalation and exhalation) expressed in fractional form.

$$Q_{\text{tidal}}(t) = \begin{cases} \dfrac{\pi V_{\text{T}}}{\left(\dfrac{120\delta_{\text{c}}}{f}\right)} \sin\left(\dfrac{2\pi t}{\left[\dfrac{120\delta_{\text{c}}}{f}\right]}\right) & 0 \leq t < \dfrac{120\delta_{\text{c}}}{f} \\[4ex] \dfrac{\pi V_{\text{T}}}{\left(\dfrac{120[(1-\delta_{\text{c}})]}{f}\right)} \sin\left(\dfrac{2\pi\left[t + \dfrac{120\delta_{\text{c}}}{f}\right]}{\left[\dfrac{120(1-\delta_{\text{c}})}{f}\right]}\right) & \dfrac{120\delta_{\text{c}}}{f} \leq t < \dfrac{60}{f} \end{cases} \tag{2-1}$$

As with DPIs, the use of sinusoidal breath profiles to examine nebulizers in combination with particle sizing via cascade impactors requires the implementation of a mixing inlet. Additional consideration must be given to the hygroscopic nature of nebulized aerosols when measuring particle sizes with cascade impactors; considerable evaporative size changes often occur with these liquid aerosols during transit through cascade impactors, as noted in the following section.

For illustrative purposes, demonstrations of the various inhalation maneuvers discussed above are presented in Figure 2-2. These profiles have been chosen arbitrarily for qualitative comparison only, and care should be taken to ensure that appropriate inhalation parameter values (e.g., peak inhalation flowrates and device resistances for DPIs, breathing frequency and tidal volume for nebulizers, etc.) are used *in vitro*.
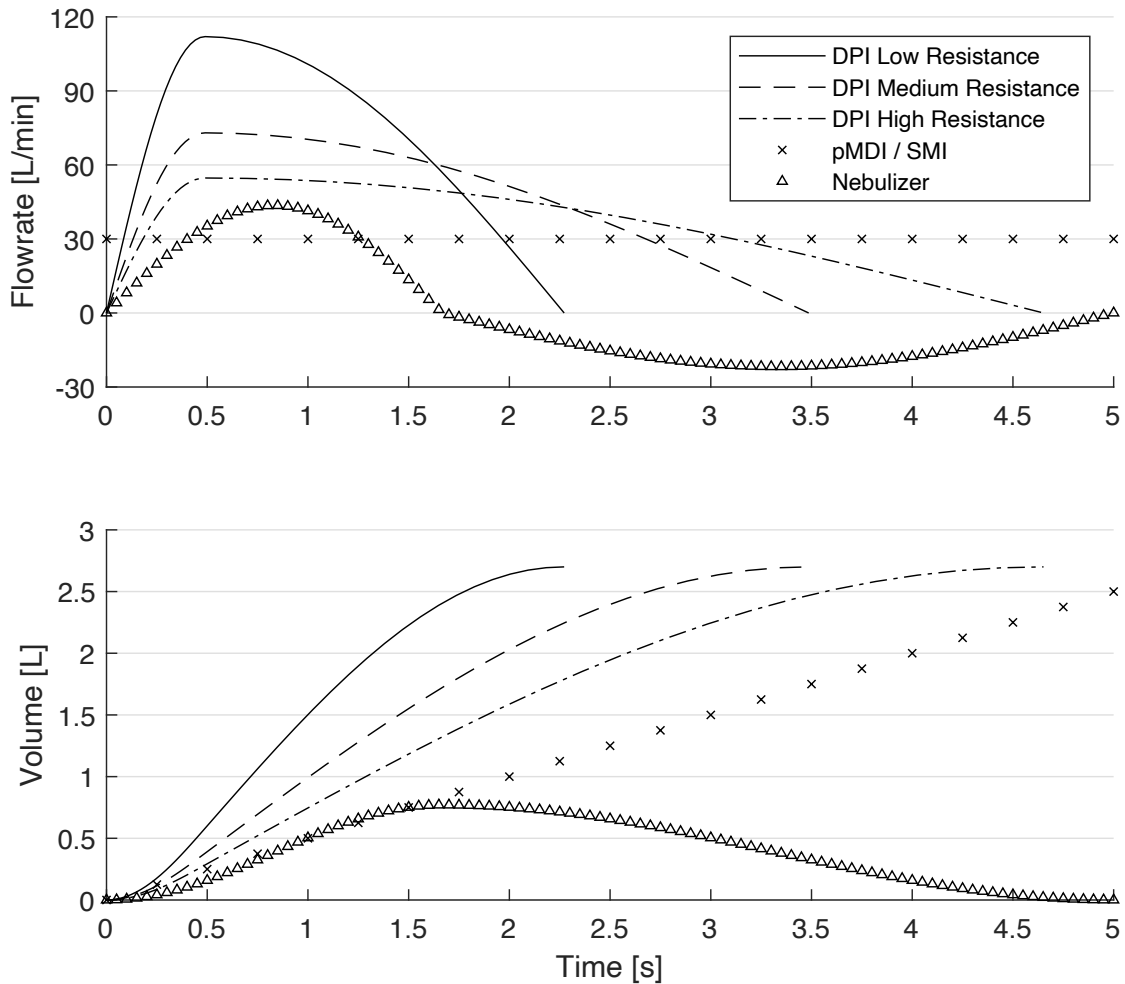
Figure 2-2: Examples of idealized inhalation maneuvers for *in vitro* performance evaluation of various devices. The top panel details the inhalation flowrate with respect to time, while the bottom details the inhaled volume with respect to time. For DPI profiles, device resistances of 0.02, 0.035, and 0.054 $kPa^{1/2}min/L$ were used as the low, medium, and high resistance DPIs, respectively, with the inhaled volume (2.7 L) and time to peak inhalation (0.49 s) chosen to match the average values in Delvadia et al (2016) for healthy adults. For the nebulizer, parameters were chosen to match the profile representative of an average adult in the Canadian Standard CAN/CSA/Z264 (Dolovich and Mitchell 2004).

2.2.3 Hygroscopic Behavior

Hygroscopic size changes due to evaporation or condensation can significantly influence *in vitro* measurements of many inhaled pharmaceutical aerosols if not considered properly. A striking example is the substantial bias towards smaller particle sizes that occurs when nebulized aerosols are measured *in vitro* using cascade impactors without steps having been taken to mitigate evaporative size changes as the aerosol transits through the instrumentation (Finlay and Stapleton 1999; Kwong, Ho, and Coates 2000). The issue of evaporative size changes in cascade impactors with hygroscopic aerosols produced by nebulizers and SMIs, together with the time required to run routine cascade impactor measurements, has led to the preferential use of laser diffraction instrumentation to characterize these aerosols (Vecellio-None et al. 2001; Ziegler and Wachtel 2005).

The challenge lies first in determining the extent to which hygroscopic size changes are important for a given aerosol, and second in determining the extent to which hygroscopic behavior in a proposed *in vitro* test may differ from hygroscopic behavior *in vivo*. In many cases the relative importance of hygroscopic effects can be estimated via non-dimensional analysis (Finlay 1998), which also provides some guidance on the steps required to mitigate or control such effects in a known manner. Yang et al. (2017) used such methods in an *in vivo* scintigraphy study on respiratory tract deposition to mitigate hygroscopic size changes of nebulized aerosols via humidification of dilution air. This approach appreciably simplified their analysis.

In considering how hygroscopic size changes *in vitro* and *in vivo* may differ, it is important to recognize that one of the defining features of the human respiratory tract is the rapid heating and humidification of inhaled air as it transits through the upper airways (Ferron 1977). Aerosols that are sensitive to hygroscopic size changes can see considerable growth via condensation in such conditions (Javaheri and Finlay 2013; Golshahi, Tian, et al. 2013), typically leading to greater respiratory tract deposition than would be assumed if the aerosol were treated as stable or constant in size. Early exploratory work described by Martonen (1990) included *in vitro* surrogate airways designed to heat and humidity inhaled air in a manner similar to what occurs *in vivo*. Temperature and humidity gradients inside "growth chambers" representing generations of the tracheobronchial airways were controlled via heat and vapour transit from water circulating in concentric annular jackets. While this work did not extend much beyond the prototyping stage, *in vitro* measurements

accounting for both hygroscopic effects and deposition in realistic airway geometries would be of great utility in better characterizing aerosol behaviour during inhalation. More recent work has seen the development of an *in vitro* setup designed to heat and humidify air during its transit through a simple induction-port-type geometry and into an Anderson Cascade Impactor (Majoral et al. 2020), but it is not clear how well such a setup can simulate the heat and mass transfer from airway walls that occurs *in vivo*, and the simple geometry of the induction port is a poor facsimile of the extrathoracic region. At present, hygroscopic behavior in the respiratory tract is perhaps best accounted for by numerical modeling using well-characterized *in vitro* data as input (Finlay 2019).

2.2.4 Real-world Use

Environmental conditions, including temperature, humidity, and pressure, can influence the generation, transport, and evolution of inhaled pharmaceutical aerosols from the device to the site of deposition. Laboratory testing is often performed under controlled environmental conditions (relative humidity of ~50% at room temperature ~20 °C) and at altitudes near sea level (ambient air pressure of ~101.3 kPa), but these conditions can span a wide range of values in real-world use. With predictive *in vitro* testing, some focus may be placed on simulating the conditions under which an inhaler—particularly pMDIs and DPIs that are commonly carried with patients during day-to-day activities—will be used outside of a controlled clinical setting.

2.2.4.1 pMDIs

PMDI performance is sensitive to extreme variations in temperature. Morin et al. (2014) found that relative to controls at 21°C the *in vitro* lung dose from four pMDIs measured downstream of an Alberta Idealized Throat decreased by an average of 70% at -12°C and increased by an average of 25% at 42°C when the inhaler and ambient environment were in thermal equilibrium. When pMDIs were instead maintained at a constant temperature of 21°C, the effects of ambient temperature decreased considerably. Shemirani et al. (2013) observed similarly increased lung dose fractions downstream of an Alberta Idealized Throat for two beclomethasone dipropionate formulations (a solution and a suspension) when pMDIs were operated at 40°C in thermal equilibrium relative to 20°C. These temperature effects on pMDI performance can be explained by two mechanisms (Shemirani et al. 2013; Morin et al. 2014): (i) altered propellant vapor pressures and subsequent effects on the atomization of a metered dose (Ivey et al. 2014) and (ii) altered evaporative rates leading to variations in droplet/particle sizes. The first mechanism can be

mitigated by keeping the pMDI at or near room temperature (e.g., stored within an inner coat pocket).

In vitro experiments also suggest that ambient humidity can influence the total lung dose achieved with some pMDIs (Shemirani et al. 2013; Ruzycki, Martin, and Finlay 2019; Ruzycki et al. 2014). Shemirani et al. (2013) found that increasing relative humidity reduced the *in vitro* total lung dose obtained with pMDIs, with the effect being greater for suspension formulations than solution formulations. A possible explanation for the difference was the much greater number of residual drug particles generated by the solution formulation, which lent a larger total surface area for hygroscopic effects to occur over in the post-actuation stage. Ruzycki, Martin and Finlay (2019) confirmed the influence of relative humidity on suspension formulations, noting considerable reductions in *in vitro* lung doses at high relative humidity for two common suspensions (Ventolin™ Evohaler™ and Flixotide® HFA).

With respect to ambient pressure, Titosky et al. (2014) found that the *in vitro* lung dose downstream of an Alberta Idealized Throat was not affected by altitudes up to 4300 m in five commercially available pMDIs, suggesting that pMDI performance is resistant to changes in altitude. This finding is well-explained by the fact that flow across a pMDI nozzle is choked, so altitude-dependent differences in the absolute pressure downstream of the pMDI nozzle have no effect on the initial atomization process.

2.2.4.2 DPIs

DPI performance can be negatively influenced by temperature and humidity during storage (Vehring 2008). Micro-particles formed by spray drying, for example, often have an energetically unfavorable state owing to their large surface areas, leaving them susceptible to conversion to more favorable states via crystallization, polymorph transition, crystal growth, or fusion of particles. Effects of temperature and humidity on device performance have been studied extensively (Young et al. 2007; Kwok and Chan 2008; Janson et al. 2016; Yu et al. 2017), with results showing that extended storage at atypical conditions leads to altered device performance. A variety of strategies have been employed to mitigate these effects during real-world use, for example, designing the glass transition temperature of an amorphous particle to be ~50°C greater than storage temperature, and using desiccants (Vehring 2008).

Effects of temperature or humidity on a freshly primed dose from a multi-dose reservoir DPI are thought to be negligible in most scenarios given the less hygroscopic nature of inhaled powders than of liquid droplets produced by nebulizers and pMDIs, and the short timescales (seconds) between priming and delivery. Limited *in vitro* data from Ruzycki et al (2014) supports this hypothesis for one commercially available DPI, the Pulmicort® Turbuhaler®.

Ambient pressure may influence DPI performance through reductions in aerodynamic forces that occur due to decreased air density at increasing altitudes. Such effects have been examined in a number of *in vitro* studies on inhaler performance at varying altitudes (Titosky et al. 2014; Buttini et al. 2016; Ruzycki et al. 2018). Ruzycki et al (2018) demonstrated that while some DPIs are somewhat sensitive to altitude, effects are device-dependent and relatively minor, particularly at flowrates representative of patients capable of generating sufficient inspiratory efforts.

2.2.4.3   Inhaler Orientation and Other Aspects of Patient Technique

Routine *in vitro* testing can be broadly described as the ideal use of inhalers in pharmacopeial experiments with well-defined and limited parameter spaces that focus on reductions in variability, providing a strong basis for quality control. More exploratory *in vitro* testing has begun to examine the effects of parameters that have typically gone unconsidered, like the effect of insertion angle of inhaler mouthpieces on extrathoracic deposition (Delvadia et al. 2013; Ruzycki, Martin, and Finlay 2019). Insertion angle can significantly influence extrathoracic deposition and the *in vitro* lung dose for DPIs with high mouthpiece exit velocities and large particles, as well as for pMDIs with high momentum spray plumes (Ruzycki, Martin, and Finlay 2019; see Chapter 3). Together with earlier *in vitro* observations of decreased extrathoracic deposition for pMDIs with lower momentum sprays (Cheng et al. 2001), these results suggest that refinement of devices and formulations may provide avenues for reducing variability in real-world use.

Aspects of real-world use related to improper operation or priming of inhalers are generally not explored experimentally, the expectation being that patients will use devices as intended by the manufacturers. As noted in the introduction, however, many patients demonstrate improper technique when using inhalers (Fink and Rubin 2005), and this issue does not appear to have improved over time (Sanchis, Gich, and Pedersen 2016). There remains room for improvement both in patient/clinician education and in device design to address improper real-world use and associated reduction in treatment efficacy.

2.3 Deposition Models

Numerical models of deposition in the respiratory tract have numerous applications beyond inhalation drug delivery, including assessments of workplace and environmental exposure and characterization of disease transmission via airborne pathogens. The past few decades have seen extensive developments in numerical deposition models thanks to improvements in medical imaging, computational fluid dynamics simulations, and *in vitro* methods used to develop empirical correlations. These are summarized in a number of recent reviews (Martin, Moore, and Finlay 2018; Hofmann 2020; Nordlund and Kuczaj 2015).

For inhaled therapies targeting the lungs, aerosol must first be generated by a device before being inhaled. The physical processes governing aerosol generation are so complex that quantitative modeling from first principles is not feasible. In practice, this necessitates the use of *in vitro* methods to provide the initial conditions for numerical models of respiratory tract deposition, but regardless of this limitation such models can provide a wealth of information for guiding the development of inhalation therapies. Inhaled pharmaceutical aerosols targeting the lungs must first transit the extrathoracic region, which acts as an efficient filter for large particles, and after reaching the thoracic airways must then deposit on airway walls to deliver the drug to target tissues without their being exhaled in any significant quantity. Addressing the unique challenge of avoiding wasted deposition in the extrathoracic airways while maximizing thoracic deposition (and even preferentially targeting specific regions of the lungs) can be aided through algebraic correlations of extrathoracic deposition and well-established one-dimensional lung deposition models, characteristics of which are discussed below.

2.3.1 Extrathoracic Deposition

The nose, mouth, and throat present a major obstacle for delivering inhaled therapeutics to the lungs without unwanted deposition in these extrathoracic airways. The high degree of inter-subject variability in lung deposition observed with some orally inhaled therapies is thought to be largely due to variation of mouth-throat deposition (Borgström, Olsson, and Thorsson 2006), making this an extremely important parameter to characterize accurately when designing new devices and formulations. Historically, the impaction parameter d^2Q provided a means of incorporating the well-known dependence of inhalation flowrate and particle size on deposition in early algebraic correlations (International Commission on Radiological Protection 1994; Cheng 2003), with scale

factors and parameters like tidal volume incorporated to capture some elements of variability in deposition with age or sex.

In recent years, the understanding of how various factors influence extrathoracic deposition has grown considerably thanks largely to thorough *in vitro* characterizations of deposition in physical airway replicas. A number of reviews summarize many of the relevant studies (Carrigy, Martin, and Finlay 2015; Carrigy et al. 2014; Martin, Moore, and Finlay 2018). Nondimensionalization of the equations governing fluid and particle behavior resulted in the identification of the Stokes and Reynolds numbers as important parameters for characterizing the deposition of many pharmaceutical aerosols of interest (Finlay 2019), leading to their inclusion in modern extrathoracic deposition correlations. The Stokes number and Reynolds numbers, which characterize particle inertia and the relative importance of inertial and viscous effects on fluid behavior, respectively, are calculated as

$$\text{Stk} = \frac{\rho_{\text{particle}} d^2 C_c U}{18 \mu D} \tag{2-2}$$

$$\text{Re} = \frac{\rho_{\text{fluid}} U D}{\mu} \tag{2-3}$$

where ρ_{particle} is the particle density, d is the particle diameter, C_c is the Cunningham correction factor, U, ρ_{fluid} and μ are the velocity, density, and dynamic viscosity of the gas phase, respectively, and D is some characteristic dimension of the geometry (note that the Stokes number is frequently written in terms of the aerodynamic diameter, with the reference density of 1000 kg/m^3 used in place of ρ_{particle}). Most correlations for extrathoracic deposition efficiency, η, are of the form

$$\eta = 1 - \frac{1}{1 + a \text{Re}^b \text{Stk}^c}. \tag{2-4}$$

The constants a, b, and c are typically determined by fitting equation (2-4) to experimental data of deposition in realistic airway replicas corresponding to a particular age range (adults, children, infants, neonates), inhalation route (nasal, oral), and inhalation profile (constant flow rate or tidal); algebraic deposition correlations are thus empirical models. Various characteristic dimensions have been proposed for extrathoracic geometries spanning different age groups and routes of

inhalation, such as the square root of the average cross sectional area of the oropharyngeal region (Golshahi, Noga, et al. 2013) or the equivalent diameter obtained by dividing the mouth-throat volume by the centerline length (Grgic et al. 2004). In practice, these characteristic dimensions and the constants a, b, and c are chosen to collapse the scatter of *in vitro* data contained in (2-4). Depending on the physics of the problem, (2-4) can be further modified to include additional parameters (Carrigy, Martin, and Finlay 2015; Martin, Moore, and Finlay 2018).

One of the major goals of the above work is the development of accurate *in vitro − in vivo* correlations. Yang et al. (2017) recently demonstrated good agreement between *in vivo* scintigraphic measurements of extrathoracic deposition of tidally-inhaled nebulized aerosols in healthy adults and predicted extrathoracic deposition using the empirical correlation of Golshahi, Noga, et al. (2013): average *in vivo* deposition of nebulized radiolabeled isotonic saline (0.193 ± 0.103, average ± standard deviation) agreed well with the average of predictions using a corrected version of the Golshahi, Noga et al. (2013) correlation (0.182 ± 0.082), particularly when compared to correlations based on the impaction parameter. However, Yang et al. (2017) also observed large errors in subject-specific predictions, with (at best) only weak correlations obtained between predictions and *in vivo* measurements of deposition in individual subjects for the five extrathoracic deposition models they used. This discrepancy was attributed to the breakdown of the assumption of geometric similarity that occurs with the transition from a limited number of well-characterized *in vitro* extrathoracic geometries used in the development of empirical correlations to the more complicated and variable situation *in vivo*.

The results of Yang et al. (2017) indicate that a single characteristic-length scale will struggle to capture the full geometrical variation of the extrathoracic airways both within and between different subjects, with the consequence that *subject-specific* predictions of extrathoracic deposition using simple algebraic correlations of the type described in equation (2-4) may be inherently limited in accuracy. However, *population-level* predictions of extrathoracic deposition, including inter-subject variability, may be achieved using algebraic correlations following the method proposed by Ruzycki et al. (2017). In this method, inter-subject variability is presumed to arise from three factors:

1. Variations between subjects in the inhalation flowrate

2. Variations between subjects in the size of the extrathoracic region (captured by the characteristic dimension D)

3. Variations between subjects in the shape of the extrathoracic region, denoted as variation resulting from geometric dissimilarity.

Ruzycki et al. (2017) describe how to obtain estimates of each source of variability based on the characteristics of the population under consideration (see also the subsequent pedagogical description by Finlay [2019]), with the overall standard deviation of deposition in the extrathoracic region, s_η, calculated as

$$s_\eta = \sqrt{s_Q^2 + s_D^2 + s_{gd}^2}. \tag{2-5}$$

Here, s_Q is the standard deviation in extrathoracic deposition due to variation in flowrate, s_D is the standard deviation due to variation in the characteristic dimension, and s_{gd} is the standard deviation arising from geometric dissimilarity. Variations in flowrate and characteristic dimensions can be measured or estimated for a given *in vivo* population, but determination of the variation due to geometric dissimilarity requires well-characterized *in vitro* data in realistic airway casts of varying shape (see Martin, Moore, and Finlay et al. [2018] for estimates of this factor for a number of deposition correlations). Note that if all geometries in a given population were simple isotropic scalings of a single mouth-throat shape, this factor would disappear, but the complexities and variation in airway shape observed between different subjects means this factor will always exist in real populations. As a case study, Ruzycki et al. (2017) applied this method to the data of Yang et al. (2017), finding excellent agreement between predicted extrathoracic deposition (0.172 ± 0.101) and that measured *in vivo* (0.193 ± 0.103) considering the first-order nature of this analysis. Each of the three sources of variability mentioned above were found to contribute significantly to inter-subject variability, with the implication that knowledge of the characteristic dimension and flowrate alone is likely insufficient to fully characterize deposition with algebraic correlations of the form of equation (2-5) that do not account for geometric dissimilarity. Figure 2-3 demonstrates how extrathoracic deposition correlations of the type described by equation (2-4) can be used to collapse scatter in deposition data about a predictive curve, particularly when compared to use of the impaction parameter alone. Figure 2-3 also demonstrates that even with

this approach, there remains some variation between predictions and measured values *in vitro*, the magnitude of which can be estimated via the method described initially by Ruzycki et al. (2017) and in more pedagogical detail by Finlay (2019).
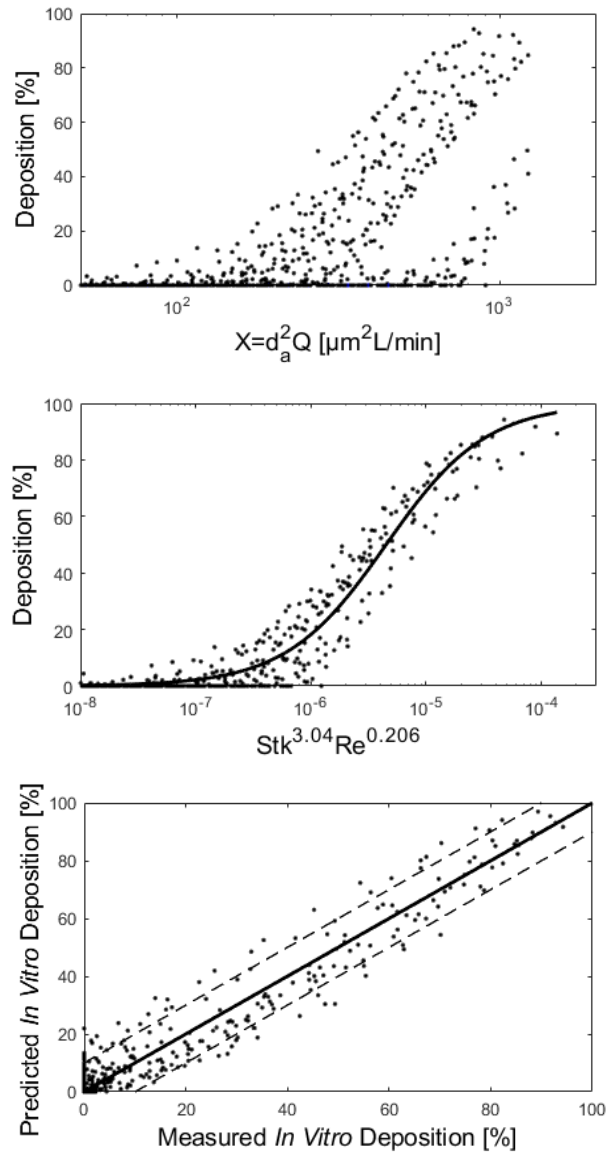
Figure 2-3: Deposition of micrometer sized particles obtained in realistic adult extrathoracic airway casts using tidal inhalations, cast in terms of (top) the impaction parameter and (middle) the Stokes and Reynolds numbers as per equation (2-4) via (Yang et al. 2017), with (bottom) the method proposed by Ruzycki et al. (2017) to quantify uncertainty due to geometric dissimilarity per equation (2-5). Data from Golshahi, Noga, et al. (2013) and Ruzycki et al. (2017).

Empirical correlations presented in the literature are generally developed using well-characterized stable particles, and most use large-diameter inlets into extrathoracic geometries that do not replicate the complicated jet effects from small mouthpiece diameter DPIs or spray plume effects from pMDIs. Numerous studies demonstrate the complications that arise when dealing with DPIs and pMDIs. As examples, DeHaan and Finlay (2004) demonstrated substantially greater deposition of particles *in vitro* when delivered through small-mouthpiece-diameter DPIs than through large-diameter straight tubes, while Ruzycki, Martin, and Finlay (2019) showed that insertion angle and ambient humidity can lead to large differences in *in vitro* deposition from pMDIs emitting high-momentum spray plumes. As a result, the extension of an algebraic correlation to a physical situation where parameters extend beyond the range used in its development can lead to erroneous or misleading predictions of device/formulation performance. Because of the complexity of modelling jet effects from small-mouthpiece-diameter DPIs and spray plume effects and subsequent hygroscopic behavior from pMDIs, current practice is to evaluate extrathoracic deposition from these devices *in vitro* using the mouth-throat geometries described in the previous section.

2.3.2 Thoracic Deposition

After a proper accounting of extrathoracic deposition comes the modeling of deposition within the lungs themselves. The thoracic airways can be broadly described as a fractal-branching structure consisting of some two dozen generations starting from the trachea and ending at the individual alveoli. Various deposition models have been proposed (see reviews by Hofmann 2020 and Martin, Moore, and Finlay 2018), but the basic properties of the one-dimensional deposition models considered here are similar. The commonly used model described by the International Commission on Radiological Protection (1994) separates the thoracic airways into distinct bronchial, bronchiolar, and alveolar regions, and treats each as a "filter" whose efficiency in removing particles from inhaled air is predicted using empirical formulae developed from analysis of *in vivo* deposition data and clearance rates.

Modern lung deposition models consider the influence on deposition in individual airways of such mechanisms as inertial impaction, gravitational sedimentation, and Brownian diffusion as air encounters an increasing number of smaller and smaller airways during inhalation. Analytical considerations of airflow properties and fluid dynamics in different regions of the lungs can direct

the selection of appropriate expressions for different deposition mechanisms (Finlay 2019). These can be mechanistic or empirical in nature. For example, Javaheri et al. (2013) use the empirical correlation of Chan and Lippmann (1980) for inertial impaction, the analytical correlations of Heyder (1975) and Heyder and Gebhart (1977) for sedimentation, and the empirical correlations of Ingham (1975) for diffusion. One-dimensional models can be further modified to account for dynamic processes like hygroscopic growth and evaporation (Ferron, Kreyling, and Haider 1988; Finlay and Stapleton 1995; Javaheri and Finlay 2013), allowing for investigations of such processes that would be extremely difficult to study in a mechanistic fashion *in situ*.

Airflow in the more analytical one-dimensional models is often considered as well-mixed turbulent flow in the larger conducting airways, classical laminar Poiseuille flow in the smaller conducting airways, and laminar plug flow in the peripheral lung. The real nature of flow in the airways will vary somewhat from the ideal behavior assumed in one-dimensional models: transitions between turbulent, laminar, and plug flow must occur. Despite such variance, the favorable comparisons of predicted regional deposition in one-dimensional lung deposition models with available experimental data suggest that these models successfully capture the major factors influencing deposition in the lungs (Hofmann 2020). A more thorough validation of deposition at the level of individual airway generations, i.e., beyond the first few conducting airways, will require advances in medical imaging to address resolution and registration issues observed with modern technologies (Darquenne et al. 2016).

One-dimensional lung deposition models can provide estimates of the mass of drug expected to deposit in various generations of the respiratory tract, but not information on localized deposition "hotspots" that can occur on, e.g., airway bifurcations—elucidation here requires computational fluid and particle dynamics simulations. Bearing this in mind, a natural progression beyond one-dimensional deposition modeling is the incorporation of models of the airway surface liquid and mucociliary clearance in the tracheobronchial airways (Finlay, Lange, King, et al. 2000; Lange et al. 2001), as the concentration of drug in the airway surface liquid is of more relevance for local drug action than the deposited mass alone. For example, Martin and Finlay (2018) recently coupled a generational lung deposition model with an airway surface liquid and mucociliary clearance model to estimate whether (and for how long) the concentration of an inhaled antibiotic exceeded the minimum inhibitory concentration required for efficacious treatment of *Pseudomonas*

aeruginosa infection in the airways. Such methods, particularly when coupled with pharmacokinetic models as discussed in the following section, may prove useful in predicting the performance of new formulations, as local effects in lung tissues will depend more on the concentration of free drug available than on the deposited mass alone (Himstedt et al. 2020).

As a final note, for devices like DPIs and pMDIs where extrathoracic deposition is difficult to predict *a priori*, an emerging trend is to use one-dimensional lung deposition models "downstream" of *in vitro* extrathoracic deposition tests. In this approach, well-characterized experimental data provide the initial conditions for modeling what occurs after aerosol transits the extrathoracic region and enters the lungs themselves (Bhagwat et al. 2017; Ruzycki et al. 2018; 2020; Tavernini et al. 2021).

2.4 Pharmacokinetic Models

Regional deposition models predict the initial distribution of drug throughout the respiratory tract. Thereafter, competing processes combine to determine the fate of deposited drug particles over time. The processes of drug dissolution or release, clearance, metabolism, and absorption from the lungs collectively influence both local and systemic exposure to inhaled drugs, with extensive reviews on these processes presented in the literature (Hastedt et al. 2016; Olsson et al. 2011; Sakagami 2006; Hickey 2014; Selo et al. 2021). Models linking broad estimates of regional deposition to these pharmacokinetic (PK) processes date to the foundational work of Byron (1986) and Gonda (1988). In recent years, models of regional or generational deposition have been combined with PK models to predict regional lung exposure and/or systemic exposure to inhaled drugs over time in a more detailed manner (Weber and Hochhaus 2013; Bhagwat et al. 2017; Bäckman, Tehler, and Olsson 2017; Bäckman et al. 2018; Martin and Finlay 2018; Boger and Fridén 2019; Ruzycki et al. 2020). Such models have been described as physiologically based pharmacokinetic (PBPK) models, wherein mechanistic descriptions of deposition and disposition in the respiratory tract are integrated with systemic PK modeling (Bäckman et al. 2018; Martin, Moore, and Finlay 2018). In this manner, the influence of regional deposition pattern on clinically relevant parameters, such as local and systemic drug concentrations, can be predicted for a given drug product.

A number of recent studies have used PK modeling to extend and interpret predictions of regional deposition models. For example, Bäckman, Tehler, and Olsson (2017) used the commercially-available Gastroplus™ model (SimulationsPlus Inc., Rochester, USA) to estimate systemic exposure to nebulizer and DPI formulations of a selective glucocorticoid receptor modulator. Regional deposition in the tracheobronchial airways, the smaller bronchiolar airways, and the alveolar spaces was predicted using a one-dimensional deposition model based on those described by the International Commission on Radiological Protection (1994) and the National Council on Radiation Protection and Measurements (1997). Additional model calculations were included to predict particle dissolution in the ASL, as well as the competing processes of mucociliary clearance and absorption. (Use of a mechanistic dissolution model incorporating solubility-limited kinetics is critical when describing the dissolution of poorly soluble drugs in the ASL). The model of Bäckman, Tehler, and Olsson (2017) was shown to accurately predict systemic exposure measured *in vivo* in healthy volunteers. Notably, predicted local exposure in the modeled lung regions was not well correlated with systemic exposure, suggesting that systemic PK data alone could not be used to infer local exposure for the poorly soluble drug that was studied.

Boger and Friden (2019) have described a coupled deposition and PK model in which the lung was further divided into 24 airway generations, as described in the Weibel A lung model (Weibel 1963). Individual lung generations were subdivided into three compartments, representing the ASL, the epithelium, and the sub-epithelium. Concentrations of inhaled salbutamol were compared in the sub-epithelium and the plasma, with higher free dru g concentrations predicted in the lung tissue than in the plasma. Lung tissue concentration was also predicted to vary over lung generations, with the sub-epithelial concentration in the 6th generation (selected by the authors as a representative target generation based on its contribution to total airway resistance) found to correlate with pharmacodynamic response.

Martin and Finlay (2018) described a three-part model in which previously developed regional deposition (Finlay et al. 1996; Finlay and Wong 1998; Javaheri et al. 2013) and ASL (Finlay, Lange, King, et al. 2000; Hoe et al. 2014; Lange et al. 2001) models provided input to a PK model incorporating drug dissolution/release, mucociliary clearance, and absorption from the lungs with traditional factors like oral absorption from the gastrointestinal tract and distribution within (and elimination from) the body. The combined model was used to compare the time course of local

(ASL) and systemic (plasma) concentrations of the inhaled antibiotic ciprofloxacin following inhalation of nebulized liposomal formulations and a DPI formulation (Martin and Finlay 2018). More recently, this model has been used to estimate local and systemic exposures to inhaled treprostinil and a prodrug form, treprostinil palmitil, through inclusion of the rate of conversion of prodrug to active drug within the lung (Martin et al. 2021).

Ruzycki et al. (2020) have recently presented a combined *in vitro-in silico* model used to predict both regional deposition and PK for budesonide DPIs–see Chapter 4 for a full description of this study. In this approach, *in vitro* experiments were conducted with the Alberta Idealized Throat and realistic inhalation maneuvers to measure the drug mass and aerodynamic particle size distribution of aerosol penetrating the throat, the latter being deemed the intrathoracic particle size distribution. Results of *in vitro* experiments were used in conjunction with regional deposition and mechanistic PK modeling to predict systemic drug concentrations for three distinct budesonide DPIs. Notably, Ruzycki et al. (2020) observed that significant differences between DPIs measured *in vitro* resulted in large differences in predicted drug masses depositing in the large (bronchial) airways and in the alveolar lung region. Conversely, less variation between DPIs was predicted in the drug mass depositing in the small (bronchiolar) airways. Furthermore, predicted PK parameters were influenced primarily by the alveolar dose or total lung dose but were poorly correlated with deposition in the large and small airways. These results suggest that PK data alone may fail to provide useful information describing drug delivery to the conducting airways, where inhaled corticosteroids such as budesonide are expected to have therapeutic effect (Barnes 2010). These results also reinforce the findings of Bäckman, Tehler, and Olsson (2017) regarding local exposure as described above. A strength of the methodology proposed by Ruzycki et al. (2020) is its ability to explore linkage between *in vitro* measured parameters, regional lung deposition, and PK parameters commonly evaluated in early-stage clinical studies. Such an approach may address limitations in similar studies that rely on traditional *in vitro* measures (e.g. stage groupings of NGI data) to estimate regional deposition without mechanistic modeling (Hochhaus et al. 2021).

2.4.1   *Characterizing Disposition*

Accurate modeling of drug behaviour after deposition in the lungs is a challenging topic owing to the various nuances that differentiate disposition in the respiratory tract and disposition in the more classical context of oral drug delivery via the gastrointestinal (GI) tract. Relative to delivery via

the GI tract, drug delivery via the respiratory tract is typically associated with a given drug mass having a much larger specific surface area, the presence of smaller liquid volumes for dissolution, more moderate pH and milder hydrodynamic considerations, and additional interactions unique to the lung environment, e.g., macrophage uptake (Hastedt et al. 2016). If an inhaled pharmaceutical aerosol is delivered in solid form (in powder form via a DPI or suspended particles in pMDIs), dissolution becomes a prerequisite for absorption and therapeutic effect, and the conditions to which a deposited particle are exposed depend on the location of deposition within the respiratory tract itself. Here, basic aspects of dissolution modeling are considered to identify important factors relevant for drug delivery via the respiratory tract.

2.4.1.1 Modeling Dissolution

A proper accounting of dissolution in the ASL is important when considering the disposition of moderately or poorly soluble compounds after their deposition in the lungs (Hastedt et al. 2016). While the current state of the art in dissolution testing *in vitro* is well summarized in recent reviews (Radivojev et al. 2019; Selo et al. 2021), it is instructive to consider how current PK models consider dissolution in the respiratory tract, whether through mechanistic or empirical means.

A classic mechanistic model of dissolution is the Nernst-Brunner type process (Dokoumetzidis and Macheras 2006). This model assumes that the dissolution process is governed primarily by the diffusion of molecules across a stagnant film of liquid (called a diffusion layer) that surrounds submerged solid particles. The general equation defining Nernst-Brunner dissolution in ASL allows for the quantification of the change of mass, m, of a submerged particle with respect to time t (see equation (4-3) in Chapter 4 and related discussion for full details). An important characteristic of this model is the relation between the thickness of the diffusion layer and the size of the particle. For particles smaller than 60 µm in diameter, the thickness of the diffusion layer is thought to be well-approximated as the particle radius (May et al. 2014; Hintz and Johnson 1989). Therefore, for most inhaled pharmaceutical aerosols, where the pulmonary dose consists of particles roughly 1 to 5 micrometers in diameter, a diffusion layer thickness equal to the particle radius is likely a reasonable model. In the tracheobronchial airways, where the ASL has a depth on the order of 10 µm (Hastedt et al. 2016), it is likewise reasonable to assume full immersion of particles in the ASL, especially given the observed tendency of particles to be displaced into the liquid phase due to the low surface tension of surfactant atop the mucus layer (Schürch et al. 1990).

At the level of individual alveoli, however, the surface liquid layer is much thinner (~0.1 μm), meaning a critical assumption used in the derivation of the Nernst-Brunner model—the existence of a diffusion layer separating the particle from the bulk liquid—is not appropriate. Strictly speaking, dissolution kinetics in the periphery of the lung are likely not well described by as a classic Nernst-Brunner process because the alveolar lining fluid is too thin to accommodate the assumed thickness of the diffusion layer. Various modifications have recently been proposed to account for differences (Bäckman and Olsson 2020; Eriksson et al. 2019), but, in the absence of an analytical model describing the dissolution of particles deposited in the very thin alveolar fluid, most PK models approximate particle dissolution and absorption in the alveolar region by a simple first order process, with a rate constant chosen to match available *in vivo* data (see e.g. Weber and Hochhaus [2013]).

2.4.1.2 Solubility and Permeability

The Nernst-Brunner model highlights the importance of drug solubility in the dissolution process. Drugs that are poorly soluble in airway surface liquid may easily saturate surrounding fluid after deposition, thereafter reducing the rate of dissolution and effectively limiting the maximum rate at which drug is made available for subsequent absorption. Competing mechanisms such as mucociliary clearance in the conducting airways can then remove deposited particles before they completely dissolve, potentially reducing the bioavailability of such therapies.

In describing solubility and dissolution it can be useful to consider the dose number, Do, the dissolution number, Dn, and the absorption number, An, proposed by Amidon et al. (1995) for use in biopharmaceutical classifications of dissolution. The dose number is calculated as

$$\text{Do} = \frac{M_0/V_0}{c_\text{S}} \tag{2-6}$$

where M_0 is the dose (mass of drug), V_0 is the volume of dissolution fluid, and c_S is the solubility. Given the dependence of Do on the volume of dissolution fluid, it's value is site-specific and will vary depending on the region of the respiratory tract where deposition occurs (Velaga et al. 2018). When Do ≪ 1, the drug has sufficient solubility to be dissolved, and subsequent disposition depends primarily on permeability and absorption rates in relevant tissues. When Do ≫ 1, the drug is considered to be dissolution-limited, and the more complicated interplay that occurs between dissolution, lung clearance mechanisms, and absorption determines local tissue concentrations and

uptake into systemic circulation. In the conducting airways, V_0 is on the order of 10 to 30 mL, allowing for the definition of a band separating fully-soluble and dissolution-limited drugs based on the dose delivered to the conducting airways and the solubility in airway surface liquid (Hastedt et al. 2016). Hastedt et al. (2016) note that while many drugs are not dissolution limited (including short-acting and long-acting bronchodilators), there are two classes of drugs that are: inhaled corticosteroids with a solubility less than 1 µg/mL (e.g., fluticasone propionate, beclomethasone dipropionate) and high dose anti-infectives with a nominal dose greater than 1 mg and a solubility less than 100 µg/mL (e.g., amphotericin B). In such cases, the accurate modeling of disposition requires the consideration of dissolution in the airway surface liquid.

The dissolution number is calculated as

$$\text{Dn} = \frac{3t_{\text{res}}D_{\text{d}}c_{\text{s}}}{\rho_{\text{particle}}r_0^2} \tag{2-7}$$

where t_{res} is the mean residence time (in the lung) and r_0 is the particle diameter. The dissolution number informs what parameters can be varied to either increase or decrease dissolution rates. For example, halving the particle size increases the dissolution rate by a factor of four (though generally speaking such large differences in particle size will be associated with large differences in regional deposition that must be borne in mind). Alterations to e.g., particle density, morphology, and crystallinity (i.e., amorphous content) that can be achieved through particle engineering processes (Vehring 2008) may also provide some degree of control over dissolution *in vivo*.

Finally, the absorption number is calculated as

$$\text{An} = t_{\text{res}}k_{\text{a}} \tag{2-8}$$

where k_{a} is an absorption rate constant that is directly proportional to permeability and absorption surface area, but whose value is difficult to quantify *a priori* and can vary with time (Hastedt et al. 2016; Velaga et al. 2018). In practice, the difficulties in establishing k_{a} in the context of inhaled therapeutics (and effects of additional active-transport phenomena besides diffusion-based permeation) prevent much use of the absorption number, but the underlying relation between absorption and permeability remains useful to consider. Optimal permeability depends on the nature of the therapy. For locally acting medications in the respiratory tract, low permeability may

aid in minimizing systemic exposure, particularly if coupled with low oral bioavailability. For systemic delivery, high permeability facilitates more rapid uptake. Dissolved low molecular weight drugs generally undergo fast absorption in the lungs (half-lives < 1 hr), with extremely fast absorption kinetics observed for lipophilic molecules (half-lives on the order of minutes or less) (Patton and Byron 2007; Patton, Fishburn, and Weers 2004). Exceptions to this behaviour can occur due to e.g., sustained binding and intracellular trapping (Hastedt et al. 2016). Lipophilic drugs (with octanol-water partition coefficients, log P, being greater than 0) are absorbed primarily through the transcellular route, while hydrophilic drugs (log P < 0) are absorbed via the paracellular route. For larger macromolecules like peptides and proteins, the rates of absorption (generally on the order of hours) are tied primarily to size, with larger molecules undergoing slower absorption through various mechanisms including receptor-mediated transcytosis, paracellular diffusion, or non-specific pinocytosis (Loira-Pastoriza, Todoroff, and Vanbever 2014).

2.4.1.3 Lung-Relevant Dissolution Testing

At present, no standardized method exists for *in vitro* dissolution testing of inhaled medications, be it for quality control, biorelevance, or clinical relevance (Radivojev et al. 2019). As such, various approaches are proposed in the literature (Floroiu et al. 2018), with some aiming to evaluate dissolution under essentially infinite sink conditions (Rohrschneider et al. 2015; May et al. 2014; Price et al. 2020) and others utilizing smaller volumes of dissolution media that may be more representative of physiological conditions in airway surface liquid (Arora et al. 2010; Tay, Liew, and Heng 2018; Gerde, Malmlöf, and Selg 2021). Even the most sophisticated *in vitro* apparatuses that aim to replicate air/blood barriers are typically of a much greater thickness than is representative of alveolar region (Gerde, Malmlöf, and Selg 2021), and it is unclear how the balance between dissolution and absorption is best considered as one transitions from the very permeable alveolar region to the less permeable conductive airways (Hastedt et al. 2016). As such, lung-relevant dissolution testing is an active area of research, and the interested reader is directed to a number of recent reviews on the topic (Selo et al. 2021; Radivojev et al. 2019; Velaga et al. 2018).

2.4.2   Considering Health or Disease

As with similar models, those proposed by Martin and Finlay (2018) and Ruzycki et al. (2020) predict regional deposition in lung geometries representative of healthy adults. These models are thus well suited for comparison with Phase 1 PK studies done in healthy subjects, and plasma drug concentration profiles predicted using these models have indeed been shown to agree well with data from Phase 1 trials (Martin and Finlay 2018; Ruzycki et al. 2020; Martin et al. 2021).

It is also of interest to develop models that can explore the influence of disease state on drug uptake due to, for example, heightened mucous production or reduced mucociliary clearance rates. The inclusion of a mechanistic ASL model for which daily mucous production rate and tracheal clearance velocity are input parameters allows the sensitivity of local and systemic drug concentrations to these parameters to be explored. For inhaled antibiotics such as ciprofloxacin, predicted drug concentrations in the ASL may be compared with minimum inhibitory concentrations against bacteria colonizing in the ASL, providing a means of estimating whether effective local drug concentrations are achieved. Figure 2-4 provides an example of such an analysis, where ASL concentrations of ciprofloxacin following inhalation of two different nominal doses delivered in a DPI formulation are modeled for three combinations of mucous production rate and tracheal clearance velocity (Martin and Finlay 2018).
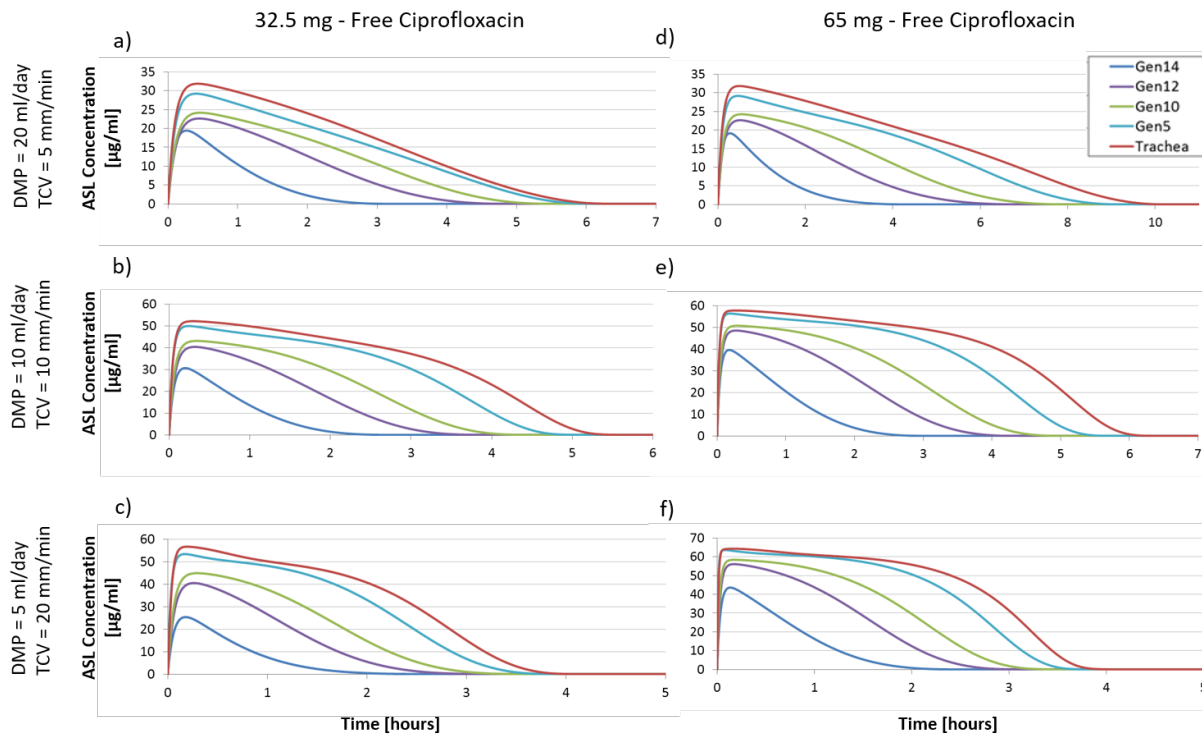
Figure 2-4: Predicted airway surface liquid (ASL) concentrations of free ciprofloxacin in the conducting airways of healthy adult subjects following inhalation of nominal dry powder doses of 32.5 mg (a-c) and 65 mg (d-f) ciprofloxacin. Results are shown for three combinations of daily mucous production (DMP) and tracheal clearance velocity (TCV). Gen *i* indicates tracheobronchial airway generation number *i*. Reprinted from Martin, Moore, and Finlay (2018) with permission from Taylor & Francis (www.tandfonline.com), *Expert Opinion on Drug Delivery*.

As seen in Figure 2-4, the longest residence times of drug in the airways are predicted for the combination of high mucous production and low clearance velocity, suggesting treatment efficacy for this class of drug may depend not only on formulation but also on physiological effects of disease. As impaired mucociliary clearance is observed in many respiratory diseases, poorly soluble drugs may be expected to persist longer in diseased lungs than in healthy lungs. Shapiro et al. (2018) adapted the model presented by Martin and Finlay (2018) to capture mucociliary clearance and ASL absorption dynamics in cystic fibrosis patients, including slow mucociliary clearance dynamics in small airways that had not been included in previous models. Such improvements may provide a method for examining the influence of cystic fibrosis treatments on mucous buildup and blockages, and on drug concentrations in ASL more generally.

2.5 Moving Towards Clinical Relevance

Of ongoing interest is the development of accurate *in vitro – in vivo* correlations for inhaled pharmaceutical aerosols. Recent research has moved towards treating *in vitro* data as the input or initial conditions for *in silico* models that can predict, through a mixture of mechanistic and empirical approaches, deposition and disposition in the lungs. This chapter has identified some of the steps involved in such approaches, including the development of *in vitro* tests that provide a more realistic measure of device performance than compendial methods, deposition models for extrathoracic and thoracic deposition, and disposition models that consider the fate of drug after deposition and under competing mechanisms of liberation, absorption, distribution, metabolism, and excretion. The research reviewed here shows great potential for extending *in vitro* measurements beyond traditional compendial methods for quality control and into prediction of clinically relevant parameters.

3   An Exploration of Factors Affecting In Vitro Deposition of Pharmaceutical Aerosols in the Alberta Idealized Throat

This chapter is published as Ruzycki, Conor A., Andrew R. Martin, and Warren H. Finlay. 2019. "An Exploration of Factors Affecting in Vitro Deposition of Pharmaceutical Aerosols in the Alberta Idealized Throat." Journal of Aerosol Medicine and Pulmonary Drug Delivery 32 (6): 405–17. Note that DPI mouthpiece velocities were calculated erroneously in the published version. Values are corrected in Table 3-2 and elsewhere. No conclusions are altered by this correction. Reproduced with permission from Mary Ann Liebert.

3.1   Abstract

Background

The development of accurate *in vitro – in vivo* correlations requires the consideration of a number of factors *in vitro*, including the emulation of upper airway geometry, inhalation maneuver, inhaler orientation, and environmental conditions. Here we examine the effects of inhaler insertion angle and humidity on deposition from a number of marketed inhalers.

Methods

Three dry powder inhalers (DPIs; Pulmicort Turbuhaler, Budelin Novolizer, and Easyhaler Budesonide) were examined at two insertion angles, one with the inhaler directed towards back of the oral cavity, the other with the inhaler directed towards the tongue. Three pressurized metered dose inhalers (pMDIs; QVAR, Ventolin Evohaler, and Flovent HFA) were examined considering the joint effects of insertion angle (as above) and relative humidity at low (15-25%) and high (> 95%) conditions. Deposited drug masses in an Alberta Idealized Throat and downstream filter were quantified via UV spectroscopy.

Results and Conclusions

Three of six inhalers showed sensitivity to insertion angle. When directed towards the tongue versus the back of the mouth, the filter dose decreased from 21.9% to 15.6% (percent delivered dose) for Easyhaler Budesonide ($P < 0.001$), from 46.5% to 26.0% for Ventolin Evohaler ($P < 0.001$), and from 56.7% to 35.7% for Flovent HFA ($P < 0.001$) for tests at ambient lab humidity. Sensitivity to insertion angle and increases in total lung dose variability may be reduced in future products using larger diameter mouthpieces and smaller particles for DPIs and lower-momentum sprays for pMDIs. Humidity influenced deposition from Ventolin Evohaler and Flovent HFA.

When oriented toward the back of the oral cavity, the filter dose decreased from 46.5% to 36.9% for Ventolin Evohaler ($P = 0.005$) and from 56.7% to 44.2% for Flovent HFA ($P < 0.001$) at high humidity relative to low. High humidity may cause a reduction in total *in vitro* lung doses for some pMDI aerosols.

3.2 Introduction

The use of the respiratory tract as a delivery route for inhaled pharmaceutical aerosols carries a number of unique challenges, one of which relates to aerosol deposition in the extrathoracic region. Extrathoracic deposition decreases the total dose of drug delivered to the lungs, reduces treatment efficacy, and contributes to the development of adverse side effects (Barnes and Pedersen 1993; Buhl 2006). Methods allowing for the accurate prediction of extrathoracic deposition are useful in developing improved inhalation therapies for the consistent and efficacious treatment of disease in clinical practice. *In vitro* methods, in particular, provide a high degree of control over experimental variables and facilitate in-depth examinations of the effects of various parameters on device and formulation performance.

Of particular interest is the development of accurate *in vitro – in vivo* correlations that allow for the prediction of *in vivo* extrathoracic and lung doses *a priori* (Byron et al. 2010). The interpretation of *in vitro* results with respect to *in vivo* performance depends on a number of factors relating to the design of the *in vitro* experiment itself. Broadly speaking, a well-designed *in vitro* test should consider modeling of (i) the upper airways, (ii) inhalation maneuver, (iii) inhaler orientation and positioning relative to the mouth, and (iv) anticipated environmental conditions including temperature, humidity, and ambient pressure.

Developments of improved upper airway models have been motivated by the tendency of the compendial United States Pharmacopeia Induction Port (USP-IP) to underestimate extrathoracic deposition in adults (Zhou, Sun, and Cheng 2011; Cheng et al. 2001). More accurate predictions of *in vivo* deposition can be obtained using extrathoracic airway models as a substitute for the USP-IP. Efforts to develop such models generally fall into one of two camps: realistic throat models aiming to replicate the fine anatomical structures in the extrathoracic region (Delvadia, Longest, and Byron 2012; Burnell et al. 2007), or idealized throat models containing mimics of important anatomical features (Stapleton et al. 2000). Wei et al. (Wei et al. 2018) demonstrated that both approaches can provide satisfactory estimates of *in vivo* deposition, as two sets of realistic

geometries (the Virginia Commonwealth University [Delvadia, Longest, and Byron 2012] and Oropharyngeal Consortium [Burnell et al. 2007] models) and the Alberta Idealized Throat (Stapleton et al. 2000) successfully replicated *in vivo* deposition of the Budelin Novolizer inhaler. An advantage of the Alberta Idealized Throat, used in the present work, stems from its manufacture to ISO 9001 standards out of metal material (Copley Scientific Limited, Nottingham, United Kingdom), the use of which avoids electrostatic surface charging effects and solvent contamination issues that can affect plastic geometries. The Alberta Idealized Throat has been shown to replicate average *in vivo* deposition for a number of pharmaceutical aerosols in adults (Zhang, Gilbertson, and Finlay 2007; Weers et al. 2015; Fink et al. 2017), making it an attractive platform for estimating extrathoracic deposition and the total dose delivered to the lungs (Finlay and Martin 2008).

Proper application of inhalation profiles depends on the device being tested. For pressurized metered dose inhalers (pMDIs), common practice is to examine deposition using a constant inhalation flowrate. Pauwels, Newman, and Borgström (1997) recommended that pMDIs be "used at a flow as low as possible," with Laube et al (2011) further specifying the ideal inhalation flowrate as 30 L/min, making this a natural choice for examining pMDI performance *in vitro*. Dry powder inhalers (DPIs) are more sensitive to the shape of inhalation profile given their passive nature, resulting in considerable flowrate-dependent performance (Weers and Clark 2017). Logically, the use of more realistic inhalation patterns with DPIs *in vitro* should better simulate typical *in vivo* performance. To this end, Delvadia et al (2016) described a procedure for defining inhaler-specific inhalation profiles for DPIs, based on device resistance, that reflect the natural tendency of patients to inhale at faster rates through device with lower resistances.

Inhaler orientation relative to the mouth is an additional parameter to consider. The effects of this parameter are understudied in the literature, with few authors explicitly examining the effect of orientation on deposition in the extrathoracic airways (Fadl et al. 2007; Delvadia et al. 2013). Fadl et al. (2007) found that aerosol penetration through a realistic *in vitro* airway cast from a metered dose inhaler suspension of 7 μm diameter particles increased considerably when the inhaler was operated at a +20° angle versus 0° (relative to horizontal), and concluded that an optimum angle exists at which aerosol penetration through the extrathoracic region is maximized. Delvadia et al (2013) extended the investigation of insertion angle on extrathoracic deposition to clinical

pharmaceutical aerosols in a series of *in vitro* experiments and computational simulations. Their results indicated that the importance of insertion angle depended on both the inhaler and formulation, with the general conclusion that aerosols with a greater momentum were more sensitive to changes in insertion angle.

Ambient environmental conditions including temperature, humidity, and pressure can influence extrathoracic deposition by affecting inhaler performance. For unstable aerosols, such conditions can also influence hygroscopic size changes. In a study on pMDI performance at extreme temperatures, Morin et al (2014) observed that the *in vitro* lung dose from four commercially available pMDIs measured downstream of an Alberta Idealized Throat decreased by an average of 70% at temperatures near -12°C relative to controls measured at 21°C when the inhaler and ambient environment were in thermal equilibrium prior to device actuation. When inhalers were instead kept at a constant temperature of 21°C, the effects of ambient temperature on *in vitro* lung dose decreased considerably. The detrimental effects of decreasing temperature on pMDI performance were explained via two mechanisms: decreased propellant vapor pressure (yielding larger initial droplet sizes upon actuation) and decreased evaporative rates at lower temperatures (potentially resulting in incomplete evaporation of propellant from drug particles). In a study on the effects of humidity on pMDI performance, Shemirani et al (2013) showed that increased relative humidity led to increased *in vitro* extrathoracic deposition and decreased *in vitro* lung deposition for both suspension and solution pMDIs. Here, increased extrathoracic deposition at higher relative humidity was thought to occur via increased condensation of ambient water vapor onto residual dry particles following propellant evaporation, leading to larger droplets and increased impaction in the mouth-throat. For such hygroscopic aerosols, the relative importance of hygroscopic effects can be estimated using non-dimensional analysis (Finlay 1998), though the quantification of hygroscopic effects on deposition in the respiratory tract requires experiment or numerical modeling. Considering DPIs, the effects of temperature and humidity on device performance have been studied extensively, with extended storage at atypical conditions leading to altered performance (Young et al. 2007; Janson et al. 2016). Over smaller time scales, i.e. the time it takes for a freshly-prepared dose to be inhaled by a patient, evidence suggests that such effects are less important (Ruzycki et al. 2014). The effects of ambient pressure have also been examined in a number of *in vitro* studies on inhaler performance at altitude (Titosky et al. 2014; Ruzycki et al. 2018). Titosky et al (2014) found that the *in vitro* lung dose downstream of an

Alberta Idealized Throat was not affected by altitudes up to 4300 m for five commercially available pMDIs, suggesting that pMDIs are relatively insensitive to changes in ambient pressure. Ruzycki et al (2018) showed that DPIs are somewhat more sensitive to altitude, though the effects of ambient pressure are variable, device-dependent, and relatively minor compared to the effects of inhalation flowrate.

Considering the above, it is clear that *in vitro* experiments require careful design to provide results that are indicative of real-world performance. In the present work, we investigate the effect of some of the aforementioned *in vitro* factors on deposition in the Alberta Idealized Throat that have been understudied in the literature. The effect of insertion angle on deposition from three DPIs of varying resistances are examined using inhaler-specific inhalation profiles following the arguments of Delvadia et al (2016). In addition, the effects of both insertion angle and relative humidity are investigated on hygroscopic aerosols emitted from three pMDIs. The results described herein may serve as guidance for those applying *in vitro* methods to characterize inhaled pharmaceutical therapies in the early stages of device development.

3.3   Materials and Methods

Six commercially available devices were selected for testing, including three DPIs (Pulmicort® Turbuhaler®, Easyhaler® Budesonide, and Budelin® Novolizer®) and three pressurized metered dose inhalers (QVAR®, Ventolin® Evohaler®, and Flovent® HFA). General properties of these inhalers are summarized in Table 3-1. DPIs were chosen to span a range of resistances typical of commercially available products (see Table 3-2), while pMDIs were chosen to span a range of spray properties (including droplet size, velocity, and momentum) based on data in the literature (Liu, Doub, and Guo 2012).

Table 3-1: Information on each inhaler selected for testing. LC = label claim.

Device	Analyte	LC (μg) / Doses	Lot Number Manufacturer	General Notes
Pulmicort Turbuhaler	budesonide	200 / 200	PASY AstraZeneca Canada Mississauga, Canada	Reservoir DPI No carrier Medium-high resistance
Easyhaler Budesonide	budesonide	200 / 200	1820769 Orion Pharma Espoo, Finland	Reservoir DPI Lactose carrier High resistance
Budelin Novolizer	budesonide	200 / 100	7A104 Meda Pharmaceuticals Takeley, UK	Reservoir DPI Lactose carrier Low resistance
QVAR	beclomethasone dipropionate	100 / 200	GTA065B Valeant Canada Laval, Canada	Solution pMDI HFA 134a propellant Ethanol cosolvent
Ventolin Evohaler	salbutamol sulfate	120 X 3* / 100	UU9R Glaxo Wellcome SA Burgos, Spain	Suspension pMDI HFA 134a propellant
Flovent HFA	fluticasone propionate	50 X 3* / 120	NF3H GlaxoSmithKline Mississauga, Canada	Suspension pMDI HFA 134a propellant

* Three actuations were used for each test with Ventolin Evohaler and Flovent HFA.

3.3.1 General Testing Procedure

Deposition from each inhaler was examined *in vitro* using a filter attached to the distal end of the Alberta Idealized Throat. Inhalers were actuated into the Alberta Idealized Throat using appropriate inhalation patterns, with deposition quantified via chemical assay. Dose depositing in the Alberta Idealized Throat was considered analogous to *in vivo* extrathoracic deposition, while the dose captured on the filter was considered analogous to the *in vivo* total delivered lung dose (including lung deposition and exhaled dose).

Prior to each experiment, both halves of the Alberta Idealized Throat were coated with silicone release spray (Molycote 316; Dow Corning, Midland, MI, USA). After allowing for solvent evaporation (~ 15 minutes), the Alberta Idealized Throat was assembled and an absolute filter (VP7100 viral/bacterial filter; KEGO corporation, London, ON, Canada) was attached downstream. An inhaler-specific adapter, designed in a manner to ensure an airtight seal, was

attached to the entrance of the Alberta Idealized Throat. With each inhaler having a unique mouthpiece shape and size, solid models of each device were replicated using scans from a laser probe on a 7-axis arm (Laser Line Probe Edge and Laser ScanArm; FARO, Lake Mary, FL, USA). Point clouds were edited and wrapped to create meshes of each inhaler using Geomagic design software (Geomagic for SOLIDWORKS; 3D Systems, Rock Hill, SC, USA), which then served as guides in the creation of solid models. Using these models and in-house templates, inhaler-specific adapters were designed (SOLIDWORKS 2017; Dassault Systèmes, Vélizy-Villacoublay, France) and prototyped out of VeroGray™ polymer using a 3D printer (Objet Eden 350V; Stratasys, Eden Prairie MN, USA). The incorporation of silicone O-rings on mating surfaces, coupled with the adapter having the local size and shape of each mouthpiece, allowed for the rapid and repeatable attachment of inhalers to the Alberta Idealized Throat during testing. Additional details on the process used to design adapters are presented in Appendix A.

For all tests, inhalers were operated following patient-use instructions. Following priming, inhalers were affixed to the Alberta Idealized Throat using the aforementioned inhaler-specific adapters. Inhalers were held in place by hand by the experimenter with a small compressive force that was not quantified, but was of a light enough magnitude to avoid compressing inhaler components. Inhalations were generated using a breathing machine for the DPIs and a vacuum pump for the pMDIs; specifics are described later in the methods. Following device actuation and inhalation, components were disassembled, and the masses of drug depositing in the Alberta Idealized Throat and downstream filter were quantified via UV spectroscopy of analytes obtained with appropriate solvents (see Quantifying Deposition section below).

Flowrates were monitored using a thermal mass flowmeter (Model 4043; TSI Incorporated, Shoreview, MN, USA) placed between the filter and the inhalation source and recorded in 50 ms intervals using a custom LabVIEW program (LabVIEW Professional Development System 2017; National Instruments, Austin, TX, USA). Environmental conditions including temperature and humidity were monitored with a digital hygrometer/thermometer (MI70 Measurement Indicator with HMP75B Humidity and Temperature Probe; Vaisala, Vantaa, Finland). Ambient conditions during testing were as follows: temperature ranged from 22°C to 24°C, relative humidity ranged from 15% to 25%, and absolute pressure ranged from 91 kPa to 94 kPa.

3.3.2 Testing with DPIs

The three DPIs selected for testing are passive and demonstrate flowrate dependent performance (Weers and Clark 2017). With each inhaler having a different airflow resistance, a subject inhaling with a given inspiratory effort through each device would be expected to generate inhalations with different peak inspiratory flowrates (Delvadia et al. 2016) (generally, subjects generate lower peak inspiratory flows through devices with higher resistances [Azouz et al. 2015]). Here, the relations of Delvadia et al (2016) are used in conjunction with the resistances of each DPI to develop specific inhalation curves for each device. These curves correspond to the 50th percentile of inhalation profiles generated by healthy adults that are trained on the proper use of each device by health care professionals (inhalation pattern B in [Delvadia et al. 2016]). Equations defining these curves are of a sinusoidal form (Delvadia et al. 2016):

$$
Q(t) = \begin{cases} Q_{\text{peak},50\%} \sin\left(\dfrac{\pi}{2}\dfrac{t}{t_{\text{peak}}}\right) & 0 \leq t \leq t_{\text{peak}} \\[2em] Q_{\text{peak},50\%} \cos\left(\dfrac{\pi(t - t_{\text{peak}})}{2(\,t_{\text{total}} - t_{\text{peak}})}\right) & t_{\text{peak}} \leq t < t_{\text{total}} \end{cases} \tag{3-1}
$$

$Q(t)$ is the flowrate at time t, t_{peak} and t_{total} are the time to peak flowrate and end of inhalation, respectively, and Q_{peak} is the peak inhalation flowrate. Q_{peak} depends on the device resistance R (Delvadia et al. 2016):

$$
Q_{\text{peak},50\%} = 1.82\left(\frac{1}{R}\right) + 21.0 \tag{3-2}
$$

From Delvadia et al (Delvadia et al. 2016) the 50th percentile value for inhalation volume of adults across genders, V, was reported as 2.7 L, while the median time required to reach the peak inhalation flow rate t_{peak} was 0.49 s, independent of device resistance. The total duration of inhalation for a given inhaler is calculated as $t_{\text{total}} = 30\pi V/Q_{\text{peak}}$. Results of the above calculations for $Q_{\text{peak},50\%}$ and t_{total} using the given values of each inhaler resistance from the literature (Delvadia et al. 2016) are summarized in Table 3-2.

Table 3-2: Inhalation parameters for each DPI calculated using the relations of Delvadia et al (2016). Mouthpiece diameters were measured using a digital caliper.[1]

Inhaler	Resistance R (kPa$^{1/2}$min/L)	Peak Inhalation Flowrate Q_{peak} (L/min)	Duration of Inhalation t_{total} (s)	Mouthpiece Exit Diameter (mm)	Mean Velocity at Q_{peak} (m/s)
Pulmicort Turbuhaler	0.0352	72.7	3.50	10.1	15.1
Easyhaler Budesonide	0.0435	62.8	4.05	5.3	47.4
Budelin Novolizer	0.0241	96.5	2.64	6.0	56.9

These inhalation profiles represent the volumetric flowrate exiting the inhaler, an important consideration addressed in the following section. Profiles were programmed into an in-house breathing machine for use in the experimental setup shown in Figure 3-1.
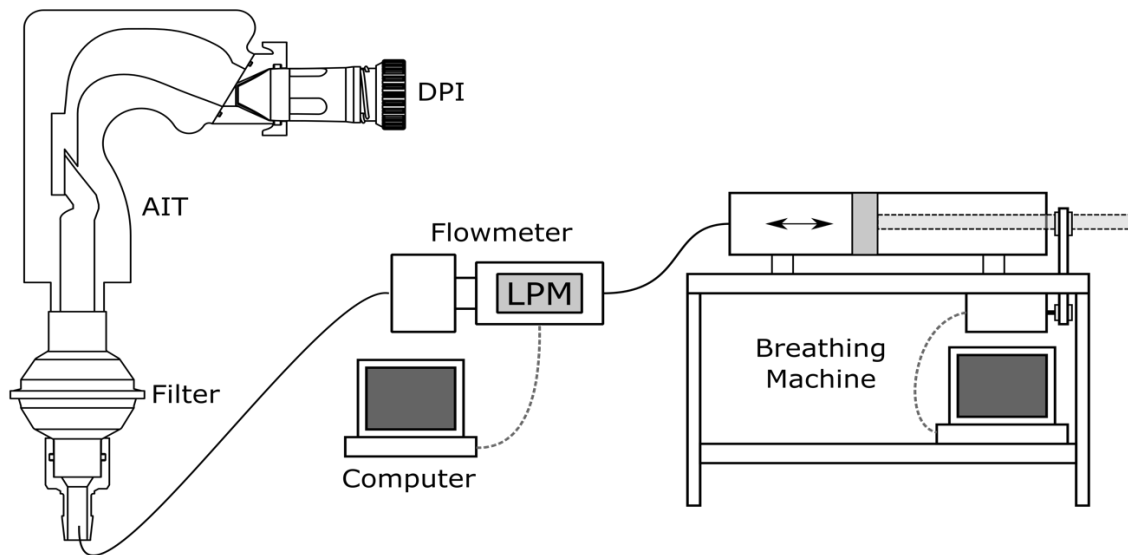
Figure 3-1: Setup used to measure in vitro extrathoracic dose and total lung dose using the Alberta Idealized Throat (AIT). DPI = dry powder inhaler.

[1] Mean velocities reported in Table 3-2 have been corrected from the published version, where the DPI mouthpiece diameter was mistaken as the radius. Published values were thus too small by a factor of 4.

3.3.2.1 Correcting for Volumetric Flowrate Exiting the Inhaler Mouthpiece

The flowmeter was calibrated by the manufacturer to measure airflow in standard L/min. Of concern here is the volumetric flowrate, which describes the actual velocity at which the gas phase travels. The standard flowrate can be converted to the volumetric flowrate using relations derived from the ideal gas law:

$$Q_{\text{vol,m}}(t) = Q_{\text{std,m}}(t) \frac{T_{\text{m}}}{T_{\text{ref}}} \frac{P_{\text{ref}}}{P_{\text{m}}} \tag{3-3}$$

$Q_{\text{std,m}}(t)$ is the standard flowrate measured by the flowmeter at a given time for airflow at conditions m, corresponding to the volumetric flowrate $Q_{\text{vol,m}}(t)$, while T_{m} (in kelvin) and P_{m} denote the measured temperature and pressure, respectively. It can be shown (see Appendix B) that to calculate the volumetric flowrate exiting the inhaler mouthpiece, the correction must consider both the ambient environmental pressure P_{amb} and the pressure drop across the inhaler ($\Delta P_{\text{DPI}}(t)$). This pressure drop, being dependent on inhalation flowrate and device resistance, is a function of time for a realistic inhalation. The resulting correction takes the form of equation (3-4), assuming that ambient environmental pressure has a negligible effect on inhaler resistance (Ruzycki et al. 2018) and that the relation between pressure drop and flowrate is quasi-steady.

$$Q_{\text{vol,DPI exit}}(t) = Q_{\text{std,m}}(t) \frac{T_{\text{m}}}{T_{\text{ref}}} \frac{P_{\text{ref}}}{\left(P_{\text{amb}} - \left[R Q_{\text{std,m}}(t) \frac{T_{\text{m}}}{T_{\text{ref}}} \frac{P_{\text{ref}}}{P_{\text{amb}}} \right]^2 \right)} \tag{3-4}$$

When programmed directly into the breathing machine, the inhalation profiles described by equation (3-1) for the volumetric flowrate exiting the inhaler mouthpiece were poorly replicated based on measurements from the in-line flowmeter and the correction described in equation (3-4). An iterative calibration on each inhalation profile was thus performed by manipulating the local size and shape of the flowrate versus time curves input to the breathing machine, allowing for the fine-tuning of each resultant profile to the ideals derived from the Delvadia et al (2016) relations. Importantly, this calibration was performed with each inhaler affixed in turn to the Alberta Idealized Throat.

3.3.3 Testing with pMDIs

PMDIs were examined using a steady inhalation flowrate of 30 L/min generated by a vacuum pump (SOGEVAC SV25; Oerlikon Leybold Vacuum, Bourg-lès-Valence, France) as shown in

Figure 3-2, in which an enclosed environmental chamber provided a measure of control over ambient test humidity. Given the low resistance of the pMDIs and the modest inhalation flowrate of 30 L/min, the volumetric flowrate correction factor in equation (3-4). was applied with the resistance R set to 0. The pMDI was held to the Alberta Idealized Throat for at least 5 seconds after actuation, providing ample time for the bolus to fully traverse the throat, after which the inhaler was removed and the vacuum pump turned off.
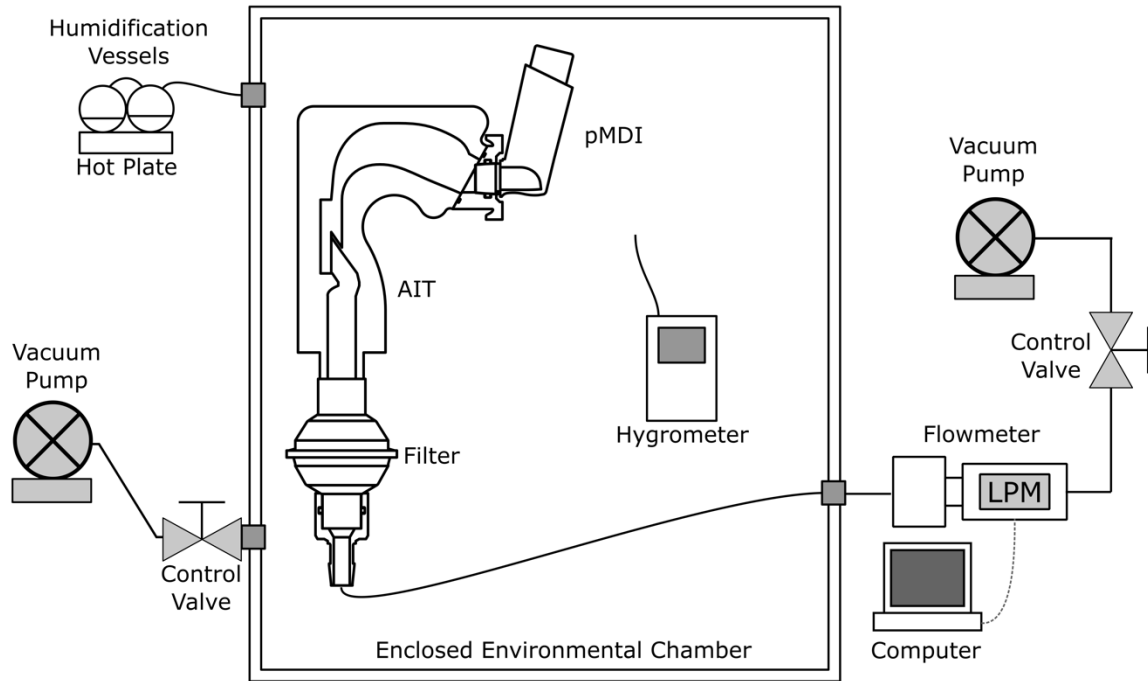
Figure 3-2: Setup used to measure in vitro extrathoracic dose and total lung dose for hygroscopic aerosols using the Alberta Idealized Throat (AIT). pMDI = pressurized metered dose inhaler.

Tests were first performed at ambient lab conditions (relative humidity ranging from 15 to 25% for Edmonton), with the environmental chamber left open. Later experiments were performed with the chamber closed off and filled with fully saturated air from a series of three humidification vessels (MR290 Humidification Chamber; Fisher & Paykel Healthcare, Auckland, New Zealand) heated to 90°C using a hotplate (Isotemp Model 11-100-49SH; Fisher Scientific, Ottawa, Canada); a slight vacuum was applied to the chamber using a secondary vacuum pump (Model 0523; Gast Manufacturing, Inc., Benton Harbor, MI, USA) to draw in saturated air until the chamber humidity exceeded 95%, after which the pressure inside was allowed to return to atmospheric pressure prior

to device actuation. With this procedure, a slight increase in temperature of 12°C relative to room temperature occurred within the box.

3.3.4 Examining Inhaler Orientation Relative to the Mouth

To examine the effect of inhaler orientation, tests were performed for each inhaler using one of two adapter designs, shown schematically in Figure 3-3. One adapter was designed to direct the inhaler towards the back of the mouth (perpendicular to the planar face defining the entrance of the Alberta Idealized Throat) corresponding to an angle of 29° relative to horizontal (Figure 3-3a). This angle is termed coaxial in the present work, after the alignment of the inhaler axis with the central axis of the oral cavity (i.e., normal to the oral cavity inlet plane). The other adapter was designed for an insertion angle of 0°, directing the inhaler towards the tongue, here termed transverse (Figure 3-3b). Both adapters were designed such that the center point of the outlet of the inhaler mouthpiece was equidistant from the entrance to the mouth-throat geometry.
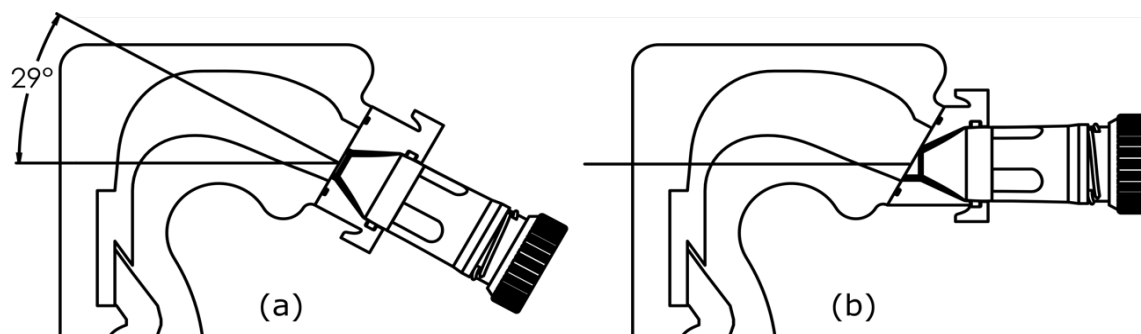
Figure 3-3: Inhaler orientation (a) coaxial; directed toward the back of the mouth and (b) transverse; directed towards the tongue.

3.3.5 Quantifying Deposition

DPIs were examined with (a) a coaxial orientation at ambient lab humidity and (b) a transverse orientation at ambient lab humidity. PMDIs were tested with (a) a coaxial orientation at ambient lab humidity, (b) a transverse orientation at ambient lab humidity, (c) a coaxial orientation at high humidity, and (d) a transverse orientation at high humidity. Each individual test was performed using a single actuation for each DPI and the QVAR pMDI, and three actuations for Ventolin Evohaler and Flovent HFA – additional actuations were used to average out some of the shot-to-shot variability that occurs with these suspension pMDIs (Hatley et al. 2016), which otherwise

complicates the statistical interpretation of results. Five repeated measures (n = 5) were taken at each experimental condition.

Masses depositing on the throat and filter were quantified via UV spectroscopy. Following each individual test, the Alberta Idealized Throat was washed twice with 10 mL of solvent, and the downstream filter was washed with 10 mL of solvent up to four times (to ensure adequate recovery from the filter material). Solvents used were HPLC grade methanol for budesonide, beclomethasone dipropionate, and fluticasone propionate, and DIUF water for salbutamol sulfate. UV absorbance was measured relative to standards at 243 nm for budesonide, 238 nm for beclomethasone dipropionate, 236 nm for fluticasone propionate, and 274 nm for salbutamol sulfate using a diode array UV-vis spectrophotometer (Cary 8454; Agilent, Santa Clara, CA, USA). Mass remaining within the device following actuation was not assayed, in accordance with real-world use following instruction leaflets.

Deposition was reported in terms of raw mass, with additional consideration given to filter deposition as a percentage of the delivered dose. The delivered dose was calculated as the sum of deposition on the Alberta Idealized Throat and downstream filter. Statistical comparisons of deposition at each test angle with each DPI were performed using Student's t-tests assuming independent samples and a significance level of 0.05. Comparisons of deposition at each test angle and test humidity for the pMDIs were performed using Two-Way ANOVA, with a significance level of 0.05. For pMDIs, post-test multiple comparisons were performed to compare cases (defined above) (a) to (b), (a) to (c), (b) to (d), and (c) to (d), following Bonferroni's correction for a familywise error rate of 0.05; P values reported for these multiple comparisons are multiplicity-adjusted. Statistics were performed in MATLAB (R2018a; The MathWorks Inc, Natick, MA, USA) using the *ttest2* (assuming unequal variance; Welch's t-test) and *anova2* functions, with a custom-script for multiple comparisons calling the *tcdf* function for values of the Student's *t*-distribution.

3.4   Results

Measured deposited masses in the Alberta Idealized Throat and downstream filter and the corresponding delivered dose are presented in Table 3-3. Raw deposition measurements from Easyhaler Budesonide, Ventolin Evohaler, and Flovent HFA showed sensitivity to insertion angle, while Flovent HFA showed sensitivity to humidity.

For Easyhaler Budesonide, the filter dose of budesonide increased from 41.9 ± 1.5 µg to 61.0 ± 5.2 µg (average $\pm$ standard deviation, $P < 0.001$) when the inhaler was directed coaxially as compared to transversely. For Ventolin Evohaler (ANOVA $P < 0.001$ for insertion angle) the filter dose of salbutamol sulfate increased from 88.5 ± 7.1 µg in the transverse orientation to 150.5 ± 29.2 µg in the coaxial orientation at ambient lab humidity ($P < 0.001$). At high humidity, the difference in filter deposition between the transverse (92.4 ± 11.8 µg) and coaxial orientations (120.0 ± 21.7 µg) failed to reach statistical significance ($P = 0.16$). For Flovent HFA (ANOVA $P < 0.001$ for insertion angle), the filter dose of fluticasone propionate increased from 45.3 ± 5.1 µg to 73.3 ± 6.3 µg at ambient lab humidity ($P < 0.001$) and from 38.2 ± 1.5 µg to 58.1 ± 4.4 µg ($P < 0.001$) at high humidity when the inhaler was directed coaxially as compared to transversely.

Of the three pMDIs, only Flovent HFA showed significant effects of humidity on raw deposition measurements, with the filter dose decreasing at high humidity relative to ambient lab humidity (ANOVA $P < 0.001$ for humidity). Differences in raw deposition due to humidity failed to reach statistical significance for Ventolin Evohaler (ANOVA $P = 0.15$). Interaction effects between insertion angle and humidity failed to reach statistical significance for filter deposition measured from any of the pMDIs (ANOVA $P = 0.30$, 0.07, and 0.07 for QVAR, Ventolin Evohaler, and Flovent HFA, respectively). No significant differences in the delivered dose were observed for any inhaler across the various test conditions.

Table 3-3: Deposition measured in the Alberta Idealized Throat (AIT) and filter for each inhaler, with the corresponding delivered dose. BUD = budesonide, BDP = beclomethasone dipropionate, SS = salbutamol sulfate, FP = fluticasone propionate. Presented as mean (standard deviation in parentheses).

Inhaler	Label Claim (µg)	Test Humidity	AIT Deposition (µg)		Filter Deposition (µg)		Delivered Dose (µg)	
			Transverse Orientation	Coaxial Orientation	Transverse Orientation	Coaxial Orientation	Transverse Orientation	Coaxial Orientation
Pulmicort Turbuhaler	200 µg BUD	Ambient	80.8 (10.5)	89.6 (16.7)	75.7 (8.2)	83.4 (8.3)	156.6 (15.9)	173.0 (23.3)
Budelin Novolizer	200 µg BUD	Ambient	153.8 (11.2)	146.8 (20.2)	54.8 (6.2)	52.6 (4.0)	208.6 (9.0)	199.3 (20.4)
Easyhaler Budesonide	200 µg BUD	Ambient	227.5 (13.6)	218.5 (22.6)	41.9 (1.5) α	61.0 (5.2)	269.4 (13.1)	279.5 (26.3)
QVAR	100 µg BDP	Ambient	25.0 (4.1)	22.5 (8.4)	60.1 (2.8)	60.8 (4.8)	85.1 (5.6)	83.3 (8.4)
		High	24.1 (2.1)	22.1 (6.3)	58.9 (4.9)	56.8 (3.4)	82.9 (6.7)	78.9 (5.9)
Ventolin Evohaler	3 X 120 = 360 µg SS	Ambient	256.5 (46.8) β	171.6 (22.5)	88.5 (7.1) β	150.5 (29.2)	344.9 (43.0)	322.1 (45.1)
		High	254.5 (35.2)	203.5 (10.2)	92.4 (11.8)	120.0 (21.7)	346.9 (40.0)	323.6 (29.1)
Flovent HFA	3 X 50 = 150 µg FP	Ambient	81.6 (6.7) β γ	56.3 (9.2)	45.3 (5.1) β γ	73.3 (6.3)	126.9 (7.1)	129.6 (9.6)
		High	90.5 (6.3)	73.6 (9.5)	38.2 (1.5)	58.1 (4.4)	128.7 (5.9)	131.6 (8.6)

α – significant difference via student's t-test

β – significant difference due to inhaler orientation via two-way ANOVA

γ – significant difference due to humidity via two-way ANOVA

Filter deposition is presented as a percent of the delivered dose in Figure 3-4. Results for Easyhaler Budesonide and Flovent HFA are consistent with those presented in Table 3-3. For Easyhaler Budesonide, filter deposition obtained with a transverse insertion angle, 15.6 (SD 1.1) % (percent of delivered dose, average with SD in parenthesis[2]) was significantly lower than that obtained with a coaxial insertion angle (21.9 [SD 1.3] %, $P < 0.001$). For Flovent HFA at ambient lab humidity, filter deposition for the transverse orientation, 35.7 (SD 3.7) %, was significantly lower than obtained with the coaxial orientation, 56.7 (SD 4.9) % ($P < 0.001$). For tests at high humidity relative to low with Flovent HFA, the filter dose decreased from 56.7 (SD 4.9) % to 44.2 (SD 4.3) % ($P < 0.001$) in the coaxial orientation. In the transverse orientation, the decrease in filter deposition for Flovent HFA between high and low humidity (29.8 [SD 1.9] % versus 35.7 [SD 3.7] %; $P = 0.11$) was not significant.

For Ventolin Evohaler, the normalization of the filter dose by the delivered dose caused additional statistical comparisons to reach significance; when expressed as a percentage of the delivered dose, deposition on the filter was significantly influenced by inhaler orientation (ANOVA $P < 0.001$) and humidity (ANOVA $P = 0.02$), with a significant interaction effect (ANOVA $P = 0.009$). In interpreting the interaction effect, the difference in filter deposition caused by inhaler orientation was greater at lower humidity. At ambient lab humidity, filter deposition with the coaxial insertion angle (46.5 [SD 4.3] %) was significantly higher ($P < 0.001$) than that obtained with the transverse orientation (26.0 [SD 4.4] %), while at high humidity, a similar but smaller difference caused by insertion angle was observed (36.9 [SD 3.6] % versus 26.7 [SD 2.8] %; $P = 0.003$). Deposition obtained with the transverse orientation was independent of humidity for Ventolin Evohaler (~26 % of delivered dose, $P = 1.0$), in contrast with the coaxial orientation, where the filter dose measured at ambient humidity, 46.5 (SD 4.3) %, exceeded that measured at high humidity, 36.9 (SD 3.6) % ($P = 0.005$).

---

[2] Results in the published version of this chapter were reported as mean $\pm$ SD % (e.g., 40 $\pm$ 10 %). To reduce ambiguity in the interpretation of this expression, results here are recast as mean (SD) %e.g., 40 (SD 10) %.
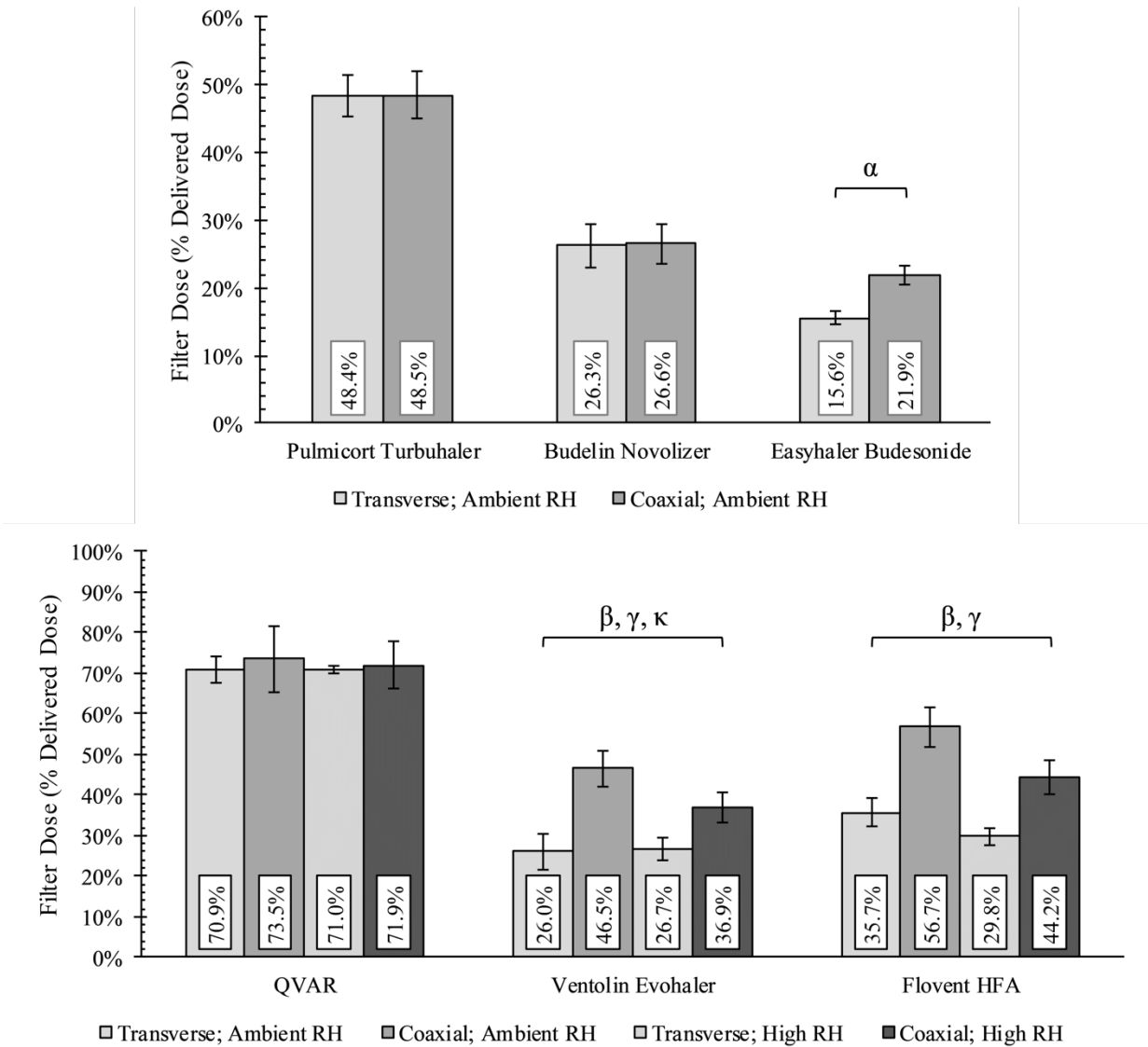
Figure 3-4: Filter dose expressed as percent delivered dose for the DPIs (top) and pMDIs (bottom). α indicates significant difference due to inhaler orientation (student's t-test), β indicates significant difference due to inhaler orientation (two-way ANOVA), γ indicates significant difference due to humidity (two-way ANOVA), κ indicates significant interaction effect between orientation and humidity (two-way ANOVA). Error bars denote standard deviation.

3.5   Discussion

Overall, three of six inhalers showed statistical sensitivity to insertion angle, including Easyhaler Budesonide, Ventolin Evohaler, and Flovent HFA. Two of three pMDIs showed sensitivity to

humidity, including Ventolin Evohaler and Flovent HFA. Effects of insertion angle are first discussed for DPIs, followed by a discussion of both insertion angle and relative humidity effects on pMDIs.

3.5.1 DPIs – Effects of Insertion Angle

Insertion angle had no effect on deposition from the Pulmicort Turbuhaler or Budelin Novolizer. In contrast, Easyhaler Budesonide showed sensitivity to insertion angle; in terms of raw mass, the average filter dose increased from 41.9 µg to 61.0 µg when the inhaler was angled toward the back of the mouth instead of directed towards the tongue, a considerable 46% increase. This is a surprising result, as the peak inhalation flowrate generated through the Easyhaler was the lowest of the three DPIs owing to its high airflow resistance. One may expect that the inhaler with the highest inhalation flowrate (Budelin Novolizer) would be most sensitive to insertion angle given that impaction is positively correlated with aerosol velocity. The present results, which contradict this expectation, suggest that flowrate and device resistance alone are insufficient parameters for predicting the importance of inhaler insertion angle with DPIs.

Some insight may be gained by considering the jet effect developed through DPI mouthpieces upon entrance into the oral cavity. DeHaan and Finlay (2004) developed an algebraic correlation for predicting oral cavity deposition from DPIs with mouthpieces of varying designs. Combining this correlation with the extrathoracic deposition correlation of Stahlhofen, Rudolf, and James (1989), which focused primarily on deposition in the larynx, they demonstrated that the majority of deposition from DPIs appears to occur in the oral cavity, upstream of the throat. Furthermore, increased probability of extrathoracic deposition from DPIs due to jet effects is expected to occur for particles in the 2 to 10 µm aerodynamic diameter range. Particles smaller than 2 µm are fairly insensitive to impaction for the flowrates used with typical DPIs, while particles larger than 10 µm are extremely likely to deposit in the mouth-throat, due to either mouthpiece jet effects in the oral cavity or the airway constriction that occurs later in the larynx.

For the DPIs used in the present work, literature suggests that Easyhaler Budesonide generates larger particles (MMAD near 4 µm (Parisini et al. 2014)) than either Pulmicort Turbuhaler (MMAD near 2.5 µm (Yoshida et al. 2017)) or Budelin Novolizer (MMAD near 2 µm (Longest et al. 2012)), indicating an increased sensitivity of this device to jet effects at equivalent velocities. However, with the inhaler-specific inhalation profiles used in the present work, and the different

mouthpiece designs of each inhaler, the average centerline velocity of the jet exiting the mouthpiece varies notably among these DPIs (see Table 3-2). Easyhaler Budesonide has a mean jet velocity of 47.4 m/s at peak inhalation flowrate, similar in value to that of the Budelin Novolizer of 56.9 m/s, while Pulmicort Turbuhaler emits a slower jet at 15.1 m/s[3]. The larger particles emitted from Easyhaler Budesonide, in combination with its relatively large jet velocity, resulted in a high amount of oral cavity deposition. Because oral cavity deposition is influenced by orientation angle, these factors may explain why Easyhaler Budesonide displays sensitivity to orientation angle, while Pulmicort Turbuhaler (with smaller particles and a slower jet) and Budelin Novolizer (with relatively small particles) were unaffected.

Test humidity was not controlled with the DPIs. Though the DPI formulations used in the present work are hygroscopically stable, humidity can certainly affect DPI performance over long durations of time (Janson et al. 2016). However, as the DPIs used here were stored at recommended conditions, and considering the short exposure time of freshly prepared doses to ambient humidity (on the order of seconds), the results obtained at the relatively dry ambient lab conditions of 15 to 25% relative humidity in Edmonton are considered to be representative of device performance at normal conditions over a range of humidity.

3.5.1.1 Realistic profiles for DPI testing

As mentioned in the methods, replication of the ideal inhalation profiles recommended by Delvadia et al (Delvadia et al. 2016) required iterative calibrations of input profiles to the breathing machine. The unsatisfactory replication of inhalation profiles using uncalibrated curves was only made obvious by monitoring in real-time the inhalation profiles generated when inhalers were attached to the Alberta Idealized Throat, when the total airflow resistance was greatest. It is unlikely that this poor replication was caused by the breathing machine itself (which operated by a motor-driven piston displacing a known volume of air over a given time) nor was an artificial signal from the flowmeter (having a quick response time of 5 ms). A potential explanation arises from fluid mechanics if one realizes that increasing airflow resistance acts to dampen transient flows. The inclusion of greater dampening reduces the response of the system to variable inputs (Beckwith, Marangoni, and Lienhard 2007), with the variable input here being the inhalation flowrate generated by the breathing machine. A related phenomenon is the alteration of flow-time

---

[3] Corrected from published version (see [1])

profiles observed in systems with varying "dead-space" or internal volume (Greguletz et al. 2010). In this regard, the *in situ* measurement of flowrates using an in-line flowmeter is a useful *in vitro* technique for confirming that inhalation profiles generated through devices are as desired.

The correction factor summarized in equation (3-4) should be incorporated in calculating the volumetric flowrate exiting the inhaler mouthpiece to avoid biased measurements. The magnitude of the correction stemming from the inclusion of device resistance depends on the flowrate through the DPI, but is of the same magnitude as the correction for the difference in pressure between the ambient and reference conditions at moderate altitudes.

3.5.2 pMDIs – Effects of Insertion Angle and Humidity

Insertion angle had negligible effects on deposition from QVAR. Ventolin Evohaler and Flovent HFA, in contrast, demonstrated a high degree of sensitivity to insertion angle. Orienting these inhalers towards the back of the mouth enhanced filter deposition considerably while decreasing deposition in the Alberta Idealized Throat. For Ventolin Evohaler at ambient humidity, average filter deposition expressed as a percent of delivered dose almost doubled (from 26.0% to 46.5%) with the inhaler oriented coaxially as compared to transversally. Flovent HFA similarly saw a large increase in filter deposition when oriented coaxially, from 35.7% to 56.7% of delivered dose, for tests at ambient lab humidity.

These results are well explained by differences in the spray/droplet velocity and droplet sizes emitted from these pMDIs. Using phase Doppler anemometry, Liu, Doub and Guo (2012) measured mean droplet velocities of 5.4 m/s for QVAR, 10.3 m/s for Ventolin HFA (equivalent to Ventolin Evohaler), and 20.1 m/s for Flovent HFA 3 cm downstream of the end of the mouthpiece. Droplet size measurements using a laser light scattering system (again at 3 cm beyond the mouthpiece) showed Flovent HFA generating droplets with the smallest volume median diameter, at 1.7 μm, compared to 2.9 μm for QVAR and 9.1 μm for Ventolin HFA. Impaction force measurements (a surrogate measure of spray momentum) 6 cm downstream of the mouthpiece suggested that Flovent HFA and Ventolin HFA generated similarly strong sprays equivalent to 5.3 g and 4.9 g masses respectively, while QVAR generated a much gentler spray equivalent to a 1.7 g mass. Overall, the measurements of Liu, Doub and Guo (2012) suggest that droplets emitted by the Ventolin Evohaler and Flovent HFA have a much higher total momentum than those emitted by QVAR. Flovent HFA, having high droplet velocities, and Ventolin HFA, having large droplets,

are more susceptible to deposition via impaction. When directed towards the tongue, droplets from Ventolin Evohaler and Flovent HFA have less time to undergo evaporative size changes, disperse with surrounding inhalation air, and decrease in velocity before reaching the interior surfaces of the Alberta Idealized Throat than when directed towards the back of the oral cavity, resulting in increased extrathoracic deposition, as is observed in the present work.

An additional factor affecting deposition from pMDIs arises from the development of sprays in a confined space (i.e., the oral cavity). *In situ* use of a pMDI has the aerosol plume surrounded by a sheath of co-flow inhalation air during inhalation. The velocity of co-flow air at 30 L/min is roughly 1.5 m/s for the three pMDIs here, as the mouthpiece of each inhaler has a cross sectional area of around 300 mm^2. The velocity of the jet emitted by QVAR is roughly 3 times greater than this co-flow, a smaller difference than is generated by Ventolin Evohaler (~7 times greater) and Flovent HFA (~13 times greater). Differences in velocity between the plume edges and the sheath air encourage shear-induced turbulence (Shemirani et al. 2013), meaning Flovent HFA should generate the most turbulent flow field inside the extrathoracic airways of these three pMDIs. As increased turbulence correlates with increased deposition in the oral cavity (Dehaan and Finlay 2004), this may account for some of the sensitivity to insertion angle and increased extrathoracic deposition observed with Ventolin Evohaler and Flovent HFA as compared to QVAR.

Aerosols emitted by pMDIs are also subject to hygroscopic effects. Evolution of the spray from a metered dose is a complicated process involving flash evaporation, two-phase flow, and atomization through the pMDI nozzle, resulting in the creation of liquid droplets containing both drug and propellant (Ivey, Vehring, and Finlay 2015). Droplets undergo further evaporative size changes, leading to the formation of cool residual dry particles that then act as condensation nuclei for ambient water vapor (Martin and Finlay 2005). Ambient conditions including temperature and humidity can influence these processes (Finlay 2019), as has been shown experimentally in previous work the Alberta Idealized Throat (Shemirani et al. 2013). In the present work, no significant effect of humidity was observed for QVAR, consistent with the observations of Shemirani et al (2013) for a similar formulation. For Ventolin Evohaler and Flovent HFA, however, humidity had a significant effect on filter deposition expressed as a percent of delivered dose, with increased humidity associated with reduced filter deposition. Ventolin Evohaler also demonstrated a significant interaction effect between humidity and insertion angle on deposition,

indicating that these effects are not independent. Generally, the effect of humidity was more noticeable when the inhaler was oriented coaxially; the filter dose decreased from 46.5% to 36.9% of delivered dose at high humidity relative to ambient for Ventolin Evohaler, and from 56.7% to 44.2% for Flovent HFA. A physical explanation for this finding may be that when these inhalers are directed towards the tongue, there is little time for hygroscopic effects to influence droplet size prior to impaction with the inner surface of oral cavity. Extrathoracic deposition is then dominated by the jet momentum of the pMDI spray plume regardless of humidity. In the coaxial orientation, however, the pMDI plume may evolve such that hygroscopic effects have more time to take hold. In this situation, high humidity likely leads to the formation of larger droplets that experience greater deposition due to impaction, as is observed in the present work.

3.5.3   On In Vitro – In Vivo Comparisons

Of common interest is the development of more accurate *in vitro* methods for predicting *in vivo* deposition. Current *in vitro* methods carry some limitations that prevent the perfect replication of *in vivo* conditions (Byron et al. 2010), including airway model rigidity, an absence of heating and humidification of inhaled air from *in vitro* airway walls, and inability to predict exhaled doses. Despite these limitations, *in vitro* methods, when designed carefully, can provide invaluable information towards the prediction of *in vivo* deposition. As noted in the introduction, a properly designed *in vitro* experiment for predicting *in vivo* deposition should consider a number of factors, including the emulation of upper airway geometry, inhalation maneuver, inhaler orientation and positioning relative to the mouth, and anticipated environmental conditions. *In vivo* deposition studies typically do not report these details fully, leaving some ambiguity in the comparison of *in vitro* with *in vivo* data. In addition, the aforementioned *in vitro* limitations can be compounded by *in vivo* limitations of different forms.

Given the subject of the present work, in which a standardized methodology was used to examine device performance using the Alberta Idealized Throat, it is useful to consider the literature detailing *in vivo* deposition of similar formulations while noting some implications for *in vitro* – *in vivo* correlations. In studies of aerosol deposition, radionuclide imaging provides an excellent resource for visualizing deposition in the respiratory tract. Each inhaler used in the present work has at least one radionuclide study reporting deposition *in vivo* in adult populations: Pulmicort Turbuhaler (Borgström et al. 1994; Newman et al. 2000; Hirst et al. 2001; Hirst, Newman, et al.

67

2002), Budelin Novolizer (Newman et al. 2000), Easyhaler Budesonide (Hirst et al. 2001), QVAR (Leach, Davidson, and Boudreau 1998; Leach et al. 2005; Leach and Colice 2010), Ventolin Evohaler (Hirst, Pitcairn, et al. 2002), and Flovent HFA (Leach and Colice 2010). One can compare the *in vivo* data with the values we measure in the present work to find generally good agreement. In establishing *in vitro – in vivo* correlations with such data, however, there are important factors to consider. For one, radionuclide imaging measures the deposition of a radiolabel rather than the pharmaceutical agent itself, making this an indirect measure of respiratory tract deposition. In addition, the process of radiolabeling a formulation is not without issue (Devadason et al. 2012; Scheuch et al. 2010), and no standard method yet exists for registering deposition in specific areas of the body in an objective manner (Newman et al. 2012; Bennett et al. 2014; Alcoforado et al. 2018). The interpretation of total activity counts with regards to label claim, metered dose, or delivered dose (useful benchmarks *in vitro*) is also unclear. Other *in vivo* methods, such as pharmacokinetic studies measuring systemic dose over time and treatment efficacy in clinical trials, provide less information that can be specifically tied to particular measures of inhaler performance, further complicating the development of *in vitro – in vivo* correlations.

Certain factors such as inhalation pattern can vary widely from target values *in vivo*. In a study involving Ventolin Evohaler, Hirst, Pitcairn, et al. (2002) observed that some subjects stopped inhaling partway through administration, explained as a reaction to the propellant spray hitting the back of the throat. Correspondingly, the averaged inhaled volume in adult subjects was only 1.5 L, lower than the 2.9 L inhaled volume achieved by the same subjects for a formulation using the same propellant (HFA-134a) with a different actuator orifice. Such an inhalation maneuver would likely cause increased extrathoracic deposition and reduced lung deposition, as was observed *in vivo*—mean lung deposition was only 14.5% of the metered dose, roughly one-half to one-third of the values predicted here for this inhaler. It is unclear whether values predicted *in vitro* in the present work for this inhaler are more representative of the *in vivo* averages when an ideal inhalation (sans-interruption) is performed.

Subjects are often coached to inhale at a specific inhalation flowrate during *in vivo* tests that may differ significantly from the inhalation patterns used in the present work. For DPIs, we used the inhaler-specific inhalation patterns proposed by Delvadia et al (2016) based on the 50th percentiles

achieved by trained healthy adult subjects. This results, for example, in a peak inhalation flowrate of 72.7 L/min with Pulmicort Turbuhaler, somewhat larger than the typical 60 L/min target used *in vivo* (Borgström et al. 1994; Hirst et al. 2001; Newman et al. 2000; Hirst, Newman, et al. 2002). Parameters such as flowrate acceleration and time to peak inhalation flowrate are typically unreported *in vivo*, making the selection of appropriately representative values ambiguous. From a regulatory and standardization perspective, it may be more practical to use well-defined inhalation profiles that reflect what a trained subject is likely to achieve *in situ* for typical use of inhalers, i.e. akin to the Delvadia et al (2016) profiles used here. The issue of altered inhalation profiles due to disease or different patient populations remains a topic for future work.

Results here highlight the importance of insertion angle and humidity on deposition in the extrathoracic region and in determining the total dose delivered to the lungs for some inhalers. Three of the six inhalers used in the present work showed sensitivity to insertion angle, meaning that the orientation of many inhalers tested *in vitro* cannot be chosen arbitrarily if one wishes to predict *in vivo* deposition. Humidity effects also play a clear role with hygroscopic aerosols emitted from pMDIs and should thus be considered when designing predictive *in vitro* experiments.

3.6 Conclusions

Inhaler insertion angle can influence *in vitro* deposition measurements in the Alberta Idealized Throat for some inhalers. Of the six devices used in the present work, three (Easyhaler Budesonide, Ventolin Evohaler, and Flovent HFA) showed significant differences in deposition at different insertion angles. For these inhalers, directing the device towards the tongue as opposed to the back of the mouth served to decrease the dose delivered to the filter downstream of the Alberta Idealized Throat; filter deposition as a percent of delivered dose decreased from 21.9 (SD 1.3) % to 15.6 (SD 1.1) % for Easyhaler Budesonide, from 46.5 (SD 4.3) % to 26.0 (SD 4.4) % for Ventolin Evohaler, and from 56.7 (SD 4.9) % to 35.7 (SD 3.7) % for Flovent HFA when tests were performed at ambient lab humidity. Sensitivity to insertion angle likely contributes to variability in lung dose for these inhalers. For DPIs, device resistance and peak inhalation flowrate were not predictive of the importance of insertion angle. Rather, the combination of high mouthpiece jet velocities and large particle sizes likely results in sensitivity to insertion angle for certain DPIs. The present results also suggest that reduced sensitivity to inhaler insertion angle may be achieved

using larger diameter inhaler mouthpieces and smaller particle sizes for DPIs, and lower-momentum sprays for pMDIs.

Humidity may also influence the deposition of hygroscopic aerosols, as was observed with two of the three pMDIs (Ventolin Evohaler and Flovent HFA). For these inhalers, increased humidity was associated with reduced filter deposition, with the effect being more noticeable in the coaxial inhaler orientation. When oriented coaxially, the filter dose (as a percent of delivered dose) decreased from 46.5 (SD 4.3) % to 36.9 (SD 3.6) % for Ventolin Evohaler and from 56.7 (SD 4.9) % to 44.2 (SD 4.3) % for Flovent HFA at high humidity relative to ambient lab humidity. A significant interaction effect may also occur between humidity and insertion angle for some inhalers. Humidity therefore influences the total *in vitro* lung dose obtained with some pMDIs.

4 Combined In Vitro-In Silico Approach to Predict Deposition and Pharmacokinetics of Budesonide Dry Powder Inhalers

This chapter is published as Ruzycki, Conor A., Brynn Murphy, Hafeez Nathoo, Warren H. Finlay, and Andrew R. Martin. 2020. "Combined in Vitro-in Silico Approach to Predict Deposition and Pharmacokinetics of Budesonide Dry Powder Inhalers." Pharmaceutical Research 37 (10): 209. Portions have been edited to reduce redundancy with other chapters in this thesis. Reproduced with permission from Springer Nature.

4.1 Abstract

Purpose

A combined *in vitro – in silico* methodology was designed to estimate pharmacokinetics of budesonide delivered via dry powder inhaler.

Methods

Particle size distributions from three budesonide DPIs, measured with a Next Generation Impactor and Alberta Idealized Throat, were input into a lung deposition model to predict regional deposition. Subsequent systemic exposure was estimated using a pharmacokinetic model that incorporated Nernst-Brunner dissolution in the conducting airways to predict the net influence of dissolution, mucociliary clearance, and absorption.

Results

DPIs demonstrated significant *in vitro* differences in deposition, resulting in large differences in simulated regional deposition in the central conducting airways and the alveolar region. Similar but low deposition in the small conducting airways was observed with each DPI. Pharmacokinetic predictions showed good agreement with *in vivo* data from the literature. Peak systemic concentration was tied primarily to the alveolar dose, while the area under the curve was more dependent on the total lung dose. Tracheobronchial deposition was poorly correlated with pharmacokinetic data.

Conclusions

Combination of realistic *in vitro* experiments, lung deposition modeling, and pharmacokinetic modeling was shown to provide reasonable estimation of *in vivo* systemic exposure from DPIs. Such combined approaches are useful in the development of orally inhaled drug products.

4.1.1 List of Symbols

ρ_p	Particle density
AUC_{24}	Area under the curve (24 hours)
c	Drug concentration
c_i	Drug concentration in i^{th} airway compartment
c_{max}	Maximum serum concentration in central compartment
c_s	Drug solubility
CL	Clearance
D_d	Diffusion coefficient
$d_{g,50}$	Particle geometric mean diameter
F_{BA}	Oral bioavailability
F_i	Fraction of dose depositing in i^{th} compartment
h	Diffusion layer thickness
k_{12}	Central to peripheral rate constant
k_{21}	Peripheral to central rate constant
k_{10}	Elimination rate constant
k_a	Oral absorption rate constant
k_{ALV}	Alveolar region absorption rate constant
$k_{diss,ALV}$	Dissolution rate constant in alveolar region
$k_{muc,i}$	Mucociliary rate constant for i^{th} airway compartment
k_{TB}	Tracheobronchial region absorption rate constant
$K_{diss,TB}$	Effective dissolution rate in tracheobronchial region
m	Drug mass
$m_{i,1}$	Drug mass (solid) in i^{th} airway compartment
$m_{i,2}$	Drug mass (dissolved) in i^{th} airway compartment
P_m	Measured Pressure
P_{ref}	Reference Pressure
Q	Flowrate
Q_{peak}	Peak inhalation flowrate

R	Inhaler resistance
S	Surface area of particles undergoing dissolution
t	Time
$t_{\max}$	Time at which maximum serum concentration occurs
t_{total}	Duration of inhalation
T_{m}	Measured Temperature
T_{ref}	Reference Temperature
$V_{\text{ASL},i}$	Volume of airway surface liquid in i^{th} airway compartment
V_{C}	Volume of central compartment
$V_{\text{d,ss}}$	Volume of distribution at steady state

Subscripts

A	gastrointestinal tract compartment
ALV	alveolar
ASL	airway surface liquid
DPI	at the inlet of the inhaler
DPI exit	immediately downstream of inhaler mouthpiece
HBM	breathing machine line
P	peripheral compartment
TB	tracheobronchial
X	central compartment
supply	building air supply line
std	standard flowrate
vacuum	vacuum line
vol	volumetric flowrate

4.2 Introduction

The unique structure and physiology of the respiratory tract make it an attractive route for the delivery of therapeutics. Pharmaceutical aerosols, including bronchodilators and anti-inflammatories, are a mainstay in the treatment of lung disease (Hossny et al. 2016; Chung et al. 2014; Vogelmeier et al. 2017), with aerosols providing a vehicle for the direct delivery of therapeutics to the site of intended action. Such targeted delivery generally reduces systemic dosing and associated adverse side effects. Paradoxically, the respiratory tract is also a useful route for the systemic delivery of some medications, as the massive surface area of the gas-exchange region of the lungs can facilitate rapid uptake. Examples of inhalable therapeutics for systemic circulation include insulin for diabetes (Pittas, Westcott, and Balk 2015), loxapine for schizophrenia (San et al. 2018), and levodopa for Parkinson's disease (Olanow and Stocchi 2018). Delivery via the inhalation route generally allows for safe and convenient self-administration by patients while bypassing first-pass metabolism.

Dosing of inhaled pharmaceutical aerosols to the lungs, however, is highly specific to individual device-formulation combinations, with considerable inter- and intra-subject variability (Martin, Moore, and Finlay 2018). The physics governing aerosol generation and transport are complex, making it difficult to estimate where particles will deposit in the respiratory tract based on their diameter alone (Finlay 2019). Post-deposition, natural defense mechanisms in the respiratory tract including mucociliary clearance, enzymatic reactions, and resident macrophages all can influence drug localization, metabolism, absorption and retention (Ruge, Kirch, and Lehr 2013; Loira-Pastoriza, Todoroff, and Vanbever 2014). These considerations highlight the importance of establishing accurate measures of device and formulation performance that enable prediction of delivered doses, and ultimately clinical efficacy.

In vitro experiments, *in silico* computational models, and *in vivo* studies of lung deposition and pharmacokinetics all provide useful data that can inform inhalation device and formulation design (Koullapis et al. 2018; Martin, Moore, and Finlay 2018; Walenga, Babiskin, and Zhao 2019). By combining *in vitro* and *in silico* methods, *in vitro* data describing delivered drug mass and particle size distribution serves as input to numerical models that predict lung deposition and pharmacokinetics. Within such an approach, realistic *in vitro* methods can be used to characterize extrathoracic deposition and the initial lung dose, as well as the intra-thoracic particle size

distribution (Wei et al. 2018; Ruzycki, Martin, and Finlay 2019), after which numerical modeling can elucidate information on thoracic deposition and disposition. Several groups have proposed *in silico* models relating regional deposition to systemic exposure or response (Bhagwat et al. 2017; Bäckman, Tehler, and Olsson 2017; Boger and Fridén 2019; Caniga et al. 2016; Martin and Finlay 2018; Weber and Hochhaus 2013) following the initial forays into this approach in the 1980s by Byron (1986) and Gonda (1988).

In the present work, we demonstrate a method for evaluating dry powder inhaler performance in terms of clinically relevant metrics using a combination of realistic *in vitro* experimentation and *in silico* numerical modeling of lung deposition, airway surface liquid, and pharmacokinetics. Three commercially available budesonide inhalers were selected for comparative study. In an earlier work (see Chapter 3, i.e., Ruzycki, Martin, and Finlay [2019]), we evaluated the influences of inhaler insertion angle on deposition from these same DPIs in the Alberta Idealized Throat (providing an *in vitro* measure of extrathoracic deposition), and a downstream filter (providing an *in vitro* measure of the total lung dose). In the present work, we extend that testing to measure the intrathoracic particle size distribution from each DPI, and in conjunction with deposition and disposition modeling, estimate regional lung deposition and the systemic concentration of budesonide achieved with each DPI under typical use. We extend existing pharmacokinetic models for inhaled corticosteroids, which broadly differentiate lung doses in terms of central and peripheral compartments (Weber and Hochhaus 2013; Bhagwat et al. 2017; Soulele, Macheras, and Karalis 2018), to consider the competing mechanisms of particle dissolution, absorption, and mucociliary clearance in each tracheobronchial airway generation. The methods exemplified in the present study are intended to help bridge the gap between *in vitro* benchtop development and early-stage human trials, wherein emphasis is often placed on the systemic dose, particularly during the development and testing of generics (Lee et al. 2015; Lu et al. 2015).

4.3   Materials and Methods

Three commercially available DPIs with formulation strengths of 200 μg budesonide per dose were selected for testing, including Pulmicort® Turbuhaler® (Lot PASY; AstraZeneca Canada Inc. Mississauga, Canada), Easyhaler® Budesonide (Lot 1820769 Orion Pharma Espoo, Finland), and Budelin® Novolizer® (Lot 7A104; Meda Pharmaceuticals Inc. Takeley, United Kingdom).

DPIs were chosen to span a representative range of device resistances expected of typical devices. General characteristics of each DPI are presented in Table 4-1.

Table 4-1: Characteristics of each DPI selected for testing, along with inhalation parameters defined using the relations of Delvadia et al (Delvadia et al. 2016).

Inhaler	Label Claim (µg budesonide)	Doses	Device Resistance (Delvadia et al. 2016) R (kPa$^{1/2}$min/L)	Peak Inhalation Flowrate Q_{peak} ("/min)	Duration of Inhalation t_{total} (s)
Pulmicort Turbuhaler	200	200	0.0352	72.7	3.50
Easyhaler Budesonide	200	200	0.0435	62.8	4.05
Budelin Novolizer	200	100	0.0241	96.5	2.64

A three-part analysis incorporating experimental and numerical methods was developed and employed to compare the performance of these three DPIs having identical label claims. First, DPIs were characterized *in vitro* using measurements in an Alberta Idealized Throat placed upstream of a Next Generation Impactor with pre-separator (Model 170 NGI and pre-separator; MSP Corporation, Shoreview, MN). Second, *in vitro* results were fed into a regional lung deposition model to provide estimates of the initial doses of budesonide depositing throughout the lungs. Third, generational deposition and airway surface liquid concentrations calculated by the lung deposition model were used as input to a pharmacokinetic model to estimate the systemic plasma concentration of budesonide over time in a typical adult human. Specifics of each part of this study are discussed in the following sections.

4.3.1 In Vitro Performance Characterization

4.3.1.1 Experimental Design

The DPIs selected for the present study are passive devices, with each exhibiting some degree of flowrate-dependent performance (Weers and Clark 2017). With each DPI having a different airflow resistance, a subject inhaling with a certain inspiratory effort would likely generate inhalations with different peak inspiratory flowrates through each device (Delvadia et al. 2016). Traditionally the examination of DPIs with cascade impactors use methods similar to those described in the United States Pharmacopeia (United States Pharmacopeia 2019a), wherein the peak inhalation flowrate of a step-inhalation is chosen to generate a 4 kPa pressure drop across the

inhaler. In the present work we instead use semi-realistic inhalation profiles whose magnitudes and durations are chosen to reflect the unique airflow resistance of each DPI.

Specifically, we used the relations of Delvadia et al (Delvadia et al. 2016) that model the inhalation flowrate as a sinusoidal function of time (equations 7 and 8 in [Delvadia et al. 2016]), and selected the profiles representative of the 50th percentile achieved by healthy adults trained on the proper use of DPIs by health care professionals. The time to peak flowrate was taken as the median value reported in (Delvadia et al. 2016), 0.49 seconds (which was observed to be independent of device resistance). The duration of inhalation was calculated with equation 10 in (Delvadia et al. 2016) for an inhaled volume of 2.7 L, the median value reported across genders. The peak flowrate was calculated based on the device resistance as per equation 5 in Delvadia et al. (2016). Table 4-1 summarizes the peak inhalation flowrate and duration of inhalation for each DPI calculated using the device resistances reported by Delvadia et al (Delvadia et al. 2016); additional detail can be found in Chapter 3 (i.e., Ruzycki, Martin, and Finlay 2019). These parameters defining the inhalation patterns correspond to the volumetric flowrate exiting the mouthpiece of each DPI.

DPI performance was characterized using the setup detailed in Figure 4-1, in which deposition of budesonide from each inhaler was measured in an Alberta Idealized Throat and Next Generation Impactor with pre-separator. A Mixing Inlet (MSP Corporation, Shoreview, MN, USA) was incorporated to allow for the use of time-varying inhalations through DPIs while maintaining a constant inhalation flowrate across the cascade impactor. Airflow through the NGI was set to provide 100 L/min (volumetric) at the inlet of the first stage, and was generated using a vacuum pump (Model 2567-V1; Gast Mfg. Corp., Benton Harbor, MI). This steady flowrate was balanced with a line connected to building supply air such that zero flow developed across the DPI when the breathing machine was not in use. Upon actuation of the breathing machine, airflow from the supply line is reduced in a time-varying manner over the course of an inhalation. As airflow through the NGI is maintained at a constant rate of 100 L/min by the vacuum pump, air is drawn through the DPI to balance the flowrates entering and exiting the mixing inlet, according to conservation of mass.
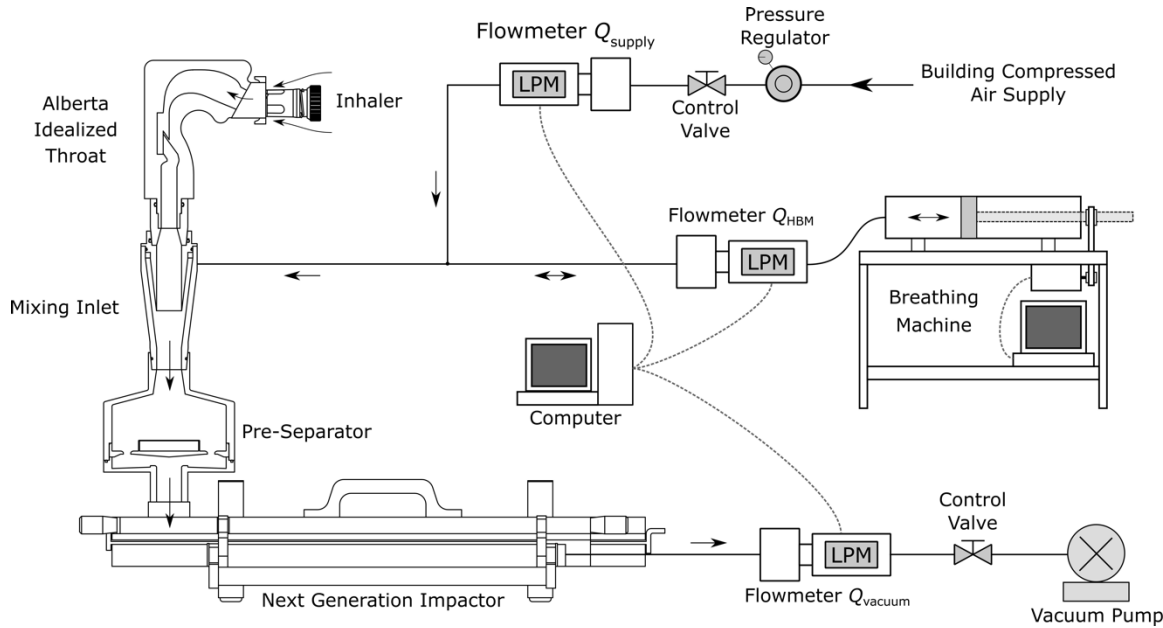
Figure 4-1: Experimental setup used to quantify deposition from dry powder inhalers. A mixing inlet downstream of the Alberta Idealized Throat allowed for experiments to be conducted with time-varying inhalation profiles while maintaining a constant flowrate through the Next Generation Impactor.

Flowrates (in standard L/min) in the supply, breathing machine, and vacuum lines were measured in 50 ms intervals using thermal mass flowmeters (Model 4043 in the supply and breathing machine lines, Model 4040 in the vacuum line; TSI Inc., Shoreview, MN, USA). The standard flowrate developed across the DPI during an inhalation, $Q_{\text{std,DPI}}(t)$, was calculated from these measurements following the conservation of mass, as shown in equation (4-1). Here the subscript "std" denotes that flowrates are reported in standard L/min, while "HBM," "vacuum," and "supply" refer to the breathing machine, vacuum, and supply lines in Figure 4-1, respectively.

$$Q_{\text{std,DPI}}(t) = Q_{\text{std,HBM}}(t) + Q_{\text{std,vacuum}}(t) - Q_{\text{std,supply}}(t) \qquad (4\text{-}1)$$

The volumetric flowrate developed at the exit of the DPI mouthpiece, $Q_{\text{vol,DPI exit}}(t)$, was then calculated using equation (3-4), which assumes that the relation between the pressure drop and flowrate is quasi-steady and that effects of ambient pressure on inhaler resistance are negligible. Full details on this derivation are presented in Appendix B.

Calculations were performed in real time using a custom LabVIEW program (LabVIEW Professional Development System 2017; National Instruments, Austin, TX, USA), coded to

display the actual inhalation profile generated across the DPI during testing. It is important to note that the inhalation profiles programmed into the breathing machine were similar, but not identical, to those described by equations 7 and 8 in Delvadia et al. (2016); as noted earlier, equations 7 and 8 in Delvadia et al. (2016) describe the volumetric flowrate *exiting the mouthpiece* of the DPI. Inhalation profiles input into the breathing machine were calibrated iteratively over the course of several test inhalations to accurately reproduce the unique profiles described by these equations for each DPI. These calibrations were performed with DPIs fixed to the Alberta Idealized Throat to account for potential damping effects of increased airflow resistance on the development of transient inhalation profiles (see discussion in Chapter 3, i.e., Ruzycki, Martin, and Finlay [2019]).

Prior to each experiment, both halves of the Alberta Idealized Throat, collection surfaces of the pre-separator, and each plate of the NGI were coated with a silicone release spray (Molycote 316; Dow Corning, Midland, MI, USA). Following solvent evaporation (~15 min), these components, together with the Mixing Inlet, were assembled as shown in Figure 4-1. Inhaler-specific adapters were fixed to the entrance of the Alberta Idealized Throat to provide airtight seals with each DPI during testing. Adapters were designed such that each DPI was aligned perpendicularly to the plane defining the entrance of the Alberta Idealized Throat, i.e., at an angle of 29° to the transverse plane. With these components in place, the vacuum pump downstream of the NGI was turned on, and the vacuum line flowrate was adjusted to provide a 100 L/min volumetric flowrate at the NGI inlet. Airflow from the supply line was then adjusted to ensure zero airflow developed across the DPI when the breathing machine was not in use.

Five actuations were used for a given inhaler during each experimental run. Prior to each actuation, the inhaler was primed following patient instruction leaflets; Pulmicort Turbuhaler was oriented vertically during priming, Budesonide Easyhaler was shaken up and down repeatedly for 3 to 5 seconds then oriented horizontally prior to priming, and Budelin Novolizer was oriented horizontally as it was primed. The inhaler was then attached to the Alberta Idealized Throat, and the breathing machine was actuated to deliver a single breath through the DPI. The inhaler was removed from the adapter, re-primed, re-attached to the adapter, and re-fired, until five total actuations had been delivered into the setup. As each DPI has a label claim of 200 µg budesonide (see Table 4-1), the total label claim for each experimental run regardless of inhaler was 1000 µg budesonide.

Components were then disassembled and washed with HPLC grade methanol to provide samples for UV spectroscopy: the Alberta Idealized Throat was washed twice with 10 ml of methanol, the pre-separator was washed three times with 10 mL of methanol, and each plate of the NGI was washed once with 5 mL of methanol. The mass of budesonide in each sample was quantified via UV absorbance relative to standards at 243 nm using a diode array UV-vis spectrophotometer (Cary 8454; Agilent, Santa Clara, CA, USA). Mass remaining within the DPI following each actuation was not assayed. The above procedure, corresponding to one experimental run, was performed five times with each DPI to allow for statistical comparisons.

Environmental conditions in the laboratory were monitored with a digital hygrometer/thermometer (MI70 Measurement Indicator with HMP75B Humidity and Temperature Probe; Vaisala, Vantaa, Finland). Ambient conditions during testing were as follows: temperature ranged from 22°C to 24°C, relative humidity ranged from 15% to 25%, and absolute pressure ranged from 91 kPa to 94 kPa.

4.3.1.2   In Vitro Data Analysis

Deposition of budesonide from each DPI (as raw mass, with a total label claim of 1000 µg, equal to 5 actuations from each 200 µg/dose DPI), was summarized using a number of common *in vitro* performance metrics (United States Pharmacopeia 2019b; 2019a; Hinds 1999). Deposition in the Alberta Idealized Throat was considered analogous to extrathoracic deposition *in vivo*. The sum of deposition on the pre-separator and each stage of the NGI was considered analogous to the total dose delivered to the lungs *in vivo* (including any exhaled fraction). Stage cutoff diameters were defined for 100 L/min using manufacturer's correlations. For simplicity, the sum of deposition in the pre-separator and NGI is referred to as the *in vitro* lung dose. Fine particle doses were defined for particles with aerodynamic diameters less than 5 µm. Extra-fine particle doses were defined for particles with aerodynamic diameters less than 2 µm. Mass median aerodynamic diameters and geometric standard deviations, along with fine-particle doses and extra-fine particle doses, were calculated via linear interpolation on particle size distributions (Hinds 1999).

Statistical comparisons of these *in vitro* performance metrics were performed using ANOVA, with post-hoc tests following Tukey's HSD criterion, at a significance level of 0.05. Comparisons were performed in MATLAB (R2018a; The MathWorks Inc, Natick, MA, USA) via the *anova1* and *multcompare* functions.

4.3.2   Lung Deposition

Assuming that the Alberta Idealized Throat approximates the extrathoracic region, the dose exiting the distal end of the Alberta Idealized Throat (i.e., the dose measured in the pre-separator and NGI) represents the *in vivo* total lung dose, while the particle size distribution measured in the pre-separator and NGI represent the initial particle size distribution of aerosol entering the thoracic airways. Here, this *in vitro* data was used as input to a well-established Lagrangian lung deposition model (Javaheri et al. 2013; Finlay, Lange, King, et al. 2000) to predict respiratory tract deposition from each DPI. Briefly, the model calculates particle deposition on a generational basis in an adult lung geometry consisting of 23 generations (Finlay, Lange, King, et al. 2000), with the trachea defined as generation 0, the tracheobronchial tree consisting of generations 0 to 14, and the alveolar region consisting of generations 15 to 23. Deposition mechanisms include inertial impaction, sedimentation, and diffusion during three phases of a breath including inhalation, breath hold, and exhalation. Inhalation parameters were set to equal those used during *in vitro* testing, i.e., an inhaled volume of 2.7 L over a time equal to those noted in Table 4-1. A breath hold of 10 sec and an exhalation time of 5.4 s were assumed for each inhaler. In the present study, hygroscopic effects were neglected through the assumption of stable particles.

Particle sizes used in the above correlations were taken as the geometric means of the bracketing cutoff diameters for the *in vitro* masses recovered from the stages of the NGI. The *in vitro* dose depositing in the pre-separator, for which there is no upper size limit, was distributed evenly among the bronchial airways (generations 0 to 8 following the International Commission on Radiological Protection [1994] model), given the low likelihood of particles greater than 10.0 μm diameter (the cutoff of the pre-separator at 100 L/min) escaping deposition in these airways for flowrates of interest (Chan and Lippmann 1980). We weigh the validity of this treatment in the discussion.

Modeling results were considered in terms of regional deposition in the bronchial (generations 0 to 8), bronchiolar (generations 9 to 14), and alveolar (generations 15 to 23) regions, in line with the lung morphology described by the International Commission on Radiological Protection (1994). Lung deposition modeling was performed only with the average measurements obtained *in vitro*, and no consideration was given to variations in lung geometry, inhalation patterns, etc. Results should therefore be considered as representative of trends expected to occur in an average adult population, rather than specific to a particular individual.

4.3.3 Airway Surface Liquid Modeling

Material depositing in the tracheobronchial airways is subject to mucociliary clearance. To capture such effects, an airway surface liquid model described in detail elsewhere (Finlay, Lange, King, et al. 2000; Martin and Finlay 2018; Lange et al. 2001) was used to predict properties of the airway surface liquid in each generation. Briefly, this model estimates the thickness of the periciliary sol and the mucous layer in each tracheobronchial airway generation for specified values of daily mucous production and tracheal clearance velocity. The periciliary sol and mucous layer are modeled as concentric annular layers. The thickness of the periciliary sol is approximated by the estimated lengths of the cilia lining the airways (Lange et al. 2001). The mucous layer thickness is estimated via mass conservation and a model of generational mucous clearance velocities based on the specified values of daily mucous production and tracheal clearance velocities (Finlay, Lange, King, et al. 2000).

The model predicts, for each tracheobronchial airway generation, the volume of airway surface liquid and the rate of clearance due to mucociliary action (quantified with the first order rate constant $k_{\text{muc},i}$). Here, the tracheal clearance velocity and daily mucus production were set to 10 mm/min and 10 mL/day, respectively, representative of typical values in healthy adults. For these values, airway surface liquid volumes in the various generations of the tracheobronchial airways fall between 0.11 and 0.36 mL. Airway surface liquid volumes were also considered independent of the amount of deposited drug, a reasonable assumption considering the small volumes of drug involved in the present work. First order rate constants describing mucociliary clearance were defined for each generation based on the ratio between the airway surface liquid volumetric flowrate at the trachea and the generational airway surface liquid volume output computed by the airway surface liquid model.

4.3.4 Pharmacokinetic Modeling of Systemic Doses

A recently developed compartmental disposition model (Martin and Finlay 2018) was used to translate predictions of lung deposition into a more traditional measure of drug exposure, i.e. the systemic dose of drug and its evolution over time. This pharmacokinetic model is shown schematically in Figure 4-2.
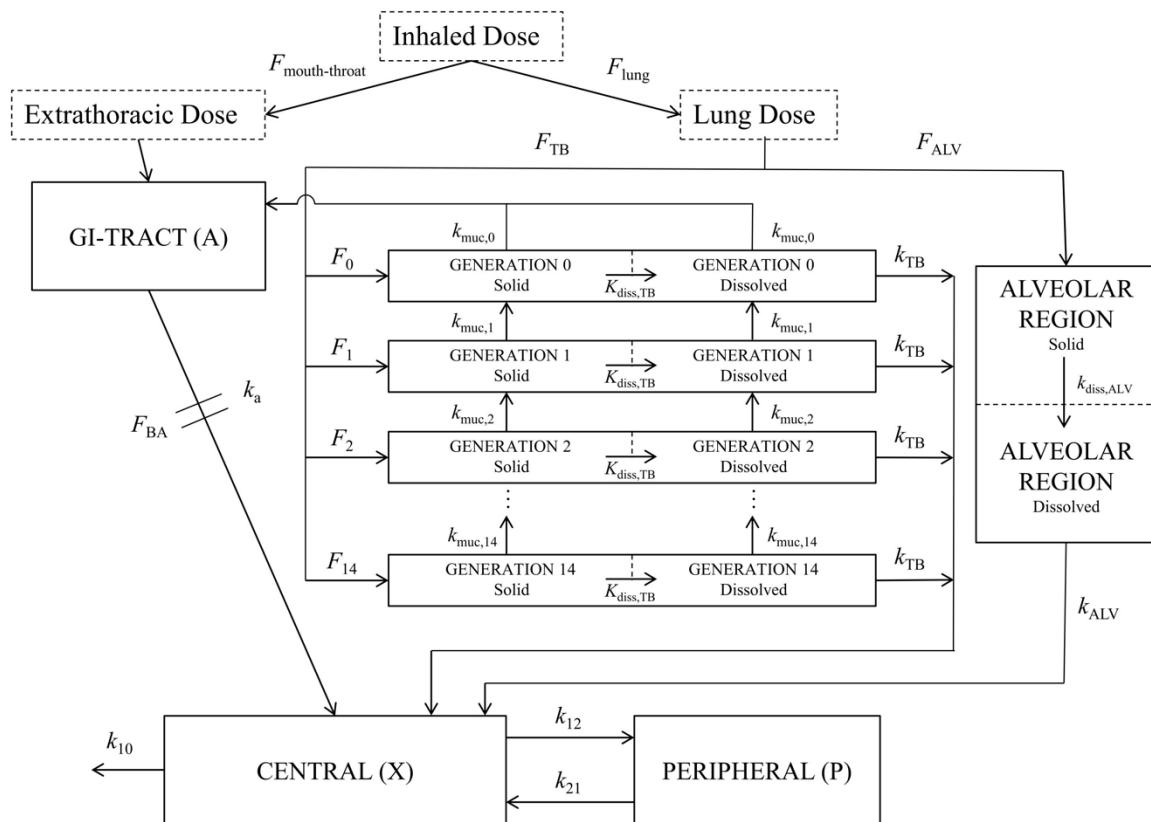
Figure 4-2: Schematic of the pharmacokinetic model used to predict systemic doses of budesonide from each DPI. First order rate constants k describe the trasition of drug among various compartments. The fraction (F) of the lung dose depositing in each generation of the trachebronchial airways and in the alveolar region is calculated via the lung deposition model. An effective rate constant $K_{diss,TB}$ is used to model dissolution in the tracheobronchial airways.

The lung is comprised of one compartment representing the alveolar region and 15 compartments representing the tracheobronchial airways. The fraction of the dose of budesonide depositing in each compartment (F) is obtained from the lung deposition model described previously. In each lung compartment, the solid and dissolved portions of drug are considered separately. Solid drug is subject to dissolution in airway surface liquid or alveolar lining fluid. In the alveolar region, this process is described using a first order rate constant $k_{diss,ALV}$, equal to 17.8 hr^{-1} for budesonide following the study of Weber and Hochhaus (2013). In the tracheobronchial airways, particle dissolution is instead modeled as a Nernst-Brunner type diffusion process (May et al. 2014), allowing for the incorporation of effects relating to particle size and drug solubility (see the

subsection titled *Dissolution Model in the Tracheobronchial Airways*). Mucociliary clearance, which acts to shuttle both dissolved and solid budesonide from deeper generations of the tracheobronchial airways towards the trachea, is characterized by first order rate constants, $k_{\mathrm{muc},i}$ (ranging from 1.8 to 5.4 hr^{-1}, as derived from the airway surface model discussed above), estimated from the airway surface liquid model. Dissolved budesonide is subject to absorption from the alveolar region according to the rate constant k_{ALV}, estimated as 20 hr^{-1} (Weber and Hochhaus 2013), and from each generation of the tracheobronchial airways according to the rate constant k_{TB}, estimated as 10 hr^{-1} (Weber and Hochhaus 2013). As discussed by Weber and Hochhaus (2013), these rate constants are arbitrarily chosen to represent fast absorption of a lipophilic substance from the alveolar region, and slightly slower absorption from the tracheobronchial airways.

A separate compartment representing the gastrointestinal tract accounts for the dose depositing in the extrathoracic region (here measured *in vitro* with the Alberta Idealized Throat) and drug removed from the lungs via mucociliary clearance. Absorption of budesonide from the gastrointestinal compartment is governed by the oral bioavailability F_{BA}, 0.107 (Ryrfeldt et al. 1982), and the rate constant k_{a}, 0.45 hr^{-1} (Weber and Hochhaus 2013). Two cases were considered for each DPI, the first using the oral bioavailability for budesonide from the literature (as above), and the second with the oral bioavailability set to zero to simulate the effects of a continual charcoal block, given the use of this technique in some pharmacokinetic studies *in vivo*.

The body itself is represented with a standard two compartment central-peripheral model, with the central compartment consisting of blood and well-perfused organs, and the peripheral compartment consisting of poorly perfused tissues. Drug transfer between these compartments is governed by rate constants k_{12} and k_{21}, equal to 20.01 hr^{-1} and 11.06 hr^{-1} for budesonide, respectively (Weber and Hochhaus 2013). Other general pharmacokinetic parameters are as follows. The volume of distribution at steady state, $V_{\mathrm{d,SS}}$, was set as 183 L (Thorsson, Edsbacker, and Conradson 1994; Hochhaus et al. 1997). Clearance, CL, was taken as 83.7 L/hr (Ryrfeldt et al. 1982). The volume of the central compartment, V_{C}, was calculated to be 65.1 L from equation (4-2), adapted from Yates and Arundel (2008). Finally, the elimination rate constant k_{10}, 1.29 hr^{-1}, was calculated by dividing the clearance by the volume of the central compartment, i.e. $k_{10} =$

CL/V_C (Yates and Arundel 2008), under the assumption that elimination occurs entirely from the central compartment.

$$V_C = \frac{V_{d,SS}}{1 + \frac{k_{12}}{k_{21}}} \qquad (4\text{-}2)$$

4.3.4.1 Dissolution Model in the Tracheobronchial Airways

Drug dissolution is commonly modelled as a Nernst-Brunner process (Dokoumetzidis and Macheras 2006), which combines the diffusion layer concept with Fick's second law of diffusion. For Nernst-Brunner dissolution, the limiting step that governs how dissolution proceeds is the diffusion of molecules across a stagnant film of liquid (the diffusion layer) surrounding submerged solids. The general equation describing this process, when written in terms of the mass of solid material m at time t, is

$$\frac{dm}{dt} = -\frac{D_d S}{h}\left(c_s - c(t)\right). \qquad (4\text{-}3)$$

D_d is the diffusion coefficient of the substance in the solvent, S is the surface area of submerged solids, h is the diffusion layer thickness, c_s is the solubility of the substance in the solvent, and $c(t)$ is the concentration of the substance in the solvent outside of the diffusion layer at a particular time.

In the present work, we assumed that particles depositing in the tracheobronchial airways are quickly drawn into the airway surface liquid and are submerged fully (Schürch et al. 1990), and that the subsequent dissolution of said particles is governed by a Nernst-Brunner process. Equation (4-3) was recast in terms of an effective rate constant $K_{diss,TB}$, and was applied to the mass of solid (undissolved) drug in each specific generation (m_i, itself varying with time), as per equation (4-4).

$$\frac{dm_i}{dt} = -K_{diss,TB} m_i(t)(c_s - c(t)) \qquad (4\text{-}4)$$

The effective rate constant $K_{diss,TB}$ was expressed in terms of the particle geometric median diameter $d_{g,50}$ (calculated from *in vitro* measurements of MMADs, assuming spherical particles), particle density ρ_p (1270 kg/m³ for budesonide), solubility of micronized budesonide in the airway

surface liquid (16 µg/mL [Hastedt et al. 2016]), and the diffusion coefficient D (6.19×10^{-6} cm²/min for budesonide in water at 37 °C [May et al. 2014]) as per equation (4-5).

$$K_{\text{diss,TB}} = \frac{12D}{\rho_{\text{P}} d_{\text{g,50}}^2} \qquad (4\text{-}5)$$

This expression for $K_{\text{diss,TB}}$ assumes that the diffusion layer thickness h was equal to the particle radius (valid for particle radii smaller than 30 µm [May et al. 2014; Hintz and Johnson 1989]) and that the total surface area and the mass of particles are well-approximated by particles with the geometric median diameter. As a further simplification, $K_{\text{diss,TB}}$ was assumed to be constant with time. These assumptions, and their influence on the systemic dose, are considered in the discussion. The effective rate constant was calculated individually for each DPI based on our *in vitro* measurements.

The pharmacokinetic model described above yielded a system of ordinary differential equations describing the mass of drug in each compartment over time. Full details regarding these equations are provided in Appendix C. This system was solved in spreadsheet format in Microsoft Excel using explicit Euler time advancement over a 24-hour period, with uniform timesteps of 0.01 hr to achieve timestep-independent results (Martin and Finlay 2018). Standard pharmacokinetic parameters including the area under the curve in 24 hours (AUC_{24}), the maximum concentration (c_{max}), and the time to maximum concentration (t_{max}) were determined from the calculated distributions. The present model did not consider variations in parameters (like the volume of distribution, absorption rates, clearance, etc.) as would occur in a population. Like the lung deposition model, results should be considered representative of trends occurring in an average adult population, rather than being specific to a particular individual. We consider the feasibility of incorporating variability in the above models in the discussion.

The *in vivo* pharmacokinetics of inhaled budesonide have been well-studied in the literature, particularly with Pulmicort Turbuhaler. Systemic concentrations as estimated in the present work were compared to a number of *in vivo* pharmacokinetic studies of inhaled budesonide in healthy or mildly asthmatic adults, including those by Thorsson, Edsbäcker, and Conradson (1994; 1000 µg via Turbuhaler, with and without charcoal block), Argenti, Shah, and Heald (2000; 600 µg via Turbuhaler), Duddu et al (2002; 800 µg via Turbuhaler, with charcoal block), Harrison and Tattersfield (2003; 1200 µg via Turbuhaler), Lähelmä et al. (2005; 1000 µg via Turbuhaler and

Easyhaler, with charcoal block), Möllmann et al. (2001; 1000 µg via Turbuhaler), Thorsson et al. (2001; 1000 µg via Turbuhaler), Mortimer et al. (2007; 800 µg via Turbuhaler), and Hämäläinen et al. (2001; 800 µg via Turbuhaler and Easyhaler) to validate model estimates of the systemic dose. For Budelin Novolizer, no pharmacokinetic data was found in the literature aside from single data points in two summary of product characteristics (SmPCs), one from the UK (Mylan Products Ltd 2018) and one from Slovenia (Meda Pharma GmbH 2017), which are included for completeness. *In vivo* pharmacokinetic profiles were scaled, where necessary, to a dose of 1000 µg under the assumption of dose linearity for inhaled budesonide (Kaiser et al. 1999). *In vivo* data reported in molar units was transformed to a gram-basis using the molecular weight of budesonide, 430.534 g/mol.

4.4   Results

Particle size distributions of budesonide measured *in vitro* are shown in Figure 4-3. A summary of relevant *in vitro* parameters, including the doses of budesonide measured in the Alberta Idealized Throat and in the NGI and pre-separator, is provided in Table 4-2. Significant differences, denoted by dashed bars in Table 4-2, are evident. Deposition in the Alberta Idealized Throat was significantly different for all DPIs (ANOVA; $p < 0.0001$), ranging from 398.0 µg with Turbuhaler to 1041.0 µg with Easyhaler. The *in vitro* lung dose was greatest with Turbuhaler (at 439.8 µg), almost twice the amount measured with Easyhaler (228.2 µg; $p < 0.0001$) or Novolizer (261.3 µg; $p < 0.0001$). The comparison of *in vitro* lung dose between Easyhaler and Novolizer was the only comparison here that failed to reach statistical significance ($p = 0.2816$). For mass median aerodynamic diameter, Easyhaler (3.62 µm) yielded larger particles than Turbuhaler (2.18 µm; $p < 0.0001$), which in turn yielded slightly larger particles than Novolizer (1.94 µm; $p = 0.0069$). The fine particle and extra fine particle doses were considerably smaller for Easyhaler (169.1 µg and 79.6 µg, respectively) than observed with the other inhalers. For Novolizer, most of the *in vitro* lung dose was contained in extra-fine particles, with an extra-fine particle dose of 210.1 µg.
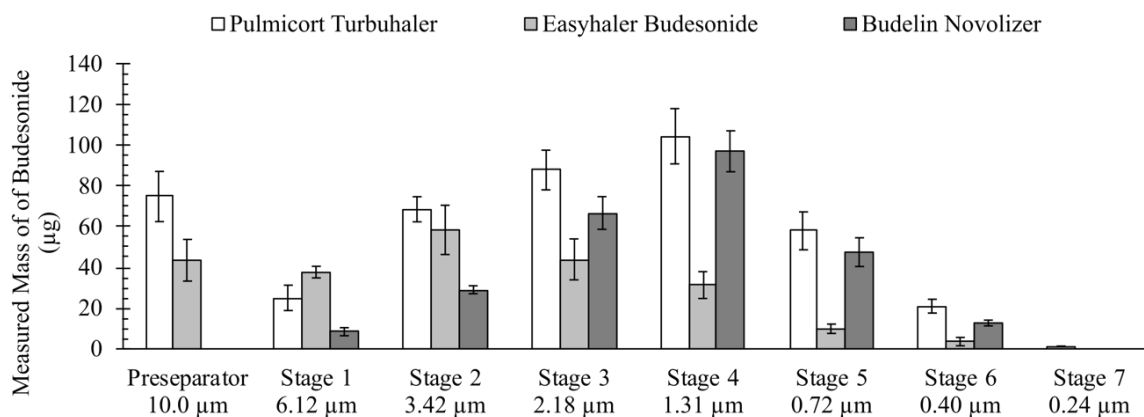
Figure 4-3: Particle size distributions measured downstream of the Alberta Idealized Throat with each DPI, expressed as the average mass of budesonide measured on the pre-separator and each stage of the Next Generation Impactor. Cutoff diameters correspond to operation of the NGI at 100 L/min. Error bars denote standard deviation.

Table 4-2: *In vitro* measurements and performance metrics, expressed as average (standard deviation in parenthesis, n = 5). Significant differences are represented by dashed bars.

Parameter	Pulmicort Turbuhaler	Easyhaler Budesonide	Budelin Novolizer
Delivered Dose (µg)	837.8 (57.0)	1269.3 (92.1)	988.7 (34.7)
Alberta Idealized Throat Deposition (µg)	398.0 (24.4)	1041.0 (119.2)	727.4 (44.5)
Next Generation Impactor + pre-separator Deposition (µg)	439.8 (36.8)	228.2 (32.6)	261.3 (27.7)
Fine Particle Dose, < 5 µm (µg)	354.6 (40.1)	169.1 (34.1)	257.8 (27.7)
Extra-fine Particle Dose, < 2 µm (µg)	253.3 (30.8)	79.6 (18.7)	210.1 (24.2)
Mass Median Aerodynamic Diameter (µm)	2.18 (0.08)	3.62 (0.15)	1.94 (0.02)
Geometric Standard Deviation (-)	2.09 (0.03)	1.99 (0.04)	1.76 (0.01)

The *in vitro* differences summarized in Table 4-2 manifested in differences in calculated regional lung deposition, as shown in Figure 4-4. Calculated bronchial deposition (generations 0 to 8) ranged from 117 µg with Turbuhaler to 27 µg with Novolizer. Calculated alveolar deposition also ranged considerably, from 263 µg with Turbuhaler to 116 µg with Easyhaler. In contrast, calculated deposition in the bronchiolar region (generations 9 to 14) was more comparable between inhalers, ranging from 37 µg with Turbuhaler to 24 µg with Novolizer.
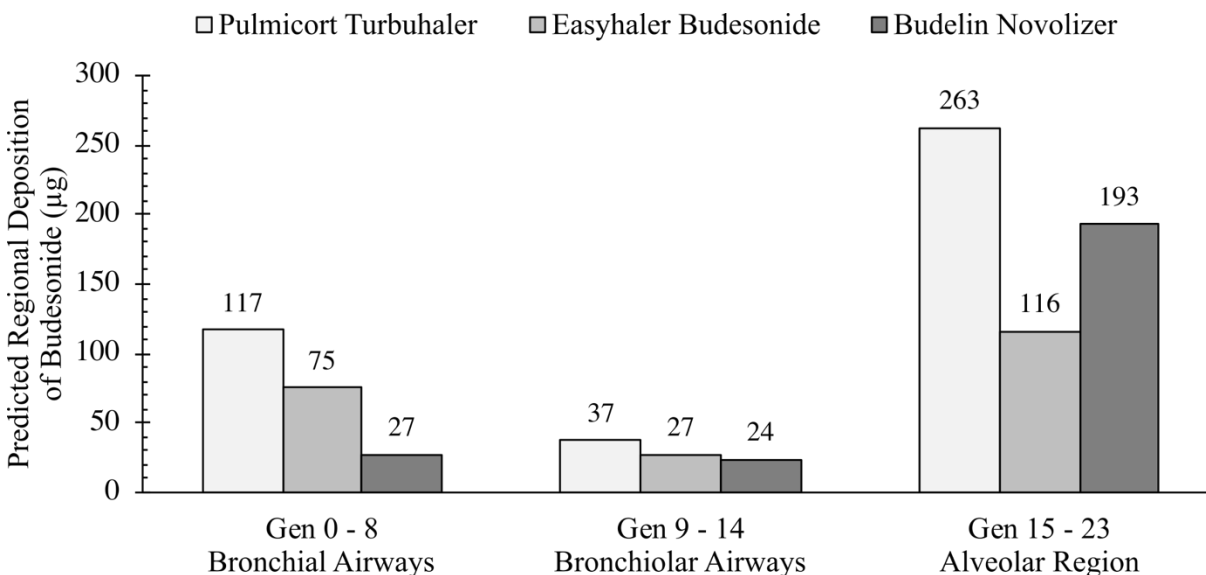
Figure 4-4: Calculated regional lung deposition of budesonide based on the particle size distributions measured *in vitro* (Figure 4-3) and the inhalations defined in Table 4-1 for the adult lung geometry of Finlay et al (2000).

For the prediction of systemic dose, the effective rate constant $K_{diss,TB}$ was first calculated for each DPI based on the *in vitro* data using equation (4-5), yielding 93.4, 34.0, and 118.0 $m^3/kg \cdot hr$ for Turbuhaler, Easyhaler, and Novolizer respectively. The system of equations comprising the model was then solved numerically. The resulting systemic profiles are shown in Figure 4-5, together with *in vivo* data from the literature for Turbuhaler, Easyhaler, and Novolizer. As noted in the methods, data was scaled to an effective dose of 1000 µg when necessary under the assumption of dose linearity for inhaled budesonide (Kaiser et al. 1999).
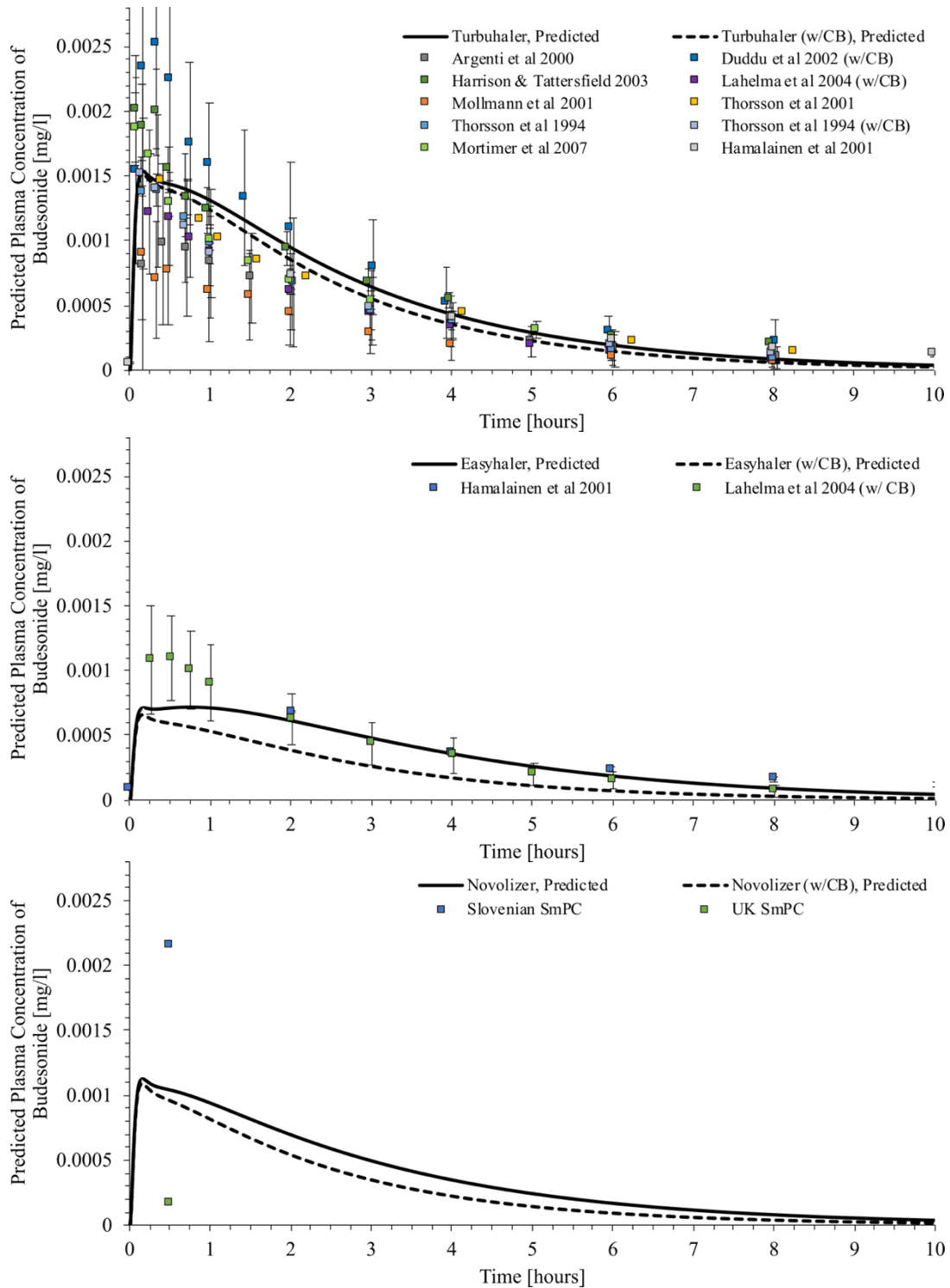
Figure 4-5: Calculated plasma concentrations with and without oral absorption for (top) Pulmicort Turbuhaler (middle) Easyhaler Budesonide and (bottom) Budelin Novolizer. *In vivo* data from the literature has been scaled, when necessary, to a dose of 1000 µg budesonide. w/CB = with charcoal block.

Standard pharmacokinetic parameters are presented in Table 4-3. For the case where no charcoal block was simulated, Turbuhaler was estimated to yield the largest area under the curve in 24 hours, at 4.87 µg·hr/l, with Easyhaler and Novolizer yielding smaller values of 3.34 and 3.73 µg·hr/l, respectively. In terms of systemic concentration, Easyhaler Budesonide demonstrated two peaks of similar values, 0.71 µg/l at 0.17 hr and 0.72 µg/l at 0.75 hr. Turbuhaler yielded the highest estimated peak concentration, at 1.54 µg/l, while Novolizer fell in the middle, at 1.13 µg/l. Time to peak concentration was the same for each DPI (0.16 to 0.17 hr). For predictions with charcoal block, the AUC decreased considerably with each inhaler, while the peak systemic concentration remained similar. The double peak occurring with Easyhaler Budesonide disappeared in the simulation with charcoal block.

Table 4-3: Summary of calculated pharmacokinetic parameters for each DPI. w/o CB = without charcoal block, w/ CB = with charcoal block.

DPI	Area Under the Curve, 24 hours AUC_{24} (μg·hr/L)		Peak Systemic Concentration c_{max} (μg/L)		Time to Peak Concentration t_{max} (hr)	
	w/o CB	w/ CB	w/o CB	w/ CB	w/o CB	w/ CB
Pulmicort Turbuhaler	4.87	4.29	1.54	1.52	0.16	0.16
Easyhaler Budesonide	3.34	1.94	0.71 / 0.72*	0.66	0.17 / 0.75*	0.16
Budelin Novolizer	3.74	2.79	1.13	1.09	0.16	0.16

* Easyhaler Budesonide demonstrated two peaks in the simulation without charcoal block, the second peak being denoted by asterisk.

4.5 Discussion

In the present study, we use *in silico modeling to* extend *in vitro* measurements of DPIs to predict regional lung deposition and systemic exposure. To illustrate the method, three marketed budesonide DPIs spanning a range of device characteristics were selected for testing. The *in vitro* results presented herein demonstrate considerable *in vitro* differences in performance between these DPIs (see Table 4-2). Subsequent *in silico* modeling permitted estimation of how these differences may or may not result in differences in regional deposition or in pharmacokinetic

parameters, such as systemic dose and peak concentration. Several interesting observations arising through these combined *in vitro – in silico* methods are discussed below.

The *in vitro* measurements indicate that despite having the same label claim of 200 µg budesonide, there is variation in the amount of drug leaving the mouthpiece between the DPIs when tested with semi-realistic inhalation profiles. Delivered doses ranged from 837.8 µg with Turbuhaler (167.6 µg per actuation) to 1269.3 µg with Easyhaler (253.9 µg per actuation), and are in excellent agreement with a recent paper by our group using the same inhalers in a different experiment (Ruzycki, Martin, and Finlay 2019). Such differences in DPI output compared to the label claim are well documented in the literature (Weers and Clark 2017), and may be partly explained by batch-to-batch variation. Of note is the agreement of our measured MMADs with values in the literature for each DPI (Parisini et al. 2014; Yoshida et al. 2017; Wei et al. 2017). Parisini et al. (2014) measured an MMAD for Easyhaler Budesonide of 3.92 (SD 0.24) µm with the NGI plus pre-separator following compendial methods, versus 3.62 (SD 0.15) µm measured here. Yoshida et al. (2017) measured an MMAD for Pulmicort Turbuhaler of 2.20 (SD 0.06) µm with the NGI plus pre-separator at a flowrate of 75 L/min, versus 2.18 (SD 0.08) µm measured here. Wei et al. (2017) measured an MMAD for Budelin Novolizer of 1.86 (SD 0.06) µm with the NGI (without pre-separator) downstream of their anatomical VCU medium mouth-throat model with a realistic inhalation similar to that used in the present work, versus 1.94 (SD 0.02) µm measured here. Our match to the data of Parisini et al. (2014) with Easyhaler Budesonide and Yoshida et al. (2017) for Pulmicort Turbuhaler despite our use of the Alberta Idealized Throat and their use of the United States Pharmacopeia Induction Port (USP-IP) can be explained through the action of the pre-separator. The USP-IP is known to significantly underestimate mouth-throat deposition, but the inclusion of the pre-separator means that larger particles that would deposit within the extrathoracic tract *in vivo* are removed by the pre-separator prior to entering the NGI itself. In the present work, the Alberta Idealized Throat acts as an analogue of the extrathoracic region (Ruzycki, Martin, and Finlay 2019), allowing for a deeper interpretation of the dose depositing on the pre-separator. The observation of a considerable dose on the pre-separator for Pulmicort Turbuhaler and Easyhaler Budesonide implies that a non-negligible dose of large particles penetrates past the extrathoracic region for some DPIs. This does not appear to be the case with Budelin Novolizer; here the dose recovered from the pre-separator with this inhaler was below quantifiable limit while only 8.4 ± 2.0 µg of budesonide were recovered from plate 1. This

corroborates well with the measurement of less than 5 µg on the first plate of the NGI (without pre-separator) from Budelin Novolizer by Wei et al (2017) downstream of their anatomical throat model. A proper investigation of the penetration of large particles through the Alberta Idealized Throat during a realistic inhalation requires additional experimentation with a measurement technology that can size large particles over a time-varying inhalation, e.g., time-of-flight aerodynamic sizers or laser light scattering systems.

Of more interest to the present discussion is how *in vitro* differences in delivered dose and particle size distributions result in more clinically relevant measures. Predicted lung deposition, shown in Figure 4-4, lends evidence to the notion that differences in performance *in vitro* can result in large differences in lung deposition. For Turbuhaler, relatively small particles (MMAD of 2.18 [SD 0.08] µm) coupled with a large *in vitro* lung dose resulted in a large predicted alveolar dose of 263 µg. For Easyhaler, larger particles (MMAD of 3.62 [SD 0.15] µm) coupled with a decreased *in vitro* lung dose resulted in a much smaller predicted alveolar dose of 116 µg. For Novolizer, whose *in vitro* lung dose was not significantly different than Easyhaler (261.3 vs. 228.2 µg respectively; $p = 0.2816$), small particle sizes (MMAD of 1.94 (SD 0.02] µm) resulted in increased alveolar deposition (at 193 µg). One factor to bear in mind with the above interpretation lies in the treatment of the un-sized portion of the *in vitro* lung dose, i.e., the dose measured in the pre-separator. As noted in the methods, the dose measured on the pre-separator was distributed evenly among the bronchial airways (corresponding to generations 0 to 8 in the present lung model), based on the low likelihood of particles greater than 10 µm (the cutoff of the pre-separator at 100 L/min) escaping deposition in these airways at flowrates of interest. For example, at a flowrate of 60 L/min (less than the peak value used with each DPI in the present work), more than 60% of particles with an aerodynamic diameter of 10 µm are predicted to deposit in generations 0 to 8 based on the correlation of Chan & Lippmann (1980). For 15 µm particles, deposition in these airways increases to more than 90%. This treatment, though rudimentary, allows for the consideration of this dose without assigning an arbitrary upper particle size (note that while deposition in the Alberta Idealized Throat has been well-characterized [Dehaan and Finlay 2004; Grgic et al. 2004], the time varying inhalations developed through the throat in the present setup preclude the definition of a useful "throat cutoff diameter," or upper size limit for the initial thoracic dose, and such a "throat cutoff diameter" would be rather coarse compared to a well-designed impactor plate regardless). It is this un-sized dose that dominates the bronchial deposition of Turbuhaler and Easyhaler in the

present model, especially when compared to Novolizer, for which deposition measured in the pre-separator was below quantifiable limit. As noted above, a thorough investigation of this effect requires use of a different measurement technique than cascade impaction. A takeaway is that one should consider both the sized and un-sized portions of the dose measured *in vitro* in predicting lung deposition; the MMAD alone may not be sufficient in describing regional lung deposition from inhalers.

Our predictions of a small deposition fraction in the bronchiolar airways (generations 9 to 14 in the present lung model) are consistent with the known difficulty in targeting deposition to these small conducting airways (Walenga and Longest 2016). Some have suggested that inhaled corticosteroids like budesonide may provide increased therapeutic benefit when targeted to the small airways (Hamid et al. 1997; Dekhuijzen 2012; Van Den Berge et al. 2013). Estimated bronchiolar deposition is similar for these DPIs despite their performance spanning a range of *in vitro* characteristics, suggesting that particle size and device design can only go so far in targeting delivery to certain lung regions. Optimizing delivery beyond the limits of these conventional approaches may require more sophisticated techniques. Two potential approaches include pulsed bolus delivery (Ostrovski et al. 2019) and enhanced condensational growth (Tian, Longest, Su, and Hindle 2011), though both techniques require technology beyond what is used in typical passive DPIs.

The lung deposition model used herein does not account for bolus effects, and thus some differences in deposition between that calculated here and what occurs *in vivo* may be expected to occur. Bolus emission of aerosols from DPIs has been studied numerically (Kopsch, Murnane, and Symons 2016), but the distribution of particles within the bolus (in terms of number and size) is not well-characterized, precluding the use of more advanced deposition modeling that incorporate bolus effects. It is also tempting to draw direct comparisons between predictions of deposition in the tracheobronchial airways and alveolar region with central-peripheral deposition measured via scintigraphy *in vivo*, some data of which exists for these inhalers (Borgström et al. 1994; Newman et al. 2000; Hirst et al. 2001; Hirst, Newman, et al. 2002). However, a direct one-to-one correlation is not possible owing to inherent difficulties in registering radioactivity to specific anatomical areas in the lungs, particularly with 2-dimensional scintigraphy data (Fleming et al. 2015).

Beyond predictions of regional lung deposition, the present methodology further allows for the modeling of systemic dosing based on the location of deposition in the lung. Calculated systemic concentrations of budesonide, shown in Figure 4-5, and the peak systemic concentrations and area under the curves, shown in Table 4-3, are in good agreement with data from the literature (Thorsson, Edsbacker, and Conradson 1994; Argenti, Shah, and Heald 2000; Duddu et al. 2002; Harrison and Tattersfield 2003; Lähelmä et al. 2005; Mollmann et al. 2001; Thorsson et al. 2001; Mortimer et al. 2007; Hämäläinen et al. 2001), suggesting the present methodology provides reasonable estimates of typical *in vivo* measures of inhaler performance. A number of observations can be made on the relationship between calculated regional lung deposition and pharmacokinetic parameters, as shown in Figure 4-6 (wherein simple linear regression was performed in Excel for the purposes of illustration) for the case where absorption from the gastrointestinal tract was considered. Firstly, peak systemic concentration correlates extremely strongly with the alveolar dose (R^2 = 0.9994; Figure 4-6a), while a weaker correlation is obtained between peak systemic concentration and the total lung dose (R^2 = 0.8414; Figure 4-6c). This is attributable to the rapid uptake of budesonide modeled from the alveolar compartment (k_{ALV} = 20 hr^{-1} (Weber and Hochhaus 2013)) as compared to the tracheobronchial region (k_{TB} = 10 hr^{-1} (Weber and Hochhaus 2013)), but also depends on the rate of dissolution for particles depositing in the alveolar liquid lining fluid versus the airway surface liquid in the tracheobronchial airways. In the present model, dissolution and uptake occurs more rapidly in the alveolar region than in the tracheobronchial region, with the end result being that the peak systemic concentration is dependent primarily on the dose depositing in the alveolar region. In contrast, the area under the curve shows a closer correlation with the total lung dose (R^2 = 0.9821; Figure 4-6d) than with the alveolar dose (R^2 = 0.9182; Figure 4-6b). Consideration of only the alveolar dose misses the significant contribution of absorption from the tracheobronchial airways that occurs over longer timespans. Figure 4-6e and Figure 4-6f show that neither the peak systemic concentration nor the area under the curve are well correlated with deposition in the tracheobronchial region (generations 0 to 14). In this region mucociliary clearance shunts a portion of the tracheobronchial dose into the gastrointestinal tract, where the low bioavailability of budesonide limits its contribution to the systemic dose. These standard pharmacokinetic parameters, therefore, do not appear to provide much useful information on the deposition of budesonide specifically in the tracheobronchial airways. Such may be the case

with other inhaled therapeutics with limited solubility in airway surface liquid and low oral bioavailability.
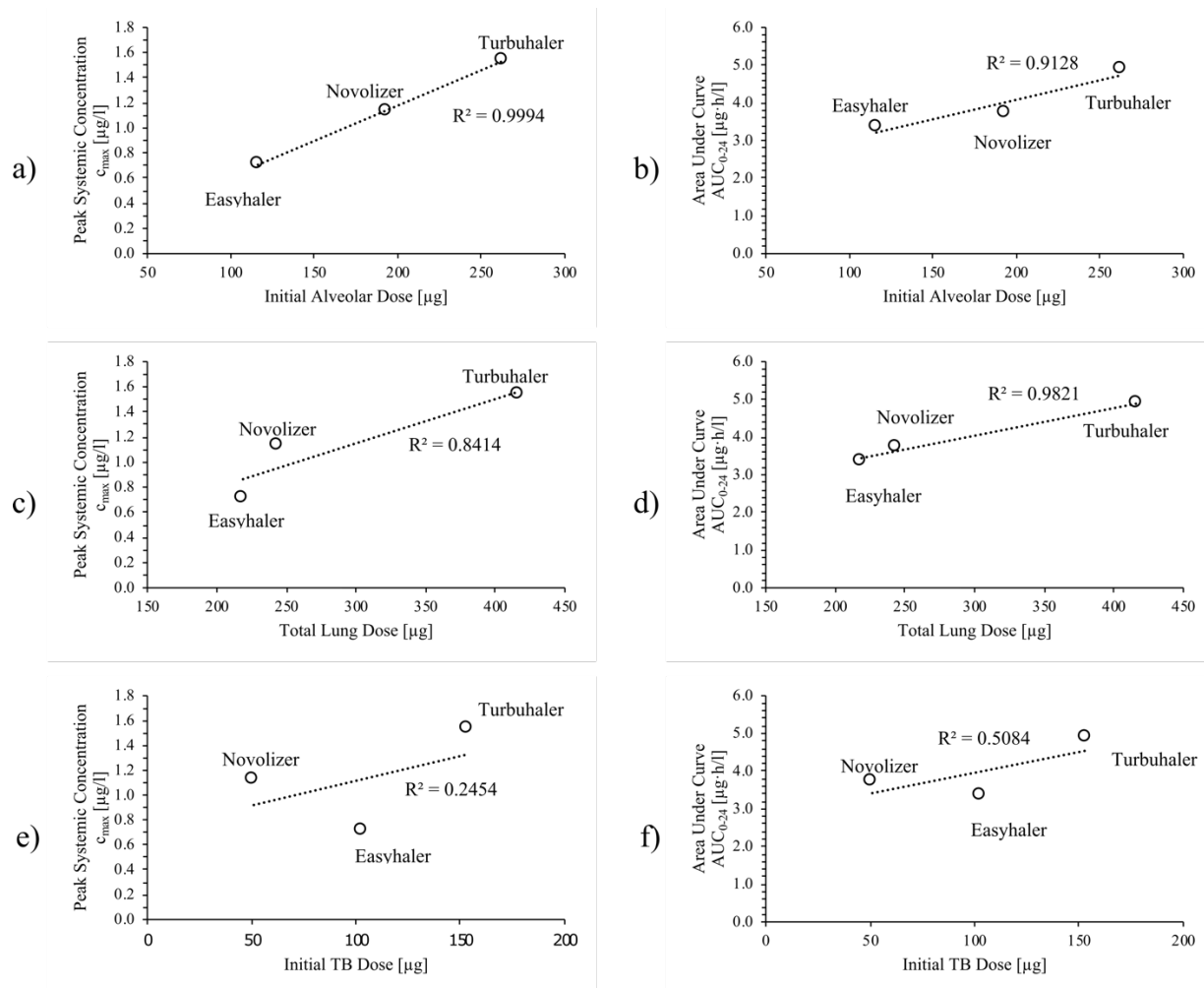
Figure 4-6: Correlations between calculated regional deposition and predicted pharmacokinetic parameters, including (a) peak systemic concentration versus initial alveolar dose, (b) area under curve versus initial alveolar dose, (c) peak systemic concentration versus total lung dose, (d) area under curve versus total lung dose, (e) peak systemic concentration versus tracheobronchial dose, and (f) area under the curve versus tracheobronchial dose, considering absorption from the gastrointestinal tract.

In the pulmonary biopharmaceutical classification system proposed by Hastedt et al (2016), budesonide lies close to the critical band defining a dissolution-limited drug (budesonide itself is not considered dissolution-limited owing to its moderate solubility). We suspect that our finding of limited correlation between tracheobronchial deposition and pharmacokinetic measures of peak

systemic concentration and area under the curve extends to dissolution-limited drugs with low oral bioavailability (e.g. beclomethasone dipropionate, fluticasone propionate, among others [Hastedt et al. 2016]), wherein mucociliary clearance removes much of the tracheobronchial dose before dissolution and absorption can occur.

The present pharmacokinetic model assumes that dissolution in the tracheobronchial airways can be modeled using a Nernst-Brunner diffusion process, but does not extend this assumption to the alveolar region. In a Nernst-Brunner process, particles are assumed to be fully submerged and are surrounded by a stagnant diffusion layer with a thickness comparable to the particle size. The assumption of full submersion may be reasonable in the conducting airways, where the airway surface liquid is sufficiently deep (Hastedt et al. 2016), and where surface tension acts to quickly draw deposited particles into the aqueous subphase below the mucous layer (Schürch et al. 1990). Regarding the assumption of stagnant diffusion layers surrounding submerged particles, we suppose that the beating action of cilia, which must induce some motion in the airway surface liquid to facilitate clearance (Smith, Gaffney, and Blake 2008), is a complicating factor that may require a deeper analysis. In the much thinner alveolar lining fluid (~ 0.2 μm [Hastedt et al. 2016]), the assumptions of full submersion of a particle and the presence of a diffusion layer of comparable thickness are more tenuous, meaning that the kinetics of dissolution in the alveolar region are probably not well-described with a classical Nernst-Brunner process. Others have suggested using modified Nernst-Brunner processes to describe dissolution in the alveolar region (Eriksson et al. 2019; Bäckman and Olsson 2020); the most sophisticated of these models necessitates experimental determination of wettability (Eriksson et al. 2019). However, an analytical model of dissolution in the extremely thin alveolar fluid has thus far eluded development. As the validity of these approaches remains to be determined, we defer to a simpler model based on *in vivo* data that models alveolar dissolution with a first order rate constant (Weber and Hochhaus 2013). Considering that each DPI used here delivers micronized budesonide, and that particles that deposit in the alveolar region will have similar diameters, we do not expect considerable differences between these DPIs in dissolution behavior, due to e.g., solubility, that are not captured by this treatment. The agreement between our model outputs and the available *in vivo* data suggests this is a reasonable approximation for micronized budesonide. For novel drugs and formulations, validated models of dissolution in the alveolar region are required before *a priori* prediction of drug disposition can be accurately performed from first principles.

The advantage of modeling dissolution as a Nernst-Brunner process arises from the ability to predict how changes to formulation factors like drug solubility and particle size influence *in vivo* performance. Experimental measurements of dissolution and solubility (May et al. 2014; Floroiu et al. 2018) can be incorporated into the present model to inform how changes in formulation affect dissolution rates and absorption in the tracheobronchial airways. Dissolution testing suggest that there is some time-dependence to the thickness of the diffusion layer surrounding particles (May et al. 2014), but the exact form of this time-dependence is unknown. Here we have assumed that the dissolution rate is constant with time, which will underestimate the speed of dissolution in the tracheobronchial region. As our modeling suggests that the alveolar dose is the driver of the peak systemic concentration, such effects are less important in the context of systemic pharmacokinetics than they are in the determination of local drug concentrations in the airway surface liquid, a topic to be explored in future work.

As noted by Weber and Hochhaus (2013), the rate constants used to model absorption from the alveolar and tracheobronchial airways were chosen arbitrarily. Physiologically-based pharmacokinetic modeling could be incorporated to inform these rate constants based on experimental measurements of membrane permeabilities and tissue retention, along with estimates of membrane surface areas and blood volumes in relevant regions of the lungs, as has been explored in a number of recent publications (Eriksson et al. 2019; Bäckman and Olsson 2020; Hochhaus et al. 2020). Noting that it remains unclear as to how best to implement the results of various methods for assessing drug permeability with absorption in different regions of the lung (Bäckman et al. 2018), and considering the general agreement between the predictions from our model and the *in vivo* data for Turbuhaler, the rate constants of Weber and Hochhaus (2013) appear reasonable in the place of more advanced physiologically-based pharmacodynamic modeling for our purposes, especially as the mathematical relationships between absorption rates and drug masses in these various models are similar. Advanced modeling techniques will certainly be indispensable, however, in extending the utility of the present methodology towards novel drugs and formulations.

A comparison of the estimated systemic concentrations with and without charcoal block, from Figure 4-5 and Table 4-3, suggests that despite the low oral bioavailability of budesonide a non-negligible amount of drug enters systemic circulation through the gastrointestinal tract (via either

the initial extrathoracic dose or dose removed from the conducting airways through mucociliary clearance). This effect is more important for inhalers that demonstrate higher extrathoracic deposition. For inhaled corticosteroids, wherein systemic pharmacokinetic data is often considered as indicative of the level of adverse side effects, use of a charcoal block during *in vivo* testing to estimate equivalence of the lung dose (Olsson et al. 2013) will mask these effects.

Available clinical evidence suggests that the budesonide DPIs used in the present work are similarly efficacious in the treatment of asthma (Chuchalin et al. 2002; Vanto et al. 2004; Schweisfurth et al. 2002). The similarity of the dose delivered to the small conducting airways may play a role here given the hypothesized importance of delivery to this region for efficacious action of inhaled corticosteroids (Hamid et al. 1997; Dekhuijzen 2012; Van Den Berge et al. 2013). Other factors to consider include whether the doses delivered to target tissues from these DPIs lie on the plateau of the dose-response curve, and whether the clinical studies used to evaluate equivalence are sufficiently powered to be able to identify any clinically meaningful difference. It is important to note that the present model does not allow for the prediction of local effects of deposited drug; a deeper interpretation of local therapeutic effects of inhaled corticosteroids requires the implementation of more advanced physiologically-based pharmacokinetic modelling (Eriksson et al. 2019; Bäckman and Olsson 2020; Hochhaus et al. 2020) together with pharmacodynamics. Budesonide itself poses an interesting problem here, as there is evidence of fatty-acid esterification and subsequent re-release of budesonide from lung tissue (Van Den Brink et al. 2008) that complicates drawing conclusions on local drug action based on free drug concentrations in the airway surface liquid post-dosing. Nevertheless, promising developments in models of drug action have recently been described (see e.g. the receptor occupancy model for inhaled corticosteroids described by Shao et al [2020]), and such models could be incorporated to the current methodology to expand its usefulness towards novel formulations.

Another limitation of the present work relates to the absence of estimates of variability in regional deposition or pharmacokinetic profiles. Extension of the present model to incorporate some inherent randomness in parameter values in the form of stochastic lung deposition modeling and population pharmacokinetics remains a topic for future work. In principle, one could couple *in vitro* testing to stochastic models of lung deposition and population pharmacokinetics to ultimately predict clinical metrics in a population. This approach is not trivial, however, as variability in one

step should inform variability in subsequent steps, and the prediction of variability *in vitro* remains an unsettled topic of investigation. *In vitro* tests on variability should incorporate not just varying inhalation parameters (Delvadia et al. 2016), but also varying throat geometries (Ruzycki et al. 2017)—and in some cases inhaler insertion angles (Ruzycki, Martin, and Finlay 2019)—to capture the large degree of variability observed between subjects, which complicates the experimental methods beyond the scope of the present work.

4.6   Conclusions

The combination of realistic *in vitro* experiment, lung deposition modeling, and pharmacokinetic modeling was shown to provide reasonable estimates of *in vivo* plasma concentration profiles of budesonide from DPIs. For the three DPIs examined here, significant differences *in vitro* resulted in large differences in calculated regional lung deposition in the upper conducting (bronchial) airways and the alveolar region. However, deposition in the small conducting (bronchiolar) airways was comparatively modest for each DPI, despite the wide range of aerosol characteristics measured *in vitro*. Results here also suggest that for budesonide, peak systemic concentration is tied primarily to the alveolar dose, while the area under the curve is more dependent on the total lung dose. Tracheobronchial deposition was poorly correlated with pharmacokinetic data, suggesting that pharmacokinetic data for systemic exposure, by itself, may fail to provide useful information on deposition specifically in the conducting airways for budesonide, and likely for more dissolution-limited drugs as well. A strength of the proposed methodology lies in the ability to estimate commonly sought-after clinical parameters from *in vitro* data.

5 In Vitro – In Silico Characterization of Nebulizers used in Methacholine Challenge Testing to Guide Provocative Dose Determinations through Hygroscopic Deposition Modeling

Portions of this chapter have been submitted as a conference abstract: Ruzycki, Conor A., David Pawluski, Eric Y.L. Wong, Warren H. Finlay, and Andrew R. Martin. Submitted November 2nd, 2021. "In Vitro – In Silico Characterization of Lung Deposition for Nebulizers used in Methacholine Challenge Testing," American Thoracic Society 2022 International Conference.

5.1 Abstract

Methacholine challenge testing (MCT) is frequently used to diagnose airway hyper-reactivity. The European Respiratory Society (ERS) technical standard on MCT supports a shift towards reporting results in terms of the provocative dose rather than the provocative concentration but does not specify a means for quantifying exhaled doses. Here, we use an *in vitro – in silico* approach based on *in vitro* measurements and hygroscopic lung deposition modeling to predict lung deposition and exhaled doses from various nebulizers proposed for MCT. We hypothesize that a significant fraction of the inhaled dose will be exhaled back out of the lungs, given the small droplet sizes produced by nebulizers traditionally used for MCT.

 Emitted doses, particle sizes, and the temperature and humidity of the nebulized airstream were measured for three nebulizers (RX160, Roxon Meditech; Hudson RCI Micro Mist (HRCI), Teleflex; AirLife Misty Max 10 (MM10), CareFusion) at methacholine chloride concentrations of 0.0625, 1, and 16 mg/mL in 0.9% saline solutions. Experimentally measured emitted doses at a concentration of 1 mg/mL were 42.0 (SD 5.1) µg from the RX160 over 120 s, 96.3 (SD 33.7) µg from the HRCI over 60 s, and 162.3 (SD 38.4) µg from the MM10 over 60 s. Dry gas flowrates used to drive the nebulizers were 9.0 L/min for the RX160 and 5.0 L/min for the HRCI and MM10. For a typical inhalation from a healthy adult breathing through a nebulizer (tidal volume 0.86 L, inhalation time 2.52 s, inspiratory:expiratory ratio of 1:1), the inhaled dose was half of the emitted dose. Predicted extrathoracic deposition fractions were very low, being negligible with the RX160 and approximately 0.05 with the HCRI and MM10. For the 1 mg/mL methacholine chloride solution, the fraction of the inhaled dose predicted to deposit in the lungs was 0.40 (8.3 µg) for the RX160, 0.62 (29.6 µg) for the HRCI, and 0.60 (48.7 µg) for the MM10. Predicted exhaled dose fractions were greatest with the RX160 (0.60), and similar for the HCRI (0.34) and MM10 (0.36).

Hygroscopic modeling thus suggests that the exhaled dose obtained during methacholine challenge testing is significant, with the characteristics of the nebulizer influencing the relative proportion of the dose that is exhaled. More accurate quantification of the provocative dose may be facilitated using the methodology described here.

5.2 Introduction

Airway hypperresponsiveness is an indication that can aide in the diagnosis of asthma (Sterk et al. 1993). The identification and quantification of airway hyperreactivity is facilitated through challenge testing that induces bronchoconstriction in a controlled manner. Various methods for inducing bronchoconstriction are described in the literature, with methacholine challenge testing (MCT) being one of the more widely used methods in modern pulmonary function laboratories (Cockcroft, Davis, and Blais 2019). In MCT, a nebulizer is used to deliver sequentially increasing doses of methacholine to a patient whose airway function is quantified after each dose, typically through measurement of the forced expiratory volume in 1 second (FEV1). Historically, the endpoint for MCT was the concentration of methacholine solution used in the nebulizer that results in a reduction of the FEV1 of 20% compared to baseline, referred to as the provocative concentration (PC_{20}). Toleration of the highest concentration of methacholine (typically 16 mg/mL) without a reduction in FEV1, considered as a negative MCT, is normally viewed as excluding a diagnosis of current asthma (Coates et al. 2017).

The recently released technical standards on MCT from the European Respiratory Society (ERS; Coates et al. 2017) sought to update best practices for MCT considering research and clinical experience subsequent to the earlier guidelines published by the American Thoracic Society (see Crapo et al. [2000]). A well-recognized limitation of MCT is the sensitivity of PC_{20} to the test method and the type of nebulizer used during administration. For example, the PC_{20} measured with the classic English Wright nebulizer, for example, can vary considerably from the PC_{20} obtained with more modern devices (El-Gammal et al. 2015). To address this limitation, the ERS standard recommends a shift to reporting test results in terms of the provocative dose of methacholine resulting in a 20% reduction in FEV1 (PD_{20}) rather than the PC_{20}. Such a shift is well justified by the action of methacholine on smooth muscle receptors, wherein the strength of the stimulus is directly related to the number of molecules (i.e., the dose) of methacholine delivered to the airways (Coates et al. 2017).

Quantification of the delivered dose of methacholine to the thoracic airways requires *in vitro* measurements to characterize nebulizer output rate and particle size distributions (Coates et al. 2018). Appendix E in the ERS technical standard suggests that the delivered dose be taken as the dose of methacholine contained in particles smaller than 5 micrometers (herein referred to as the fine particle fraction, or FPF), under the assumption that particles smaller than 5 micrometers penetrate into the lungs and deposit fully (Coates et al. 2017). An *in vitro* experiment to determine the output rate of methacholine (in mg/min) may involve the use of a suitable chemical tracer or surrogate, while particle size can be measured using conventional techniques like laser diffraction. The delivered dose obtained with such a method is taken simply as the output rate of methacholine from the nebulizer, $\dot{m}_{MC}$, multiplied by the FPF and the inhalation time, t_{in} (the portion of the time spent tidal breathing where the patient is inhaling):

$$F_{dose} = \dot{m}_{MC} \cdot \text{FPF} \cdot t_{in}. \tag{5-1}$$

Studies using this approach to estimate the PD_{20} have generally found more consistent correlations of results across disparate protocols than are provided by the PC_{20} (Dell et al. 2015; Schulze et al. 2009; Davis et al. 2017; Blais et al. 2017).

One of the challenges with this approach is the characterization of particle size distributions from legacy devices. For example, the legacy English Wright nebulizer, the prototypical device used in MCT (Crapo et al. 2000), has a very low solution nebulization rate (calibrated to 0.13 mg/mL during MCT) and emits particles that may be too small to reliably measure via laser diffraction (Coates, Leung, and Dell 2014). Measurements with alternative techniques suggest that the English Wright nebulizer emits aerosols with a mass median diameter (MMD) of approximately 0.75 to 1.5 µm (Ryan et al. 1981; Crapo et al. 2000) so that a considerable fraction of particles are below the lower detection diameter limit of optical laser diffraction equipment.

A related issue concerns the shift to conducting MCT using modern nebulizers, which emit much larger aerosols at greater nebulization rates, with the consequence that considerably higher doses of methacholine can be delivered to the patient during MCT, absent appropriate adjustments to protocols. The ERS standard also recommends, as an inhalation protocol, tidal breathing with an inhalation period of at least 1 min (Coates et al. 2017). This effectively sets a lower limit for delivered dose that can be much higher with high-output-rate modern nebulizers than with legacy

nebulizers. For example, Coates, Leung, and Dell (Coates, Leung, and Dell 2014) predict that the AeroEclipse II breath actuated nebulizer would deliver in 12 s the same dose that the English Wright would deliver over 120 s for a given stock concentration of methacholine. As such, the selection of appropriate devices and protocols for MCT requires careful consideration.

As noted in the ERS technical standard, "some of the inhaled aerosol may be exhaled before it has time to deposit in the lungs" (Coates et al. 2017, p.9). Equation (5-1), while attractive in its simplicity, does not allow for an estimation of this exhaled dose. The exhaled dose is itself dependent on multiple factors (Finlay 2019) including the nature of the inhaled aerosol (e.g., particle size distribution and hygroscopicity), the breathing pattern (e.g., tidal volume, flowrate, use of a breath hold), and characteristics of the patient (e.g., geometry of the respiratory tract). For tidal inhalations without a lengthy breath hold, the exhaled dose for micrometer-sized and sub-micrometer-sized particles can be significant (International Commission on Radiological Protection 1994). In the context of MCT, accurate estimation of the exhaled dose obtained with disparate devices and protocols would aide in quantifying the delivered dose and in improving correlations of results based on the clinical endpoint of PD_{20}. However, estimation of exhaled doses is complicated by the potential for hygroscopic behaviour of nebulized methacholine aerosols in the respiratory tract. Strong evaporative effects are known to occur with the English Wright nebulizer, and the saline stock solution used with MCT carries a high potential for hygroscopic growth within the respiratory tract upon inhalation (Javaheri et al. 2013; Golshahi, Tian, et al. 2013; Javaheri and Finlay 2013). As such, hygroscopic effects may have large impacts on deposition in the lungs, and their consideration is important when aiming to quantify both the delivered and exhaled doses.

In the present work, we develop an *in vitro – in silico* methodology to characterize the performance of various nebulizers proposed for use with MCT. *In vitro* experiments were performed to evaluate (a) emitted doses, (b) the airstream conditions exiting the nebulizers, and (c) residual particle sizes, allowing for back-calculation of aerosol characteristics upon exiting the nebulizer mouthpiece. Resulting data provided the initial conditions for a previously-validated hygroscopic lung deposition model (Javaheri et al. 2013; Finlay, Lange, King, et al. 2000) with modifications to capture the behavior of MCT aerosols. Lung deposition modeling allowed for the quantification of the mass of drug depositing in the respiratory tract and the mass of drug exhaled for different

devices and stock concentrations of methacholine. Further consideration was given to deposition in the tracheobronchial airways, the region of the lungs where the target tissue (smooth muscle; see Coates et al. [2017]) for methacholine is predominantly located (Ochs and Weibel 2015). The approach described herein may aide in providing more accurate quantification of the PD_{20} for MCT obtained with different test protocols and delivery devices.

5.3 Material and Methods

Three nebulizers (RX160 Wright-Type, Roxon Meditech; Hudson RCI Micro Mist (HRCI), Teleflex; AirLife Misty Max 10 (MM10), CareFusion) were selected for testing. The RX160 is essentially a modern version of the English Wright nebulizer, for which instructions for use with MCT follow the original ATS guidelines (i.e., calibrate the compressed air flow to the nebulizer to obtain a solution nebulization rate of 0.13 mg/min, administer each dose of methacholine with the 2 minute tidal breathing method; Crapo et al. 2000). The HRCI and MM10 are disposable unvented jet nebulizers that, when compared to the RX160, provide higher drug output rates and larger particle sizes based on manufacturer specifications. Both the HRCI and MM10 have been used to conduct MCT in Canadian pulmonary function laboratories and are proposed as replacements for the RX160.

5.3.1 In Vitro Nebulizer Characterization

Nebulizers were driven with compressed dry air, with the driving pressure measured via pressure gauge (general-purpose stainless-steel gauge, 0 to 30 psi; Swagelok) and flowrate measured via thermal mass flowmeter (Model 4043; TSI Incorporated, Shoreview, MN, USA). RX160 nebulizers used in the present work were operated at flowrates calibrated to provide a solution nebulization rate of 0.13 mg/min (quantified by measuring the nebulizer before and after testing). For the three RX160s used in the present work, the calibrated flowrates were 8.9, 9.0, and 9.1 L/min (at which the corresponding gauge pressure was 18.5 psi). The HRCI and MM10 were operated with compressed dry air at a flowrate of 5.0 L/min (with gauge pressures of 10 and 12.5 psi, respectively), the minimum flowrate for which information on device performance is supplied by the manufactures. This minimum flowrate was chosen to reduce as much as possible the nebulization rate provided by these higher output rate nebulizers without jeopardizing device performance. Unless otherwise noted, RX160 nebulizers were operated for a 2 min period, while the HRCI and MM10 were operated for 1 min, with an initial fill volume of 3 mL.

In vitro performance of each nebulizer was evaluated in a three-part analysis to quantify emitted doses, airstream conditions including temperature and humidity, and residual particle sizes. Emitted dose tests were performed using a 1 mg/mL ciprofloxacin surrogate in 9 mg/mL saline. Airstream conditions and residual particle sizes were measured using three solutions relevant for MCT: low (0.0625 mg/mL methacholine chloride in 9 mg/mL saline), medium (1 mg/mL methacholine chloride in 9 mg/mL saline), and high (16 mg/mL methacholine chloride in 9 mg/mL saline) concentrations of methacholine, in addition to measurements taken with the diluent only (9 mg/mL saline).

5.3.1.1   Emitted Dose

Methacholine for inhalation is formulated from methacholine chloride added to isotonic saline (i.e., 9 mg/mL aqueous solution of NaCl) to obtain methacholine chloride concentrations ranging from 0.0625 mg/mL to 16 mg/mL. Methacholine itself is challenging to assay, with the ERS standards suggesting that a suitable surrogate can be used to evaluate nebulizer emitted doses (Coates et al. 2017). Here, ciprofloxacin (via ciprofloxacin hydrochloride hydrate) was used as a surrogate owing to its ease of assay via UV spectroscopy.

Stock solutions of 1 mg/mL ciprofloxacin (prepared as 1.16 mg/mL ciprofloxacin hydrochloride hydrate) in 9 mg/mL saline were used to evaluate emitted doses. A glass fiber filter (VP7100 viral/bacterial filter; KEGO corporation, London, ON, Canada) was placed immediately downstream of the nebulizer output (RX160) or Tee-piece (HRCI and MM10) to capture nebulized aerosol, with flowrate through the filter generated by a vacuum pump (Model RV5; Edwards Ltd., Crawley, West Sussex, England). An open configuration (i.e., not air-tight) was used to avoid over-pressuring nebulizers prior to testing, with the vacuum pump operating at a flowrate of 30 L/min (well above that of the driving flowrate for the nebulizer) to ensure that all emitted aerosol was captured on the filter (see Figure 5-1). A simple on-off valve and stopwatch were used to manually control the delivery time from each nebulizer. After reaching the prescribed delivery time, the air supply to the nebulizer and the vacuum pump were turned off, and the filter was disconnected for chemical assay.

The dose of ciprofloxacin captured on the filter—the emitted dose—was recovered using a 7:3 volumetric mixture of DIUF water and methanol as solvent (methanol was added to facilitate wetting of the hydrophobic filter surface). Ciprofloxacin content was quantified using a diode array

UV-vis spectrophotometer (Cary 8454; Agilent, Santa Clara, CA, USA), using the spectrum peak at 277 nm and valley at 302 nm. Three rinses (first with 25 mL, the second and third with 10 mL each) of the filter gave sufficient recovery, with subsequent rinses giving below quantifiable limit. Additional details, including an evaluation of dose linearity for different concentrations of ciprofloxacin, are presented in Appendix D. Nebulizers were weighed before and after each test with a digital mass balance to determine the solution nebulization rate.
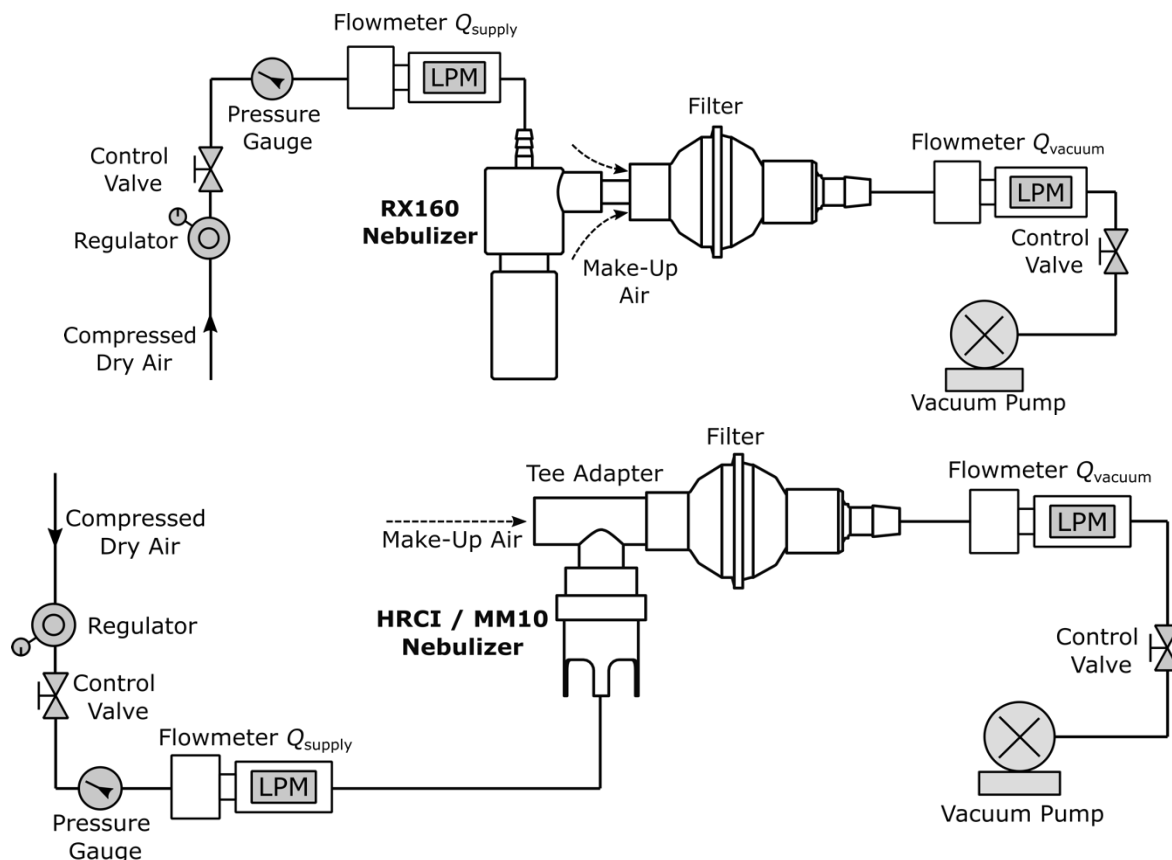
Figure 5-1: Setup used to quantify the emitted dose of methacholine (via a ciprofloxacin surrogate). Slight difference in setup between (top) the RX160 nebulizer and (bottom) the HRCI and MM10 nebulizers were necessitated by differences in device design.

Three RX160 nebulizers were obtained for testing, and five repeated measurements of the emitted dose were performed for each individual nebulizer (total n = 15). Five HRCI and five MM10 were tested as well, with three repeated measurements of emitted dose for each individual nebulizer (likewise, total n = 15). Statistical comparisons of emitted doses from each type of nebulizer were performed using ANOVA, with post-hoc tests following Tukey's HSD criterion, at a significance level of 0.05. Comparisons were performed in MATLAB (R2018a; The MathWorks Inc, Natick,

MA, USA) via the *anova1* and *multcompare* functions. Though we use ciprofloxacin as a surrogate for quantifying the emitted dose, results in the remainder of this chapter are discussed in terms of the emitted dose of methacholine chloride for the sake of clarity.

5.3.1.2   Airstream Conditions

The temperature and humidity of the airstream emitted by the nebulizer were recorded with a calibrated digital hygrometer/thermometer (HMP75B Humidity and Temperature Probe with MI70 Measurement Indicator, accuracy ±1.0 % RH for 0 to 90% RH, ± 1.7% RH for 90 to 100% RH; Vaisala, Vantaa, Finland). Using a tee connector as an access port, the probe head was placed directly in the emitted airstream of the nebulizer with a small foil shroud used to prevent droplet impaction on its surface (see Figure 5-2). The probe was also operated in "sensor preheat" mode to avoid condensation on the sensor during testing. Temperature and humidity were measured and recorded in 1 s intervals, with the averages calculated over the appropriate interval (2 min for RX160, 1 min for HRCI and MM10) taking into consideration the response time of the HMP75B probe itself (see Appendix E for additional details).

One RX160 was used for testing, with five replicated measures obtained with each solution of interest (i.e., low, medium, and high methacholine concentrations, plus diluent only). Five HCRIs and five MM10s were used to examine each solution of interest once. Among each type of nebulizer, measurements of the average temperature and humidity over the administration time at each solution of interest were compared with ANOVA using the *anova1* function in MATLAB, with a significance level of 0.05.
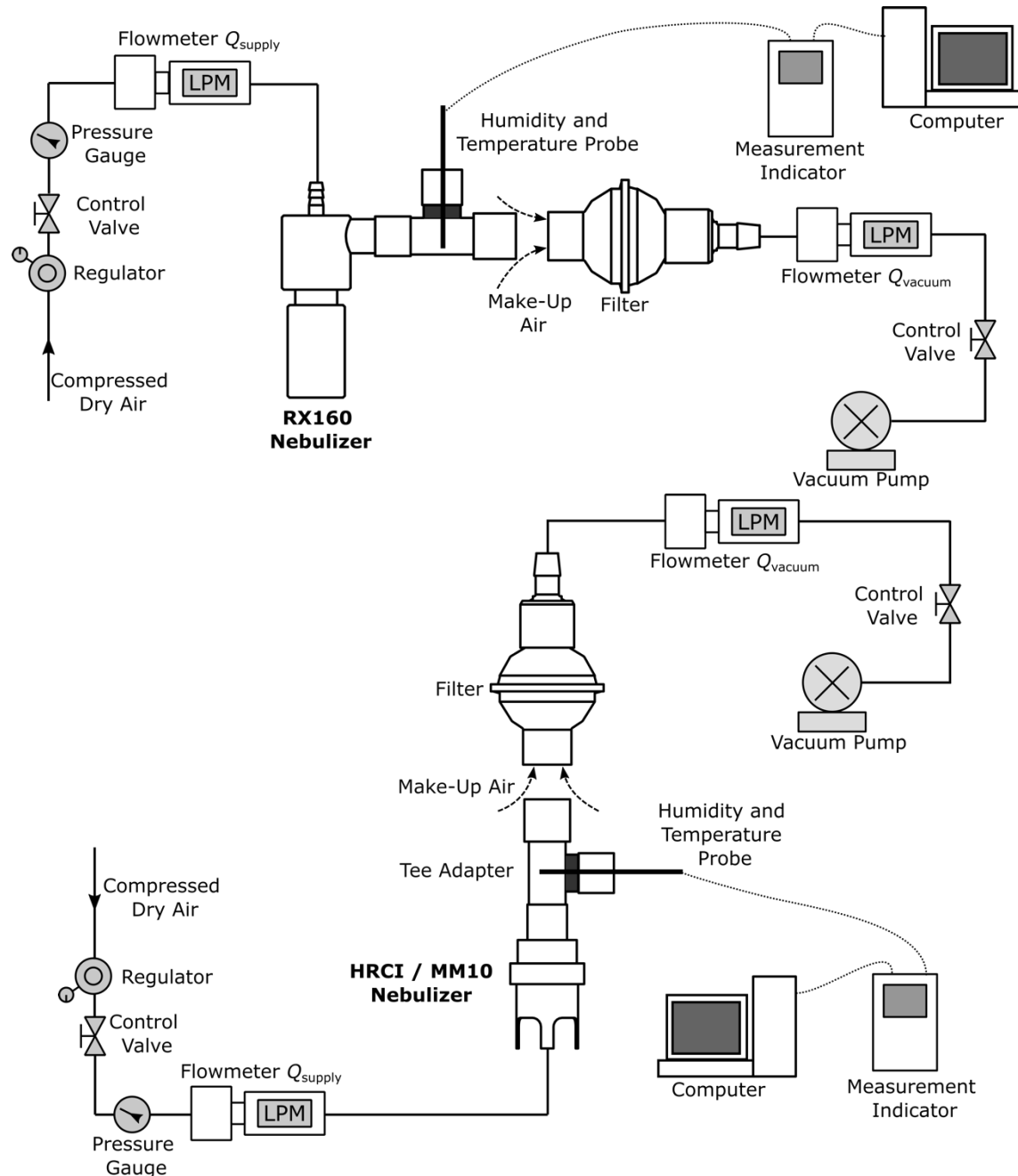
Figure 5-2: Setup used to quantify the temperature and humidity of the airstream emitted from nebulizers. Slight difference in setup between (top) the RX160 nebulizer and (bottom) the HRCI and MM10 nebulizers were necessitated by differences in device design.

5.3.1.3 Residual Particle Size Distributions

The low output rate and small droplet sizes emitted by Wright-type nebulizers complicates the use of laser diffraction for characterizing particle size distributions with these devices (Coates, Leung,

and Dell 2014). To circumvent this issue while using the same sizing instrument for all nebulizers, we opted to measure residual particle size distributions with an electric low pressure impactor (ELPI+; Dekati, Kangasala, Finland: airflow provided by a Model nXDS20i vacuum pump; Edwards, Burgess Hill, UK) using the setup shown in Figure 5-3. Nebulizers were operated as above, with the aerosol conditioned to facilitate the measurement of dry particles remaining after the evaporation of water. In particular, emitted aerosol was first directed through a Kr-85 charge neutralizer (Aerosol Neutralizer 3054; TSI Incorporated, Shoreview, MN, USA) before entering a drying column filled with silica gel and wrapped with heat tape to create a high-temperature, low-humidity environment. The resulting dry and charge-neutralized particles were subsequently characterized with the ELPI+ at the nominal flowrate of 10 L/min following standard procedures, with oil-saturated sintered collection plates used to reduce potential issues related to particle bounce within the impactor during operation (Marjamäki et al. 2000).

Size distribution data was recorded in 1 s intervals, with the averages calculated over the appropriate interval (2 min for RX160, 1 min for HRCI and MM10, with consideration given to the transit time between nebulization and measurement with the ELPI+). Measurements of particle sizes were taken for low, medium, and high concentrations of methacholine (as described above), and diluent-only. One RX160 was used for testing, with five replicated measures obtained with each solution of interest, while five HCRIs and five MM10s were used to examine each solution of interest once. This procedure yielded n = 5 measurements for each type of nebulizer with each solution of interest.
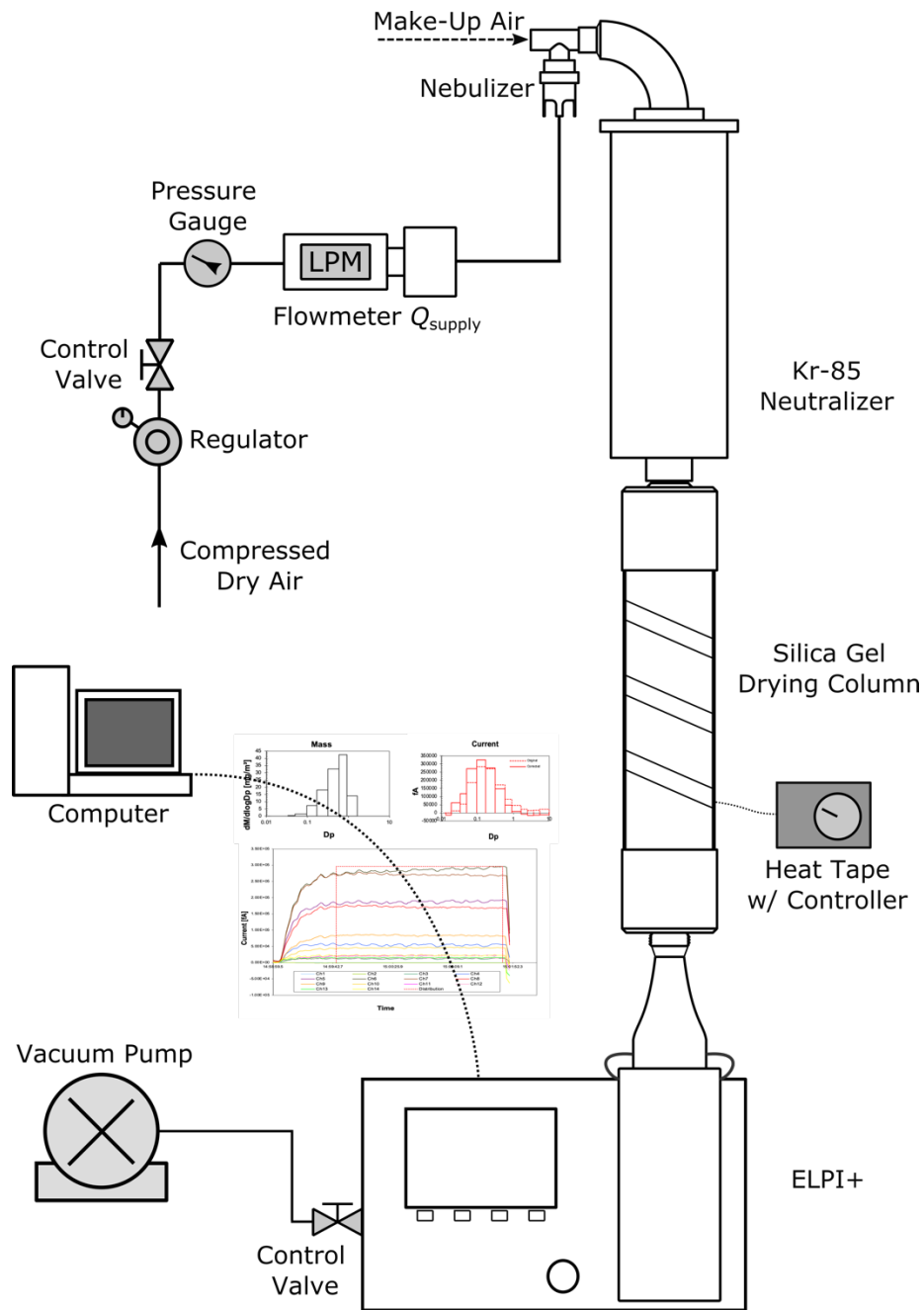
Figure 5-3: Setup used to quantify residual particle size distributions from each nebulizer with the ELPI+ electric low pressure impactor.

The data inversion algorithm used by the ELPI+ to quantify the mass of particles depositing on each stage requires an estimate of particle density. Residual particle densities (ρ_{res}) were estimated assuming ideal volume mixing behavior between sodium chloride ($\rho_{NaCl} = 2.165$ kg/m^3) and methacholine chloride ($\rho_{MC} = 1.03325$ kg/m^3; Yaws [2017]) based on the initial concentrations of these solutes ($c_{NaCl} = 9$ mg/mL, c_{MC} equaling 0.0625, 1, or 16 mg/mL) in the stock solution:

$$\rho_{\text{res}} = \frac{c_{\text{NaCl}} + c_{\text{MCl}}}{\frac{c_{\text{NaCl}}}{\rho_{\text{NaCl}}} + \frac{c_{\text{MCl}}}{\rho_{\text{MCl}}}}. \tag{5-2}$$

5.3.2 Emitted Droplet Sizes

In vitro data on residual particle size and emitted airstream temperature and humidity were used to back-calculate, via hygroscopic theory, the initial size of droplets emitted from each nebulizer, assuming that emitted droplets are in hygroscopic equilibrium with the gas phase upon exiting the nebulizer mouthpiece. Each cut-point from the ELPI+ was treated as the residual particle size corresponding to an initial droplet diameter emitted by the nebulizer at the measured conditions of RH and T. Hygroscopic theory provided a means to estimate these initial emitted diameters for each stage of the ELPI+, in essence providing a mapping from measured residual dry particles to emitted droplets. Measured size distribution data for the ELPI+ (expressed in terms of emitted droplet diameters in place of the measured residual particles) were then fit to log-normal distributions to estimate the mass median diameter (MMD) and geometric standard deviation (GSD) of aerosol emitted by each nebulizer. Equilibrium droplets MMDs were compared across each solution concentration via ANOVA using the *anova1* function in MATLAB, with a significance level of 0.05.

5.3.2.1 Hygroscopic Theory

For a solute-containing water droplet, the concentration of water vapour at the droplet surface, c_{s}, is a function of the water activity coefficient S_{sol} (accounting for the influence of dissolved solutes), the Kelvin effect K (accounting for the influence of surface curvature), and the concentration of water vapour that would occur over a flat surface of pure water, $c_{\text{s,pure}}$:

$$c_{\text{s}} = S_{\text{sol}} K c_{\text{s,pure}}. \tag{5-3}$$

Various empirical expressions for $c_{\text{s,pure}}$ as a function of temperature are presented in the literature. Here we use the correlation for $c_{\text{s,pure}}$ (in kg/m³) from Ferron, Haider, and Kreyling (1988) based on temperature T (in °C):

$$c_{\text{s,pure}} = 4.95133 \times 10^{-3} + (3.14787 \times 10^{-4})T + (1.0118 \times 10^{-5})T^2 \\ + (1.96539 \times 10^{-7})T^3 + (1.93574 \times 10^{-9})T^4 \tag{5-4}$$

For a droplet at equilibrium with the surrounding environment, the ratio of c_{s} and $c_{\text{s,pure}}$ is equal to the relative humidity, RH. Equation (5-3) can be re-expressed as

$$RH = S_{sol}K. \tag{5-5}$$

The water activity coefficient (S_{sol}) is a function of droplet diameter and solute content, while the Kelvin effect is a function of droplet diameter d_d, solution surface tension σ_{sol}, the molecular weight of the solvent (in this case, water) M_w, the density of the solvent (water) ρ_w, the temperature of the droplet T (in K), and the universal gas constant R_u (Gysel, Weingartner, and Baltensperger 2002):

$$K = \exp\left(\frac{4\sigma_{sol}M_w}{R_u\rho_w d_d T}\right). \tag{5-6}$$

As the relative humidity is measured experimentally (see 5.3.1.2 above), equation (5-5) allows for the calculation of the equilibrium droplet size as long as an appropriate expressions relating the water activity coefficient to droplet size and solute content can be derived.

Droplet size, d_d, can be also be expressed as a function of the residual particle diameter (d_{res}, the size if all solvent were to be evaporated), the density of the residual particle and the density of water (ρ_{res} and ρ_w, respectively, with ρ_w taken as 1000 kg/m^3), and the solute content expressed as a mass percent of the solution, Y_{sol} (O'Shaughnessy et al. 2020):

$$d_d = d_{res}\left[\frac{\rho_{res}}{\rho_w}\left(\frac{1}{Y_{sol}/100} - 1\right) + 1\right]^{1/3}. \tag{5-7}$$

Solutions used in the present work are either binary mixtures of sodium chloride in water or ternary mixtures of sodium chloride and methacholine chloride in water. Various methods are proposed for estimating water activity coefficients of binary and ternary mixtures (Rowland and May 2018; O'Shaughnessy et al. 2020), many of which require well-characterized experimental data that does not exist for methacholine chloride. We use a relatively simple approach based on Raoult's law for multiple components, allowing for the use of extensive literature on sodium chloride in both dilute and concentrated solutions while incorporating the potential effects of methacholine chloride. Note that on a molar basis, sodium chloride ($M_{NaCl} = 58.44$ g/mol) is responsible for the majority of solute content in each of the solutions examined here, even compared to methacholine chloride ($M_{MCl} = 195.69$ g/mol) at its highest initial concentration of 16 mg/mL.

Existing correlations for the water activity of aqueous solutions of sodium chloride as a function of Y_{NaCl} (e.g., Cinkotai [1971], O'Shaughnessy et al. [2020]) typically extend to a salt content of

~27% ($Y_{\text{NaCl}} \approx 27$) at a relative humidity of 76% ($S_{\text{NaCl}} = 0.76$), the point at which saturation occurs for salt in water. However, aqueous droplets of salt can exist in states of supersaturation at lower humidity (Tang, Munkelwitz, and Wang 1986; M. D. Cohen, Flagan, and Seinfeld 1987), with the efflorescence RH of NaCl being approximately 45% (Gregson et al. 2019). We derive a new correlation for the water activity of sodium chloride in water, S_{NaCl}, based on the classic data of Robinson and Stokes (1970) and the droplet-based data of Tang, Munkelwitz, and Wang (1986), corresponding to Y_{NaCl} from 0 to 43.0 and S_{NaCl} from 1 to 0.48, to capture this extended range of behaviour:

$$S_{\text{NaCl}} = 1 - (0.006154)Y_{\text{NaCl}} + (6.527 \times 10^{-5})Y_{\text{NaCl}}^2 \\ - (1.073 \times 10^{-5})Y_{\text{NaCl}}^3 + (1.403 \times 10^{-7})Y_{\text{NaCl}}^4. \tag{5-8}$$

Incorporation of the influence of methacholine was achieved through a modified form of Raoult's law, which for multiple component solutions can be expressed as (Finlay 2019)

$$S_{\text{sol}} \approx 1 - \frac{\sum_j i_j x_{sj}}{x_{\text{w}}} \tag{5-9}$$

where x_{w} is the molar concentration of water, x_{sj} is the molar concentration of solute j, and i_j is the van't Hoff factor for solute j, which for ideal solutions is equal to the number of ions a molecule dissociates into upon dissolution. For real solutions, the van't Hoff factor captures non-ideal behaviour and it is itself a function of solute concentration (Low 1969). Logically, equation (5-8) captures the same behaviour expected by equation (5-9) for sodium chloride, expressed in a different form (i.e., in terms of the solution mass content of sodium chloride, Y_{NaCl}, rather than the molar concentration x_{NaCl}). As such, equation (5-9) can be re-expressed as:

$$S_{\text{sol}} \approx S_{\text{NaCl}} - \frac{i_{\text{MCl}} x_{\text{MCl}}}{x_{\text{w}}} \tag{5-10}$$

Equation (5-10) was used to develop correlations of the form of (5-8) for each solution of methacholine used in the present work (i.e., low, medium, and high). Ideal behaviour was assumed to occur with methacholine chloride, i.e., $i_{\text{MCl}} = 2$. The ratio of methacholine chloride and sodium chloride held constant as the total solute content was increased from zero concentration ($Y_{\text{sol}} = 0$, $S_{\text{sol}} = 1$) to highly concentrated ($S_{\text{sol}} \approx 0.45$), with Y_{sol} simply taken as the summation of Y_{NaCl} and Y_{MCl}. Resulting correlations are shown in Figure 5-4, with additional details in Appendix F.
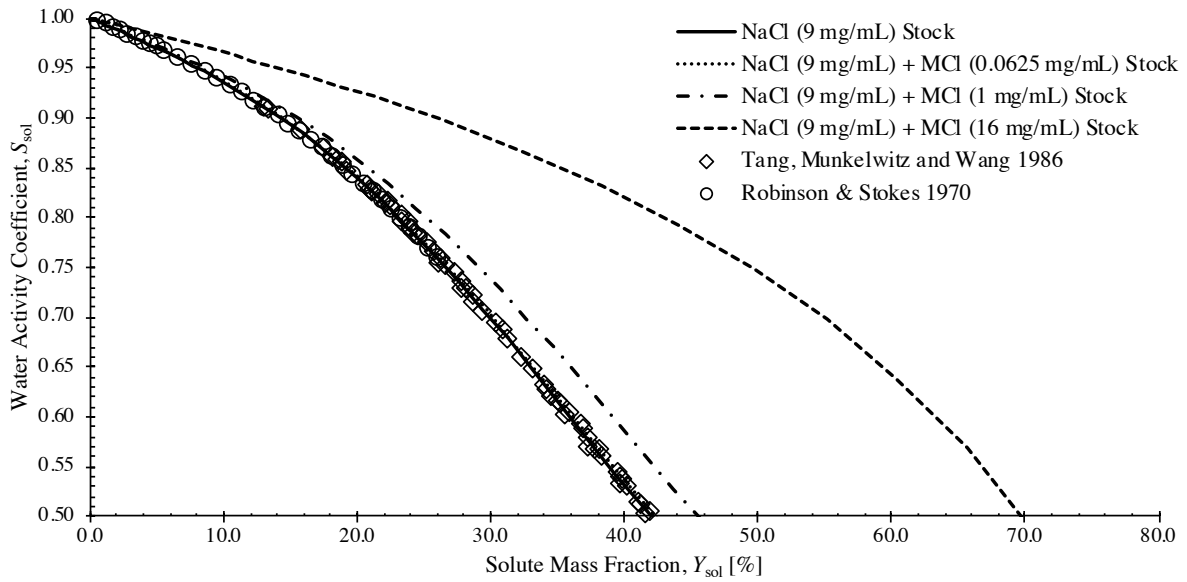
Figure 5-4: Correlations of water activity coefficient vs. solute mass fraction for the various solutions used in the present work, together with literature data for NaCl. Note that the low methacholine concentration curve (9 mg/mL NaCl + 0.0625 mg/mL MCl) is practically indistinguishable from NaCl alone.

Equations (5-6), (5-7), and (5-10) were substituted into (5-5), providing an implicit equation whose solution gave the droplet diameter $d_{d,eq}$ and solute mass content Y_{sol} corresponding to a particular residual particle size d_{res} (taken as the ELPI+ cut-points on the bases of Stokes diameter). Calculations with this method were performed using the nonlinear root-finder function *fzero* in MATLAB for each cut-point of the ELPI+ to provide estimates of the corresponding droplet diameters at the experimentally measured airstream conditions of RH and T.

5.3.2.2 Droplet Size Distribution

Cumulative mass distribution data from the ELPI+ provided size distributions in terms of residual particle sizes, and together with the above mapping from residual particles to emitted droplets allowed for estimation of the emitted aerosol characteristics. Cumulative mass distribution data from the ELPI+ (mapped to emitted droplets) were fit to lognormal distributions to determine MMDs and GSDs of aerosol upon emission from the nebulizers via the *logncdf* function in MATLAB's *Curve Fitting* Toolbox. Residual particle MMDs were calculated similarly.

5.3.3 Lung Deposition Modeling

A validated hygroscopic lung deposition model (Finlay et al. 1996; Finlay, Stapleton, and Zuberbuhler 1998; Finlay, Lange, Li, et al. 2000; Javaheri et al. 2013; Javaheri and Finlay 2013) was adapted for use in the present work to incorporate characteristics of aqueous aerosols containing methacholine chloride and sodium chloride. As the framework of the model is described extensively by Javaheri et al. (2013) and earlier works, only a summary is included here.

The hygroscopic model considered two-way coupling of heat and mass transfer between inhaled droplets and the carrier gas (air), as well as heat and mass transfer from the airway. Initial properties of the carrier gas were calculated assuming instantaneous adiabatic mixing between the nebulized airstream with experimentally measured RH and T (see section 5.3.1.2) and inhaled make-up air (taken as 20°C and 50% relative humidity). The inhalation profile was modeled as tidal with a volume of 860 cm^3, an average inhalation flowrate of 20.5 L/min, an inspiratory:expiratory ratio of 1:1, and no breath hold, a profile representative of adults breathing through nebulizers (Finlay 2019; A. P. Roth, Lange, and Finlay 2003; Yang et al. 2017). The total volume of droplets inhaled per breath was calculated via a mass balance of water considering the solution nebulization rate and the nebulized airstream RH.

Inhaled aerosol is discretized from a continuous lognormal distribution defined by the MMD and GSD into $N = 200$ bins spaced in 0.1 μm increments from 0.1 to 20 μm. Initial droplet characteristics including droplet density and solute weight fraction are determined by the procedure outlined in section 5.3.2. The differential equations describing the change in droplet diameter representing each bin, $d_{d,i}$, with time t are:

$$\frac{dd_{d,i}}{dt} = -\frac{4D_v(c_{s,i} - c_\infty)}{\rho_d d_i}. \tag{5-11}$$

D_v is the diffusion coefficient of water vapour in the carrier gas, c_∞ is the saturation water vapour concentration in the ambient phase far from the droplet surface, and ρ_d is the droplet density.

The differential equation describing the droplet temperatures T_i involves the specific heat capacity of the droplet, $c_{p,i}$, the latent heat of evaporation of water, L, the thermal conductivity of air, k_{air}, and the temperature of the ambient gas phase far from the droplet surface, T_∞:

$$\rho_\mathrm{d} c_{\mathrm{p},i} \frac{d_{\mathrm{d},i}^2}{12} \frac{dT_i}{dt} = -LD_\mathrm{v}\big(c_{\mathrm{s},i} - c_\infty\big) - k_\mathrm{air}(T_i - T_\infty). \tag{5-12}$$

The differential equation describing the water vapour concentration in the ambient phase in a particular airway generation involves the average mass transfer coefficient $\bar{g}$ (see Javaheri et al. [2013]), the internal area (A) and volume (V) of the airway, the concentration of water vapour at the airway surface, c_wall, the number of droplets with diameter $d_{\mathrm{d},i}$, n_i:

$$\frac{dc_\infty}{dt} = \frac{\bar{g}A}{V}(c_\mathrm{wall} - c_\infty) + \sum_{i=1}^{N} 2\pi D_\mathrm{v} n_i \, d_{\mathrm{d},i}\big(c_{\mathrm{s},i} - c_\infty\big). \tag{5-13}$$

Finally, the differential equation describing the temperature in the ambient phase in a particular airway generation is

$$\rho_\mathrm{air} c_{\mathrm{p,air}} \frac{dT_i}{dt} = \frac{\bar{h}A}{V}(T_\mathrm{wall} - T_\infty) + \sum_{i=1}^{N} 2\pi k_\mathrm{air} n_i \, d_{\mathrm{d},i}(T_i - T_\infty) \tag{5-14}$$

where ρ_air (1.139 kg/m³) and $c_{\mathrm{p,air}}$ (1010 J/kg·K) are the density and specific heat capacity of air, respectively, T_wall is temperature of the airway walls (taken as 37°C), and $\bar{h}$ is an average heat transfer coefficient (see Javaheri et al. [2013]).

Calculation of deposition is facilitated by first dividing the inhaled aerosol into 1000 small hypothetical boluses that achieve varying degrees of penetration into the lungs.[4] The dose delivered by each of these boluses to a particular generation depends on its final penetration depth (a function of tidal volume and airway geometry), the size of particles contained in the bolus in a particular generation (via equations (5-11) through (5-14)), and the breathing pattern (consisting of inhalation, pause, and exhalation phases; the profile used here is noted above). For the thoracic airways, the predominant deposition mechanisms are impaction, sedimentation, and diffusion. Impaction is calculated using the correlation of Chan and Lippmann (1980), sedimentation via the relations of Heyder (1975) and Heyder and Gebhart (1977), and diffusion via the relations of

---

[4] Axial dispersion (e.g., Taylor dispersion) of these hypothetical boluses is not considered in the present model, and indeed this is a common limitation of many 1D Lagrangian lung deposition models. Such effects would cause mixing between adjacent parcels of inhaled air. Investigation and implementation of these effects is a topic for future work.

Ingham (1975). Extrathoracic deposition is calculated using the Yang et al. (2017) correction of the Golshahi et al. (2013) correlation for tidal oral breathing:

$$\eta = 1 - \frac{1}{[2.23 \times 10^5 (\text{Stk}^{3.04} \text{Re}^{0.206}) + 1]}. \tag{5-15}$$

Stk and Re are the Stokes and Reynolds numbers (see equations (2-2) and (2-3)) whose characteristic diameter is the square root of the average cross-sectional area of the oropharyngeal region.

Equations (5-11), (5-12), (5-13), and (5-14) represent a moderately stiff system of $2N + 2$ coupled ordinary differential equations, solved here using the CVODE solver (S. D. Cohen and Hindmarsh 1994) with the implicit Backward Differentiation Formula scheme for dense linear systems (CVDENSE). Solution output was tracked over increments of 1.0×10^{-6} s. Deposition is calculated on a per-breath basis, and results are scaled to reflect the multiple breaths obtained over the appropriate administration time for the nebulizers used here, i.e., 2 min for the RX160 and 1 min for the HCRI and MM10. Validations of the model incorporating the equations outlined in section 5.3.2.1 were performed via comparison to an earlier Fortran version known to provide good agreement with *in vivo* scintigraphy data (Finlay et al. 1996; Finlay, Stapleton, and Zuberbuhler 1998; Finlay, Lange, Li, et al. 2000). A test case of initially 9 mg/mL saline droplets with an MMD of 4.5 µm and GSD of 1.5 showed less than a 2.5% difference in the total lung dose (in mg of saline) between these models, which we considered to be acceptable agreement.

5.4   Results

The emitted doses of methacholine chloride from an initially 1 mg/mL methacholine chloride solution in 9 mg/mL saline are shown in Figure 5-5. Differences in the emitted doses observed between each nebulizer were statistically significant, varying from an average of 42.0 (SD 5.1) µg with the RX160 over a 2 min period, 112.1 (SD 39.2) with the HRCI over a 1 min period, and 162.3 (SD 38.4) µg with the MM10 over a 1 min period. The solution nebulization rates for the RX160, HRCI, and MM10 measured during emitted dose tests were 0.131 (SD 0.005), 0.205 (SD 0.040), and 0.265 (SD 0.038) mg/min, respectively. Additional scoping runs (see Appendix D) confirmed a linear relationship between the emitted dose and stock solution concentration.
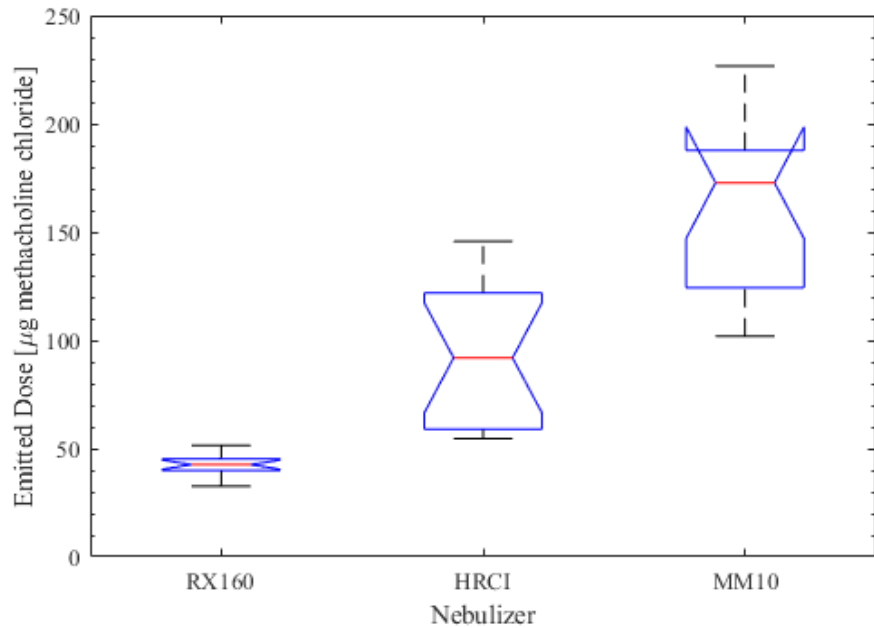
Figure 5-5: Notched box-and-whisker plot of emitted doses of an initially 1 mg/mL methacholine chloride in 9 mg/mL saline solution from the RX160 nebulizer over a 2 min period and the HRCI and MM10 nebulizers over a 1 min period (n = 15).

Airstream conditions (averaged over the appropriate administration period) were found to be independent of the solution concentration (via ANOVA, $p > 0.05$), and were thus pooled into single values for each nebulizer. Measured temperature and relative humidity are presented in Table 5-1 (where the temperature is reported relative to ambient), together with estimates of the inhaled volume of droplets based on a mass balance of water vapour. The RX160 emitted aerosol at considerably lower temperature and relative humidity than both the HRCI and MM10.

Table 5-1: Airstream conditions measured with each nebulizer (pooled across each solution of interest, n = 20), together with the estimated emitted volume of droplets per minute.

Nebulizer	Temperature (Relative to Ambient) [°C]	Relative Humidity [%]	Dry Gas Flowrate [L/min]	Emitted Volume of Droplets [mL/min]
RX160	-4.0 (SD 0.5)	78.5 (SD 1.0)	9.0	0.036
HRCI	-2.0 (SD 0.3)	88.3 (SD 1.5)	5.0	0.138
MM10	-1.7 (SD 0.3)	89.9 (SD 0.9)	5.0	0.196

119

Table 5-2: Lognormal size distributions characterized by the mass median diameters (MMDs) of residual particles and corresponding equilibrium droplets calculated via hygroscopic theory at each solution of interest for each nebulizer, together with the predicted total solute concentration of these droplets. GSD = geometric standard deviation, NaCl = sodium chloride, MCl = methacholine chloride.

Nebulizer	Parameter	Stock Solution Concentration			
		NaCl (9 mg/mL)	NaCl (9 mg/mL) + MCl (0.0625 mg/mL)	NaCl (9 mg/mL) + MCl (1 mg/mL)	NaCl (9 mg/mL) + MCl (16 mg/mL)
RX160	Residual MMD [μm]	0.26 (SD 0.03)	0.26 (SD 0.01)	0.27 (SD 0.01)	0.46 (SD 0.01)
	Equilibrium Droplet MMD [μm]	0.51 (SD 0.06)	0.50 (SD 0.03)	0.51 (SD 0.02)	0.62 (SD 0.01)
	Solute Concentration [mg/mL]	283.5	285.2	308.2	507.8
	GSD [-]	1.92 (SD 0.07)	1.89 (SD 0.05)	1.86 (SD 0.04)	1.98 (SD 0.02)
HRCI	Residual MMD [μm]	0.97 (SD 0.07)	1.00 (SD 0.07)	1.03 (SD 0.10)	1.50 (SD 0.09)
	Equilibrium Droplet MMD [μm]	2.23 (SD 0.17)	2.31 (SD 0.16)	2.24 (SD 0.22)	2.40 (SD 0.14)
	Solute Concentration [mg/mL]	175.6	176.5	189.8	310.3
	GSD [-]	1.76 (SD 0.02)	1.74 (SD 0.03)	1.75 (SD 0.04)	1.72 (SD 0.02)
MM10	Residual MMD [μm]	1.02 (SD 0.11)	0.98 (SD 0.07)	0.95 (SD 0.07)	1.42 (SD 0.04)
	Equilibrium Droplet MMD [μm]	2.43 (SD 0.25)	2.34 (SD 0.16)	2.15 (SD 0.16)	2.46 (SD 0.25)
	Solute Concentration [mg/mL]	156.4	157.2	169.1	274.3
	GSD [-]	1.78 (SD 0.06)	1.77 (SD 0.06)	1.77 (SD 0.05)	1.77 (SD 0.05)

Residual particle MMDs and corresponding equilibrium droplet MMDs calculated using hygroscopic theory are presented in Table 5-2. Droplet MMDs emitted from the HRCI and MM10 are on the order of 2 to 2.5 µm, with the RX160 emitting considerably smaller droplets. Differences in equilibrium droplet MMDs as a function of the stock concentration are not significant for the HRCI or MM10, whereas with the RX160 the equilibrium droplet MMDs generated from the highest stock concentration of methacholine (0.62 µm) are larger than at other concentrations (≈0.5 µm). Equilibrium droplets were predicted to be at least an order of magnitude more concentrated than the stock solutions, with the highest concentration occurring with the RX160.

5.4.1 Hygroscopic Lung Deposition Modeling
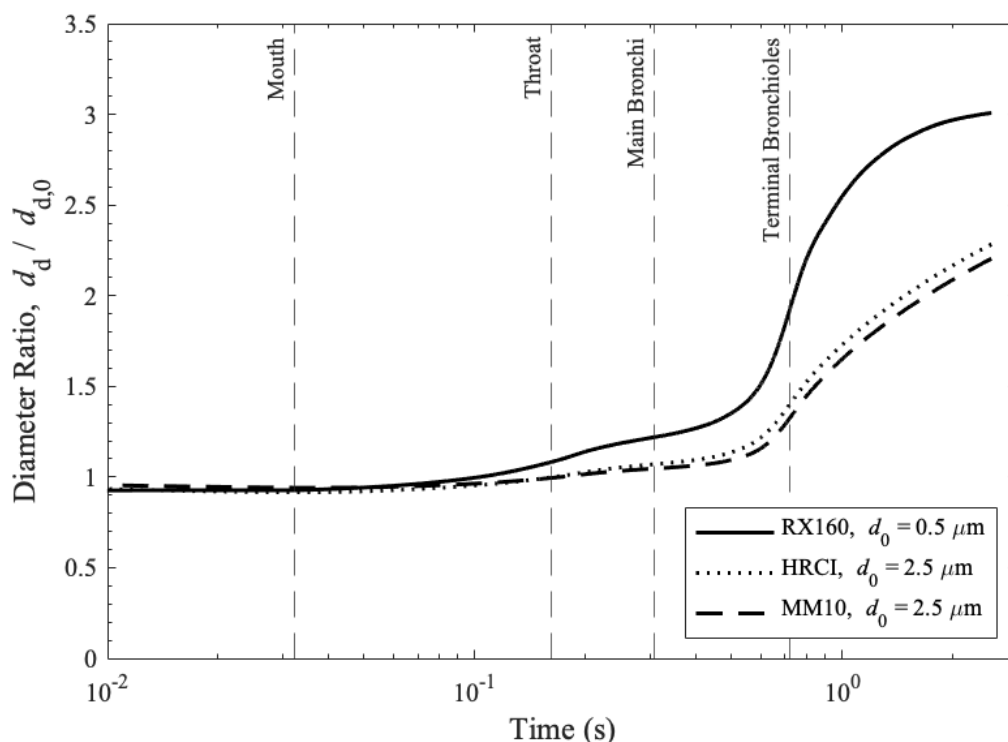
Figure 5-6: Evolution of droplet size during transit through the respiratory tract for 9 mg/mL NaCl + 1 mg/mL MCl stock solutions in each nebulizer. Vertical lines identify the time required to reach the specified generation of the respiratory tract, with the inhalation beginning at $t = 0$.

Hygroscopic behaviour of droplets representative of the MMD emitted by each nebulizer is shown in Figure 5-6 based on data for the 9 mg/mL NaCl + 1 mg/mL MCl stock solution. Just prior to inhalation, a small degree of droplet shrinkage occurs due to mixing with make-up air at a lower humidity than the nebulized emitted airstream. Droplets are relatively stable in size during transit

of the extrathoracic region, with growth accelerating towards the middle of the conducting airways and throughout the alveolar region. The most significant growth occurs with aerosols from the RX160 nebulizer, where droplets are predicted to increase in diameter by a factor of 3 by the end of the inhalation. For a 0.5 μm droplet, this corresponds to an increase in diameter to 1.5 μm. The HRCI and MM10 nebulizers see more modest but still considerable growth, with increases in droplet diameters by a factor of approximately 2.2 by the end of inhalation (for a 2.5 μm droplet, this corresponds to an increase in diameter to 5.5 μm).
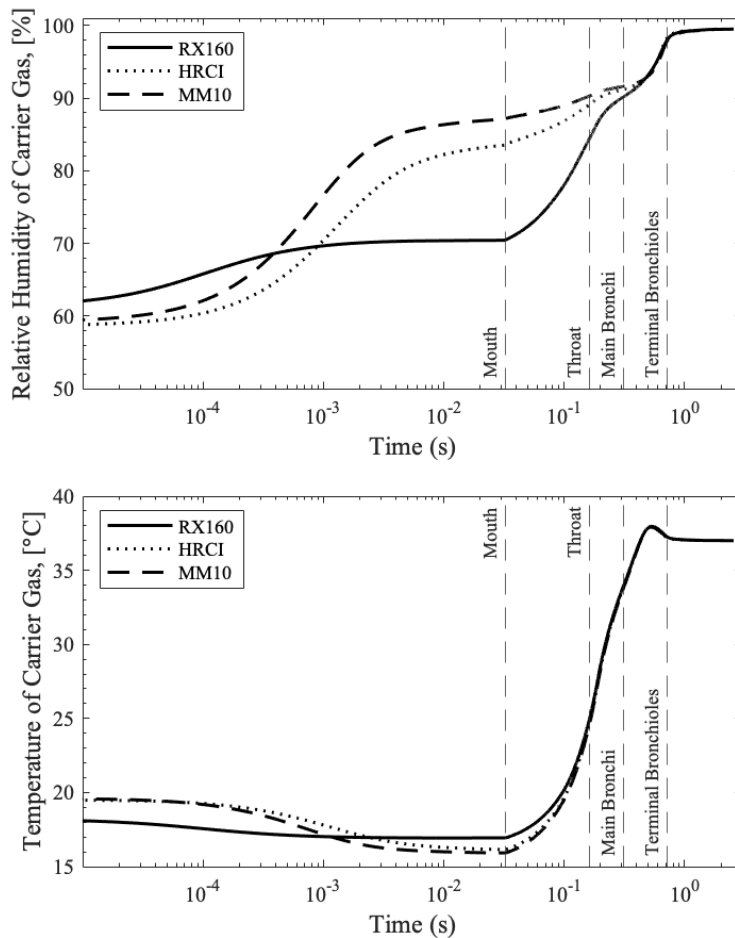
Figure 5-7: Evolution of carrier gas temperature (top) and relative humidity (bottom) during transit through the respiratory tract for 9 mg/mL NaCl + 1 mg/mL MCl stock solutions. Vertical lines identify the time required to reach the specified generation of the respiratory tract, with the inhalation beginning at time $t = 0$.

Evolution of the carrier gas is shown in Figure 5-7. Carrier gas temperature increases rapidly during transit through the extrathoracic region, topping out slightly above body temperature (~38 ºC) in the conducting airways before returning to 37ºC in the alveolar region. Relative humidity increases steadily upon inhalation, reaching 99.5% shortly after transiting the terminal bronchioles.

Predicted regional deposition of inhaled aerosol is shown in Figure 5-8 for data corresponding to 1 mg/mL MCl in 9 mg/mL NaCl stock solutions. The inhaled dose is half the emitted dose (as summarized in Figure 5-5) based on the chosen inhalation profile. The lung dose varies considerably with the nebulizer type, ranging from 8.3 µg with the RX160 to 48.7 µm with the MM10, (approximately a 6-fold difference despite using the same stock concentration). Extrathoracic deposition is negligible with the RX160 and very small with the HRCI and MM10 (less than 5% of the inhaled dose). The proportion of the inhaled dose depositing in the lungs with the RX160 (40%) is considerably smaller than that predicted to occur with the HRCI and MM10 (62% and 60%, respectively). Correspondingly, the proportion of the dose exhaled is considerably larger with the RX160 (60% of inhaled) than with the HRCI and MM10 (35% and 37%).
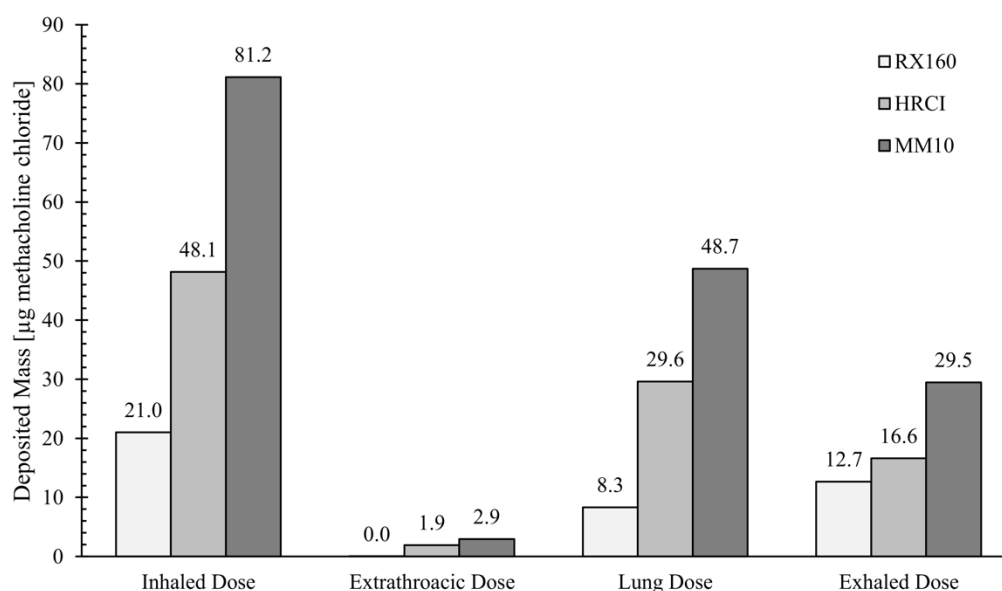
Figure 5-8: Predicted regional deposition of methacholine chloride for each nebulizer corresponding to 1 mg/mL MCl + 9 mg/mL NaCl stock solutions. MCl = methacholine chloride, NaCl = sodium chloride

The effect of stock concentration on regional deposition (expressed as a percent of the inhaled dose) is presented in Figure 5-9, with predictions of deposited mass presented in Table 5-3.

Predictions for the low (0.0625 mg/mL) and high (16 mg/mL) concentrations of methacholine chloride are consistent with those for the 1 mg/mL solution, with no major differences observed in predictions of extrathoracic, tracheobronchial, or total lung deposition, when expressed as a percent of the inhaled dose. Tracheobronchial deposition as percent of the inhaled dose with the RX160 is approximately 9%, roughly half of that obtained with the HRCI and MM10.

Table 5-3: Predictions of deposited mass of methacholine chloride as a function of stock solution concentration. MCl = methacholine chloride, NaCl = sodium chloride.

Nebulizer	Dose [µg MCl]	Stock Solution Concentration		
		NaCl (9 mg/mL) + MCl (0.0625 mg/mL)	NaCl (9 mg/mL) + MCl (1 mg/mL)	NaCl (9 mg/mL) + MCl (16 mg/mL)
RX160	Inhaled Dose	1.3	21.0	336.0
	Extrathoracic Deposition	0.0	0.0	0.4
	Total Lung Deposition	0.5	8.3	143.2
	Tracheobronchial Deposition	0.1	1.9	32.4
	Exhaled Dose	0.8	12.7	192.4
HRCI	Inhaled Dose	3.0	48.1	770.4
	Extrathoracic Deposition	0.1	1.9	34.3
	Total Lung Deposition	1.9	29.6	480.2
	Tracheobronchial Deposition	0.5	8.4	140.9
	Exhaled Dose	1.0	16.6	255.9
MM10	Inhaled Dose	5.1	81.2	1298.4
	Extrathoracic Deposition	0.2	2.9	69.4
	Total Lung Deposition	3.1	48.7	791.4
	Tracheobronchial Deposition	0.9	13.2	230.2
	Exhaled Dose	1.8	29.5	437.6
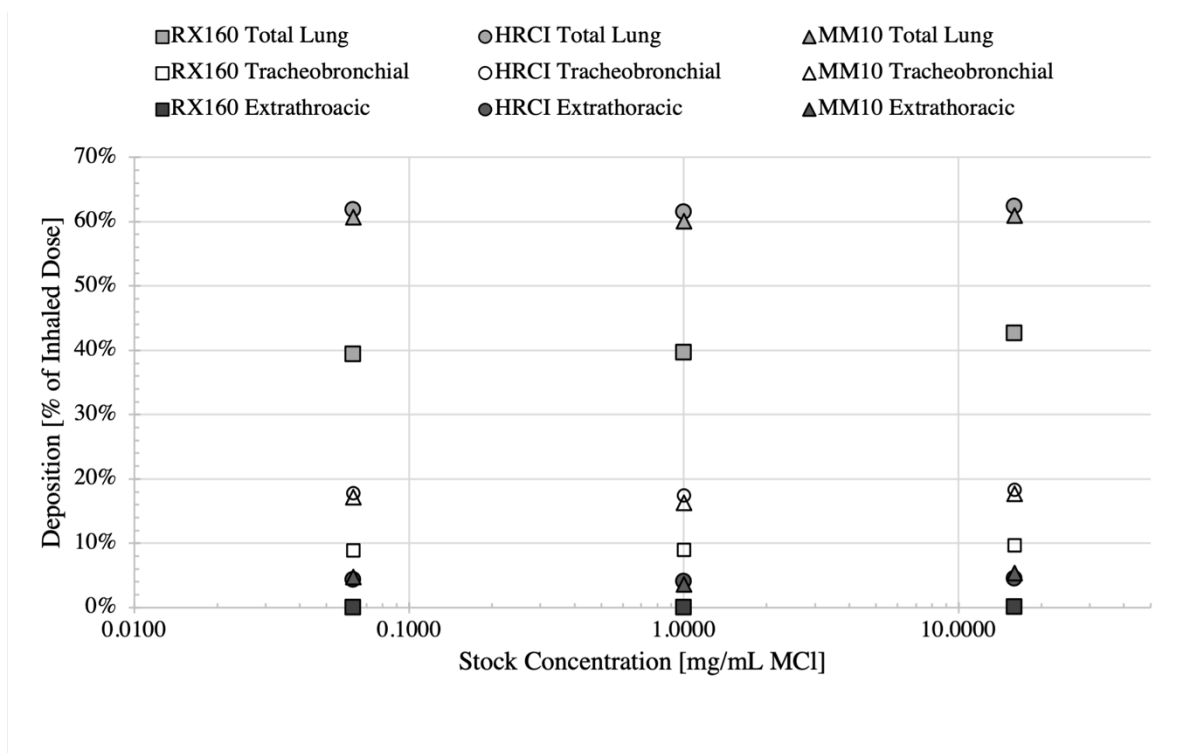
Figure 5-9: Predictions of regional deposition for each nebulizer at varying stock solution concentrations, expressed as a percent of inhaled dose.

5.5 Discussion

5.5.1 Provocative Dose

Results from the present work suggest that the exhaled dose obtained using the tidal breathing method with methacholine challenge testing is considerable. For the RX160, whose functional heritage is the low output rate and small droplet generating English Wright nebulizer, predictions here indicate that more than half of the inhaled dose of methacholine (roughly 60%) is subsequently exhaled without depositing in the lungs. The higher output rate HRCI and MM10 nebulizers are predicted to have a lower but still considerable exhaled dose, roughly 35% of the inhaled dose. These results suggest that assuming all fine particles depositing in the lungs, as per equation (5-1), will significantly overestimates the provocative dose obtained during methacholine challenge testing. Such a finding is not unexpected, as the exhaled dose obtained with tidal inhalations from nebulizers can be considerable. For example, Yang et al. (2017) measured *in vivo* exhalation fractions of 27.3 (SD 10.3) % of the inhaled dose for adults performing tidal inhalations with nebulizers emitting aerosols larger than those modeled here (MMDs of ~3.7 μm, GSDs of ~2.0). That being said, the degree of exhalation predicted here for the very small aerosol emitted

125

by the RX160 (MMD of ~0.5 μm) is not as high as one may expect based on deposition models that do not account for hygroscopic growth (International Commission on Radiological Protection 1994; National Council on Radiation Protection and Measurements 1997; Yeh et al. 1996), where for a 0.5 μm particle one may expect total respiratory tract deposition of 15 to 25 %. With the present model, one can "turn off" hygroscopic effects related to droplet size by setting the right-hand sides of equations (5-11) through (5-14) to zero. For the RX160, the exhaled fraction calculated with this change increases to ~65% from ~60%, with decreased deposition occurring in the alveolar region. This suggests that while hygroscopic effects certainly influence deposition and are important for accurate quantification of regional doses, there is a practical limit on how much they can increase respiratory tract deposition for the types of aerosols used here. While other works have suggested various approaches to increase lung deposition via manipulation of hygroscopic effects, these measures require much more control over variables than occurs during typical MCT (Golshahi, Tian, et al. 2013; Tian, Longest, Su, and Hindle 2011; Javaheri and Finlay 2013; Tian et al. 2013).

Characterization of the provocative dose is best illustrated via demonstration. Consider a patient who responds to a 1 mg/mL methacholine chloride concentration during MCT with each of the nebulizers used in the present work. For the RX160, the non-cumulative PD_{20} calculated using the ERS method is $(42.0\ \mu g\ /\ 120\ s) \cdot (1) \cdot (60\ s) = 21.0\ \mu g$, where the FPF has been taken as 1. Notably, this is in excellent agreement with the expected value of 23.75 μg as described in the ERS technical standard (Coates et al. 2017). For the HRCI and MM10, we require an estimate of the FPF, which we obtain via integration of the lognormal distribution defined by the MMDs and GSDs as summarized in Table 5-2[5]. For the HRCI, with an average MMD of 2.30 μm and GSD of 1.74, the FPF is 0.919, while for the MM10 with an MMD of 2.35 μm and GSD of 1.77 the FPF is 0.907. Thus, the estimated non-cumulative PD_{20} for the HRCI is $(112.1\ \mu g\ /\ 60\ s) \cdot (0.919) \cdot (30\ s) = 51.5\ \mu g$, and for the MM10 is $(162.3\ \mu g/60\ s\ ) \cdot (0.907) \cdot (30\ s) = 73.6\ \mu g$. These estimates are considerably larger than the predictions of the lung dose obtained with hygroscopic deposition modeling in the present work, at 8.3, 29.6, and 48.7 μg for the RX160, HRCI, and MM10 nebulizers, respectively. The difference is greatest with the RX160, where predicted lung

---

[5] For a lognormal distribution defined by the frequency distribution $f(x) = \frac{1}{x\sqrt{2\pi}\ln \text{GSD}} \exp\left[-\frac{(\ln x - \ln \text{MMD})^2}{2(\ln \text{GSD})^2}\right]$ the fraction of particles smaller than size d can be calculated as $F(d) = \frac{1}{2}\left[1 + \text{erf}\left(\frac{\ln x - \ln \text{MMD}}{\sqrt{2}\ln \text{GSD}}\right)\right]$.

deposition accounting for hygroscopic effects less than half of that calculated with the ERS method. Differences with the HRCI and MM10 are notable as well, with hygroscopic predictions of lung dose being approximately two-thirds of predictions suggested by equation (5-1). Such overestimations of the PD_{20} using equation (5-1) might not be of practical concern if the bias were consistent across different makes and models of nebulizers. Unfortunately, our results suggest that the type of nebulizer does influence the relative proportion of the dose depositing in the lungs. This complicates the use of generalized rules of the form of equation (5-1), and suggests that more advanced methods may be required if accurate characterization of the PD_{20} is of interest when comparing MCT results across disparate labs and methodologies.

Beyond the total lung dose, the current methodology also allows for estimation of the dose delivered to specific regions that may be more relevant to the action of methacholine. As noted by Coates et al. (2017), methacholine interacts with muscarinic receptors in airway smooth muscle to cause contraction and airway narrowing. Smooth muscle is located predominantly in the tracheobronchial airways, meaning it may be that dose depositing here is more relevant to patient response during MCT than the dose depositing deeper in the alveolar region. Our calculations suggest that approximately 9% of the inhaled dose deposits in the tracheobronchial airways for the RX160, and about 18% for the HRCI and MM10. For the above example with a stock solution of 1 mg/mL MCl, this translates into tracheobronchial doses of 1.9, 8.4, and 13.2 µg for the RX160, HRCI, and MM10 nebulizers, respectively. Similar to the total lung dose, the type of nebulizer influences the relative proportion of the dose depositing in the tracheobronchial region. A comparative clinical study wherein nebulizers with known characteristics are used with MCT, similar to that described by Dell et al. (2015), would be useful in determining whether the incorporation of hygroscopic lung deposition modeling in predictions of total lung and tracheobronchial doses of methacholine yields better correlations of results.

5.5.2 Considerations of Hygroscopic Behaviour

The experimental measurements of airstream conditions suggest that full saturation of the emitted airstream with water vapour (to 99.5% for isotonic solutions) does not occur with these nebulizers, in contrast to suggestions from earlier literature that typically consider nebulizers driven via compressors using room air with non-negligible water vapour content (Ferron and Gebhart 1988; Stapleton and Finlay 1995; Ferron et al. 1997). In the present work, very dry building air (RH <

1%) was used to drive nebulizers, meaning that essentially all water (as either vapour or liquid) in the emitted airstream originates from the stock solution. Assuming that the initial number and size of primary droplets produced during nebulization is independent of the driving gas humidity (a reasonable assumption considering the variables involved [Finlay 2019]), and that the aerodynamic behaviour of droplets within the nebulizer itself is similar as well, one may expect a lower output humidity from the nebulizer when driven with dry air. As few studies have directly measured the humidity of the airstream emitted by nebulizers, rather relying on estimates via mass balance considerations, additional work is required to investigate this phenomenon.

Likely the largest unknown in the present work is whether emitted droplets are truly at equilibrium with the surrounding airstream at the nebulizer exit. Arguments in favour of equilibrium relate to the stability in particle size upon emission and before mixing with ambient air that has been demonstrated experimentally (Stapleton and Finlay 1995) and hygroscopic modeling of the droplet nebulization process and transit throughout nebulizers (Finlay and Stapleton 1995). Considering that expected droplet lifetimes for sizes of interest (less than 5 µm) at the experimentally measured conditions here are on the order of 1 s or less (Ferron et al. 1997), and that transit times from the droplet production region to the exit of the nebulizer are of a similar timescale, the assumption of droplets being near equilibrium is likely reasonable. For equilibrium to be achieved here, droplets generated from stock solutions of known concentration must undergo considerable evaporation within the nebulizer after production to humidify the dry compressed airstream, and indeed Table 5-2 suggests emitted droplets are considerably more concentrated than the stock. For example, with the RX160 the predicted equilibrium droplet concentration of aerosol produced from 9 mg/mL saline (0.9% weight-by-volume) is 283.6 mg/mL, roughly 25% weight by volume, at the measured RH of 79%. Such highly concentrated droplets are predicted to experience considerable hygroscopic growth upon inhalation into the respiratory tract as air is heated and humidified to near full saturation (99.5% RH) at body temperature, as shown in Figure 5-6. But regardless of whether the emitted aerosol is in complete equilibrium with the carrier gas at the exit of the nebulizer, the addition of make-up air (here taken as 50% RH and 20 ºC) in the mouthpiece leads to additional hygroscopic changes prior to inhalation that appear to largely stabilize prior to reaching the respiratory tract (demonstrated in Figure 5-7). Even if droplets are not truly in a state of equilibrium at the point of emission from the nebulizer (and thus the droplet sizes reported in

the present work are biased towards smaller sizes), this additional mixing step will drive droplets towards smaller sizes prior to inhalation.

One can calculate the content equivalent diameters of droplets produced by each of the nebulizers here, which represents the diameter of the droplet were it to have the same solute concentration of some reference solution (C. Roth and Gebhart 1996; Ivey et al. 2014). Using the concentration of the stock solutions in the present work as the reference concentrations, the content equivalent MMDs generated by the RX160, HRCI, and MM10 are approximately 1.6, 5.9, and 5.8 µm, in line with what has been reported elsewhere for content equivalent diameters from nebulizers (C. Roth and Gebhart 1996). This estimate of the content equivalent diameter is essentially an upper limit of droplet MMD and is the size one would expect to measure if there were negligible evaporation occurring between droplet production and emission. Existing measurements of aerosol characteristics from nebulizers vary considerably, being highly dependent on experimental design. Ryan et al. (1981) measured mass median aerodynamic diameters ranging from 0.75 to 1.48 for the English Wright nebulizer using a low-flow Mercer impactor. Coates, Leung, and Dell (Coates, Leung, and Dell 2014) more recently used a Next Generation Impactor, but did not provide specifics of the particle size distribution aside from describing it as "very small" with a fine particle fraction of unity. Naji et al. (2013) report a mass median aerodynamic diameter of 1 µm from the RX160 based on manufacturer information, but do not validate this value. No measurements of either the English Wright or RX160 were found in the literature for techniques other than cascade impaction. With the HRCI and MM10, literature values of droplet size show large discrepancies and are heavily dependent on experimental design and instrumentation. Wang et al. (2017) measured MMADs ranging from 4 to 5 µm from the MM10 using an aerodynamic particle sizer, Sharma et al. (2017) measured a bimodal distribution from the MM10 with half of the mass contained in particles smaller than 1.5 µm using an Anderson Cascade Impactor, and MMDs measured via laser diffraction include 5.5 µm via Itoga et al. (2014) and 3.56 µm via Ari et al. (2018). Interestingly, Song et al. (2016) noted that droplet size measurements obtained with laser diffraction and cascade impaction show poor agreement even when environmental conditions are controlled to reduce hygroscopic size changes. Validated comparisons between disparate methods would be of value in determining the accuracy of various approaches in characterizing emitted droplet sizes, particularly given the desire to move towards laser diffraction as a means for characterizing nebulized aerosols (Vecellio-None et al. 2001; Ziegler and Wachtel 2005).

Compared to measurements via laser diffraction for the HRCI and MM10, the equilibrium droplet sizes estimated in the present work are somewhat lower than expected. There are a few possibilities in terms of potential errors in the present work that may result in underestimation of emitted droplet sizes. First, the ELPI+ may measure smaller residual particle sizes than occur in reality with pharmaceutical aerosols. Conflicting data exists here. Telko, Kujanpää, and Hickey (2007) found excellent agreement between simultaneous ELPI and Anderson Cascade Impactor measurements for DPIs, while Kotian et al. (2009) reported the ELPI as significantly underestimating particle sizes for pMDIs via comparisons to separate measurements in an Anderson Cascade Impactor. Note that pMDI aerosols are hygroscopic in nature, and Kotian et al. (2009) did not consider whether the much lower pressure obtained within the ELPI as compared to the Anderson Cascade Impactor would influence droplet evolution. As such, their measurements may be indicative of differences in hygroscopic droplet behaviour within the instrumentation itself rather than inherent biases from the ELPI. In the present work, we mitigate hygroscopic effects by drying particles completely prior to measurement with the ELPI+, and as the ELPI+ demonstrates similar performance to the ELPI (Järvinen et al. 2014), we suspect that our measurements of residual particle size are reasonable. Second, our measurements of the emitted airstream conditions may be lower than expected, but as noted above additional work is required to investigate the dependence of emitted airstream conditions on driving gas properties. Third, droplets may exist in some state between the content equivalent diameter and the equilibrium diameter, and as such would be larger than predicted. As noted above, subsequent mixing with room temperature air at a lower humidity will mitigate differences that would otherwise occur with stable particles, and associated minor differences in droplet sizes upon inhalation are not of a magnitude that will alter the main conclusions.

It is instructive to consider the case where rather than being highly concentrated, emitted droplets are equal in concentration to the stock solution. Such a hypothetical case for the RX160 with 1 mg/mL MCl in 9 mg/mL NaCl is considered in Figure 5-10, where the only factors changed from the original calculations are the initial equilibrium droplet solute concentration and density[6].

---

[6] In reality, a difference in the emitted droplet concentration would also be associated with a difference in droplet size and carrier gas conditions like temperature and humidity. Such effects are ignored here for the sake of simplicity.
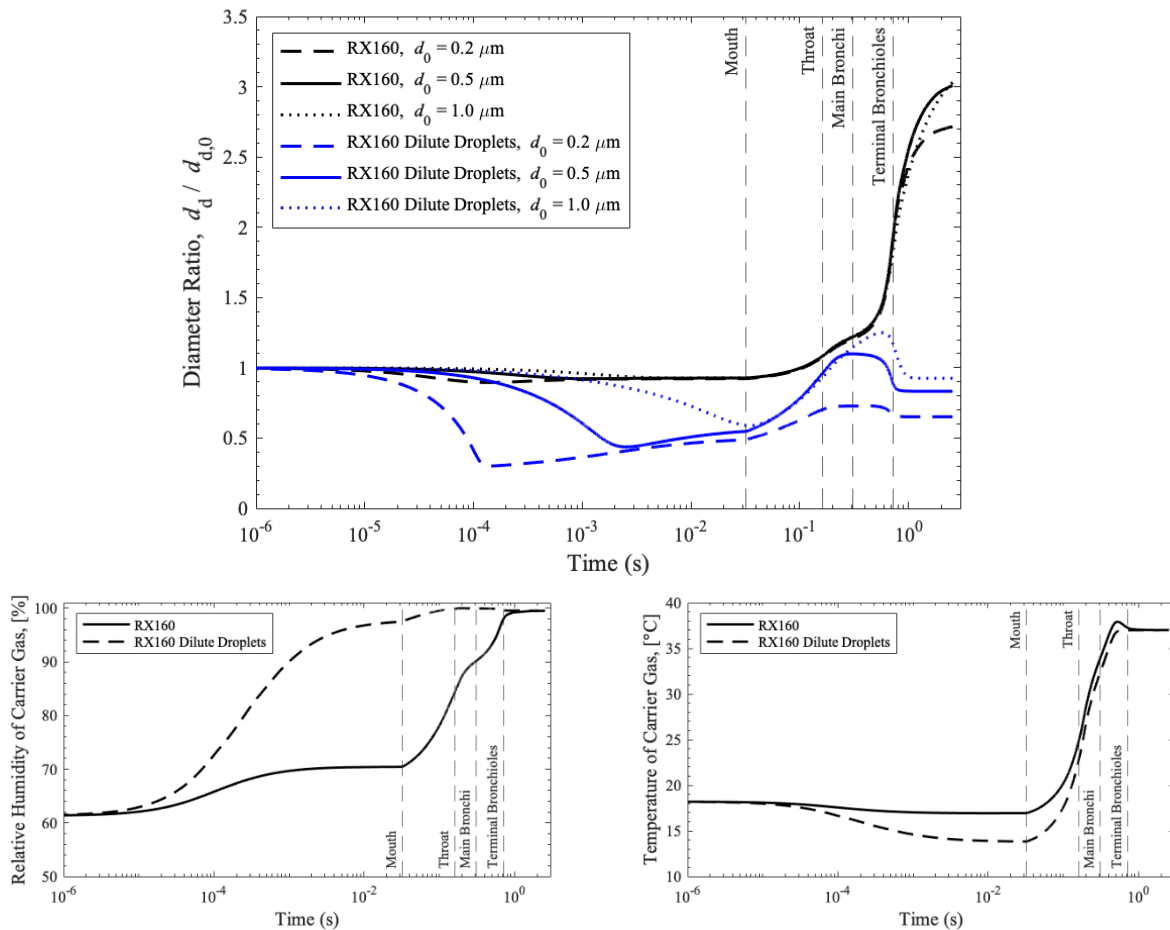
Figure 5-10: Comparison of cases where emitted droplets from the RX160 are concentrated as predicted in Table 5-2 versus the hypothetical situations where droplets are equal in concentration to the stock solution of 9 mg/mL NaCl + 1 mg/mL MCl stock solutions in each nebulizer (i.e., Dilute Droplets). Top shows evolution of different droplet sizes over time, bottom left the change in carrier gas relative humidity, and bottom right the change in temperature.

For the dilute solute droplet case, significant evaporation occurs prior to inhalation as water vapour from droplets drives humidification of the carrier gas. After inhalation and during transit of the tracheobronchial region, there is a period where supersaturation occurs in the inhaled air, driving condensational growth onto inhaled droplets and increasing their size (Javaheri et al. 2013). This contrasts with the predictions for more concentrated droplets from the present work, where supersaturation does not occur. The high solute content of concentrated droplets leads to considerable reductions in vapor pressure at the droplet surface, driving rapid absorption of water vapour from the carrier gas that prevents a state of supersaturation from occurring while facilitating

131

significant condensational growth. Evidently, the solution concentration of droplets when emitted from the nebulizer can considerably influence their hygroscopic behaviour upon inhalation.

The derivation of correlations for water activity coefficients as a function of solute content used a modified form of Raoult's law to incorporate the extensive empirical data on sodium chloride solutions in literature while accounting for potential (ideal) effects of methacholine chloride. Strictly speaking, the form of Raoult's law used here is valid only for dilute solutions, as it does not account for non-ideal interactions that are often observed in solutions that are more concentrated. Various mixing laws are proposed to take into account non-ideal behaviour (Rowland and May 2018; Wexler 2019), though generally these require high quality experimental data on each component used in the mixture, the accuracy of predictions at high concentrations (nearing or surpassing saturation) is unknown, and the rules provide largely equivalent predictions when considering experimental uncertainty. We explored the use of one of these rules—the additivity rule described by Robinson and Bower (1965)—but found that errors between this method and the Raoult's law approach described previously were negligible. Barring high quality experimental data on methacholine chloride solutions, the modified Raoult's law approach was considered sufficient for considering hygroscopic effects during lung deposition modeling.

5.6 Conclusions

Hygroscopic modeling suggests that the exhaled dose obtained during methacholine challenge testing is significant, with the characteristics of the nebulizer influencing the relative proportion of the dose that is exhaled. The low output rate and small droplet sizes (equilibrium droplet MMDs near 0.5 μm) emitted from the RX160 resulted in predicted total lung deposition of only 40% of the inhaled dose. The higher output rate HRCI and MM10 nebulizers, both of which emitted droplets with equilibrium MMDs near 2.5 μm, were predicted to yield higher total lung deposition at approximately 60% of the inhaled dose. Measurements of airstream conditions at the nebulizer exit suggested that emitted droplets existed at a state of high concentration relative to the stock solution, and sequentially considerable hygroscopic growth was predicted to occur during transit through the airways. Existing methods for estimating the lung dose overestimated the predictions here by a factor of 2.5 for the RX160, 1.7 for the HRCI, and 1.5 for the MM10. More accurate quantification of the provocative dose obtained during MCT with disparate devices and methodologies may be facilitated using the methods described here.

6 Conclusions

6.1 Summary

This thesis investigated and developed experimental and numerical methods for characterizing the performance of inhaled pharmaceutical aerosols, with the aim of developing more clinically relevant measures of performance than are provided by existing techniques. Work described here provides a framework for improving upon the standard pharmacopeial methods used to characterize pharmaceutical aerosol performance, with the incorporation of numerical modeling allowing for more in-depth interpretation of *in vitro* data. With increased focus on the use of inhaled aerosols as a delivery route for both local and systemic delivery of medication, such methods are of interest for streamlining the drug development process and in optimizing future devices and formulations.

Chapter 2 reviewed relevant literature and identified various factors to consider when developing more predictive *in vitro* and *in silico* methods. Clinical measures used to evaluate treatment efficacy were briefly reviewed, and the limitations of existing pharmacopeial methods were described. Factors influencing *in vitro* methods were characterized in terms of airway geometry, inhalation maneuver, hygroscopic behaviour, and considerations of real-world use. Deposition models characterizing extrathoracic and thoracic deposition were reviewed, together with pharmacokinetic models and associated factors like mucociliary clearance and dissolution.

Chapter 3 explored the influence of inhaler insertion angle and relative humidity on deposition of pharmaceutical aerosols in the Alberta Idealized Throat. Inhaler insertion angle was found to significantly influence *in vitro* deposition measurements for some inhalers. Of the six tested devices, three showed significant differences in deposition at different insertion angles, wherein directing the device towards the tongue as opposed to the back of the mouth decreased the *in vitro* lung dose. With DPIs, device resistance and peak inhalation flowrate were not predictive of the importance of insertion angle. Instead, DPI sensitivity to insertion angle was related to the combination of high mouthpiece jet velocities and large aerodynamic particle sizes. For pMDIs, high spray momentum was associated with sensitivity to insertion angle. Conclusions of this chapter are two-fold. First, measurements here suggest that one must consider factors beyond inhalation flowrate and extrathoracic geometry when interpreting *in vitro* measurements of deposition from some pharmaceutical inhalers. Second, reduced sensitivity to inhaler insertion

angle in real-world patient use may be facilitated with DPIs using larger diameter inhaler mouthpieces and smaller aerodynamic particle sizes and with pMDIs using lower momentum sprays. As the variability in extrathoracic deposition is considered a primary source of variability in the lung dose, such considerations in future device and formulation design may aid in achieving greater consistency in therapeutic effects for patients using pMDIs and DPIs.

In Chapter 4 a combined *in vitro – in silico* methodology was developed and shown to successfully replicate *in vivo* plasma concentrations of budesonide from dry powder inhalers based solely on experimental data, regional deposition modeling, and pharmacokinetic modeling using parameter values from literature. As no extraneous fit factors were required to achieve good agreement, the combination of advanced *in vitro* measurement of intrathoracic particle size distributions, regional deposition modeling, and disposition modeling accounting for mucociliary clearance and dissolution in the conducting airways appears robust. Despite notable *in vitro* differences in performance, predicted deposition in the small conducting airways was comparably modest for each DPI. Peak systemic concentration of budesonide was dependent primarily on the total lung dose, whereas tracheobronchial deposition was poorly correlated with pharmacokinetic data. This suggests that the reliance of similarities in pharmacokinetic data for establishing bioequivalence of inhaled locally acting pharmaceutical therapies may not properly elucidate differences between formulations. The establishment of bioequivalence for generics should thus consider additional information beyond systemic exposure, and the proposed methodology here provides a template for such investigations.

Chapter 5 saw the development of a novel *in vitro* methodology for characterizing nebulizer performance that, when coupled with hygroscopic theory and lung deposition modeling, allowed for the quantification of regional deposition obtained with methacholine aerosols used in bronchial provocation testing. Measurements of airstream conditions suggested that the nebulizers used in the present work emitted droplets at very high concentrations, and subsequent deposition modeling suggested considerable hygroscopic growth occurs with such aerosols during inhalation. Results further suggest that existing methods for characterization of the provocative dose overestimate the relevant dose significantly, with the magnitude of the error depending on characteristics of the nebulizer used during testing. As such, the method outlined in Chapter 5 may prove useful in

standardizing the determination of the provocative dose in methacholine challenge testing and in improving the translatability of results obtained with disparate methods and protocols.

6.2 Contributions

The following list summarized new contributions to knowledge developed in this thesis:

- Demonstration of the influence of insertion angle on extrathoracic deposition in the Alberta Idealized Throat for pharmaceutical aerosols and identification of factors influencing sensitivity of deposition to inhaler insertion angle
- Utilization of calibrated semi-realistic inhalation patterns coupled with cascade impactor measurements downstream of an Alberta Idealized Throat to characterize intrathoracic particle size distributions
- Derivation of flowrate correction factors incorporating the influence of device resistance and ambient pressure for more accurate determination of volumetric flowrates
- Successful use of advanced *in vitro* experimentation, regional deposition modeling, and pharmacokinetic modeling to replicate *in vivo* systemic dosing of budesonide from DPIs
- Derivation of a Nernst-Brunner dissolution model based on mass median aerodynamic diameters to capture effect of particle size on disposition
- Demonstration of a lack of correlation between tracheobronchial deposition and systemic exposure for budesonide, reinforcing that pharmacokinetics alone are not sufficient in characterizing orally inhaled locally acting therapies
- Development of a methodology to back-calculate emitted droplet sizes from nebulizers based on residual particle size and airstream conditions
- Measurement of airstream conditions in nebulized airstreams suggesting the typical assumption of saturation may not hold for some nebulizers
- Development of correlations for water activity coefficients of highly concentrated droplets using a modified Raoult's law approach
- Characterization of provocative doses for challenge testing that incorporates mechanistic lung deposition modeling and hygroscopic effects
- Quantification of significant exhaled fractions obtained with methacholine aerosols used during challenge testing

6.3   Recommendations for Future Work

Further investigation of the factors influencing sensitivity to insertion angle in terms of extrathoracic deposition may be warranted, particularly for pMDIs as new propellants are investigated for use in new formulations. Extension of the methods to investigate deposition in the Alberta Idealized Child Throat would be valuable in investigating whether similar trends in sensitivity to insertion angle and humidity hold in the smaller extrathoracic airways more representative of younger patients.

The success of the methodology proposed in Chapter 4 to replicate systemic exposure is promising, but elucidation of local effects requires more advanced physiologically based pharmacokinetic and pharmacodynamic modeling. Future work may consider implementing such PBPK/PD models with the ultimate aim of predicting local effects in lung tissue. Budesonide was chosen as a demonstrator drug given the availability of literature data on various pharmacokinetic parameters, but extension to novel therapies will require the implementation of additional methods (e.g., *ex vivo* work, *in vitro* cell studies, etc.) to inform the selection of appropriate values for rate constants. Additional work investigating the influence of patient use characteristics like inhalation flowrates may help inform how variability in the intrathoracic particle size distribution that may result from real-world use manifests in systemic measures like the peak systemic concentration and area under the curve. Future work may also consider improving the lung deposition model to incorporate bolus effects expected to occur during a typical inhalation through a DPI.

Further work is required to investigate the state of droplets upon emission from nebulizers to confirm the observation of unsaturated airstream conditions and better characterize their state relative to equilibrium. Experimental measurements of water activity with the mixtures used here may also prove useful in validating the Raoult's law approach for estimating hygroscopic behaviour of sodium chloride plus methacholine chloride droplets, and by extension, other mixtures of interest. A comparative study of MCT using the nebulizers investigated here would serve as a useful validation of the proposed method for characterizing the provocative dose relative to existing methods. Considering the use of challenge testing in pediatric populations, further work extending the deposition model towards a geometry representative of children would be of value.

References

Agertoft, L., and S. Pedersen. 1993. "Importance of the Inhalation Device on the Effect of Budesonide." *Archives of Disease in Childhood* 69 (1): 130–33.

Alcoforado, Luciana, Armèle Dornelas de Andrade, Joaquin L. Herraiz, Simone Cristina Soares Brandão, Jacqueline de Melo Barcelar, James B. Fink, and Jose G. Venegas. 2018. "Anatomically Based Analysis of Radioaerosol Distribution in Pulmonary Scintigraphy: A Feasibility Study in Asthmatics." *Journal of Aerosol Medicine and Pulmonary Drug Delivery* 31 (5): 298–310.

Amidon, G L, H Lennernäs, V P Shah, and J R Crison. 1995. "A Theoretical Basis for a Biopharmaceutic Drug Classification: The Correlation of in Vitro Drug Product Dissolution and in Vivo Bioavailability." *Pharmaceutical Research* 12 (3): 413–20.

Argenti, Domenick, Bharti Shah, and Donald Heald. 2000. "A Study Comparing the Clinical Pharmacokinetics, Pharmacodynamics, and Tolerability of Triamcinolone Acetonide HFA-134a Metered-Dose Inhaler and Budesonide Dry-Powder Inhaler Following Inhalation Administration." *Journal of Clinical Pharmacology* 40 (5): 516–26.

Ari, Arzu, Truong Dang, Fahad H. Al Enazi, Mohammed M. Alqahtani, Abdulrahman Alkhathami, Rowaida Qoutah, Ahmad S. Almamary, and James B. Fink. 2018. "Effect of Heat Moisture Exchanger on Aerosol Drug Delivery and Airway Resistance in Simulated Ventilator-Dependent Adults Using Jet and Mesh Nebulizers." *Journal of Aerosol Medicine and Pulmonary Drug Delivery* 31 (1): 42–48.

Arora, Deepika, Kumar A. Shah, Matthew S. Halquist, and Masahiro Sakagami. 2010. "In Vitro Aqueous Fluid-Capacity-Limited Dissolution Testing of Respirable Aerosol Drug Particles Generated from Inhaler Products." *Pharmaceutical Research* 27 (5): 786–95.

Azouz, Wahida, Philip Chetcuti, Harold S.R. Hosker, Dinesh Saralaya, John Stephenson, and Henry Chrystyn. 2015. "The Inhalation Characteristics of Patients When They Use Different Dry Powder Inhalers." *Journal of Aerosol Medicine and Pulmonary Drug Delivery* 28 (1): 35–42.

Bäckman, Per, Sumit Arora, William Couet, Ben Forbes, Wilbur de Kruijf, and Amrit Paudel. 2018. "Advances in Experimental and Mechanistic Computational Models to Understand Pulmonary Exposure to Inhaled Drugs." *European Journal of Pharmaceutical Sciences* 113 (October 2017): 41–52.

Bäckman, Per, and Bo Olsson. 2020. "Pulmonary Drug Dissolution, Regional Retention and Systemic Absorption: Understanding Their Interactions Through Mechanistic Modeling." *Respiratory Drug Delivery 2020* 50: 113–22.

Bäckman, Per, Ulrika Tehler, and Bo Olsson. 2017. "Predicting Exposure after Oral Inhalation of the Selective Glucocorticoid Receptor Modulator, AZD5423, Based on Dose, Deposition Pattern, and Mechanistic Modeling of Pulmonary Disposition." *Journal of Aerosol Medicine and Pulmonary Drug Delivery* 30 (2): 108–17.

Barnes, Peter J. 2010. "Inhaled Corticosteroids." *Pharmaceuticals* 3 (3): 514–40.

Barnes, Peter J., and Soren Pedersen. 1993. "Efficacy and Safety of Inhaled Corticosteroids in Asthma. Report of a Workshop Held in Eze, France, October 1992." *American Review of Respiratory Disease* 148 (4 Pt 2): S1-26.

Basheti, Iman A., Helen K. Reddel, Carol L. Armour, and Sinthia Z. Bosnic-Anticevich. 2007. "Improved Asthma Outcomes with a Simple Inhaler Technique Intervention by Community Pharmacists." *Journal of Allergy and Clinical Immunology* 119 (6): 1537–38.

Bateman, E. D., S. S. Hurd, P. J. Barnes, J. Bousquet, J. M. Drazen, J.M. FitzGerald, P. Gibson, et al. 2008. "Global Strategy for Asthma Management and Prevention: GINA Executive Summary." *European Respiratory Journal* 31 (1): 143–78.

Beasley, Richard, James Harper, Grace Bird, Ingrid Maijers, Mark Weatherall, and Ian D. Pavord. 2019. "Inhaled Corticosteroid Therapy in Adult Asthma Time for a New Therapeutic Dose Terminology." *American Journal of Respiratory and Critical Care Medicine* 199 (12): 1471–77.

Beckwith, T. G., R. D. Marangoni, and J. H. Lienhard. 2007. *Mechanical Measurements*. 6th ed. Saddle River, NJ: Pearson Prentice Hall.

Bennett, William D., Miao Xie, Kirby Zeman, Harry Hurd, and Scott Donaldson. 2014. "Heterogeneity of Particle Deposition by Pixel Analysis of 2D Gamma Scintigraphy Images." *Journal of Aerosol Medicine and Pulmonary Drug Delivery* 28 (3): 211–18.

Berge, M. Van Den, N. H.T. Ten Hacken, E. Van Der Wiel, and D. S. Postma. 2013. "Treatment of the Bronchial Tree from Beginning to End: Targeting Small Airway Inflammation in Asthma." *Allergy: European Journal of Allergy and Clinical Immunology* 68 (1): 16–26.

Bhagwat, Sharvari, Uta Schilling, Mong Jen Chen, Xiangyin Wei, Renishkumar R. Delvadia, Mohammad Absar, Bhawana Saluja, and Günther Hochhaus. 2017. "Predicting Pulmonary Pharmacokinetics from In Vitro Properties of Dry Powder Inhalers." *Pharmaceutical Research* 34 (12): 2541–56.

Bjermer, Leif. 2011. "Targeting Small Airways, a Step Further in Asthma Management." *Clinical Respiratory Journal* 5 (3): 131–35.

Blais, Christianne M., Donald W. Cockcroft, Justine Veilleux, Marie-Ève Boulay, Louis-Philippe Boulet, Gail M. Gauvreau, Tara X. Scime, Richard M. Watson, Paul M. O'Byrne, and Beth E. Davis. 2017. "Methacholine Challenge: Comparison of Airway Responsiveness Produced by a Vibrating Mesh Nebulizer Versus a Jet Nebulizer." *Journal of Aerosol Medicine and Pulmonary Drug Delivery* 31 (2): 88–93.

Boger, Elin, and Markus Fridén. 2019. "Physiologically Based Pharmacokinetic/Pharmacodynamic Modeling Accurately Predicts the Better Bronchodilatory Effect of Inhaled Versus Oral Salbutamol Dosage Forms." *Journal of Aerosol Medicine and Pulmonary Drug Delivery* 32 (1): 1–12.

Borgström, Lars, E. Bondesson, F. Moren, E. Trofast, and Stephen P. Newman. 1994. "Lung Deposition of Budesonide Inhaled via Turbuhaler®: A Comparison with Terbutaline Sulphate in Normal Subjects." *European Respiratory Journal* 7 (1): 69–73.

Borgström, Lars, Bo Olsson, and Lars Thorsson. 2006. "Degree of Throat Deposition Can Explain

the Variability in Lung Deposition of Inhaled Drugs." *Journal of Aerosol Medicine* 19 (4): 473–83.

Borojeni, Azadeh A.T., Michelle L. Noga, Andrew R. Martin, and Warren H. Finlay. 2015. "Validation of Airway Resistance Models for Predicting Pressure Loss through Anatomically Realistic Conducting Airway Replicas of Adults and Children." *Journal of Biomechanics* 48 (10): 1988–96.

Brink, Karen I.Maassen Van Den, Martin Boorsma, A. Jeske Staal-Van Den Brekel, Staffam Edsbäcker, Emiel F. Wouters, and Lars Thorsson. 2008. "Evidence of the in Vivo Esterification of Budesonide in Human Airways." *British Journal of Clinical Pharmacology* 66 (1): 27–35.

Broeders, Mariëlle E.A.C., Joaquin Sanchis, Mark L. Levy, Graham K. Crompton, and P. N.Richard Dekhuijzen. 2009. "The ADMIT Series - Issues in Inhalation Therapy. 2) Improving Technique and Clinical Effectiveness." *Primary Care Respiratory Journal* 18 (2): 76–82.

Buhl, R. 2006. "Local Oropharyngeal Side Effects of Inhaled Corticosteroids in Patients with Asthma." *Allergy: European Journal of Allergy and Clinical Immunology* 61 (5): 518–26.

Burnell, Patricia K. P., Lars Asking, Lars Borgström, Steve C. Nichols, Bo Olsson, David Prime, and Ian Shrubb. 2007. "Studies of the Human Oropharyngeal Airspaces Using Magnetic Resonance Imaging IV - the Oropharyngeal Retention Effect for Four Inhalation Delivery Systems." *Journal of Aerosol Medicine* 20 (3): 269–81.

Buttini, Francesca, James Hannon, Kristi Saavedra, Irene Rossi, Anna Giulia Balducci, Hugh Smyth, Andy Clark, and Paolo Colombo. 2016. "Accessorized DPI: A Shortcut towards Flexibility and Patient Adaptability in Dry Powder Inhalation." *Pharmaceutical Research* 33 (12): 3012–20.

Byron, Peter R. 1986. "Prediction of Drug Residence Times in Regions of the Human Respiratory Tract Following Aerosol Inhalation." *Journal of Pharmaceutical Sciences* 75 (5): 433–38.

Byron, Peter R., Michael Hindle, Carlos F. Lange, P. Worth Longest, Donald Mcrobbie, Michael J. Oldham, Bo Olsson, Charles G. Thiel, Herbert Wachtel, and Warren H. Finlay. 2010. "In Vivo – In Vitro Correlations: Predicting Pulmonary Drug Deposition from Pharmaceutical Aerosols." *Journal of Aerosol Medicine and Pulmonary Drug Delivery* 23 (Supplement 2): S59–69.

Caillaud, Denis, Charles Le Merre, Yan Martinat, Bernard Aguilaniu, and Demetri Pavia. 2007. "A Dose-Ranging Study of Tiotropium Delivered via Respimat® Soft Mist™ Inhaler or HandiHaler® in COPD Patients." *International Journal of COPD* 2 (4): 559–65.

Caniga, Michael, Antonio Cabal, Khamir Mehta, David S. Ross, Malgorzata A. Gil, Janice D. Woodhouse, Joseph Eckman, et al. 2016. "Preclinical Experimental and Mathematical Approaches for Assessing Effective Doses of Inhaled Drugs, Using Mometasone to Support Human Dose Predictions." *Journal of Aerosol Medicine and Pulmonary Drug Delivery* 29 (4): 362–77.

Carrigy, Nicholas B., Andrew R. Martin, and Warren H. Finlay. 2015. "Use of Extrathoracic

Deposition Models for Patient-Specific Dose Estimation during Inhaler Design." *Current Pharmaceutical Design* 21 (27): 3984–92.

Carrigy, Nicholas B., Conor A. Ruzycki, Laleh Golshahi, and Warren H. Finlay. 2014. "Pediatric In Vitro and In Silico Models of Deposition via Oral and Nasal Inhalation." *Journal of Aerosol Medicine and Pulmonary Drug Delivery* 27 (3): 149–69.

Cazzola, M., C. P. Page, L. Calzetta, and M. G. Matera. 2012. "Pharmacology and Therapeutics of Bronchodilators." *Pharmacological Reviews* 64 (3): 450–504.

Chan, Tai L., and Morton Lippmann. 1980. "Experimental Measurements and Empirical Modelling of the Regional Deposition of Inhaled Particles in Humans." *American Industrial Hygiene Association Journal* 41 (6): 399–409.

Chen, John Z., M Kiaee, Andrew R. Martin, and Warren H. Finlay. 2020. "In Vitro Assessment of an Idealized Nose for Nasal Spray Testing: Comparison with Regional Deposition in Realistic Nasal Replicas." *International Journal of Pharmaceutics* 582.

Cheng, Yung-Sung. 2003. "Aerosol Deposition in the Extrathoracic Region." *Aerosol Science and Technology* 37 (8): 659–71.

Cheng, Yung-Sung, C S Fu, D Yazzie, and Y Zhou. 2001. "Respiratory Deposition Patterns of Salbutamol PMDI with CFC and HFA-134a Formulations in a Human Airway Replica." *Journal of Aerosol Medicine* 14 (2): 255–66.

Cheng, Yung-Sung, Yue Zhou, and Bean T. Chen. 1999. "Particle Deposition in a Cast of Human Oral Airways." *Aerosol Science and Technology* 31 (4): 286–300.

Chuchalin, A.G., H.-J. Kremer, P. Metzenauer, E. O'Keefe, and R. Hermann. 2002. "Clinical Equivalence Trial on Budesonide Delivered Either by the Novolizer® Multidose Dry Powder Inhaler or the Turbuhaler® in Asthmatic Patients." *Respiration* 69 (6): 502–8.

Chung, Kian Fan, Sally E. Wenzel, Jan L. Brozek, Andrew Bush, Mario Castro, Peter J. Sterk, Ian M. Adcock, et al. 2014. "International ERS/ATS Guidelines on Definition, Evaluation and Treatment of Severe Asthma." *European Respiratory Journal* 43 (2): 343–73.

Ciciliani, Anna Maria, Peter Langguth, and Herbert Wachtel. 2017. "In Vitro Dose Comparison of Respimat® Inhaler with Dry Powder Inhalers for COPD Maintenance Therapy." *International Journal of COPD* 12: 1565–77.

Cinkotai, F. F. 1971. "The Behaviour of Sodium Chloride Particles in Moist Air." *Journal of Aerosol Science* 2 (3): 325–29.

Clark, Andrew R. 2012. "Understanding Penetration Index Measurements and Regional Lung Targeting." *Journal of Aerosol Medicine and Pulmonary Drug Delivery* 25 (4): 179–87.

Coates, Allan L., Bruce Culver, Donald Cockcroft, Teal Hallstrand, Jeffrey Haynes, David Kaminsky, Neil MacIntyre, and Jack Wanger. 2018. "Characterizing Nebulizer Performance for Methacholine Challenge Tests." *American Journal of Respiratory and Critical Care Medicine* 198 (8): 988–90.

Coates, Allan L., Kitty Leung, and Sharon D. Dell. 2014. "Developing Alternative Delivery

Systems for Methacholine Challenge Tests." *Journal of Aerosol Medicine and Pulmonary Drug Delivery* 27 (1): 66–70.

Coates, Allan L., Jack Wanger, Donald W. Cockcroft, Bruce H. Culver, Kai Håkon Carlsen, Zuzana Diamant, Gail Gauvreau, et al. 2017. "ERS Technical Standard on Bronchial Challenge Testing: General Considerations and Performance of Methacholine Challenge Tests." *European Respiratory Journal* 49 (5): 1–17.

Cockcroft, Donald W., Beth E. Davis, and Christianne M. Blais. 2019. "Direct Bronchoprovocation Test Methods: History 1945–2018." *Expert Review of Respiratory Medicine* 13 (3): 279–89.

Cohen, Mark D., Richard C. Flagan, and John H. Seinfeld. 1987. "Studies of Concentrated Electrolyte Solutions Using the Electrodynamic Balance. 2. Water Activities for Mixed-Electrolyte Solutions." *Journal of Physical Chemistry* 91 (17): 4575–82.

Cohen, Scott D., and Alan C. Hindmarsh. 1994. "CVODE User Guide, Technical Report UCRL-MA-118618." Livermore, California.

Crapo, Robert O., Richard Casaburi, Allan L. Coates, Paul L. Enright, John L. Hankinson, Charles G. Irvin, Neil R. MacIntyre, et al. 2000. "Guidelines for Methacholine and Exercise Challenge Testing-1999. Official Statement of the American Thoracic Society." *American Journal of Respiratory and Critical Care Medicine* 161 (1): 309–29.

Dahl, Ronald, Bo Lundback, Jean-Luc Malo, Jorge. A. Mazza, Markku M. Nieminen, Pekka Saarelainen, and Helen Barnacle. 1993. "A Dose-Ranging Study of Fluticasone Propionate in Adult Patients with Moderate Asthma." *Chest* 104 (5): 1352–58.

Daley-Yates, Peter T. 2015. "Inhaled Corticosteroids: Potency, Dose Equivalence and Therapeutic Index." *British Journal of Clinical Pharmacology* 80 (3): 372–80.

Daley-Yates, Peter T., Noushin Brealey, Sebin Thomas, Daren Austin, Shaila Shabbir, Tim Harrison, Dave Singh, and Neil Barnes. 2021. "Therapeutic Index of Inhaled Corticosteroids in Asthma: A Dose–Response Comparison on Airway Hyperresponsiveness and Adrenal Axis Suppression." *British Journal of Clinical Pharmacology* 87 (2): 483–93.

Darquenne, Chantal, John S. Fleming, Ira Katz, Andrew R. Martin, Jeffry Schroeter, Omar S. Usmani, Jose Venegas, and Otmar Schmid. 2016. "Bridging the Gap Between Science and Clinical Efficacy: Physiology, Imaging, and Modeling of Aerosols in the Lung." *Journal of Aerosol Medicine and Pulmonary Drug Delivery* 29 (2): 107–26.

Davis, Beth E., Samuel K. Simonson, Christianne M. Blais, and Donald W. Cockcroft. 2017. "Methacholine Challenge Testing: A Novel Method for Measuring PD20." *Chest* 152 (6): 1251–57.

Dehaan, Wes H., and Warren H. Finlay. 2004. "Predicting Extrathoracic Deposition from Dry Powder Inhalers." *Journal of Aerosol Science* 35: 309–31.

Dekhuijzen, P. N. Richard. 2012. "Anti-Inflammatory Drug Targeting in Asthma. Should Inhaled Corticosteroids Reach the Small Airways?" *Current Drug Therapy* 7 (4): 248–54.

Dell, Sharon D., Sundeep S. Bola, Richard G. Foty, Laura C. Marshall, Kathleen A. Nelligan, and

Allan L. Coates. 2015. "Provocative Dose of Methacholine Causing a 20% Drop in FEV1 Should Be Used to Interpret Methacholine Challenge Tests with Modern Nebulizers." *Annals of the American Thoracic Society* 12 (3): 357–63.

Delvadia, Renishkumar R., Michael Hindle, P. Worth Longest, and Peter R. Byron. 2012. "In Vitro Tests for Aerosol Deposition II: IVIVCs for Different Dry Powder Inhalers in Normal Adults." *Journal of Aerosol Medicine and Pulmonary Drug Delivery* 26 (3): 138–44.

Delvadia, Renishkumar R., P. Worth Longest, and Peter R. Byron. 2012. "In Vitro Tests for Aerosol Deposition. I : Scaling a Physical Model of the Upper Airways to Predict Drug Deposition Variation in Normal Humans." *Journal of Aerosol Medicine and Pulmonary Drug Delivery* 25 (1): 32–40.

Delvadia, Renishkumar R., P. Worth Longest, Michael Hindle, and Peter R. Byron. 2013. "In Vitro Tests for Aerosol Deposition. III: Effect of Inhaler Insertion Angle on Aerosol Deposition." *Journal of Aerosol Medicine and Pulmonary Drug Delivery* 26 (3): 145–56.

Delvadia, Renishkumar R., Xiangyin Wei, P. Worth Longest, Jurgen Venitz, and Peter R. Byron. 2016. "In Vitro Tests for Aerosol Deposition. IV: Simulating Variations in Human Breath Profiles for Realistic DPI Testing." *Journal of Aerosol Medicine and Pulmonary Drug Delivery* 29 (2): 196–206.

Devadason, Sunalene G., Hak-Kim Chan, Sabine Haeussermann, Claudius Kietzig, Philip J. Kuehl, Stephen Newman, Knut Sommerer, and Glyn Taylor. 2012. "Validation of Radiolabeling of Drug Formulations for Aerosol Deposition Assessment of Orally Inhaled Products." *Journal of Aerosol Medicine and Pulmonary Drug Delivery* 25 (S1): S-6-S-9.

Dokoumetzidis, Aristides, and Panos Macheras. 2006. "A Century of Dissolution Research: From Noyes and Whitney to the Biopharmaceutics Classification System." *International Journal of Pharmaceutics* 321 (1–2): 1–11.

Dolovich, Myrna B, and Jolyon P Mitchell. 2004. "Canadian Standards Association Standard CAN/CSA/Z264." *Canadian Respiratory Journal* 11 (7): 489–95.

Döring, Gerd, Patrick Flume, Harry Heijerman, and J. Stuart Elborn. 2012. "Treatment of Lung Infection in Patients with Cystic Fibrosis: Current and Future Strategies." *Journal of Cystic Fibrosis* 11 (6): 461–79.

Dorosz, Agata, Agata Penconek, and Arkadiusz Moskal. 2016. "In Vitro Study on the Aerosol Emitted from the DPI Inhaler under Two Unsteady Inhalation Profiles." *Journal of Aerosol Science* 101: 104–17.

Duddu, Sarma P., Steven A. Sisk, Yulia H. Walter, Thomas E. Tarara, Kevin R. Trimble, Andrew R. Clark, Michael A. Eldon, et al. 2002. "Improved Lung Delivery from a Passive Dry Powder Inhaler Using an Engineered PulmoSphere® Powder." *Pharmaceutical Research* 19 (5): 689–95.

El-Gammal, Amani I., Kieran J. Killian, Tara X. Scime, Suzanne Beaudin, Abbey Schlatman, Donald W. Cockcroft, and Gail M. Gauvreau. 2015. "Comparison of the Provocative Concentration of Methacholine Causing a 20% Fall in FEV1 between the AeroEclipse II Breath-Actuated Nebulizer and the Wright Nebulizer in Adult Subjects with Asthma." *Annals*

of the American Thoracic Society 12 (7): 1039–43.

Eriksson, Johanna, Helena Thörn, Erik Sjögren, Lisa Holmstén, Katarina Rubin, and Hans Lennernäs. 2019. "Pulmonary Dissolution of Poorly Soluble Compounds Studied in an Ex Vivo Rat Lung Model." *Molecular Pharmaceutics* 16: 3053–64.

Esposito-Festen, Jose E., B Ates, Frans J. M. van Vliet, Antonius F. M. Verbraak, Johan C. de Jongste, and Harm A.W.M. Tiddens. 2004. "Effect of a Facemask Leak on Aerosol Delivery from a PMDI-Spacer System." *Journal of Aerosol Medicine* 17 (1): 1–6.

European Medicines Agency Committee for Medical Products for Human Use. 2006. *Guidleline on the Pharmaceutical Quality of Inhalation and Nasal Products*. London.

European Pharmacopeia. 2019. *Ph Eur 9.8 General Chapter 2.9.18 Preparations for Inhalation: Aerodynamic Assessment of Fine Particles*. Strasbourg, France.

Everard, Mark L., Sunalene G. Devadason, and Peter N. Le Souëf. 1997. "Flow Early in the Inspiratory Manoeuvre Affects the Aerosol Particle Size Distribution from a Turbuhaler." *Respiratory Medicine* 91: 624–28.

Fadl, Ahmed, Jinbo Wang, Zongqin Zhang, and Yung-Sung Cheng. 2007. "Effects of MDI Spray Angle on Aerosol Penetration Efficiency through an Oral Airway Cast." *Journal of Aerosol Science* 38 (8): 853–64.

Ferron, George A. 1977. "The Size of Soluble Aerosol Particles as a Function of the Humidity of the Air. Application to the Human Respiratory Tract." *Journal of Aerosol Science* 8 (4): 251–67.

Ferron, George A., and Josef Gebhart. 1988. "Estimation of the Lung Deposition of Aerosol Particles Produced with Medical Nebulizers." *Journal of Aerosol Science* 19 (7): 1083–86.

Ferron, George A., B Haider, and W G Kreyling. 1988. "Inhalation of Salt Aerosol Particles—I. Estimation of the Temperature and Relative Humidity of the Air in the Human Upper Airways." *Journal of Aerosol Science* 19 (3): 343–63.

Ferron, George A., Wolfgang G. Kreyling, and B Haider. 1988. "Inhalation of Salt Aerosol Particles—II. Growth and Deposition in the Human Respiratory Tract." *Journal of Aerosol Science* 19 (5): 611–31.

Ferron, George A., Christa Roth, B. Busch, and E. Karg. 1997. "Estimation of the Size Distribution of Aerosols Produced by Jet Nebulizers as a Function of Time." *Journal of Aerosol Science* 28 (5): 805–19.

Fink, James B., Lisa Molloy, John S. Patton, Valdecir Castor Galindo-Filho, Jacqueline de Melo Barcelar, Luciana Alcoforado, Simone Cristina Soares Brandão, and Armèle Dornelas de Andrade. 2017. "Good Things in Small Packages: An Innovative Delivery Approach for Inhaled Insulin." *Pharmaceutical Research* 34 (12): 2568–78.

Fink, James B., and Bruce K. Rubin. 2005. "Problems with Inhaler Use: A Call for Improved Clinician and Patient Education." *Respiratory Care* 50 (10): 1360–75.

Finlay, Warren H. 1998. "Estimating the Type of Hygroscopic Behavior Exhibited by Aqueous

Droplets." *Journal of Aerosol Medicine* 11 (4): 221–29.

———. 2019. *The Mechanics of Inhaled Pharmaceutical Aerosols : An Introduction*. 2nd ed. San Diego: Academic Press.

Finlay, Warren H., and M. G. Gehmlich. 2000. "Inertial Sizing of Aerosol Inhaled from Two Dry Powder Inhalers with Realistic Breath Patterns versus Constant Flow Rates." *International Journal of Pharmaceutics* 210 (1–2): 83–95.

Finlay, Warren H., Carlos F. Lange, Malcolm King, and David P. Speert. 2000. "Lung Delivery of Aerosolized Dextran." *American Journal of Respiratory and Critical Care Medicine* 161: 91–97.

Finlay, Warren H., Carlos F. Lange, WI. Li, and M. Hoskinson. 2000. "Validating Deposition Models in Disease : What Is Needed ?" *Journal of Aerosol Medicine* 13 (4): 381–86.

Finlay, Warren H., and Andrew R. Martin. 2008. "Recent Advances in Predictive Understanding of Respiratory Tract Deposition." *Journal of Aerosol Medicine and Pulmonary Drug Delivery* 21 (2): 189–206.

Finlay, Warren H., and Kevin W. Stapleton. 1995. "The Effect on Regional Lung Deposition of Coupled Heat and Mass Transfer between Hygroscopic Droplets and Their Surrounding Phase." *Journal of Aerosol Science* 26 (4): 655–70.

———. 1999. "Undersizing of Droplets from a Vented Nebulizer Caused by Aerosol Heating during Transit through an Anderson Impactor." *Journal of Aerosol Science* 30 (1): 105–9.

Finlay, Warren H., Kevin W. Stapleton, Hak-Kim Chan, Peter C. Zuberbuhler, and Igor Gonda. 1996. "Regional Deposition of Inhaled Hygroscopic Aerosols: In Vivo SPECT Compared with Mathematical Modeling." *Journal of Applied Physiology* 81 (1): 374–83.

Finlay, Warren H., Kevin W. Stapleton, and Peter C. Zuberbuhler. 1998. "Variations in Predicted Regional Lung Deposition of Salbutamol Sulphate between 19 Nebulizer Types." *Journal of Aerosol Medicine: Deposition, Clearance, and Effects in the Lung* 11 (2): 65–80.

Finlay, Warren H., and Jonathan P. Wong. 1998. "Regional Lung Deposition of Nebulized Liposome-Encapsulated Ciprofloxacin." *International Journal of Pharmaceutics* 167 (1–2): 121–27.

Fleming, John, Joy Conway, Caroline Majoral, Ira Katz, Georges Caillibotte, Marine Pichelin, Spyridon Montesantos, and Michael Bennett. 2015. "Controlled, Parametric, Individualized, 2-D and 3-D Imaging Measurements of Aerosol Deposition in the Respiratory Tract of Asthmatic Human Subjects for Model Validation." *Journal of Aerosol Medicine and Pulmonary Drug Delivery* 28 (6): 432–51.

Floroiu, Andreea, Martin Klein, Johannes Krämer, and Claus Michael Lehr. 2018. "Towards Standardized Dissolution Techniques for in Vitro Performance Testing of Dry Powder Inhalers." *Dissolution Technologies* 25 (3): 6–18.

Frijlink, Henderik W., and Anne H. De Boer. 2005. "Dry Powder Inhalers for Pulmonary Drug Delivery." *Expert Opinion on Drug Delivery* 1 (1): 67–86.

Geller, David E., William H. Pitlick, Pasqua A. Nardella, William G. Tracewell, and Bonnie W. Ramsey. 2002. "Pharmacokinetics and Bioavailability of Aerosolized Tobramycin in Cystic Fibrosis." *Chest* 122 (1): 219–26.

Gerde, Per, Maria Malmlöf, and Ewa Selg. 2021. "In Vitro to Ex Vivo/In Vivo Correlation (IVIVC) of Dissolution Kinetics from Inhaled Particulate Solutes Using Air/Blood Barrier Models: Relation between in Vitro Design, Lung Physiology and Kinetic Output of Models." *Journal of Aerosol Science* 151 (October 2020): 105698.

Golshahi, Laleh, and Warren H. Finlay. 2012. "An Idealized Child Throat That Mimics Average Pediatric Oropharyngeal Deposition." *Aerosol Science and Technology* 46 (5): i–iv.

Golshahi, Laleh, Michelle L. Noga, and Warren H. Finlay. 2012. "Deposition of Inhaled Micrometer-Sized Particles in Oropharyngeal Airway Replicas of Children at Constant Flow Rates." *Journal of Aerosol Science* 49: 21–31.

Golshahi, Laleh, Michelle L. Noga, Reinhard Vehring, and Warren H. Finlay. 2013. "An in Vitro Study on the Deposition of Micrometer-Sized Particles in the Extrathoracic Airways of Adults during Tidal Oral Breathing." *Annals of Biomedical Engineering* 41 (5): 979–89.

Golshahi, Laleh, Geng Tian, Mandana Azimi, Yoen Ju Son, Ross Walenga, P. Worth Longest, and Michael Hindle. 2013. "The Use of Condensational Growth Methods for Efficient Drug Delivery to the Lungs during Noninvasive Ventilation High Flow Therapy." *Pharmaceutical Research* 30 (11): 2917–30.

Gonda, Igor. 1988. "Drugs Administered Directly into the Respiratory Tract: Modeling of the Duration." *Journal of Pharmaceutical Sciences* 77 (4): 340–46.

Gregson, Florance K.A., Joshua F. Robinson, Rachael E.H. Miles, C. Paddy Royall, and Jonathan P. Reid. 2019. "Drying Kinetics of Salt Solution Droplets: Water Evaporation Rates and Crystallization." Research-article. *Journal of Physical Chemistry B* 123 (1): 266–76.

Greguletz, Roland, Pontus U. Andersson, Andy Cooper, Frank Chambers, Mark A. Copley, Geoff Daniels, Melanie Hamilton, et al. 2020. "A Cross-Industry Assessment of the Flow Rate-Time Profiles of Test Equipment Typically Used for Dry-Powder Inhaler (DPI) Testing: Part 1–Compendial Apparatuses." *Aerosol Science and Technology* 54 (12): 1424–47.

Greguletz, Roland, Jan Arp, Chris Blatchford, Frank Chambers, Mark A. Copley, Volker Glaab, Teresa Iley, et al. 2010. "A Collaborative Study by the European Pharmaceutical Aerosol Group (EPAG) to Assess the Flow-Time Profile of Test Equipment Typically Used for PMDI/DPI Testing – Part 1: Volume Test." *Ddl 2010*, no. December: 1–5.

Grgic, Biljana, Warren H. Finlay, Patricia K. P. Burnell, and Anthony F. Heenan. 2004. "In Vitro Intersubject and Intrasubject Deposition Measurements in Realistic Mouth – Throat Geometries." *Journal of Aerosol Science* 35: 1025–40.

Grgic, Biljana, Andrew R. Martin, and Warren H. Finlay. 2006. "The Effect of Unsteady Flow Rate Increase on in Vitro Mouth-Throat Deposition of Inhaled Boluses." *Journal of Aerosol Science* 37 (10): 1222–33.

Gross, Nicholas J., and Peter J. Barnes. 2017. "New Therapies for Asthma and Chronic Obstructive Pulmonary Disease." *American Journal of Respiratory and Critical Care Medicine* 195 (2):

159–66.

Guilmette, Raymond A., Jeffrey D. Wicks, and Ronald K. Wolff. 1989. "Morphometry of Human Nasal Airways In Vivo Using Magnetic Resonance Imaging." *Journal of Aerosol Medicine* 2 (4): 365–77.

Gysel, M, E Weingartner, and U Baltensperger. 2002. "Hygroscopicity of Aerosol Particles at Low Temperatures. 2. Theoretical and Experimental Hygroscopic Properties of Laboratory Generated Aerosols." *Environmental Science & Technology* 36 (1): 63–68.

Hämäläinen, K. M., M. Granander, P. Toivanen, and A. Malinen. 2001. "Assessment of the Systemic Effects of Budesonide Inhaled from Easyhaler® and from Turbuhaler® in Healthy Male Volunteers." *Respiratory Medicine* 95 (11): 863–69.

Hamid, Qutayba, Yunling Song, Thomas C. Kotsimbos, Eleanor Minshall, Tony R. Bai, Richard G. Hegele, and James C. Hogg. 1997. "Inflammation of Small Airways in Asthma." *Journal of Allergy and Clinical Immunology* 100 (1): 44–51.

Hämmerlein, Andrea, Uta Müller, and Martin Schulz. 2011. "Pharmacist-Led Intervention Study to Improve Inhalation Technique in Asthma and COPD Patients." *Journal of Evaluation in Clinical Practice* 17 (1): 61–70.

Harrison, T. W., and A. E. Tattersfield. 2003. "Plasma Concentrations of Fluticasone Propionate and Budesonide Following Inhalation from Dry Powder Inhalers by Healthy and Asthmatic Subjects." *Thorax* 58 (3): 258–60.

Hastedt, Jayne E., Per Bäckman, Andrew R. Clark, William Doub, Anthony Hickey, Guenther Hochhaus, Phil J. Kuehl, et al. 2016. "Scope and Relevance of a Pulmonary Biopharmaceutical Classification System AAPS/FDA/USP Workshop March 16-17th, 2015 in Baltimore, MD." *American Association of Pharmaceutical Scientists Open* 2 (1): 1.

Hatley, Ross H.M., Jacob Parker, John N. Pritchard, and Dirk von Hollen. 2016. "Variability in Delivered Dose from Pressurized Metered-Dose Inhaler Formulations Due to a Delay Between Shake and Fire." *Journal of Aerosol Medicine and Pulmonary Drug Delivery* 30 (1): 71–79.

Heyder, J. 1975. "Gravitational Deposition of Aerosol Particles within a System of Randomly Oriented Tubes." *Aerosol Science* 6 (3): 133–37.

Heyder, J, and Josef Gebhart. 1977. "Gravitational Deposition of Particles from Laminar Aerosol Flow Through Inclined Circular Tubes." *Journal of Aerosol Science* 8 (1972): 289–95.

Hickey, Anthony J. 2014. "Controlled Delivery of Inhaled Therapeutic Agents." *Journal of Controlled Release* 190: 182–88.

Himstedt, Anneke, Clemens Braun, Sebastian Georg Wicha, and Jens Markus Borghardt. 2020. "Towards a Quantitative Mechanistic Understanding of Localized Pulmonary Tissue Retention—a Combined in Vivo/in Silico Approach Based on Four Model Drugs." *Pharmaceutics* 12 (5).

Hinds, William C. 1999. *Aerosol Technology : Properties, Behavior, and Measurement of Airborne Particles*. 2nd ed. Hoboken, NJ: Wiley.

Hintz, Rebecca J., and Kevin C. Johnson. 1989. "The Effect of Particle Size Distribution on Dissolution Rate and Oral Absorption." *International Journal of Pharmaceutics* 51 (1): 9–17.

Hira, Daiki, Hiroyoshi Koide, Shigemi Nakamura, Toyoko Okada, Kazunori Ishizeki, Masafumi Yamaguchi, Setsuko Koshiyama, et al. 2018. "Assessment of Inhalation Flow Patterns of Soft Mist Inhaler Co-Prescribed with Dry Powder Inhaler Using Inspiratory Flow Meter for Multi Inhalation Devices." *PLoS ONE* 13 (2): 1–12.

Hirst, Peter H., R. E. Bacon, Gary R. Pitcairn, M. Silvasti, and Stephen P. Newman. 2001. "A Comparison of the Lung Deposition of Budesonide from Easyhlaler®, Turbuhaler® and PMDI plus Spacer in Asthmatic Patients." *Respiratory Medicine* 95 (9): 720–27.

Hirst, Peter H., Stephen P. Newman, David A. Clark, and Michaël G.L. Hertog. 2002. "Lung Deposition of Budesonide from the Novel Dry Powder Inhaler Airmax^{TM}." *Respiratory Medicine* 96 (6): 389–96.

Hirst, Peter H., Gary R. Pitcairn, Jeffry G. Weers, T. E. Tarara, Andrew R. Clark, L. A. Dellamary, G. Hall, J. Shorr, and Stephen P. Newman. 2002. "In Vivo Lung Deposition of Hollow Porous Particles from a Pressurized Metered Dose Inhaler." *Pharmaceutical Research* 19 (3): 258–64.

Hochhaus, Günther, Mong-jen Chen, Jagdeep Shur, Abhinav Kurumaddali, Uta Schilling, Yuanyuan Jiao, Stefanie K Drescher, et al. 2020. "Unraveling the Pulmonary Fate of Fluticasone and Friends : Meeting the Physiologic and Pharmacokinetic Challenges." *Respiratory Drug Delivery 2020*, 139–46.

Hochhaus, Günther, Mong Jen Chen, Abhinav Kurumaddali, Uta Schilling, Yuanyuan Jiao, Stefanie K. Drescher, Elham Amini, et al. 2021. "Can Pharmacokinetic Studies Assess the Pulmonary Fate of Dry Powder Inhaler Formulations of Fluticasone Propionate?" *AAPS Journal* 23 (3): 1–14.

Hochhaus, Günther, Helmut Möllmann, Hartmut Derendorf, and Ricardo J. Gonzalez-Rothi. 1997. "Pharmacokinetic/Pharmacodynamic Aspects of Aerosol Therapy Using Glucocorticoids as a Model." *Journal of Clinical Pharmacology* 37 (10): 881–92.

Hoe, Susan, James W. Ivey, Mohammed A. Boraey, Abouzar Shamsaddini-Shahrbabak, Emadeddin Javaheri, Sadaf Matinkhoo, Warren H. Finlay, and Reinhard Vehring. 2014. "Use of a Fundamental Approach to Spray-Drying Formulation Design to Facilitate the Development of Multi-Component Dry Powder Aerosols for Respiratory Drug Delivery." *Pharmaceutical Research* 31 (2): 449–65.

Hofmann, Werner. 2020. "Regional Deposition: Deposition Models." *Journal of Aerosol Medicine and Pulmonary Drug Delivery* 33 (5): 239–48.

Hossny, Elham, Nelson Rosario, Bee Wah Lee, Meenu Singh, Dalia El-Ghoneimy, Jian Yi Soh, and Peter Le Souef. 2016. "The Use of Inhaled Corticosteroids in Pediatric Asthma: Update." *World Allergy Organization Journal* 9 (1): 1–24.

Huynh, Bao K., Daniela Traini, Dale R. Farkas, P. Worth Longest, Michael Hindle, and Paul M. Young. 2018. "The Development and Validation of an In Vitro Airway Model to Assess

Realistic Airway Deposition and Drug Permeation Behavior of Orally Inhaled Products Across Synthetic Membranes." *Journal of Aerosol Medicine and Pulmonary Drug Delivery* 31 (2): 103–8.

Ingham, D B. 1975. "Diffusion of Aerosols from a Stream Flowing Through a Cylindrical Tube." *Aerosol Science* 6 (1): 125–32.

International Commission on Radiological Protection. 1994. *Human Respiratory Tract Model for Radiological Protection : A Report of a Task Group of the International Commission on Radiological Protection.* Vol. 24 1-3. Oxford, Eng. :Tarrytown, N.Y.: published for the International Commission on Radiological Protection by Pergamon.

Itoga, Nathan K., Christopher K. Kinoshita, Stephen M. Masutani, and Loren G. Yamamoto. 2014. "Mechanical Factors Affecting Nebulized Albuterol Aerosol Particle Sizes for Asthma Drug Delivery." *American Journal of Emergency Medicine* 32 (6): 569–72.

Ivey, James W., David Lewis, Tanya Church, Warren H. Finlay, and Reinhard Vehring. 2014. "A Correlation Equation for the Mass Median Aerodynamic Diameter of the Aerosol Emitted by Solution Metered Dose Inhalers." *International Journal of Pharmaceutics* 465 (1–2): 18–24.

Ivey, James W., Reinhard Vehring, and Warren H. Finlay. 2015. "Understanding Pressurized Metered Dose Inhaler Performance." *Expert Opinion on Drug Delivery* 12 (6): 901–16.

Janson, Christer, Thomas Loöf, Gunilla Telg, Georgios Stratelis, and Folke Nilsson. 2016. "Difference in Resistance to Humidity between Commonly Used Dry Powder Inhalers: An in Vitro Study." *Npj Primary Care Respiratory Medicine* 26 (June): 1–5.

Janssens, Hettie M., Johan C. de Jongste, Wytske J. Fokkens, Simon G.F. Robben, Kris Wouters, and Harm A.W.M. Tiddens. 2002. "The Sophia Anatomical Infant Nose-Throat (Saint) Model: A Valuable Tool to Study Aerosol Deposition in Infants." *Journal of Aerosol Medicine* 14 (4): 433–41.

Järvinen, A., M. Aitomaa, A. Rostedt, J. Keskinen, and J. Yli-Ojanperä. 2014. "Calibration of the New Electrical Low Pressure Impactor (ELPI+)." *Journal of Aerosol Science* 69: 150–59.

Javaheri, Emadeddin, and Warren H. Finlay. 2013. "Size Manipulation of Hygroscopic Saline Droplets: Application to Respiratory Drug Delivery." *International Journal of Heat and Mass Transfer* 67: 690–95.

Javaheri, Emadeddin, Laleh Golshahi, and Warren H. Finlay. 2013. "An Idealized Geometry That Mimics Average Infant Nasal Airway Deposition." *Journal of Aerosol Science* 55: 137–48.

Javaheri, Emadeddin, Farzin M Shemirani, Marine Pichelin, Ira M Katz, Georges Caillibotte, Reinhard Vehring, and Warren H. Finlay. 2013. "Deposition Modeling of Hygroscopic Saline Aerosols in the Human Respiratory Tract : Comparison between Air and Helium – Oxygen as Carrier Gases." *Journal of Aerosol Science* 64: 81–93.

Jen-Ping Chen. 1994. "Theory of Deliquescence and Modified Kohler Curves." *Journal of the Atmospheric Sciences* 51 (23): 3505–16.

Kaiser, H., D. Aaronson, R. Dockhorn, S. Edsbäcker, P. Korenblat, and A. Källén. 1999. "Dose-Proportional Pharmacokinetics of Budesonide Inhaled via Turbuhaler®." *British Journal of*

Clinical Pharmacology 48 (3): 309–16.

Kakavas, Sotirios, Ourania S. Kotsiou, Fotis Perlikos, Maria Mermiri, Georgios Mavrovounis, Konstantinos Gourgoulianis, and Ioannis Pantazopoulos. 2021. "Pulmonary Function Testing in COPD: Looking beyond the Curtain of FEV1." *Npj Primary Care Respiratory Medicine* 31 (1).

Kamin, Wolfgang E.S., Tilman Genz, Sascha Roeder, Gerhard Scheuch, Thomas Trammer, Ralf Juenemann, and Rolf M. Cloes. 2002. "Mass Output and Particle Size Distribution of Glucocorticosteroids Emitted from Different Inhalation Devices Depending on Various Inspiratory Parameters." *Journal of Aerosol Medicine* 15 (1): 65–73.

Kaviratna, Anubhav, Geng Tian, Xiaofei Liu, Renishkumar R. Delvadia, Sau Lee, and Changning Guo. 2019. "Evaluation of Bio-Relevant Mouth-Throat Models for Characterization of Metered Dose Inhalers." *AAPS PharmSciTech* 20 (3): 130.

Keller, Lea Adriana, Olivia Merkel, and Andreas Popp. 2021. "Intranasal Drug Delivery: Opportunities and Toxicologic Challenges during Drug Development." *Drug Delivery and Translational Research* Jan 25: 1–25.

Kerwin, Edward M., Donald P. Tashkin, Thomas R. Murphy, George W. Bensch, Tony Marrs, Mary Z. Luo, and Jack Y. Zhang. 2020. "A Dose-Ranging Study of Epinephrine Hydrofluroalkane Metered-Dose Inhaler (Primatene® MIST) in Subjects with Intermittent or Mild-to-Moderate Persistent Asthma." *Journal of Aerosol Medicine and Pulmonary Drug Delivery* 33 (4): 186–93.

Kiaee, Milad, Herbert Wachtel, Michelle L. Noga, Andrew R. Martin, and Warren H. Finlay. 2018. "Regional Deposition of Nasal Sprays in Adults: A Wide Ranging Computational Study." *International Journal for Numerical Methods in Biomedical Engineering* 34 (5): 1–13.

———. 2019. "An Idealized Geometry That Mimics Average Nasal Spray Deposition in Adults: A Computational Study." *Computers in Biology and Medicine* 107 (November 2018): 206–17.

Kopsch, Thomas, Darragh Murnane, and Digby Symons. 2016. "Optimizing the Entrainment Geometry of a Dry Powder Inhaler: Methodology and Preliminary Results." *Pharmaceutical Research* 33 (11): 2668–79.

Kotian, Reshma, Joanne Peart, Joan Bryner, and Peter R. Byron. 2009. "Calibration of the Modified Electrical Low-Pressure Impactor (ELPI) for Use with Pressurized Pharmaceutical Aerosols" 22 (1): 55–65.

Koullapis, Pantelis, Stravos C. Kassinos, Jefferson Muela, Carlos D. Perez-Segarra, Joaquim Rigola, Oriol Lehmkuhl, Yan Cui, et al. 2018. "Regional Aerosol Deposition in the Human Airways: The SimInhale Benchmark Case and a Critical Assessment of in Silico Methods." *European Journal of Pharmaceutical Sciences* 113 (June 2017): 77–94.

Kwok, Philip Chi Lip, and Hak Kim Chan. 2008. "Effect of Relative Humidity on the Electrostatic Charge Properties of Dry Powder Inhaler Aerosols." *Pharmaceutical Research* 25 (2): 277–88.

Kwong, W. T. Jenny, Sharon L. Ho, and Allan L. Coates. 2000. "Comparison of Nebulized Particle

Size Distribution with Malvern Laser Diffraction Analyzer Versus Andersen Cascade Impactor and Low-Flow Marple Personal Cascade Impactor." *Journal of Aerosol Medicine* 13 (4): 303–14.

Lähelmä, Satu, Merja Kirjavainen, Marjo Kela, Jukka Herttuainen, Mikko Vahteristo, Matti Silvasti, and Marjut Ranki-Pesonen. 2005. "Equivalent Lung Deposition of Budesonide in Vivo: A Comparison of Dry Powder Inhalers Using a Pharmacokinetic Method." *British Journal of Clinical Pharmacology* 59 (2): 167–73.

Lange, Carlos F., Robert E.W. Hancock, John Samuel, and Warren H. Finlay. 2001. "In Vitro Aerosol Delivery and Regional Airway Surface Liquid Concentration of a Liposomal Cationic Peptide." *Journal of Pharmaceutical Sciences* 90 (10): 1647–57.

Laube, Beth L., Hettie M. Janssens, Frans H.C. De Jongh, Sunalene G. Devadason, Rajiv Dhand, Patrice Diot, Mark L. Everard, et al. 2011. "What the Pulmonary Specialist Should Know about the New Inhalation Therapies." *European Respiratory Journal* 37 (6): 1308–31.

Laube, Beth L., Gail Sharpless, Charles Shermer, Vincent Sullivan, and Kenneth Powell. 2012. "Deposition of Dry Powder Generated by Solovent in Sophia Anatomical Infant Nose-Throat (SAINT) Model." *Aerosol Science and Technology* 46 (5): 514–20.

Leach, Chet L., and Gene L. Colice. 2010. "A Pilot Study to Assess Lung Deposition of HFA-Beclomethasone and CFC-Beclomethasone from a Pressurized Metered Dose Inhaler with and without Add-On Spacers and Using Varying Breathhold Times." *Journal of Aerosol Medicine and Pulmonary Drug Delivery* 23 (6): 355–61.

Leach, Chet L., Patricia J. Davidson, and Robert J. Boudreau. 1998. "Improved Airway Targeting with the CFC-Free HFA-Beclomethasone Metered- Dose Inhaler Compared with CFC-Beclomethasone." *European Respiratory Journal* 12 (6): 1346–53.

Leach, Chet L., Patricia J. Davidson, Bruce E. Hasselquist, and Robert J. Boudreau. 2005. "Influence of Particle Size and Patient Dosing Technique on Lung Deposition of HFA-Beclomethasone from a Metered Dose Inhaler." *Journal of Aerosol Medicine* 18 (4): 379–85.

Lee, Sau L., Bhawana Saluja, Alfredo García-Arieta, Gustavo Mendes Lima Santos, Ying Li, Sarah Lu, Shuguang Hou, et al. 2015. "Regulatory Considerations for Approval of Generic Inhalation Drug Products in the US, EU, Brazil, China, and India." *The AAPS Journal* 17 (5): 1285–1304.

Liu, Xiaofei, William H. Doub, and Changning Guo. 2012. "Evaluation of Metered Dose Inhaler Spray Velocities Using Phase Doppler Anemometry (PDA)." *International Journal of Pharmaceutics* 423 (2): 235–39.

Loira-Pastoriza, Cristina, Julie Todoroff, and Rita Vanbever. 2014. "Delivery Strategies for Sustained Drug Release in the Lungs." *Advanced Drug Delivery Reviews* 75: 81–91.

Longest, P. Worth, Geng Tian, Renishkumar R. Delvadia, and Michael Hindle. 2012. "Development of a Stochastic Individual Path (SIP) Model for Predicting the Deposition of Pharmaceutical Aerosols: Effects of Turbulence, Polydisperse Aerosol Size, and Evaluation of Multiple Lung Lobes." *Aerosol Science and Technology* 46 (12): 1271–85.

Low, Richard D H. 1969. "A Generalized Equation for the Solution Effect in Droplet Growth."

Journal of Atmospheric Sciences 26 (3): 608–11.

Lu, Dongmei, Sau L. Lee, Robert A. Lionberger, Stephanie Choi, Wallace Adams, Hoainhon N. Caramenico, Badrul A. Chowdhury, et al. 2015. "International Guidelines for Bioequivalence of Locally Acting Orally Inhaled Drug Products: Similarities and Differences." *AAPS Journal* 17 (3): 546–57.

Majoral, Caroline, Allan L. Coates, Alain Le Pape, and Laurent Vecellio. 2020. "Humidified and Heated Cascade Impactor for Aerosol Sizing." *Frontiers in Bioengineering and Biotechnology* 8: 1313.

Marjamäki, Marko, Jyrki Ristimäki, Annele Virtanen, Mikko Moisio, R Luoma, and Jorma Keskinen. 2000. "Testing Porous Metal as a Collection Substrate in ELPI." *Journal of Aerosol Science* 31: 76–77.

Martin, Andrew R., and Warren H. Finlay. 2005. "The Effect of Humidity on the Size of Particles Delivered from Metered-Dose Inhalers." *Aerosol Science and Technology* 39 (4): 283–89.

———. 2018. "Model Calculations of Regional Deposition and Disposition for Single Doses of Inhaled Liposomal and Dry Powder Ciprofloxacin." *Journal of Aerosol Medicine and Pulmonary Drug Delivery* 31 (1): 49–60.

Martin, Andrew R., Valdimir S. Malinin, David. Cipolla, and Warren H. Finlay. 2021. "Modeling Regional Deposition and Pharmacokinetics for Inhaled Prodrug Treprostinil Palmitil." *Journal of Aerosol Medicine and Pulmonary Drug Delivery* 34 (5): A-12.

Martin, Andrew R., Charles P. Moore, and Warren H. Finlay. 2018. "Models of Deposition, Pharmacokinetics, and Intersubject Variability in Respiratory Drug Delivery." *Expert Opinion on Drug Delivery* 15 (12): 1175–88.

Martonen, T. B. 1990. "Development of Surrogate Lung Systems with Controlled Thermodynamic Environments to Study Hygroscopic Particles: Air Pollutants and Pharmacologic Drugs." *Particulate Science and Technology* 8 (1–2): 1–20.

Maselli, Diego J, Holly Keyt, and Marcos I Restrepo. 2017. "Inhaled Antibiotic Therapy in Chronic Respiratory Diseases." *International Journal of Molecular Sciences* 18 (5): 1062.

May, Sabine, Birte Jensen, Claudius Weiler, Markus Wolkenhauer, Marc Schneider, and Claus Michael Lehr. 2014. "Dissolution Testing of Powders for Inhalation: Influence of Particle Deposition and Modeling of Dissolution Profiles." *Pharmaceutical Research* 31 (11): 3211–24.

McRobbie, Donald W., and Susan E. Pritchard. 2005. "Studies of the Human Oropharyngeal Airspaces Using Magnetic Resonance Imaging. III. The Effects of Device Resistance with Forced Maneuver and Tidal Breathing on Upper Airway Geometry." *Journal of Aerosol Medicine* 18 (3): 325–36.

McRobbie, Donald W., Susan Pritchard, and Rebecca A. Quest. 2003. "Studies of the Human Oropharyngeal Airspaces Using Magnetic Resonance Imaging. I. Validation of a Three-Dimensional MRI Method for Producing Ex Vivo Virtual and Physical Casts of the Oropharyngeal Airways During Inspiration." *Journal of Aerosol Medicine* 16 (4): 401–15.

Meda Pharma GmbH. 2017. "Budelin Novolizer 200 Mikrogramov/Odmerek Prašek Za Inhaliranje." Bad Homburg, Germany.

Minocchieri, Stefan, Juerg Martin Burren, Marc Aurel Bachmann, Georgette Stern, Johannes Wildhaber, Stefan Buob, Ralf Schindel, Richard Kraemer, Urs Peter Frey, and Mathias Nelle. 2008. "Development of the Premature Infant Nose Throat-Model (PrINT-Model)-an Upper Airway Replica of a Premature Neonate for the Study of Aerosol Delivery." *Pediatric Research* 64 (2): 141–46.

Mitchell, Jolyon P., and Myrna B. Dolovich. 2012. "Clinically Relevant Test Methods to Establish In Vitro Equivalence for Spacers and Valved Holding Chambers Used with Pressurized Metered Dose Inhalers (PMDIs)." *Journal of Aerosol Medicine and Pulmonary Drug Delivery* 25 (4): 217–42.

Mitchell, Jolyon P., Jason Suggett, and Mark Nagel. 2016. "Clinically Relevant In Vitro Testing of Orally Inhaled Products—Bridging the Gap Between the Lab and the Patient." *AAPS PharmSciTech* 17 (4): 787–804.

Mohammed, Hlack, Daryl L. Roberts, Mark A. Copley, Mark Hammond, Steven C. Nichols, and Jolyon P. Mitchell. 2012. "Effect of Sampling Volume on Dry Powder Inhaler (DPI)-Emitted Aerosol Aerodynamic Particle Size Distributions (APSDs) Measured by the Next-Generation Pharmaceutical Impactor (NGI) and the Andersen Eight-Stage Cascade Impactor (ACI)." *AAPS PharmSciTech* 13 (3): 875–82.

Mollmann, Helmut, Melanie Wagner, Sriram Krishnaswami, Hristina Dimova, Yufei Tang, Christine Falcoz, Peter T. Daley-Yates, et al. 2001. "Single-Dose and Steady-State Pharmacokinetic and Pharmacodynamic Evaluation of Therapeutically Clinically Equivalent Doses of Inhaled Fluticasone Propionate and Budesonide, given as Diskus?? Or Turbohaler?? Dry-Powder Inhalers to Healthy Subjects." *Journal of Clinical Pharmacology* 41 (12): 1329–38.

Montanaro, Anthony, Steven Weinstein, Carolyn Beaudot, Sue M. Scott, and George Georges. 2021. "Efficacy and Safety of Inhaled Extrafine Beclomethasone Dipropionate in Adults with Asthma: A Randomized, Parallel-Group, Dose-Ranging Study (BEAM)." *Journal of Asthma*, AHEAD-OF-PRINT:1-10.

Morin, Chelsea M. D., James W. Ivey, Jordan T. F. Titosky, Jonathan D. Suderman, Jason S. Olfert, Reinhard Vehring, and Warren H. Finlay. 2014. "Performance of Pressurized Metered-Dose Inhalers at Extreme Temperature Conditions." *Journal of Pharmaceutical Sciences* 103 (11): 3553–59.

Mortimer, Kevin J., Anne E. Tattersfield, Yufei Tang, Kai Wu, Sarah Lewis, Gunther Hochhaus, and Tim W. Harrison. 2007. "Plasma Concentrations of Fluticasone Propionate and Budesonide Following Inhalation: Effect of Induced Bronchoconstriction." *British Journal of Clinical Pharmacology* 64 (4): 439–44.

Mylan Products Ltd. 2018. "Budelin Novolizer 200 Micrograms per Actuation Inhalation Powder." Potters Bar, UK.

Naji, Nizar, Elaine Keung, Suzanne Beaudin, James Kane, Kieran J. Killian, and Gail M. Gauvreau. 2013. "The Effects of Particle Size on Measurement of Airway

Hyperresponsiveness to Methacholine." *Annals of Allergy, Asthma and Immunology* 110 (5): 359–63.

National Council on Radiation Protection and Measurements. 1997. *Deposition, Retention, and Dosimetry of Inhaled Radioactive Substances : Recommendations of the National Council on Radiation Protection and Measurements.* NCRP Report. Bethesda, MD: National Council on Radiation Protection and Measurements.

Newman, Stephen P., William D. Bennett, Martyn Biddiscombe, Sunalene G. Devadason, Myrna B. Dolovich, John Fleming, Sabine Haeussermann, et al. 2012. "Standardization of Techniques for Using Planar (2D) Imaging for Aerosol Deposition Assessment of Orally Inhaled Products." *Journal of Aerosol Medicine and Pulmonary Drug Delivery* 25 (S1): S-10-S-28.

Newman, Stephen P., Joanne Brown, Karen P. Steed, Sandra J. Reader, and Heinrich Kladders. 1998. "Lung Deposition of Fenoterol and Flunisolide Delivered Using a Novel Device of Inhaled Medicines." *Chest* 113 (4): 957–63.

Newman, Stephen P., Gary R. Pitcairn, Peter H. Hirst, R. E. Bacon, E. O'Keefe, M. Reiners, and R. Hermann. 2000. "Scintigraphic Comparison of Budesonide Deposition from Two Dry Powder Inhalers." *European Respiratory Journal* 16 (1): 178–83.

Newman, Stephen P. 2017. "Drug Delivery to the Lungs: Challenges and Opportunities." *Therapeutic Delivery* 8 (8): 647–61.

Nordlund, Markus, and Arkadiusz K Kuczaj. 2015. "Aerosol Dosimetry Modeling Using Computational Fluid Dynamics." In *Computational Systems Toxicology*, edited by Julia Hoeng and Manuel C Peitsch, 393–427. New York, NY: Springer New York.

O'Shaughnessy, Patrick T, Lawrence LeBlanc, Alessandra Pratt, Ralph Altmaier, Prathish K Rajaraman, Ross Walenga, and Ching-Long Lin. 2020. "Assessment and Validation of a Hygroscopic Growth Model with Different Water Activity Estimation Methods." *Aerosol Science and Technology* 54 (10): 1169–82.

Ochs, Matthias, and Ewald R Weibel. 2015. "Functional Design of the Human Lung for Gas Exchange." In *Fishman's Pulmonary Diseases and Disorders, 5e*, edited by Michael A Grippi, Jack A Elias, Jay A Fishman, Robert M Kotloff, Allan I Pack, Robert M Senior, and Mark D Siegel. New York, NY: McGraw-Hill Education.

Olanow, C. Warren, and Fabrizio Stocchi. 2018. "Levodopa: A New Look at an Old Friend." *Movement Disorders* 33 (6): 859–66.

Olsson, Bo, Eva Bondesson, Lars Borgström, Staffam Edsbäcker, Stefan Eirefelt, Katarina Ekelund, Lena Gustavsson, and Tove Hegelund-Myrbäck. 2011. "Pulmonary Drug Metabolism, Clearance, and Absorption." In *Controlled Pulmonary Drug Delivery*, edited by Hugh D.C. Smyth and Anthony J Hickey, 21–50. Controlled Release Society; Springer.

Olsson, Bo, Lars Borgström, Hans Lundbäck, and Mårten Svensson. 2013. " Validation of a General In Vitro Approach for Prediction of Total Lung Deposition in Healthy Adults for Pharmaceutical Inhalation Products ." *Journal of Aerosol Medicine and Pulmonary Drug Delivery* 26 (6): 355–69.

Ostrovski, Yan, Simon Dorfman, Maksim Mezhericher, Stavros Kassinos, and Josué Sznitman. 2019. "Targeted Drug Delivery to Upper Airways Using a Pulsed Aerosol Bolus and Inhaled Volume Tracking Method." *Flow, Turbulence and Combustion* 102 (1): 73–87.

Parisini, Irene, Sean J. Cheng, Digby D. Symons, and Darragh Murnane. 2014. "Potential of a Cyclone Prototype Spacer to Improve in Vitro Dry Powder Delivery." *Pharmaceutical Research* 31 (5): 1133–45.

Parumasivam, Thaigarajan, Hak-Kim Chan, Warwick John Britton, Sharif Abdelghany, Tian Tian Ye, and Rachel Yoon Kyung Chang. 2016. "Dry Powder Inhalable Formulations for Anti-Tubercular Therapy." *Advanced Drug Delivery Reviews* 102: 83–101.

Patton, John S., and Peter R. Byron. 2007. "Inhaling Medicines: Delivering Drugs to the Body through the Lungs." *Nature Reviews Drug Discovery* 6 (1): 67–74.

Patton, John S., C. Simone Fishburn, and Jeffry G. Weers. 2004. "The Lungs as a Portal of Entry for Systemic Drug Delivery." *Proceedings of the American Thoracic Society* 1 (4): 338–44.

Pauwels, R., Stephen P. Newman, and Lars Borgström. 1997. "Airway Deposition and Airway Effects of Antiasthma Drugs Delivered from Metered-Dose Inhalers." *European Respiratory Journal* 10 (9): 2127–38.

Pellegrino, Robert, Giovanni Viegi, Vito Brusasco, Robert O. Crapo, Felip Burgos, Richard Casaburi, Allan L. Coates, et al. 2005. "Interpretative Strategies for Lung Function Tests." *European Respiratory Journal* 26 (5): 948–68.

Phalen, Robert F., Michael J. Oldham, and Ronald K. Wolff. 2008. "The Relevance of Animal Models for Aerosol Studies." *Journal of Aerosol Medicine and Pulmonary Drug Delivery* 21 (1): 113–24.

Pittas, Anastassios G., Gregory P. Westcott, and Ethan M. Balk. 2015. "Efficacy, Safety, and Patient Acceptability of Technosphere Inhaled Insulin for People with Diabetes: A Systematic Review and Meta-Analysis." *The Lancet Diabetes and Endocrinology* 3 (11): 886–94.

Price, Robert, Jagdeep Shur, William Ganley, Gonçalo Farias, Nikoletta Fotaki, Denise S. Conti, Renishkumar Delvadia, Mohammad Absar, Bhawana Saluja, and Sau Lee. 2020. "Development of an Aerosol Dose Collection Apparatus for In Vitro Dissolution Measurements of Orally Inhaled Drug Products." *AAPS Journal* 22 (2): 1–9.

Pritchard, Susan E, and Donald W McRobbie. 2004. "Studies of the Human Oropharyngeal Airspaces Using the Influence of Mouthpiece Diameter and Resistance of Inhalation Devices on the Oropharyngeal Airspace Geometry." *Journal of Aerosol Medicine* 17 (4): 310–24.

Quon, Bradley S, Christopher H Goss, and Bonnie W Ramsey. 2014. "Inhaled Antibiotics for Lower Airway Infections." *Annals of the American Thoracic Society* 11 (3): 425–34.

Radivojev, Snezana, Sarah Zellnitz, Amrit Paudel, and Eleonore Fröhlich. 2019. "Searching for Physiologically Relevant in Vitro Dissolution Techniques for Orally Inhaled Drugs." *International Journal of Pharmaceutics* 556 (December 2018): 45–56.

Ramsey, B W, M S Pepe, J M Quan, K L Otto, A B Montgomery, J Williams-Warren, M Vasiljev-K, et al. 1999. "Intermittent Administration of Inhaled Tobramycin in Patients with Cystic

Fibrosis. Cystic Fibrosis Inhaled Tobramycin Study Group." *The New England Journal of Medicine* 340 (1): 23–30.

Reddel, Helen K., D. Robin Taylor, Eric D. Bateman, Louis Philippe Boulet, Homer A. Boushey, William W. Busse, Thomas B. Casale, et al. 2009. "An Official American Thoracic Society/European Respiratory Society Statement: Asthma Control and Exacerbations - Standardizing Endpoints for Clinical Asthma Trials and Clinical Practice." *American Journal of Respiratory and Critical Care Medicine* 180 (1): 59–99.

Réminiac, François, Laurent Vecellio, Ronan Mac Loughlin, Deborah Le Pennec, Maria Cabrera, Nathalie Heuzé Vourc'h, James B. Fink, and Stephan Ehrmann. 2016. "Nasal High Flow Nebulization in Infants and Toddlers: An in Vitro and in Vivo Scintigraphic Study." *Pediatric Pulmonology* 52 (3): 337–44.

Robinson, R A, and V E Bower. 1965. "An Additivity Rule for the Vapor Pressure Lowering of Aqueous Solutions." *Journal of Research of the National Bureau of Standards. Section A, Physics and Chemistry* 69A (4): 365–67.

Robinson, R A, and R H Stokes. 1970. *Electrolyte Solutions : The Measurement and Interpretation of Conductance, Chemical Potential, and Diffusion in Solutions of Simple Electrolytes.* 2nd ed., r. London: Butterworths.

Rohrschneider, Marc, Sharvari Bhagwat, Raphael Krampe, Victoria Michler, Jörg Breitkreutz, and Günther Hochhaus. 2015. "Evaluation of the Transwell System for Characterization of Dissolution Behavior of Inhalation Drugs: Effects of Membrane and Surfactant." *Molecular Pharmaceutics* 12 (8): 2618–24.

Roth, A. P., Carlos F. Lange, and Warren H. Finlay. 2003. "The Effect of Breathing Pattern on Nebulizer Drug Delivery." *Journal of Aerosol Medicine* 16 (3): 325–39.

Roth, Christa, and Josef Gebhart. 1996. "Aqueous Droplet Sizing by Inertial Classification." *Particle and Particle Systems Characterization* 13 (3): 192–95.

Rowland, Darren, and Peter M. May. 2018. "A Comparative Investigation of Mixing Rules for Property Prediction in Multicomponent Electrolyte Solutions." *Journal of Solution Chemistry* 47 (1): 107–26.

Ruge, Christian C., Julian Kirch, and Claus Michael Lehr. 2013. "Pulmonary Drug Delivery: From Generating Aerosols to Overcoming Biological Barriers-Therapeutic Possibilities and Technological Challenges." *The Lancet Respiratory Medicine* 1 (5): 402–13.

Ruzycki, Conor A., Laleh Golshahi, Reinhard Vehring, and Warren H. Finlay. 2014. "Comparison of in Vitro Deposition of Pharmaceutical Aerosols in an Idealized Child Throat with in Vivo Deposition in the Upper Respiratory Tract of Children." *Pharmaceutical Research* 31 (6): 1525–35.

Ruzycki, Conor A., Andrew R. Martin, and Warren H. Finlay. 2019. "An Exploration of Factors Affecting in Vitro Deposition of Pharmaceutical Aerosols in the Alberta Idealized Throat." *Journal of Aerosol Medicine and Pulmonary Drug Delivery* 32 (6): 405–17.

Ruzycki, Conor A., Andrew R. Martin, Reinhard Vehring, and Warren H. Finlay. 2018. "An in Vitro Examination of the Effects of Altitude on Dry Powder Inhaler Performance." *Journal*

of Aerosol Medicine and Pulmonary Drug Delivery 31 (4): 221–36.

Ruzycki, Conor A., Brynn Murphy, Hafeez Nathoo, Warren H. Finlay, and Andrew R. Martin. 2020. "Combined in Vitro-in Silico Approach to Predict Deposition and Pharmacokinetics of Budesonide Dry Powder Inhalers." *Pharmaceutical Research* 37 (10): 209.

Ruzycki, Conor A., Michael Yang, Hak-Kim Chan, and Warren H. Finlay. 2017. "Improved Prediction of Intersubject Variability in Extrathoracic Aerosol Deposition Using Algebraic Correlations." *Aerosol Science and Technology* 51 (6): 667–73.

Ryan, G., Myrna B. Dolovich, G. Obminski, Donald W. Cockcroft, Elizabeth F. Juniper, F. E. Hargreave, and Michael T. Newhouse. 1981. "Standardization of Inhalation Provocation Tests: Influence of Nebulizer Output, Particle Size, and Method of Inhalation." *Journal of Allergy and Clinical Immunology* 67 (2): 156–61.

Ryrfeldt, A, P Andersson, S Edsbacker, M Tonnesson, D Davies, and R Pauwels. 1982. "Pharmacokinetics and Metabolism of Budesonide, a Selective Glucocorticoid." *European Journal of Respiratory Diseases* 63 (S 122): 86–95.

Sakagami, Masahiro. 2006. "In Vivo, in Vitro and Ex Vivo Models to Assess Pulmonary Absorption and Disposition of Inhaled Therapeutics for Systemic Delivery." *Advanced Drug Delivery Reviews* 58 (9–10): 1030–60.

San, Luis, Gemma Estrada, Natalia Oudovenko, Francisco Montañés, Natalia Dobrovolskaya, Olga Bukhanovskaya, Mikhail Popov, and Eduard Vieta. 2018. "PLACID Study: A Randomized Trial Comparing the Efficacy and Safety of Inhaled Loxapine versus Intramuscular Aripiprazole in Acutely Agitated Patients with Schizophrenia or Bipolar Disorder." *European Neuropsychopharmacology* 28 (6): 710–18.

Sanchis, Joaquin, Ignasi Gich, and Soren Pedersen. 2016. "Systematic Review of Errors in Inhaler Use: Has Patient Technique Improved Over Time?" *Chest* 150 (2): 394–406.

Santos Cavaiola, Tricia, and Steven Edelman. 2014. "Inhaled Insulin: A Breath of Fresh Air? A Review of Inhaled Insulin." *Clinical Therapeutics* 36 (8): 1275–89.

Scheuch, Gerhard, William Bennett, Lars Borgström, Andy Clark, Richard Dalby, Myrna Dolovich, John Fleming, et al. 2010. "Deposition, Imaging, and Clearance: What Remains to Be Done?" *Journal of Aerosol Medicine and Pulmonary Drug Delivery* 23 (S2): S-39-S-57.

Schulze, Johannes, Martin Rosewich, Carsten Riemer, Melanie Dressler, Markus A. Rose, and Stefan Zielen. 2009. "Methacholine Challenge - Comparison of an ATS Protocol to a New Rapid Single Concentration Technique." *Respiratory Medicine* 103 (12): 1898–1903.

Schürch, Samuel, Peter Gehr, Vinzenz Im Hof, Marianne Geiser, and Francis Green. 1990. "Surfactant Displaces Particles toward the Epithelium in Airways and Alveoli." *Respiration Physiology* 80 (1): 17–32.

Schweisfurth, H., A. Malinen, T. Koskela, P. Toivanen, and M. Ranki-Pesonen. 2002. "Comparison of Two Budesonide Powder Inhalers, Easyhaler® and Turbuhaler®, in Steroid-Naïve Asthmatic Patients." *Respiratory Medicine* 96 (8): 599–606.

Scichilone, Nicola, Salvatore Battaglia, Salvatore Taormina, Viviana Modica, Elena Pozzecco,

and Vincenzo Bellia. 2013. "Alveolar Nitric Oxide and Asthma Control in Mild Untreated Asthma." *Journal of Allergy and Clinical Immunology* 131 (6): 1513–17.

Selo, Mohammed Ali, Johannes A. Sake, Kwang Jin Kim, and Carsten Ehrhardt. 2021. "In Vitro and Ex Vivo Models in Inhalation Biopharmaceutical Research — Advances, Challenges and Future Perspectives." *Advanced Drug Delivery Reviews* 177 (October): 113862.

Shao, Jie, James Talton, Yaning Wang, Lawrence Winner, and Guenther Hochhaus. 2020. "Quantitative Assessment of Pulmonary Targeting of Inhaled Corticosteroids Using Ex Vivo Receptor Binding Studies." *AAPS Journal* 22 (2): 1–10.

Shapiro, Gail, Edwin A. Bronsky, Craig F. LaForce, Louis Mendelson, David Pearlman, R. H. Schwartz, and Stanley J. Szefler. 1998. "Dose-Related Efficacy of Budesonide Administered via a Dry Powder Inhaler in the Treatment of Children with Moderate to Severe Persistent Asthma." *Journal of Pediatrics* 132 (6): 976–82.

Shapiro, Monica E., Timothy E. Corcoran, Carol A. Bertrand, Florencio Serrano Castillo, and Robert S. Parker. 2018. "Physiologically-Based Model of Fluid Absorption and Mucociliary Clearance in Cystic Fibrosis." *IFAC-PapersOnLine* 51 (19): 102–3.

Sharma, Pawan, Roslyn Yi, Ajay P. Nayak, Nadan Wang, Francesca Tang, Morgan J. Knight, Shi Pan, Brian Oliver, and Deepak A. Deshpande. 2017. "Bitter Taste Receptor Agonists Mitigate Features of Allergic Asthma in Mice." *Scientific Reports* 7 (April): 1–14.

Shemirani, Farzin M., Susan Hoe, David Lewis, Tanya Church, Reinhard Vehring, and Warren H. Finlay. 2013. "In Vitro Investigation of the Effect of Ambient Humidity on Regional Delivered Dose with Solution and Suspension MDIs." *Journal of Aerosol Medicine and Pulmonary Drug Delivery* 26 (4): 215–22.

Shur, Jagdeep, Robert Price, Tim Rouse, David Lewis, Dilraj Singh, Bradley Morrical, and Stephen Edge. 2019. "Defining the Dosage Strength for Labeling of DPIs : Use, Limitations and Relevance of in Vitro Data." *Inhalation Magazine* 13 (1): 7–13.

Singh, Dave, Helena Pujol, Anna Ribera, Beatriz Seoane, Eric Massana, Carol Astbury, Sandrine Ruiz, and Gonzalo de Miquel. 2014. "A Dose-Ranging Study of the Bronchodilator Effects of Abediterol (LAS100977), a Long-Acting B2-Adrenergic Agonist, in Asthma; a Phase II, Randomized Study." *BMC Pulmonary Medicine* 14 (1): 1–10.

Smaldone, Gerald C., Elna Berg, and Kurt Nikander. 2005. "Variation in Pediatric Aerosol Delivery: Importance of Facemask." *Journal of Aerosol Medicine* 18 (3): 354–63.

Smith, D. J., E. A. Gaffney, and J. R. Blake. 2008. "Modelling Mucociliary Clearance." *Respiratory Physiology and Neurobiology* 163 (1–3): 178–88.

Song, Xinghan, Junhua Hu, Shuyao Zhan, Rui Zhang, and Wen Tan. 2016. "Effects of Temperature and Humidity on Laser Diffraction Measurements to Jet Nebulizer and Comparison with NGI." *AAPS PharmSciTech* 17 (2): 380–88.

Soulele, K., P. Macheras, and V. Karalis. 2018. "On the Pharmacokinetics of Two Inhaled Budesonide/Formoterol Combinations in Asthma Patients Using Modeling Approaches." *Pulmonary Pharmacology and Therapeutics* 48 (July 2017): 168–78.

Stahlhofen, W, G Rudolf, and A C James. 1989. "Intercomparison of Experimental Regional Aerosol Deposition Data." *Journal of Aerosol Medicine* 2 (3).

Stapleton, Kevin W. 2018. "Orally Inhaled Migraine Therapy: Where Are We Now?" *Advanced Drug Delivery Reviews* 133: 131–34.

Stapleton, Kevin W., and Warren H. Finlay. 1995. "Determining Solution Concentration within Aerosol Droplets Output by Jet Nebulizers." *Journal of Aerosol Science* 26 (1): 137–45.

Stapleton, Kevin W., E. Guentsch, M. K. Hoskinson, and Warren H. Finlay. 2000. "On the Suitability of K-Epsilon Turbulence Modeling for Aerosol Deposition in the Mouth and Throat: A Comparison with Experiment." *Journal of Aerosol Science* 31 (6): 739–49.

Stein, Stephen W., and Charles G. Thiel. 2016. "The History of Therapeutic Aerosols: A Chronological Review." *Journal of Aerosol Medicine and Pulmonary Drug Delivery* 30 (1): 20–41.

Sterk, Peter J., Leonardo M. Fabbri, Philip H. Quanjer, Donald W. Cockcroft, Paul M. O'Byrne, S. D. Anderson, Elizabeth F. Juniper, and J. L. Malo. 1993. "Airway Responsiveness. Standardized Challenge Testing with Pharmacological, Physical and Sensitizing Stimuli in Adults." *European Respiratory Journal* 6 (16): 53–83.

Szczesniak, Rhonda, Sonya L Heltshe, Sanja Stanojevic, and Nicole Mayer-Hamblett. 2017. "Use of FEV(1) in Cystic Fibrosis Epidemiologic Studies and Clinical Trials: A Statistical Perspective for the Clinical Researcher." *Journal of Cystic Fibrosis* 16 (3): 318–26.

Tang, Ignatius N., H. R. Munkelwitz, and Ning Wang. 1986. "Water Activity Measurements with Single Suspended Droplets: The NaCl-H2O and KCl-H2O Systems." *Journal of Colloid And Interface Science* 114 (2): 409–15.

Tarrant, Benjamin J., Caitlin Le Maitre, Lorena Romero, Ranjana Steward, Brenda M. Button, Bruce R. Thompson, and Anne E. Holland. 2017. "Mucoactive Agents for Chronic, Non-Cystic Fibrosis Lung Disease: A Systematic Review and Meta-Analysis." *Respirology* 22 (6): 1084–92.

Tavernini, Scott, Tanya K. Church, David A. Lewis, Andrew R. Martin, and Warren H. Finlay. 2018. "Scaling an Idealized Infant Nasal Airway Geometry to Mimic Inertial Filtration of Neonatal Nasal Airways." *Journal of Aerosol Science* 118: 14–21.

Tavernini, Scott, Dino J. Farina, Andrew R. Martin, and Warren H. Finlay. 2021. "Using Filters to Estimate Regional Lung Deposition with Dry Powder Inhalers." *Pharmaceutical Research* 38: 1601–13.

Tavernini, Scott, Milad Kiaee, Dino J. Farina, Andrew R. Martin, and Warren H. Finlay. 2019. "Development of a Filter That Mimics Tracheobronchial Deposition of Respirable Aerosols in Humans." *Aerosol Science and Technology* 53 (7): 802–16.

Tay, Justin Yong Soon, Celine Valeria Liew, and Paul Wan Sia Heng. 2018. "Dissolution of Fine Particle Fraction from Truncated Anderson Cascade Impactor with an Enhancer Cell." *International Journal of Pharmaceutics* 545 (1–2): 45–50.

Telko, Martin J., Jukka Kujanpää, and Anthony J. Hickey. 2007. "Investigation of Triboelectric

Charging in Dry Powder Inhalers Using Electrical Low Pressure Impactor (ELPI™).” *International Journal of Pharmaceutics* 336 (2): 352–60.

Tepper, Stewart J. 2013. “Orally Inhaled Dihydroergotamine: A Review.” *Headache* 53 (SUPPL.2): 43–53.

Thorsson, Lars, Staffan Edsbacker, and T. B. Conradson. 1994. “Lung Deposition of Budesonide from Turbuhaler® Is Twice That from a Pressurized Metered-Dose Inhaler P-MDI.” *European Respiratory Journal* 7 (10): 1839–44.

Thorsson, Lars, Staffan Edsbacker, Anders Kallen, and Claes-Goran Lofdahl. 2001. “Pharmacokinetics and Systemic Activity of Fluticasone via Diskus and PMDI, and of Budesonide via Turbuhaler.” *Br J Clin Pharmacol* 52: 529–38.

Tian, Geng, P. Worth Longest, Xiang Li, and Michael Hindle. 2013. “Targeting Aerosol Deposition to and Within the Lung Airways Using Excipient Enhanced Growth.” *Journal of Aerosol Medicine and Pulmonary Drug Delivery* 26 (5): 248–65.

Tian, Geng, P. Worth Longest, Guoguang Su, and Michael Hindle. 2011. “Characterization of Respiratory Drug Delivery with Enhanced Condensational Growth Using an Individual Path Model of the Entire Tracheobronchial Airways.” *Annals of Biomedical Engineering* 39 (3): 1136–53.

Tian, Geng, P. Worth Longest, Guoguang Su, Ross L. Walenga, and Michael Hindle. 2011. “Development of a Stochastic Individual Path (SIP) Model for Predicting the Tracheobronchial Deposition of Pharmaceutical Aerosols: Effects of Transient Inhalation and Sampling the Airways.” *Journal of Aerosol Science* 42 (11): 781–99.

Titosky, Jordan T.F., Chelsea M.D. Morin, Jonathan D. Suderman, Jason S. Olfert, Warren H. Finlay, and Reinhard Vehring. 2014. “The Effect of Altitude on Inhaler Performance.” *Journal of Pharmaceutical Sciences* 103 (7): 2116–24.

Ung, Keith T., and Hak Kim Chan. 2016. “Effects of Ramp-up of Inspired Airflow on in Vitro Aerosol Dose Delivery Performance for Certain Dry Powder Inhalers.” *European Journal of Pharmaceutical Sciences* 84: 46–54.

Ung, Keith T., Nagaraja Rao, Jeffry G. Weers, Daniel Huang, and Hak Kim Chan. 2016. “Design of Spray Dried Insulin Microparticles to Bypass Deposition in the Extrathoracic Region and Maximize Total Lung Dose.” *International Journal of Pharmaceutics* 511 (2): 1070–79.

United States Pharmacopeia. 2019a. *USP 44(5) General Chapter <601> Inhalation and Nasal Drug Products - Aerosols, Sprays, and Powders - Performance Quality Tests*. Rockville, MD.

———. 2019b. *USP 45(2) Informative Chapter <1604> Data Interpretation of Aerodynamic Particle Size Distribution Measurements for Orally Inhaled Products.* Rockville, MD.

US FDA Center for Drug Evaluation and Research (CDER). 2018. *Metered Dose Inhaler (MDI) and Dry Powder Inhaler (DPI) Products - Quality Considerations Guidance for Industry (Draft)*. Revision 1. Rockville, MD.

Usmani, Omar S., and Peter J. Barnes. 2012. “Assessing and Treating Small Airways Disease in Asthma and Chronic Obstructive Pulmonary Disease.” *Annals of Medicine* 44 (2): 146–56.

Usmani, Omar S., Martyn F. Biddiscombe, and Peter J. Barnes. 2005. "Regional Lung Deposition and Bronchodilator Response as a Function of B2-Agonist Particle Size." *American Journal of Respiratory and Critical Care Medicine* 172 (12): 1497–1504.

Usmani, Omar S., Dave Singh, Monica Spinola, Andrea Bizzi, and Peter J. Barnes. 2016. "The Prevalence of Small Airways Disease in Adult Asthma: A Systematic Literature Review." *Respiratory Medicine* 116: 19–27.

Vanto, T., K.M. Hämäläinen, M. Vahteristo, S. Wille, F. Njå, and N. Hyldebrandt. 2004. "Comparison of Two Budesonide Dry Powder Inhalers in the Treatment of Asthma in Children." *Journal of Aerosol Medicine: Deposition, Clearance, and Effects in the Lung* 17 (1): 15–24.

Vecellio-None, Laurent, Daniel Grimbert, Eric Boissinot, Alain Le Pape, Etienne Lemarié, Patrice Diot, Marie-Helene H (3) Becquemin, et al. 2001. "Validation of Laser Diffraction Method as a Substitute for Cascade Impaction in the European Project for a Nebulizer Standard." *Journal of Aerosol Medicine: Deposition, Clearance, and Effects in the Lung* 14 (1): 107–14.

Vehring, Reinhard. 2008. "Pharmaceutical Particle Engineering via Spray Drying." *Pharmaceutical Research* 25 (5): 999–1022.

Velaga, Sitaram P., Jelena Djuris, Sandra Cvijic, Stavroula Rozou, Paola Russo, Gaia Colombo, and Alessandra Rossi. 2018. "Dry Powder Inhalers: An Overview of the in Vitro Dissolution Methodologies and Their Correlation with the Biopharmaceutical Aspects of the Drug Products." *European Journal of Pharmaceutical Sciences* 113 (August 2017): 18–28.

Versteeg, Hendrik K., Daryl L. Roberts, Frank Chambers, Andy Cooper, Mark A. Copley, Jolyon P. Mitchell, and Hlack Mohammed. 2020. "A Cross-Industry Assessment of the Flow Rate-Elapsed Time Profiles of Test Equipment Typically Used for Dry-Powder Inhaler (DPI) Testing: Part 2– Analysis of Transient Air Flow in the Testing of DPIs with Compendial Cascade Impactors." *Aerosol Science and Technology* 54 (12): 1448–70.

Vogelmeier, Claus F., Gerard J. Criner, Fernando J. Martinez, Antonio Anzueto, Peter J. Barnes, Jean Bourbeau, Bartolome R. Celli, et al. 2017. "Global Strategy for the Diagnosis, Management, and Prevention of Chronic Obstructive Lung Disease 2017 Report." *American Journal of Respiratory and Critical Care Medicine* 195 (5): 557–82.

Walenga, Ross L., Andrew H. Babiskin, and Liang Zhao. 2019. "In Silico Methods for Development of Generic Drug–Device Combination Orally Inhaled Drug Products." *CPT: Pharmacometrics and Systems Pharmacology* 8 (6): 359–70.

Walenga, Ross L., and P. Worth Longest. 2016. "Current Inhalers Deliver Very Small Doses to the Lower Tracheobronchial Airways: Assessment of Healthy and Constricted Lungs." *Journal of Pharmaceutical Sciences* 105 (1): 147–59.

Wang, Sheena H, Afton L Thompson, Anthony J Hickey, and Herman F Staats. 2012. "Dry Powder Vaccines for Mucosal Administration: Critical Factors in Manufacture and Delivery." In *Mucosal Vaccines: Modern Concepts, Strategies, and Challenges*, edited by Pamela A Kozlowski, 121–56. Berlin, Heidelberg: Springer Berlin Heidelberg.

Wang, Yang, Jiayu Li, Anna Leavey, Caroline O'Neil, Hilary M. Babcock, and Pratim Biswas.

2017. "Comparative Study on the Size Distributions, Respiratory Deposition, and Transport of Particles Generated from Commonly Used Medical Nebulizers." *Journal of Aerosol Medicine and Pulmonary Drug Delivery* 30 (2): 132–40.

Weber, Benjamin, and Guenther Hochhaus. 2013. "A Pharmacokinetic Simulation Tool for Inhaled Corticosteroids." *The American Association of Pharmaceutical Sciences Journal* 15 (1): 159–71.

Weers, Jeffry G., Andrew R. Clark, Nagaraja Rao, Keith Ung, Alfred Haynes, Sanjeev K. Khindri, Sheryl A. Perry, Surendra Machineni, and Paul Colthorpe. 2015. "*In Vitro–In Vivo* Correlations Observed With Indacaterol-Based Formulations Delivered with the Breezhaler ®." *Journal of Aerosol Medicine and Pulmonary Drug Delivery* 28 (4): 268–80.

Weers, Jeffry G., and Andy Clark. 2017. "The Impact of Inspiratory Flow Rate on Drug Delivery to the Lungs with Dry Powder Inhalers." *Pharmaceutical Research* 34 (3): 507–28.

Wei, Xiangyin, Michael Hindle, Renishkumar R Delvadia, and Peter R. Byron. 2017. "In Vitro Tests for Aerosol Deposition. V: Using Realistic Testing to Estimate Variations in Aerosol Properties at the Trachea." *Journal of Aerosol Medicine and Pulmonary Drug Delivery* 30 (5): 339–48.

Wei, Xiangyin, Michael Hindle, Anubhav Kaviratna, Bao K. Huynh, Renishkumar R. Delvadia, Dennis Sandell, and Peter R. Byron. 2018. "In Vitro Tests for Aerosol Deposition. VI: Realistic Testing with Different Mouth–Throat Models and In Vitro—In Vivo Correlations for a Dry Powder Inhaler, Metered Dose Inhaler, and Soft Mist Inhaler." *Journal of Aerosol Medicine and Pulmonary Drug Delivery* 31 (0): 358–71.

Weibel, Ewald R. 1963. *Morphometry of the Human Lung*. Berlin: Springer.

Wexler, Anthony S. 2019. "Raoult Was Right after All." *ACS Omega* 4 (7): 12848–52.

Xi, Jinxiang, and P. Worth Longest. 2007. "Transport and Deposition of Micro-Aerosols in Realistic and Simplified Models of the Oral Airway." *Annals of Biomedical Engineering* 35 (4): 560–81.

Yang, Michael Y., Conor A. Ruzycki, Jordan Verschuer, Andrew Katsifis, Stefan Eberl, Keith Wong, Laleh Golshahi, John D. Brannan, Warren H. Finlay, and Hak Kim Chan. 2017. "Examining the Ability of Empirical Correlations to Predict Subject Specific in Vivo Extrathoracic Aerosol Deposition during Tidal Breathing." *Aerosol Science and Technology* 51 (3): 363–76.

Yates, James W.T., and Philip A. Arundel. 2008. "On the Volume of Distribution at Steady State and Its Relationship with Two-Compartmental Models." *Journal of Pharmaceutical Sciences* 97 (1): 111–22.

Yaws, Carl L. 2017. "Table 2. Physical Properties - Organic Compounds." In *Yaws' Critical Property Data for Chemical Engineers and Chemists*. Knovel.

Yeh, Hsu Chi, Richard G. Cuddihy, Robert F. Phalen, and I. Yiin Chang. 1996. "Comparisons of Calculated Respiratory Tract Deposition of Particles Based on the Proposed NCRP Model and the New ICRP66 Model." *Aerosol Science and Technology* 25 (2): 134–40.

Yeh, Hsu Chi, and G.M Schum. 1980. "Models of Human Lung Airways and Their Application to Inhaled Particle Deposition." *Bulletin of Mathematical Viology* 42 (3): 461–80.

Yoshida, Hiroyuki, Akemi Kuwana, Hiroko Shibata, Ken-ichi Izutsu, and Yukihiro Goda. 2017. "Comparison of Aerodynamic Particle Size Distribution Between a Next Generation Impactor and a Cascade Impactor at a Range of Flow Rates." *AAPS PharmSciTech* 18 (3): 646–53.

Young, Paul M., Adrian Sung, Daniela Traini, Philip Kwok, Herbert Chiou, and Hak Kim Chan. 2007. "Influence of Humidity on the Electrostatic Charge and Aerosol Performance of Dry Powder Inhaler Carrier Based Systems." *Pharmaceutical Research* 24 (5): 963–70.

Yu, Jiaqi, Jennifer Wong, Ari Ukkonen, Jonna Kannosto, and Hak-Kim Chan. 2017. "Effect of Relative Humidity on Bipolar Electrostatic Charge Profiles of Dry Powder Aerosols." *Pharmaceutical Research* 34 (8): 1707–15.

Zhang, Yu, Kyle Gilbertson, and Warren H. Finlay. 2007. "In Vivo–In Vitro Comparison of Deposition in Three Mouth–Throat Models with Qvar® and Turbuhaler® Inhalers." *Journal of Aerosol Medicine* 20 (3): 227–35.

Zhou, Yue, Jaijie Sun, and Yung-Sung Cheng. 2011. "Comparison of Deposition in the USP and Physical Mouth – Throat Models with Solid and Liquid Particles." *Journal of Aerosol Medicine and Pulmonary Drug Delivery* 24 (6): 277–84.

Ziegler, Jochen, and Herbert Wachtel. 2005. "Comparison of Cascade Impaction and Laser Diffraction for Particle Size Distribution Measurements." *Journal of Aerosol Medicine* 18 (3): 311–24.

Appendix A. Design of Improved Adapters for Inhaler Testing

Commercially available inhalers can vary widely in form and function. In benchtop testing it is often necessary to fix these inhalers to sampling apparatuses including filters and induction ports. For repeated and consistent testing it is advantageous to have well-designed adapters that allow for consistent replication of parameters like inhaler insertion angle and distance from the end of the mouthpiece to the entrance of the sampling apparatus while also ensuring an airtight seal such that all inhaled air passes through the inhaler itself. This appendix briefly summarizes the procedure developed to create adapters to fit inhalers with proprietary designs to sampling apparatuses of interest.

Creation of adapters for fitting inhalers to sampling apparatuses has typically been through an iterative process requiring rough approximations of mouthpiece sizes and shapes with dimensions characterized with e.g., handheld calipers. Such a process often required repeated printing of parts to improve the design over time, and minor variations between inhalers and these designs often necessitated the use of vacuum grease to develop airtight seals with the inhaler and sampling apparatus. The methodology described here uses 3D scanning technology and solid modeling to create adapters better able to seal with inhalers at insertion angles of interest.

General methodology

- Scan the inhaler with a laser probe (FAROArm Fusion 7 axis 6 ft model, with FARO Laser ScanArm Laser Line Probe) to obtain a 3D point cloud

- Create a dimensionally accurate 3D model replication of the inhaler

- Utilize the 3D model and a general adapter template with a particular inhaler orientation to create inhaler-specific adapters for rapid prototyping

Scanning Inhalers

Prior to scanning, inhalers of interest were coated twice with matte white spray paint to provide a surface with uniform optical properties (Painter's Touch Flat White Multi-Purpose Paint; Rust-oleum). Geomagic for SOLIDWORKS was used to control the FAROArm laser line probe and obtain scans directly into the SOLIDWORKS environment. The FAROArm's 3 mm ball probe was calibrated using a 9 point hole compensation. The laser probe was calibrated via plate

compensation. After compensation, the laser probe was operated on high accuracy mode, with a scan rate of 1:1, scan density of 1:1, thresholds of 5, 50, and 15 for width, peak, and noise respectively, and the normal algorithm for a white matte surface.

The inhaler was then scanned from multiple orientations and angles (generally requiring approximately 10 scans to obtain a sufficiently detailed point cloud of the entire inhaler). Resulting point clouds were merged and "cleaned up" first by manually deleting obviously erroneous points, then applying the Reduce Noise (typically level 2) and Sampling (typically 50% at curvature 7) operations as appropriate.

From Scan to Model

A mesh model of the inhaler was created from the point cloud using the Wrap Mesh command in Geomagic. The resulting mesh was repaired and improved in an iterative process using manual manipulation in erratic areas together with the Repair, Remove Spikes (typically 50% or 75% smoothness), Remove Detached Triangles, Smooth, Fill Holes, Re-mesh, and Simplify (typically 50% at curvature 7) tools. The mesh provided the bases for defining reference geometries and regions that characterized the disparate designs of each inhaler. Particularly important here were the main central axis of the inhaler mouthpiece and cross-sectional planes defining its tip and base. These reference geometries (axes, points, planes, etc.) were used to build up a solid model consisting of relatively simple shapes to coincide with the existing mesh, making use of various tools like surface extractions or guide curves and multiple cross sections to recreate more complicated aspects of e.g., mouthpiece geometry. As a final check, the Deviation Analysis tool was used to confirm that the solid model created through this process was sufficiently similar to the mesh derived from scans of each inhaler, here taken as deviations within 0.01" on critical sections (i.e., the mouthpiece). The following figure shows an example of the transitions from the scanned point cloud, to the mesh, to the final solid model that occurs, in this case for the Turbuhaler DPI.
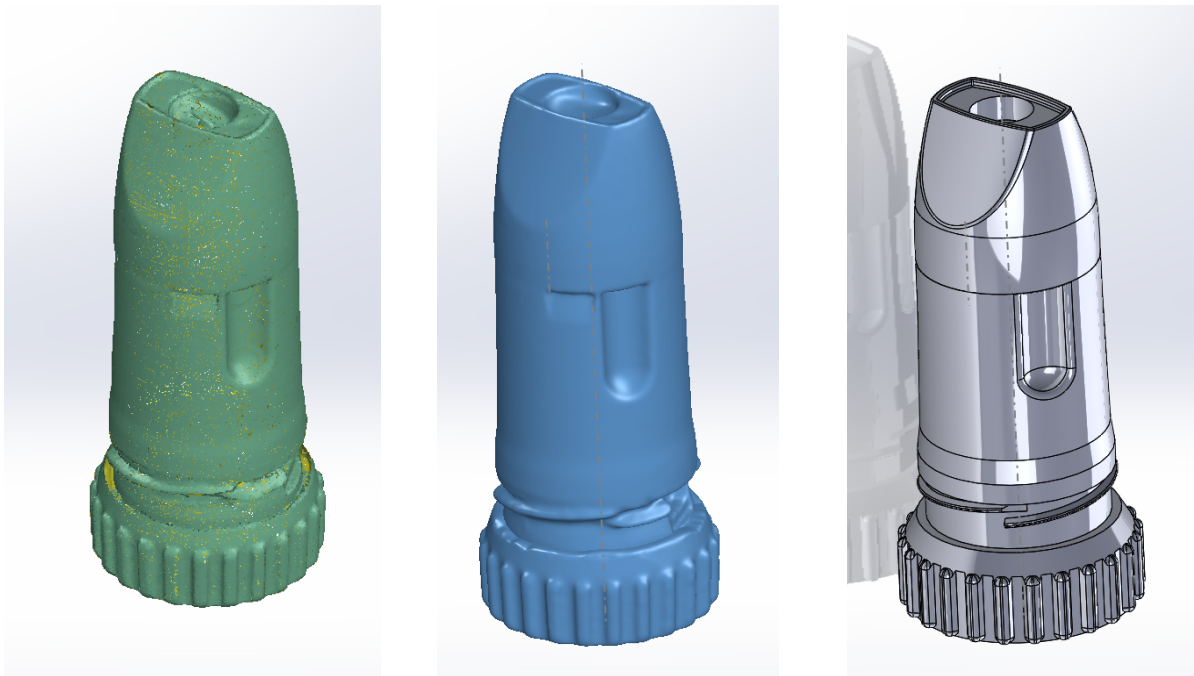
Figure A-1: Scanned point cloud (left), treated mesh (centre), and solid model (right) of the Turbuhaler DPI.

Crafting the Inhaler Adapters

With an accurate solid model of the inhaler, the creation of adapters from a universal template was straightforward. The template files are based on the in-house Aerosol Research Lab of Alberta version of the Alberta Idealized Throat, where adapters are affixed to the entrance of the AIT with four #10 socket head cap screws. These template adapters contain an O-ring groove on the surface that mates with the entrance of the AIT, to incorporate a 2-024 O-ring (fractional width = 1/16", inner diameter of 1 and 1/8"). In a SOLIDWORKS assembly file, the solid model of the inhaler was superimposed over top of the adapter template. The mouthpiece of the inhaler was used to create a cavity (Cavity Feature, with a uniform scaling of 1.5% to allow for clearance) in the adapter file. An additional O-ring (fractional width of 3/32'', inner diameter dependent on the geometry of the inhaler, e.g., a size 2-121 O-ring is used with the Turbuhaler DPI) was incorporated into the inner surface of the cavity to create an airtight seal between the inhaler and the adapter during us. The exact location of this inner O-ring groove was chosen to avoid the creation of thin features that may compromise the integrity of the adapter over repeated uses (note that the holes for the socket head cap screws acted as constraints). Resulting adapter files were

prototyped as desired. Examples of the final adapters are shown in the drawings and rendered images below.
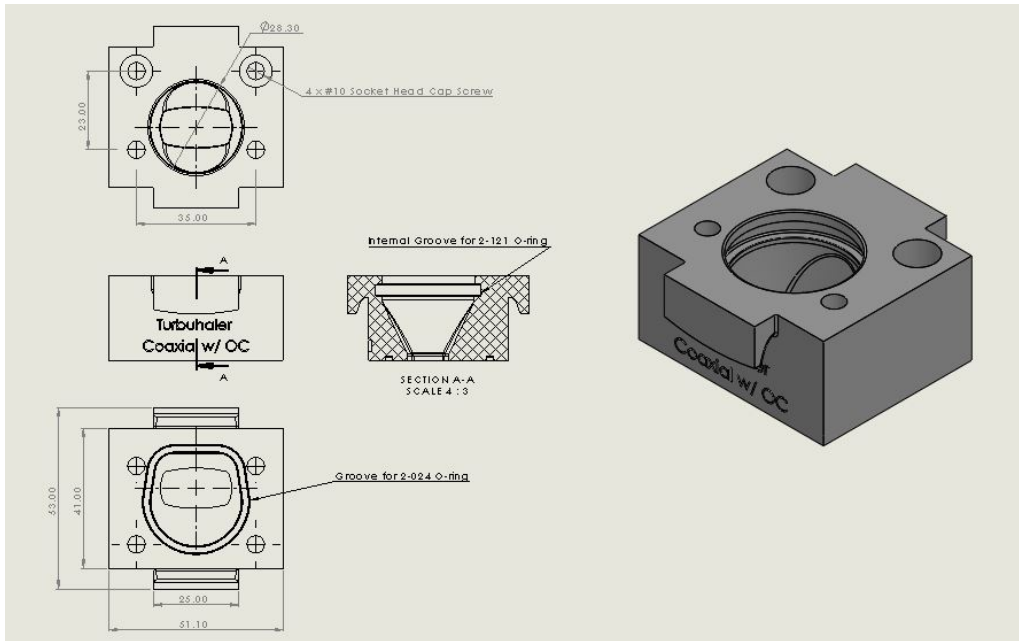

Figure A-2: Turbuhaler DPI adapter designed for a coaxial insertion angle into the Alberta Idealized Throat. Dimensions in [mm].
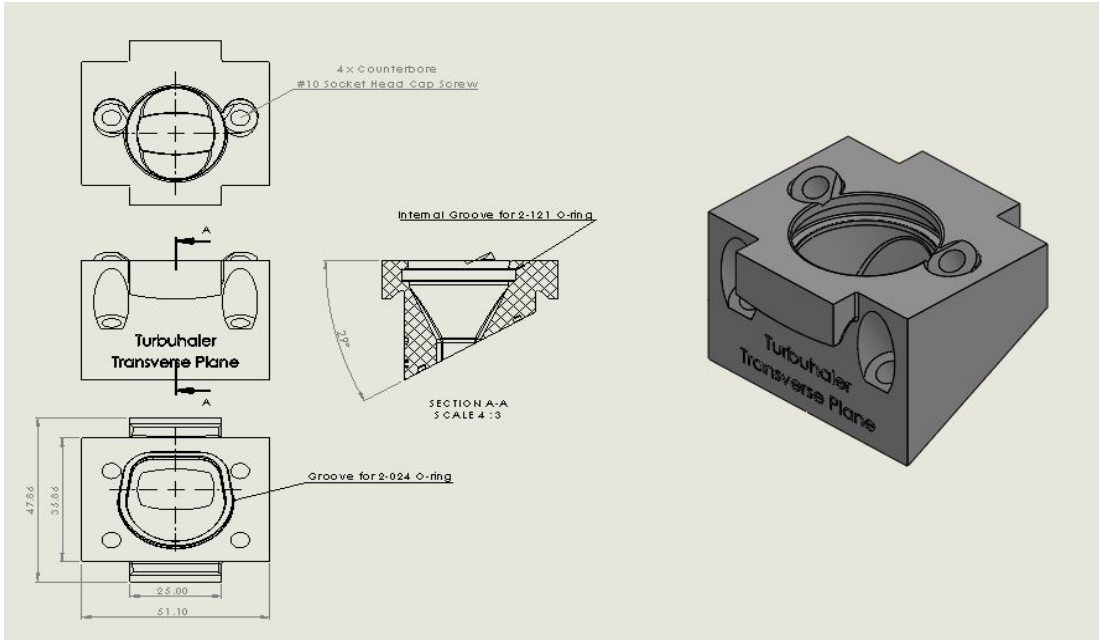
Figure A-3: Turbuhaler DPI adapter designed for a transverse insertion angle into the Alberta Idealized Throat. Dimensions in [mm]
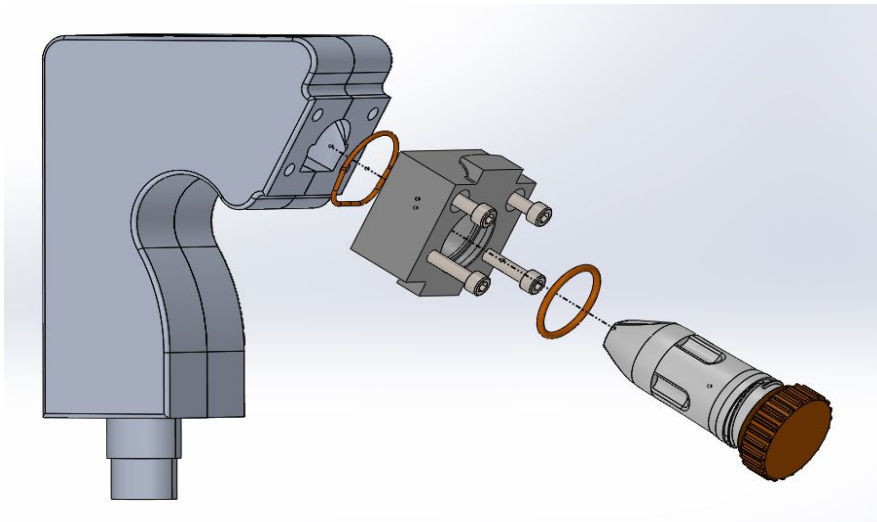

Figure A-4: Exploded view of the coaxial insertion angle demonstrating the location and assembly of components.
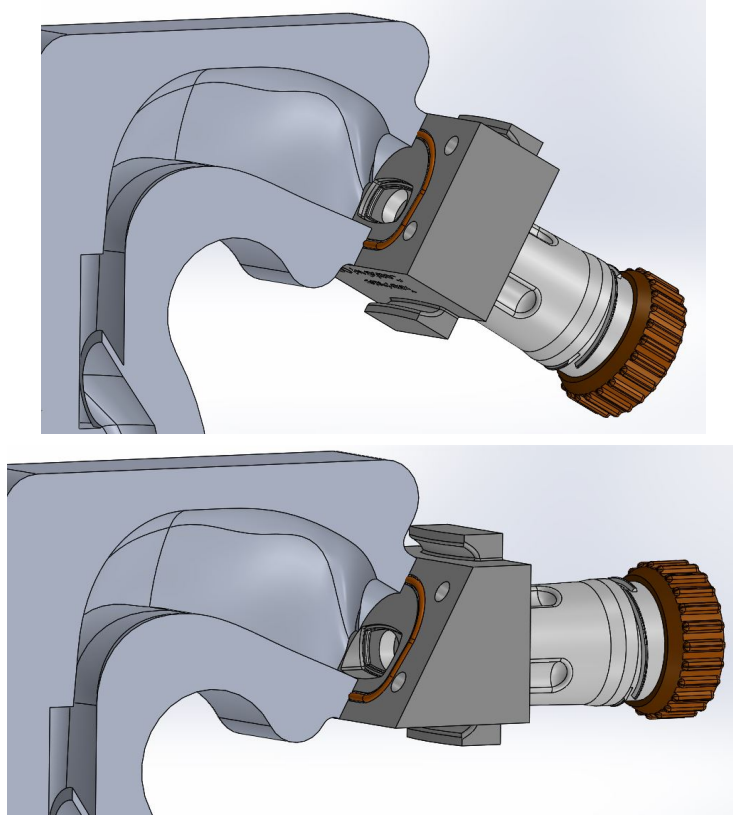
Figure A-5: Comparison of adapters for (top) coaxial and (bottom) transverse orientations with the Turbuhaler DPI attached to the Alberta Idealized Throat.

Appendix B. Volumetric Flowrate Correction Factors

The model 4043 TSI flowmeter is calibrated to measure airflow in standard L/min, defined as a temperature T_{ref} of 21.11 °C and pressure P_{ref} of 101.3 kPa for instruments from TSI Incorporated. Of more concern in aerosol physics is the volumetric flowrate, which describes the actual velocity at which the aerosol and gas phase travel. The standard flowrate can be converted to the volumetric flowrate using the ideal gas law:

$$Q_{vol,m}(t) = Q_{std,m}(t) \frac{T_m}{T_{ref}} \frac{P_{ref}}{P_m}. \tag{B-1}$$

$Q_{std,m}(t)$ is the measured standard flowrate for air at conditions m, having a pressure and temperature of P_m and T_m respectively. $Q_{vol,m}(t)$ denotes the volumetric flowrate at time t. In the setup shown in Figure 3-1, the volumetric flowrate of air entering the DPI is calculated using the values for ambient temperature, T_{amb}, and pressure, P_{amb}.

To calculate the volumetric flowrate exiting the inhaler mouthpiece, the standard flowrate measured by the meter must be corrected considering both the ambient pressure and the pressure drop across the inhaler, ΔP_{DPI}. Equation (B-1) for this condition becomes

$$Q_{vol,DPI\ exit}(t) = Q_{std,m}(t) \frac{T_m}{T_{ref}} \frac{P_{ref}}{\left(P_{amb} - \Delta P_{DPI}(t)\right)}. \tag{B-2}$$

The pressure drop across the DPI depends on the device resistance and flowrate through the inhaler, making it variable over the course of the inhalation, i.e., $\Delta P_{DPI}(t)$. Assuming a quasi-steady relation between pressure drop and flowrate (a reasonable assumption given the small internal volume of the DPI relative to the inhaled volume and inhalation flowrate, resulting in a responsive flow-field with a short time constant inside the DPI) gives

$$\Delta P_{DPI}(t) = \left[R Q_{vol,amb}(t)\right]^2. \tag{B-3}$$

The inhaler resistance is a function of ambient pressure P_{amb} (Titosky et al. 2014), but given the moderate altitudes involved in the present work the effect is taken as negligible, i.e. $R = R_{ref}$, where R_{ref} is the value measured at sea level. The volumetric flowrate occurring at the mouthpiece exit becomes

$$Q_{\text{vol,DPI exit}}(t) = Q_{\text{std,m}}(t)\frac{T_\text{m}}{T_\text{ref}}\frac{101.3}{\left(P_\text{amb} - \left[R\ Q_{\text{vol,amb}}(t)\right]^2\right)}. \tag{B-4}$$

Expressing $Q_{\text{vol,amb}}(t)$ in terms of the standard flowrate leads to the expression detailing the volumetric flowrate exiting the inhaler mouthpiece,

$$Q_{\text{vol,DPI exit}}(t) = Q_{\text{std,m}}(t)\frac{T_\text{m}}{T_\text{ref}}\frac{101.3}{\left(P_\text{amb} - \left[RQ_{\text{std,m}}(t)\frac{T_\text{m}}{T_\text{ref}}\frac{101.3}{P_\text{amb}}\right]^2\right)}. \tag{B-5}$$

The derivation of equation (B-5), also presented as equation (3-4) in Chapter 3, assumes that the effect of ambient pressure on inhaler resistance is negligible (reasonable for moderate altitudes; see Ruzycki et al. [2018]) and that the relation between pressure drop and flowrate is quasi-steady (a reasonable assumption given the small volume of the inhaler relative to the inhalation flowrate).

Correction Factors with Realistic Inhalations

The Delvadia et al semi-idealized inhalation profiles are presented in terms of the volumetric flowrate exiting the inhaler mouthpiece. The setup in Figure 4-1 can provide an indirect measure of this flowrate by considering a mass balance of flow. Consider a control volume encompassing the supply line, the breathing machine line, the vacuum line downstream of the NGI, and the airflow entering the DPI. The equation for conservation of mass in this control volume is:

$$\frac{dm}{dt} = \sum \dot{m}_\text{in} - \sum \dot{m}_\text{out}. \tag{B-6}$$

The time rate of change of mass inside the control volume, dm/dt, is considered negligible relative to the magnitudes of the inlet and outlet flows. This assumption is justified by noting that all flows here have Mach numbers less than 0.3 (i.e., flow can be considered incompressible, so changes in density are small) and the walls of the control volume are rigid (i.e., the actual volume of gas contained in the control volume remains constant). Noting that $m = \rho V$ (mass equals density times volume), expanding with the product rule for differentiation, and using the above physical reasoning (incompressible flow and a rigid control volume), dm/dt is:

$$\frac{dm}{dt} = \frac{d(\rho V)}{dt} = \rho\frac{dV}{dt} + Q\frac{d\rho}{dt} = 0. \tag{B-7}$$

The equation for conservation of mass becomes, after expressing the inlet and outlet flows in terms of their volumetric flowrates $Q_{vol,supply}$, $Q_{vol,HBM}$, $Q_{vol,vacuum}$, and $Q_{vol,DPI}$:

$$\rho_{supply}Q_{vol,supply} + \rho_{DPI}Q_{vol,DPI} = \rho_{HBM}Q_{vol,HBM} + \rho_{vacuum}Q_{vol,vacuum}. \qquad \text{(B-8)}$$

This equation can be recast in terms of standard flowrates using the ideal gas law as follows. The volumetric flowrate at a particular temperature and pressure relates to the standard flowrate as:

$$Q_{vol,m}(t) = Q_{std,m}(t)\frac{P_{ref}}{T_{ref}}\frac{T_m}{P_m}. \qquad \text{(B-9)}$$

From the ideal gas law:

$$\rho_m = \frac{P_m}{R_{specific}T_m}. \qquad \text{(B-10)}$$

Equation (B-9) can then be expressed as:

$$\rho_m Q_{vol,m}(t) = \rho_{ref}Q_{std,m}(t). \qquad \text{(B-11)}$$

Here ρ_m is the air density at which the volumetric flowrate is desired (dependent on temperature and pressure), while ρ_{ref} is a reference density (equal to approximately 1.2 kg/m^3 for TSI calibrated flowmeters). With suitable substitutions, equation (B-8) takes a simple form as all density terms become ρ_{ref}. Further rearranging to solve for the unmeasured flowrate entering the DPI, equation (B-8) becomes:

$$Q_{std,DPI}(t) = Q_{std,HBM}(t) + Q_{std,vacuum}(t) - Q_{std,supply}(t). \qquad \text{(B-12)}$$

Flowrates on the right hand side of equation (B-12) are known (measured with the setup shown in Figure 4-1), allowing for the straightforward calculation of the standard flowrate generated through the DPI, $Q_{std,DPI}$. Calculation of the volumetric flowrate exiting the DPI mouthpiece can then be performed using equation (B-5), i.e., equation (3-4) in Chapter 3.

Appendix C. Description of the Pharmacokinetic Model Described in Chapter 4.

The equations describing the pharmacokinetic model shown schematically in Figure 4-2 of the main text are summarized here. Note that initial deposited masses in each generation of the tracheobronchial airways and in the alveolar region (F_i, $0 \leq i \leq 14$, and F_{ALV}, respectively) come directly from the regional deposition model discussed in the main text, while the initial dose in the gastrointestinal tract is taken as the dose measured in the Alberta Idealized Throat *in vitro*. Rate constants describing mucociliary clearance ($k_{muc,i}$) and the volume of the airway surface liquid in each generation $V_{ASL,i}$ come from the airway surface liquid model discussed in the main text. Values for other rate constants and critical parameters are provided in the main text with references to the literature.

Gastrointestinal tract compartment drug mass, m_A:

$$\frac{dm_A}{dt} = -k_a m_A + k_{muc,0}(m_{0,1} + m_{0,2}). \qquad \text{(C-1)}$$

Equation (C-1) is subject to the initial condition m_A equal to the dose measured in the Alberta Idealized Throat at time $t = 0$.

Central compartment drug mass, m_X:

$$\frac{dm_X}{dt} = -(k_{12} + k_{01})m_X + F_{BA}k_a m_A + k_{21}m_P + k_{ALV}m_{ALV,2} + k_{TB} \sum_{i=0}^{14} m_{i,2}. \qquad \text{(C-2)}$$

Equation (C-2) is subject to the initial condition $m_X = 0$ at time $t = 0$.

Central compartment drug concentration, c_X:

$$c_X = \frac{m_X}{V_C} \qquad \text{(C-3)}$$

where the volume of distribution, V_C, was calculated via (4-2) as discussed in the main text.

Peripheral compartment drug mass, m_P:

$$\frac{dm_P}{dt} = k_{12}m_X - k_{21}m_P. \qquad \text{(C-4)}$$

Equation (C-4) is subject to the initial condition $m_P = 0$ at time $t = 0$.

i^{th} tracheobronchial airway compartment drug mass, m_i ($0 \le i < 14$):

$$\frac{dm_{i,1}}{dt} = -K_{\text{diss,TB}} m_{i,1} (c_S - c_i) - k_{\text{muc},i} m_{i,1} + k_{\text{muc},i+1} m_{i+1,1}, \qquad \text{(C-5)}$$

$$\frac{dm_{i,2}}{dt} = K_{\text{diss,TB}} m_{i,1} (c_S - c_i) - k_{\text{muc},i} m_{i,2} + k_{\text{muc},i+1} m_{i+1,2} - k_{\text{TB}} m_{i,2}. \qquad \text{(C-6)}$$

$K_{\text{diss,TB}}$ is calculated with (4-5) in the main text.

i^{th} tracheobronchial airway compartment drug mass, m_i ($i = 14$):

$$\frac{dm_{i,1}}{dt} = -K_{\text{diss,TB}} m_{i,1} (c_S - c_i) - k_{\text{muc},i} m_{i,1}, \qquad \text{(C-7)}$$

$$\frac{dm_{i,2}}{dt} = K_{\text{diss,TB}} m_{i,1} (c_S - c_i) - k_{\text{muc},i} m_{i,2} - k_{\text{TB}} m_{i,2}. \qquad \text{(C-8)}$$

i^{th} tracheobronchial airway compartment drug concentration, c_i ($0 \le i \le 14$):

$$c_i = \frac{m_{i,2}}{V_{\text{ASL},i}}. \qquad \text{(C-9)}$$

Alveolar compartment drug mass, m_{ALV}:

$$\frac{dm_{\text{ALV},1}}{dt} = -k_{\text{diss,ALV}} m_{\text{ALV},1}, \qquad \text{(C-10)}$$

$$\frac{dm_{\text{ALV},2}}{dt} = k_{\text{diss,ALV}} m_{\text{ALV},1} - k_{\text{ALV}} m_{\text{ALV},2}. \qquad \text{(C-11)}$$

Equations (C-5), (C-7), and (C-10) are subject to the initial condition $m_{i,1} = F_i$ at time $t = 0$. Equations (C-6), (C-8), and (C-11) are subject to the initial condition $m_{i,2} = 0$ at time $t = 0$.

Appendix D. Assays to Quantify Nebulizer Emitted Dose

UV Spectroscopy Calibration Curve

Emitted doses from each nebulizer were measured using the setup detailed in Figure 5-1 and described in section 5.3.1.1, where a ciprofloxacin surrogate (formulated from ciprofloxacin hydrochloride hydrate, CHH) was used in place of methacholine chloride. A standard calibration curve for UV-spectroscopic measurements was developed by dissolving known amounts of ciprofloxacin hydrochloride hydrate in 9 mg/mL saline and diluting with a 7:3 (volume basis) mixture of DIUF water and methanol (the rinsate used with filter samples). The resulting standards showed a strong linear correlation ($R^2 = 0.9967$) using the absorbance peak at 277 nm (background correction at 302 nm) for ciprofloxacin hydrochloride hydrate concentrations up to 21.7 µg/mL (equivalent to 18.6 µg/mL ciprofloxacin), as shown Figure D-1. The slope of the calibration curve, 0.0722 AU/(µg/mL), was used to translate UV spectroscopic measurements of absorbance maxima into ciprofloxacin concentrations for each rinsate sample.
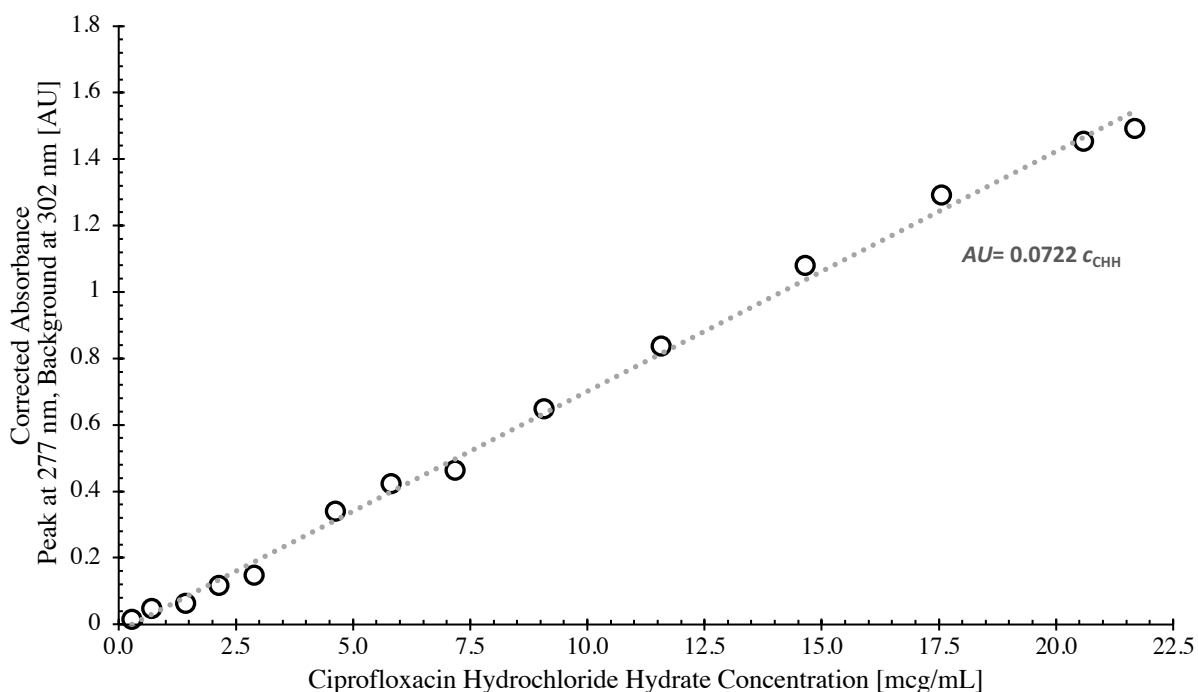

Figure D-1: Calibration curve for ciprofloxacin hydrochloride hydrate.

Drug Recovery

A check of total mass recovery on the filter, nebulizer, and tee-piece was performed for the HRCI nebulizer using a procedure modified from section 5.3.1.1. Modifications included use of a 0.25 mg/mL ciprofloxacin surrogate in 9 mg/mL sodium chloride, running the HRCI nebulizer until sputtering occurred regularly (approximately 5 minutes with the HRCI), and assaying for dose remaining in the nebulizer and depositing in the tee-piece with 50 mL and 10 mL, respectively, of 7:3 DIUF water to methanol. A nominal fill volume of 3 mL, corresponding to 871 µg of ciprofloxacin hydrochloride hydrate for the stock solution concentration of 0.29 mg/mL, was used for each test. Weighing the nebulizer empty and after filling with the ciprofloxacin solution of known concentration allowed for estimation of the actual mass of ciprofloxacin added to the nebulizer (density of the solution was assumed to be 1.0046 g/mL, that of isotonic saline). The sum of the mass recovered from the filter, nebulizer, and tee-piece was compared to this nominal value to assess if adequate drug recovery was achieved with the assay described in 5.3.1.1. Results are shown in Table D-1. The observed excellent recovery, 93.7 (SD 1.1) % of the total expected dose, confirms the assay procedure yields adequate recovery of the ciprofloxacin surrogate.

Table D-1: Recovered dose as a percent of the nominal mass with the HRCI nebulizer (n = 3).

	Percent of Nominal [%]
Filter	22.1 (SD 2.6)
Nebulizer	71.4 (SD 3.6)
Tee-piece	0.2 (SD 0.1)
Total	93.7 (SD 1.1)

Table 4 in the ERS technical standard (Coates et al. 2017) suggests that the delivered dose from nebulizers used with MCT is a linear function of the concentration of the solution the nebulizer is filled with. We examined this relationship using ciprofloxacin surrogates with concentrations of 0.25, 1, and 4 mg/mL (all in 9 mg/mL saline), otherwise following the procedure outlined in section 5.3.1.1. Results are shown in Figure D-2, which confirmed this linear trend, at least up to concentrations of 4 mg/mL of the surrogate. We assume this holds for other nebulizers as well.
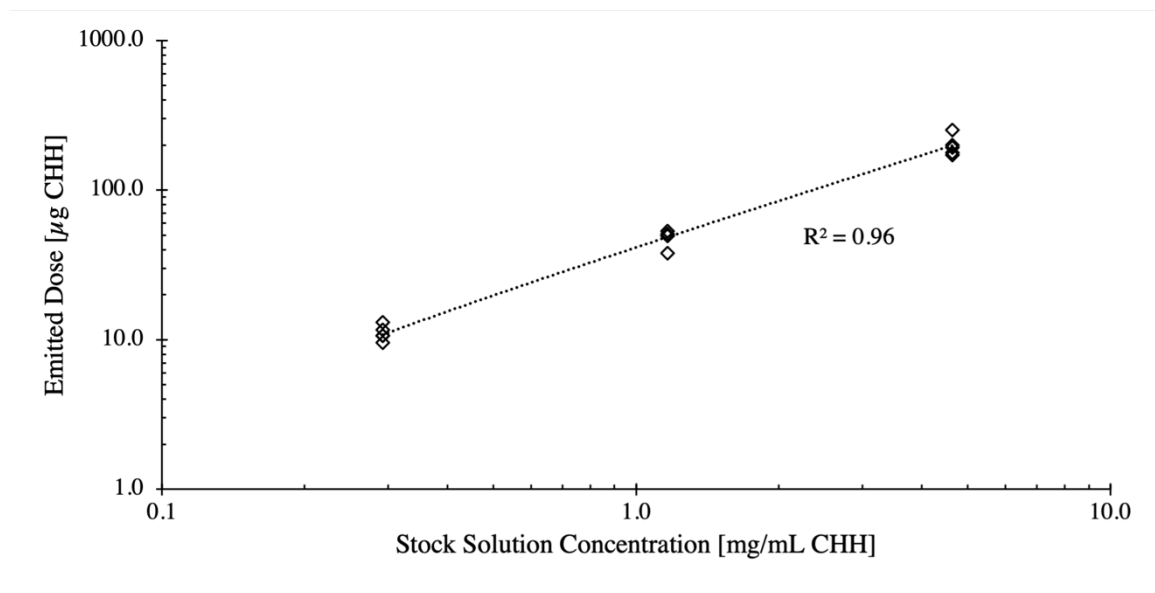

Figure D-2: Linearity of the dose emitted from RX160 nebulizers for ciprofloxacin hydrochloride hydrate (CHH) surrogates in 9 mg/mL saline.

Appendix E.   Measurements of Nebulized Airstream Conditions

As noted in 5.3.1.2 the temperature and humidity of the airstream emitted by the nebulizer were recorded with a calibrated digital hygrometer/thermometer (HMP75B Humidity and Temperature Probe with MI70 Measurement Indicator; Vaisala, Vantaa, Finland) as per the setup in Figure 5-2. The probe was also operated in "sensor preheat" mode to avoid condensation on the sensor during testing, and the temperature and humidity were measured and recorded in 1 s intervals. Typical examples of the recorded profiles are shown in Figure E-1
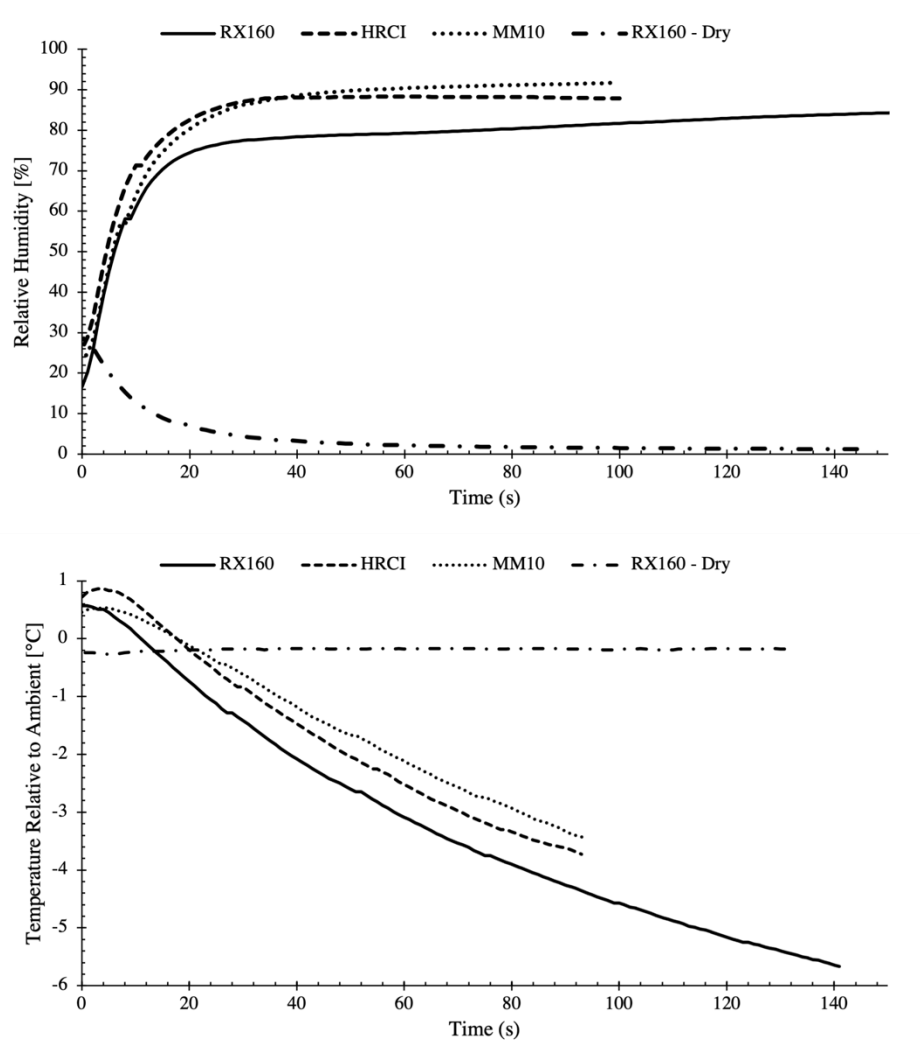

Figure E-1: Typical examples of (top) humidity and (bottom) temperature profiles measured in the airstream emitted from nebulizers using 9 mg/mL saline. A dry run with the RX160 is included to show the conditions of building air sans nebulized aerosol.

The response time (to 90% of final value) of the HMP75B probe is stated by the manufacturer to be 17 s, which for a first order system equates to a time constant of 7.4 s. Some time is also required for the nebulizer to begin emitting aerosol after the air supply is turned on, though this time is much less than 7.4 s. For a first order system, the measured value reaches 95% of the final value within three time constants, here equal to 22 s. Thus, averages of the humidity and temperature were taken starting 22 s after the instrument began responding to the change in temperature and humidity and for the appropriate time duration according to the emitted dose tests described in section 5.3.1.1 (i.e., 2 min for RX160, 1 min for HRCI and MM10). One RX160 was used for testing, with five replicated measures obtained with each solution of interest (i.e., low, medium, and high methacholine concentrations, plus diluent only). Five HCRIs and five MM10s were used to examine each solution of interest once. This procedure yielded n = 5 measurements for each type of nebulizer at each solution of interest, or a total n = 20, as summarized in Table E-1. For each nebulizer, differences measured between the various stock solution concentrations are not statistically significant. Values were pooled into single estimates of humidity and temperature.

Table E-1: Average humidity and temperature of the nebulized airstream.

Nebulizer	Initial Solution	Relative Humidity [%]	Temperature (Relative to Ambient) [ºC]
RX160	9 mg/mL NaCl	78.7 (SD 1.6)	-4.0 (SD 0.4)
	9 mg/mL NaCl + 0.0625 mg/mL MCl	78.9 (SD 1.0)	-3.9 (SD 0.5)
	9 mg/mL NaCl + 1 mg/mL MCl	78.4 (SD 0.4)	-3.9 (SD 0.7)
	9 mg/mL NaCl + 16 mg/mL MCl	78.0 (SD 0.9)	-4.0 (SD 0.4)
HRCI	9 mg/mL NaCl	89.3 (SD 1.0)	-2.1 (SD 0.3)
	9 mg/mL NaCl + 0.0625 mg/mL MCl	88.8 (SD 2.1)	-2.2 (SD 0.2)
	9 mg/mL NaCl + 1 mg/mL MCl	87.6 (SD 1.2)	-1.8 (SD 0.2)
	9 mg/mL NaCl + 16 mg/mL MCl	87.6 (SD 1.3)	-2.1 (SD 0.3)
MM10	9 mg/mL NaCl	89.5 (SD 0.6)	-1.7 (SD 0.7)
	9 mg/mL NaCl + 0.0625 mg/mL MCl	89.8 (SD 1.5)	-1.7 (SD 0.2)
	9 mg/mL NaCl + 1 mg/mL MCl	90.4 (SD 0.7)	-1.5 (SD 0.2)
	9 mg/mL NaCl + 16 mg/mL MCl	89.7 (SD 0.6)	-1.7 (SD 0.4)

Appendix F. Additional Description of Hygroscopic Models

Correlations for the predicted water activity of different concentrations of methacholine chloride (MCl) in 9 mg/mL sodium chloride (NaCl) are shown in Figure 5-4. The correlation for NaCl, equation (5-8), was developed by fitting a 4th degree polynomial to literature data (Tang, Munkelwitz, and Wang 1986; Robinson and Stokes 1970) with the *Curve Fitting Toolbox* in MATLAB, with the intercept set to 1 and no weighting. The R^2 of 0.9998 and SSE of 0.0005168 imply an excellent fit.

Using equation (5-10), correlations for varying concentrations of methacholine chloride were developed and are presented here in explicit form. Correlations are expressed in terms of the total solute mass content Y_{sol} and are defined for low, medium, and high concentrations of MCl (0.0625, 1, and 16 mg/mL, respectively). Y_{sol} is expressed as a percent point, i.e., 20.6% solute mass content in a solution is equal to $Y_{sol} = 20.6$.

Table F-1: Correlations for water activity coefficient as a function of solute content.

Initial Solution	Expression for Water Activity Coefficient, S [-]
9 mg/mL NaCl	$S_{NaCl} = 1 - (0.006154)Y_{NaCl} + (6.527 \times 10^{-5})Y_{NaCl}^2 - (1.073 \times 10^{-5})Y_{NaCl}^3 + (1.403 \times 10^{-7})Y_{NaCl}^4$
9 mg/mL NaCl + 0.0625 mg/mL MCl	$S_{low} = 1 - (0.006124)Y_{sol} + (6.422 \times 10^{-5})Y_{sol}^2 - (1.051 \times 10^{-5})Y_{sol}^3 + (1.364 \times 10^{-7})Y_{sol}^4$
9 mg/mL NaCl + 1 mg/mL MCl	$S_{medium} = 1 - (0.00572)Y_{sol} + (5.044 \times 10^{-5})Y_{sol}^2 - (7.807 \times 10^{-6})Y_{sol}^3 + (9.122 \times 10^{-8})Y_{sol}^4$
9 mg/mL NaCl + 16 mg/mL MCl	$S_{high} = 1 - (0.003149)Y_{sol} - (3.569 \times 10^{-5})Y_{sol}^2 + (5.737 \times 10^{-7})Y_{sol}^3 - (1.269 \times 10^{-8})Y_{sol}^4$

Droplet Density

The density of droplets comprised of varying concentrations of solute was calculated using an ideal volumetric mixing model, a simple approach that neglects non-ideal behaviour but allows for calculations absent well-characterized experimental data for the various solutions of interest and is consistent with the method used to estimate residual particle density, i.e., equation (5-2).

$$\rho_d = \frac{m_{NaCl} + m_{MCl} + m_w}{\frac{m_{NaCl}}{\rho_{NaCl}} + \frac{m_{MCl}}{\rho_{MCl}} + \frac{m_w}{\rho_w}}. \tag{F-1}$$

This equation was recast in terms of the solute mass content Y_{sol} and approximated with 2nd order polynomial fits for each solution of interest (i.e., diluent only and low, medium, and high concentrations of MCl) to facilitate inclusion in the coding of the hygroscopic model.

Table F-2: Correlations for droplet density as a function of solute content.

Initial Solution	Expression for Droplet Density, ρ_d [kg/m^3]
9 mg/mL NaCl	$\rho_{d,NaCl} = 1000 + 5.205 Y_{NaCl} + 0.04133 Y_{NaCl}^2$
9 mg/mL NaCl + 0.0625 mg/mL MCl	$\rho_{d,low} = 1000 + 5.171 Y_{sol} + 0.04133 Y_{sol}^2$
9 mg/mL NaCl + 1 mg/mL MCl	$\rho_{d,medium} = 1000 + 4.714 Y_{sol} + 0.03399 Y_{sol}^2$
9 mg/mL NaCl + 16 mg/mL MCl	$\rho_{d,high} = 1000 + 2.122 Y_{sol} + 0.005657 Y_{sol}^2$

Figure F-1 shows these density values over a range of solute mass fractions for each solution of interest. Also shown are predictions accounting for non-ideal behaviour with sodium chloride via Köhler theory (Gysel, Weingartner, and Baltensperger 2002). Differences in the predicted droplet density between the ideal method described in equation (F-1) and Köhler theory are small (less than 5%), suggesting the ideal method is a reasonable approximation for present purposes.
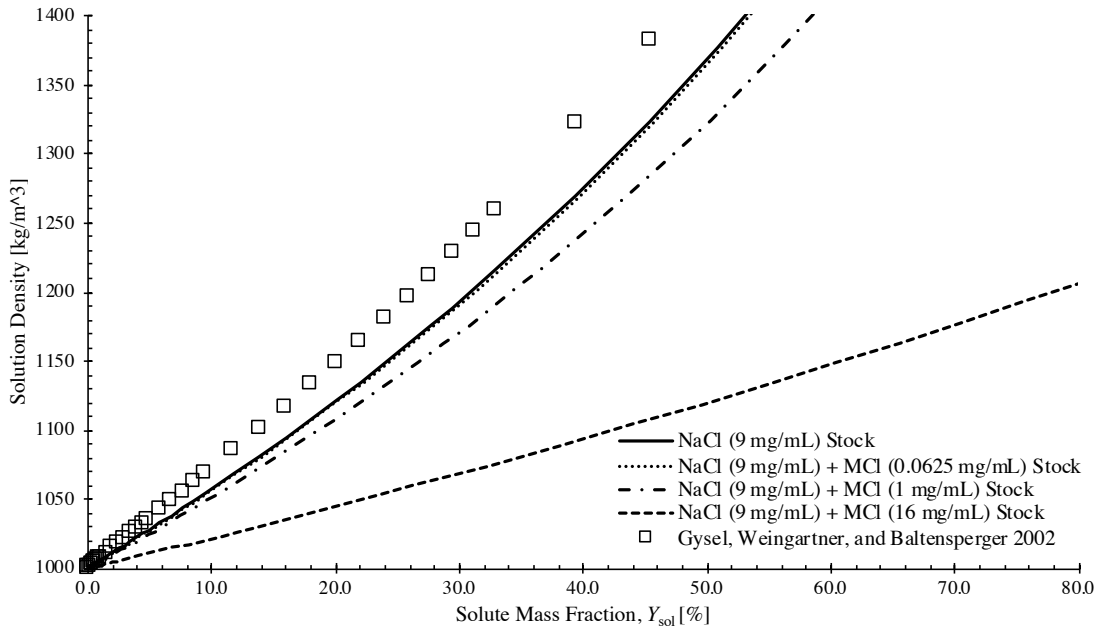

Figure F-1: Predicted density for each solution of interest versus solute content.

Surface Tension

Calculation of the Kelvin effect in equation (5-6) requires an estimate of the surface tension of the solution under consideration, σ_{sol}. For dilute aqueous solutions the surface tension shows an approximately linear relation to the concentration (Jen-Ping Chen 1994; Gysel, Weingartner, and Baltensperger 2002). Surface tension is also observed to be a function of temperature. These effects were considered via the method of Gysel, Weingartner, and Baltensperger (2002),

$$\sigma_{sol} = 0.0761 - (1.55 \times 10^{-4})T + \sum_i \beta_i b_i, \tag{F-2}$$

where β_i is a salt-specific coefficient and b_i is the molality of salt i. β for sodium chloride is 0.00164 [Nm^{-1}M^{-1}], which we also take as the β for methacholine chloride owing to a lack of better literature. This allows for b_i to be expressed as the total solution molality. Solution molality, calculated as the number of moles of solute per kg of solvent, was calculated in conjunction with other values above and approximated as 2nd order polynomials of solute mass content Y_{sol}.

Table F-3: Correlations for solution molality as a function of solute content.

Initial Solution	Expression for Solution Molality, b [mol/mL]
9 mg/mL NaCl	$b_{NaCl} = 0.1413Y_{NaCl} + 0.003621Y_{NaCl}^2$
9 mg/mL NaCl + 0.0625 mg/mL MCl	$b_{low} = 0.14Y_{sol} + 0.003627Y_{sol}^2$
9 mg/mL NaCl + 1 mg/mL MCl	$b_{medium} = 0.1205Y_{sol} + 0.003764Y_{NaCl}^2$
9 mg/mL NaCl + 16 mg/mL MCl	$b_{high} = 0.01468Y_{sol} + 0.003935Y_{NaCl}^2$

Specific Heat Capacity

Specific heat capacity of droplets, c_p, was calculated as an ideal mixture between water ($c_{p,w} = 4180$ J/kg·K) and solute. Owing to a lack of information on methacholine chloride, we use the c_p of sodium chloride ($c_{p,NaCl} = 880$ J/kg·K) as representative of the solute content in each solution of interest in the present work.

$$c_p = \frac{\left[Y_{sol}c_{p,NaCl} + (100 - Y_{sol})c_{p,w}\right]}{100} \tag{F-3}$$

Equilibrium Solute Mass Content

The hygroscopic theory outlined in section 5.3.2 leads to the estimation of the equilibrium size of droplets corresponding to residual particle sizes measured by the ELPI+. Because of the relation between the water activity coefficient and the Kelvin effect, smaller droplets are, at equilibrium, more concentrated than larger droplets. Implementation of the code for lung deposition required an estimate of the initial solute mass content (i.e., concentration) of droplets upon inhalation, where the concentration is a function of many factors including equilibrium droplet size and airstream conditions. Correlations expressing the equilibrium solute mass content (i.e., concentration) for each nebulizer and solution of interest were developed from the predictions in section 5.3.2 using power fits of the form $ax^b + c$. Examples of the interplay between equilibrium solute content and droplet size are shown for saline using the data for the RX160, HRCI, and MM10 nebulizers in Figure F-2. To simplify implementation in the lung deposition model, the initial solute mass content of droplets (and correspondingly, the droplet density per equation (F-1)) for each nebulizer and solution of interest were calculated using the singular values of predicted MMDs, rather than across entire distributions. Such an approximation is reasonable considering majority of mass is contained in droplets larger than 0.1 μm, above which the effects of the Kelvin effect on equilibrium size are less pronounced in the current problem.
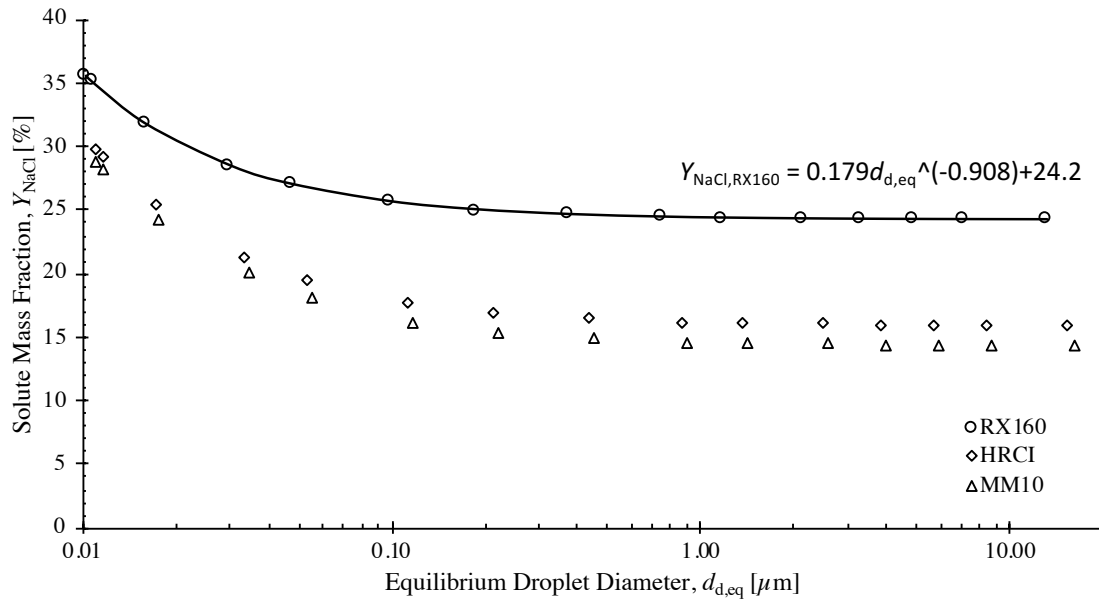

Figure F-2: Relation between equilibrium droplet diameter and solute mass fraction for the RX160, HRCI, and MM10 nebulizers delivering sodium chloride.

For completeness, the correlations for each nebulizer and solution are included in Table F-4.

Table F-4: Correlations for equilibrium solute mass content as a function of droplet diameter.

Nebulizer	Initial Solution	Expression for Equilibrium Solute Mass Content Y_{sol} [%] as a Function of Droplet Diameter $d_{d,eq}$ [µm]
RX160	9 mg/mL NaCl	$Y_{NaCl} = 0.179(d_{d,eq})^{-0.908} + 24.2$
	9 mg/mL NaCl + 0.0625 mg/mL MCl	$Y_{low} = 0.1804(d_{d,eq})^{-0.9076} + 24.34$
	9 mg/mL NaCl + 1 mg/mL MCl	$Y_{medium} = 0.2006(d_{d,eq})^{-0.9043} + 26.35$
	9 mg/mL NaCl + 16 mg/mL MCl	$Y_{high} = 0.5841(d_{d,eq})^{-0.7609} + 44.88$
HRCI	9 mg/mL NaCl	$Y_{NaCl} = 0.3038(d_{d,eq})^{-0.8486} + 15.94$
	9 mg/mL NaCl + 0.0625 mg/mL MCl	$Y_{low} = 0.3061(d_{d,eq})^{-0.8482} + 16.03$
	9 mg/mL NaCl + 1 mg/mL MCl	$Y_{medium} = 0.3386(d_{d,eq})^{-0.8463} + 17.27$
	9 mg/mL NaCl + 16 mg/mL MCl	$Y_{high} = 0.9497(d_{d,eq})^{-0.7409} + 28.59$
MM10	9 mg/mL NaCl	$Y_{NaCl} = 0.3392(d_{d,eq})^{-0.8362} + 14.34$
	9 mg/mL NaCl + 0.0625 mg/mL MCl	$Y_{low} = 0.3417(d_{d,eq})^{-0.8359} + 14.41$
	9 mg/mL NaCl + 1 mg/mL MCl	$Y_{medium} = 0.3771(d_{d,eq})^{-0.8343} + 15.51$
	9 mg/mL NaCl + 16 mg/mL MCl	$Y_{high} = 1.012(d_{d,eq})^{-0.7408} + 25.4$